DESIGN, DEVELOPMENT AND FLIGHT TEST OF THE SUPER LOKI DART METEOROLOGICAL ROCKET SYSTEMS

Bruce Bollermann, et al

Space Data Corporation

Prepared for:

Air Force Cambridge Research Laboratories

30 May 1972

AFCRL - 72 - 0382

DESIGN, DEVELOPMENT AND FLIGHT TEST OF THE SUPER LOKI DART METEOROLOGICAL ROCKET SYSTEMS

Bruce Bollermann
Robert L. Walker

SPACE DATA CORPORATION
1331 S. 26th Street
Phoenix, Arizona 85034

CONTRACT NO. F19628-69-C-0212

PROJECT NO. 6682
TASK NO. 668202
WORK UNIT NO. 66820201

FINAL REPORT
Period Covered 1 February 1969 through 30 May 1972

30 May 1972

Contract Monitor: John B. Wright
Meteorology Laboratory

Prepared for:

AIR FORCE CAMBRIDGE RESEARCH LABORATORIES
AIR FORCE SYSTEMS COMMAND
UNITED STATES AIR FORCE
Bedford, Massachusetts 01730

Qualified requestors may obtain additional copies from the Defense Documentation Center. All others should apply to the Clearinghouse for Federal Scientific and Technical Information.

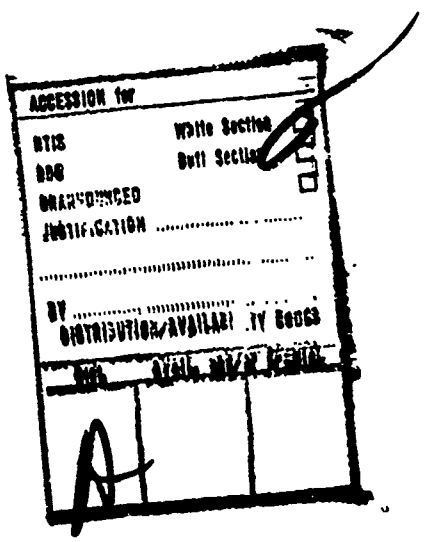

Unclassified

Security Classification

DOCUMENT CONTROL DATA - R & D

(Security classification of title, body of abstract and indexing annotation must be entered when the overall report is classified)

1 ORIGINATING ACTIVITY (Corporate author) Space Data Corporation 1331 S. 26th St. Phoenix, Arizona 85034	2a. REPORT SECURITY CLASSIFICATION Unclassified 2b GROUP

3 REPORT TITLE

DESIGN, DEVELOPMENT AND FLIGHT TEST OF THE SUPER LOKI DART METEOROLOGICAL ROCKET SYSTEMS

4 DESCRIPTIVE NOTES (Type of report and inclusive dates)
Scientific Final. 1 February 1969 - 30 May 1972 Approved 26 July 1972

5 AUTHOR(S) (First name, middle initial, last name)
Bruce Bollermann
Robert L. Walker

6 REPORT DATE 30 May 1972	7a. TOTAL NO OF PAGES ~~222~~ 236	7b. NO OF REFS
8a. CONTRACT OR GRANT NO F19629-69-C-0212 b PROJECT, TASK, AND WORK UNIT NO. 6682-02-01 c DOD ELEMENT 6570/F d. DOD SUBELEMENT 676682	9a. ORIGINATOR'S REPORT NUMBER(S) 9b. OTHER REPORT NO(S) (Any other numbers that may be assigned this report) AFCRL-72-0382	

10 DISTRIBUTION STATEMENT

A - Approved for public release;distribution unlimited.

11 SUPPLEMENTARY NOTES TECH., OTHER	12 SPONSORING MILITARY ACTIVITY Air Force Cambridge Research Laboratories (LY) L. G. Hanscom Field, Bedford MA 01730

13 ABSTRACT

The Super Loki Dart Meteorological Rocket Systems have been developed to obtain high altitude temperature, density and wind measurements by means of small inexpensive rocket systems. The Super Loki Robin Dart System was designed as a replacement for the larger and more expensive Viper Robin Dart to obtain falling sphere density and wind data from an altitude of 30 km to 90 km. The Super Loki Transponder Dart was also developed in order to offer better wind and temperature data from 25 km to a higher altitude, 70 km, than the more expensive Arcas Transponder system. The Super Loki Transmitter Dart was developed as a candidate to replace the Loki Dart by also offering improved data to higher altitudes. By development of the three Super Loki systems which have commonality of motors and other parts, simplification of the inventory requirements of the U. S. Meteorological Rocket Network is possible.

Details of illustrations in this document may be better studied on microfiche.

DD FORM 1 NOV 1473

Unclassified

Security Classification

I-A

Unclassified

Security Classification

14 KEY WORDS	LINK A		LINK B		LINK C	
	ROLE	WT	ROLE	WT	ROLE	WT
Probe, Meteorological						
Meteorological Probe						
Meteorological Rocket						
Sounding Rocket						
Rocket, Sounding						
Rocket, Meteorological						

Unclassified

Security Classification

I-B

AFCRL - 72 - 0382

DESIGN, DEVELOPMENT AND FLIGHT TEST

OF THE

SUPER LOKI DART METEOROLOGICAL ROCKET SYSTEMS

Bruce Bollermann
Robert L. Walker

SPACE DATA CORPORATION
1331 S. 26th Street
Phoenix, Arizona 85034

CONTRACT NO. F19628-69-C-0212

PROJECT NO. 6682
TASK NO. 668202
WORK UNIT NO. 66820201

FINAL REPORT
Period Covered 1 February 1969 through 30 May 1972

30 May 1972

Contract Monitor: John B. Wright
Meteorology Laboratory

Prepared for:

AIR FORCE CAMBRIDGE RESEARCH LABORATORIES
AIR FORCE SYSTEMS COMMAND
UNITED STATES AIR FORCE
Bedford, Massachusetts 01730

I-1

FOREWORD

This report is authorized by Contract No. F19628-69-C-0212 which has been sponsored by the Vertical Sounding Techniques Branch (LYV) of the Meteorology Laboratory, Air Force Cambridge Research Laboratory.

Space Data Corporation wishes to express appreciation to Mr. Robert Leviton, Branch Chief, Mr. John B. Wright, Contract Monitor, and to other members of the Vertical Sounding Techniques Branch -- Mr. Ted Georgian, Mr. Anthony Matthews, Mr. Jack Griffin and Gordon Canning, whose combined efforts have made the Super Loki development program a success. Appreciation is also expressed to Mr. Robert Turner, R-AERO-Y, of the Marshall Space Flight Center, NASA, for his financial assistance to the program. The efforts of Mr. O. H. Daniel and Mr. Dan Hanson of the Pan American Airways, Range Contractor at Cape Kennedy, are also appreciated and significantly added to the success of the program

ABSTRACT

The Super Loki Dart Meteorological Rocket Systems have been developed to obtain high altitude temperature, density and wind measurements by means of small inexpensive rocket systems. The Super Loki Robin Dart System was designed as a replacement for the larger and more expensive Viper Robin Dart to obtain falling sphere density and wind data from an altitude of 30 km to 90 km. The Super Loki Transponder Dart was also developed in order to offer better wind and temperature data from 25 km to a higher altitude, 70 km, than the more expensive Arcas Transponder system. The Super Loki Transmitter Dart was developed as a candidate to replace the Loki Dart by also offering improved data to higher altitudes. By development of the three Super Loki systems which have commonality of motors and other parts, simplification of the inventory requirements of the U.S. Meteorological Rocket Network is possible.

LIST OF CONTRIBUTORS

Space Data Corporation

Ray Crum
Garwood Baybrook
Ed Morgan
Bernard Welinski
Ed Schaefer

TABLE OF CONTENTS

TABLE OF CONTENTS
Continued

TABLE OF CONTENTS
Continued

TABLE OF CONTENTS
Continued

LIST OF FIGURES

LIST OF FIGURES
Continued

LIST OF FIGURES
Continued

LIST OF FIGURES
Continued

LIST OF FIGURES
Continued

LIST OF FIGURES
Continued

LIST OF TABLES

LIST OF TABLES
Continued

SUMMARY

Three Super Loki Dart Meteorological Rocket Systems have been developed and successfully flight tested for the United States Air Force to provide low cost meteorological measurements to altitudes from 20 km to 90 km. Two basic rocket vehicles were developed to carry three required payloads to apogee altitudes of 75 km and 115 km.

The Super Loki Robin Dart system has been developed to obtain falling sphere density and wind data from an altitude of 30 km to 90 km. This system can replace the more expensive Viper Robin Dart.

The Super Loki Transponder Dart system has been developed to obtain atmospheric temperature and wind data from an altitude of 20 km to 70 km by means of an AN/GMD-4 ground-station receiving set. Since this system includes a transponder, radar tracking is not required, and remote site operation is made possible. This Super Loki system can replace the more expensive Arcas AN/DMQ-9 transponder system.

The Super Loki Transmitter Dart system has been developed as an outgrowth of the transponder system. The transponder instrument ranging receiver has been deleted from the transponder instrument for those launch sites where tracking radars are available, thereby reducing the system's cost. Since it attains a 70 km altitude, it provides data to higher altitudes than the Loki Darts. Slower descending sondes in both the Transponder and Transmitter systems theoretically provide improved data over that obtained by currently operational systems.

INTRODUCTION

The U. S. Air Force has requirements for routine direct measurement of atmospheric temperatures, density and wind profiles from the earth surface to an altitude of 90 km. Balloon-borne radiosondes are used to satisfy these measurement requirements to a ceiling of about 30 km. Rocket systems are required to extend the measured profiles up to 90 km.

From about 1963 to 1969 the Arcas meteorological rocket was used to conduct routine temperature and wind soundings to about 60 km. A transmitter instrument was used with the AN/GMD-1 ground-station receiving equipment. Thus, tracking radar was required to obtain space position data. During the mid 1960's, an AN/DMQ-9 transponder instrument was developed for the Arcas rocket so that soundings could be made at remote sites without the need for tracking radar. Soon after this period, the Loki Dart system was developed for the Air Force to replace the more costly Arcas.

Although the transmitter instrument version of the Loki Dart (PWN-8B) was immediately successful, the dart second-stage appeared to be too small to incorporate the larger transponder instrument. Two programs to develop a transponder instrument for the small Loki Dart ended in failure. Because of this, it was proposed to scale the Loki system up in size to make more payload volume available for the transponder instrument. It was decided that a higher apogee altitude should be achieved than for either the Arcas or the Loki, and that a larger decelerator should be developed to achieve reasonable descent rates at the higher altitudes with the heavier transponder instrument. This new system is the Super Loki which is the subject of this report.

During the latter 1960's, the Viper Robin Dart system was developed to obtain falling sphere density and wind profiles to 100 km. Although this system was operational for only two years, the Air Force decided to replace it with a smaller and lower cost Super Loki falling sphere system. For the sake of a unified booster system and logistics simplification, the Air Force also decided to develop a Super Loki transmitter system by eliminating the ranging receiver from the transponder system. Thus, three Super Loki systems, ie., the transponder, transmitter and Robin falling sphere have been developed under the program reported herein. A discussion of the evolution of meteorological rockets, in particular the Super Loki development, is given in Reference 1.

3.

ROCKET MOTOR FINAL DESIGN

3.1 Introduction

The Super Loki rocket motor was originally developed by scaling up the Loki motor from a 3.0 - inch diameter to a 4.0 - inch diameter for NASA-MSFC to power a chaff dart second-stage to 115 km. The rocket motor was modified and adapted to the Air Force dart systems during the current program.

3.2 Description

The Super Loki rocket motor shown in Figure 3.1 consists of an aluminum case with an internal burning cast-in-case solid propellant. An aluminum headcap and interstage coupling is located at the forward end of the rocket motor. A graphite nozzle insert backed by a steel retaining ring is located at the aft end of the motor. The propellant fuel is a polysulfide polymer with an ammonium perchlorate oxidizer. The igniter consists of two parallel 1 watt/1 ampere no-fire squibs and an ignition charge of cupric oxide and aluminum power. The igniter is separable from the rocket motor and is installed at the launch site.

A cross-section view of the Super Loki rocket motor is presented in Figure 3.2. Major design characteristics are presented in Table 3.1, and the propellant characteristics are presented in Table 3.2. The propellant burning rate and area ratio curves vs. chamber pressure are presented in Figure 3.3.

3.3 Performance

A summary of the rocket motor performance data is presented in Table 3.3. A nominal pressure and thrust vs. time curve is presented in Figure 3.4.

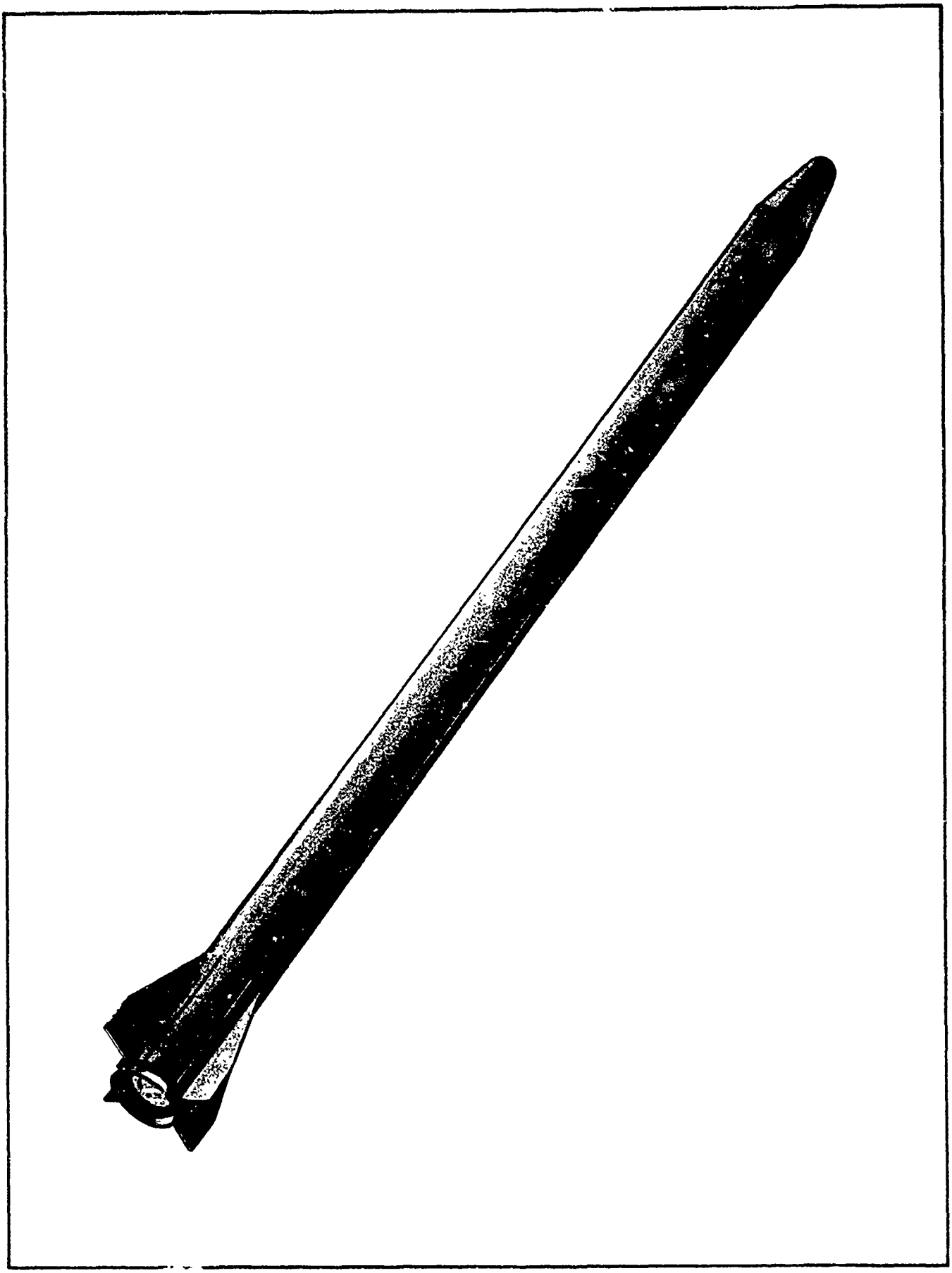

FIGURE 3.1 SUPER LOKi ROCKET MOTOR

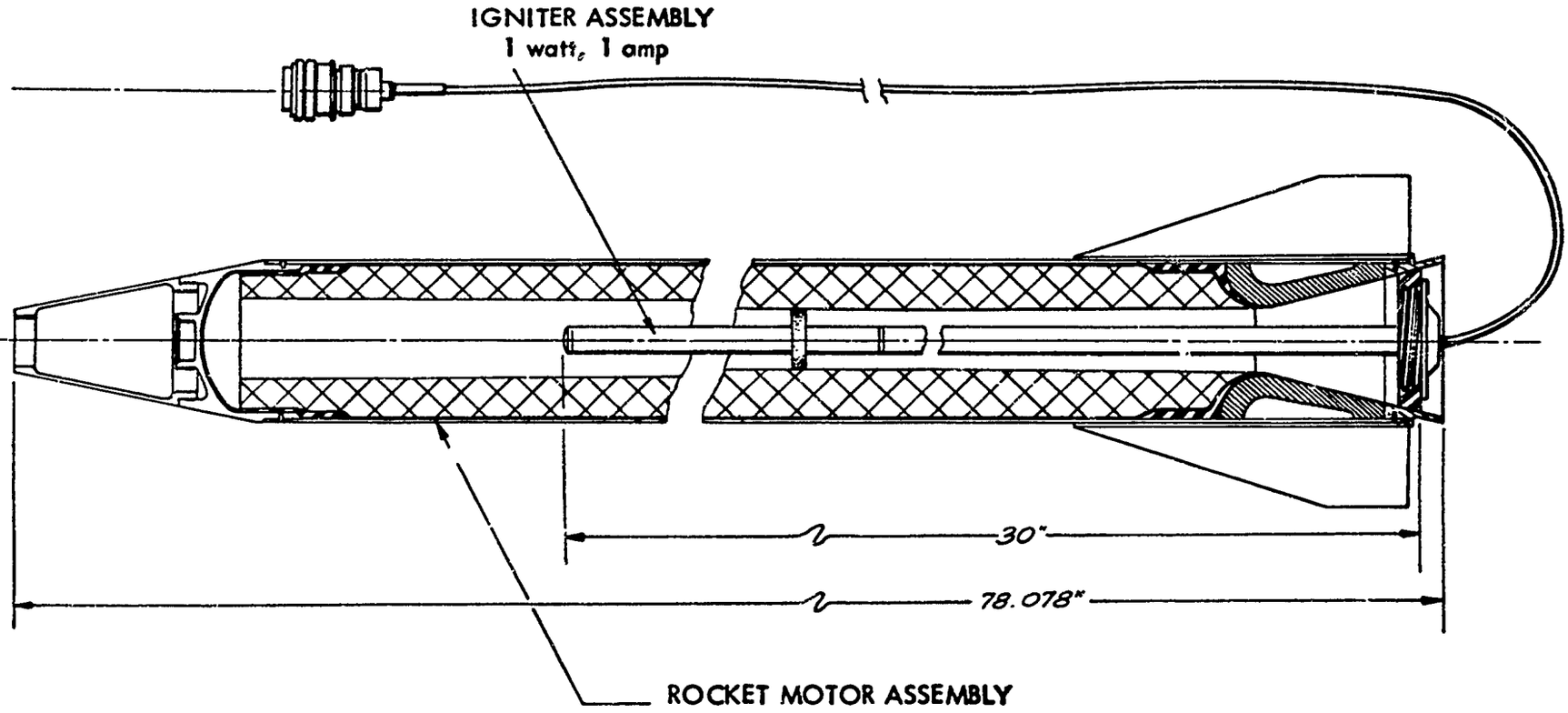

FIGURE 3.2 CROSS-SECTION VIEW OF SUPER LOKI ROCKET MOTOR WITH IGNITER INSTALLED

TABLE 3.1

SUPER LOKI ROCKET MOTOR DESIGN CHARACTERISTICS

Length	78.3	in.
Diameter	4.0	in.
Fin Span	8.00	in.
Fin Tip Chord	2.00	in.
Fin Root Chord	8.00	in.
Fin Area (each)	10.0	$in.^2$ per fin
Weights:		
Motor Case with Fins and Nozzle	10.63	lb.
Headcap and Interstage	1.37	lb.
Robin Dart Interstage Adaptor	0.67	lb.
Propellant	37.51	lb.
Liner	0.69	lb.
Total	50.87	lb.
Igniter	0.40	lb.
Motor Case Wall	0.083" 2014-T6 Aluminum	
Motor Case Proof Pressure	1500	psi
Motor Case Yield Pressure (min)	2320	psi
Motor Case Burst Pressure	2700	psi
Nozzle Throad Area	2.326 in^2	
Storage Temperature Limits	$-40^{\circ}F$ to $+140^{\circ}F$	
Operational Temperature Limits	$-40^{\circ}F$ to $+140^{\circ}F$	
Storage Life	2 years	
Explosives Classification	ICC Class B	

TABLE 3.2

PROPELLANT CHARACTERISTICS

Propellant Composition

Material	Purpose	Parts by Weight (Nominal)
Polysulfide Polymer, Liquid	Fuel and Binder	16.40
Quinonedioximine	Curing Agent	1.20
Sulfur, Flowers of	Curing Catalyst	0.10
Diphenylguanidine	Curing Accelerator	0.10
Ammonium Perchlorate (as received)	Oxidizer	46.20
Ammonium Perchlorate (after grinding)	Oxidizer	30.80
Dibutyl Phthalate	Plasticizer	2.80
Magnesium Oxide	Curing Catalyst	0.60
Aluminum	Resonance Suppressor	1.80

Grain Size Distribution for Ammonium Perchlorate Blend

As received AP retained on:	REQUIREMENTS Min.	Max.
USS 18%	-0-	-0-
USS 50%	3%	11%
USS 100%	50	82
USS 140%	85	98
USS 325%	98	100
Ground AP % Below:		
10 Microns	12	32
20 Microns	40	60
30 Microns	58	78

Ballistic Properties

Temperature coefficient of chamber pressure	0.308 per deg Kelvin
Temperature coefficient of burn rate	0.0488 per deg Kelvin
Pressure exponent	0.435
Characteristic exhaust velocity	4702 fps
Ratio of specific heats	1.217
Heat of Explosion	1200 cal/g
Adiabatic Flame Temperature	2784°K

TABLE 3.2 (Continued)

PROPELLANT CHARACTERISTICS

Physical Properties	
Density	0.062 lb/in^3
Hardness	70 - 90 Shore A
Tensile Strength	200 - 250 psi maximum
Elongation	18 - 45% maximum
Modulus	2100 - 2800 psi
Autoignition Temperature	275°F

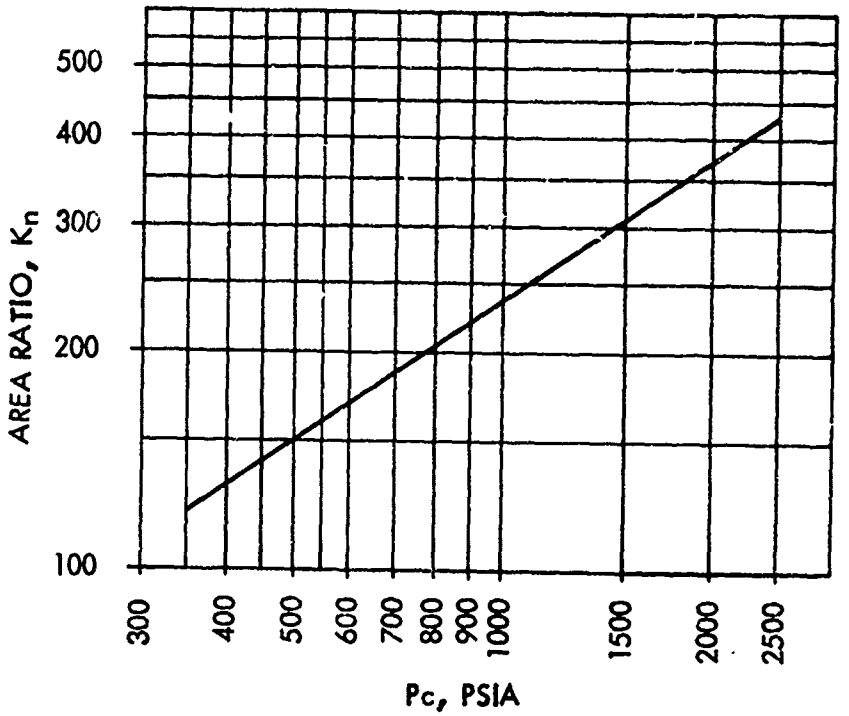

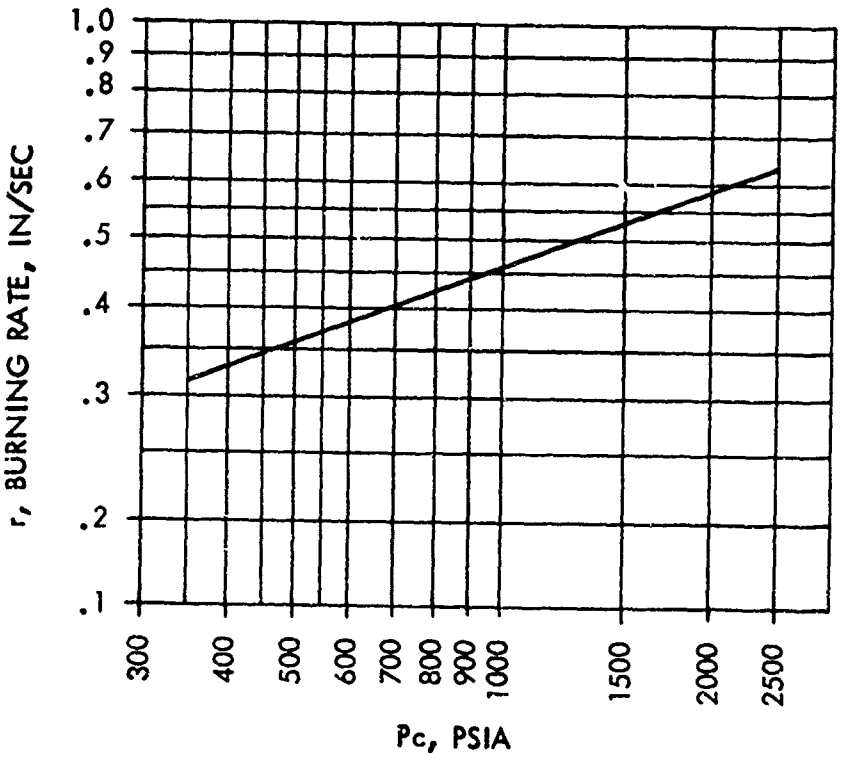

FIGURE 3.3 SUPER LOKI ROCKET MOTOR INTERNAL BALLISTICS DATA
AMBIENT TEMPERATURES

TABLE 3.3

ROCKET MOTOR PERFORMANCE SUMMARY

(SEA LEVEL FIRING)

Average Thrust (lbf)	4021
Average Chamber Pressure (psia)	1212
Total Impulse (lbf-sec)	8511
Action Time (sec)	2.11
Maximum Thrust (lbf)	5524
Maximum Chamber Pressure (psia)	1543
Specific Impulse (sec)	232

FIGURE 3.4 SUPER LOKI ROCKET MOTOR
SEA LEVEL CHAMBER PRESSURE AND
THRUST VS. TIME AT +59°F.

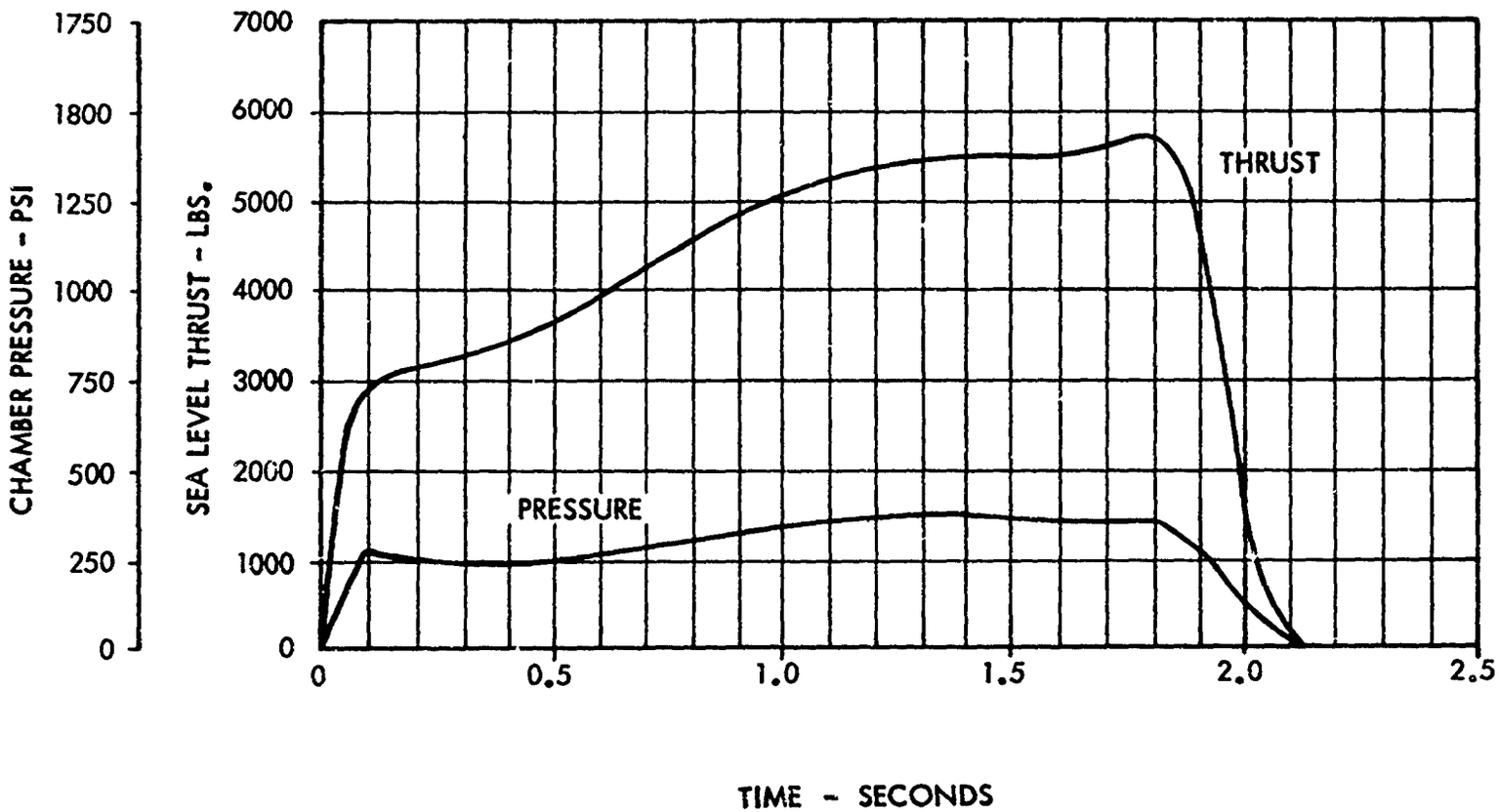

4.

ROBIN SYSTEM FINAL DESIGN

4.1 Introduction

The Super Loki Robin Dart vehicle as shown in Figure 4.1 consists of a 1.625-inch diameter dart second-stage with the Super Loki rocket motor. The dart body is coated with an ablative material to reduce the effect of rather severe aerodynamic heating upon the inflatable sphere payload. The sphere inflator contains a percussion initiated time delay charge to initiate sphere inflation through a two-stage chamber after deployment from the dart body at an altitude of 115 km. Atmospheric density and wind data are derived from a precise radar track of the descending inflated sphere.

4.2 Vehicle Description

The Super Loki Robin Dart is a two-stage vehicle which consists of the Super Loki rocket motor as the first or booster stage and a non-propulsive 1.625-inch diameter dart second stage. The vehicle configuration is shown in Figure 4.2, and detailed dimensions are included in Figure 4.3.

The rocket motor interstage has been designed to accept the larger diameter transponder dart. Therefore, an interstage adapter ring is used with the smaller diameter Robin dart.

A summary of the vehicle mass properties is presented in Table 4.1. The vehicle center-of-gravity vs time is presented in Figure 4.4, and pitch moment-of-inertia vs time is presented in Figure 4.5.

The aerodynamic data for the vehicle are presented as follows:

Figure 4.6	Normal Force Coefficient, First Stage
Figure 4.7	Normal Force Coefficient, Dart
Figure 4.8	Center-of-Pressure, First Stage
Figure 4.9	Center-of-Pressure, Dart

The Super Loki Robin Dart is stable during two-stage propulsive flight at essentially a zero degree angle of attack. After dart separation at motor burnout, the dart coasts to apogee in a stable flight mode at essentially a zero degree angle of attack in the sensible atmosphere. After rocket motor burnout and stage separation, the expended booster becomes unstable and tumbles. Eventually the booster descends in a flat spin to impact at a relatively slow rate of speed. The drag coefficients for the various stage configurations are presented in Table 4.2.

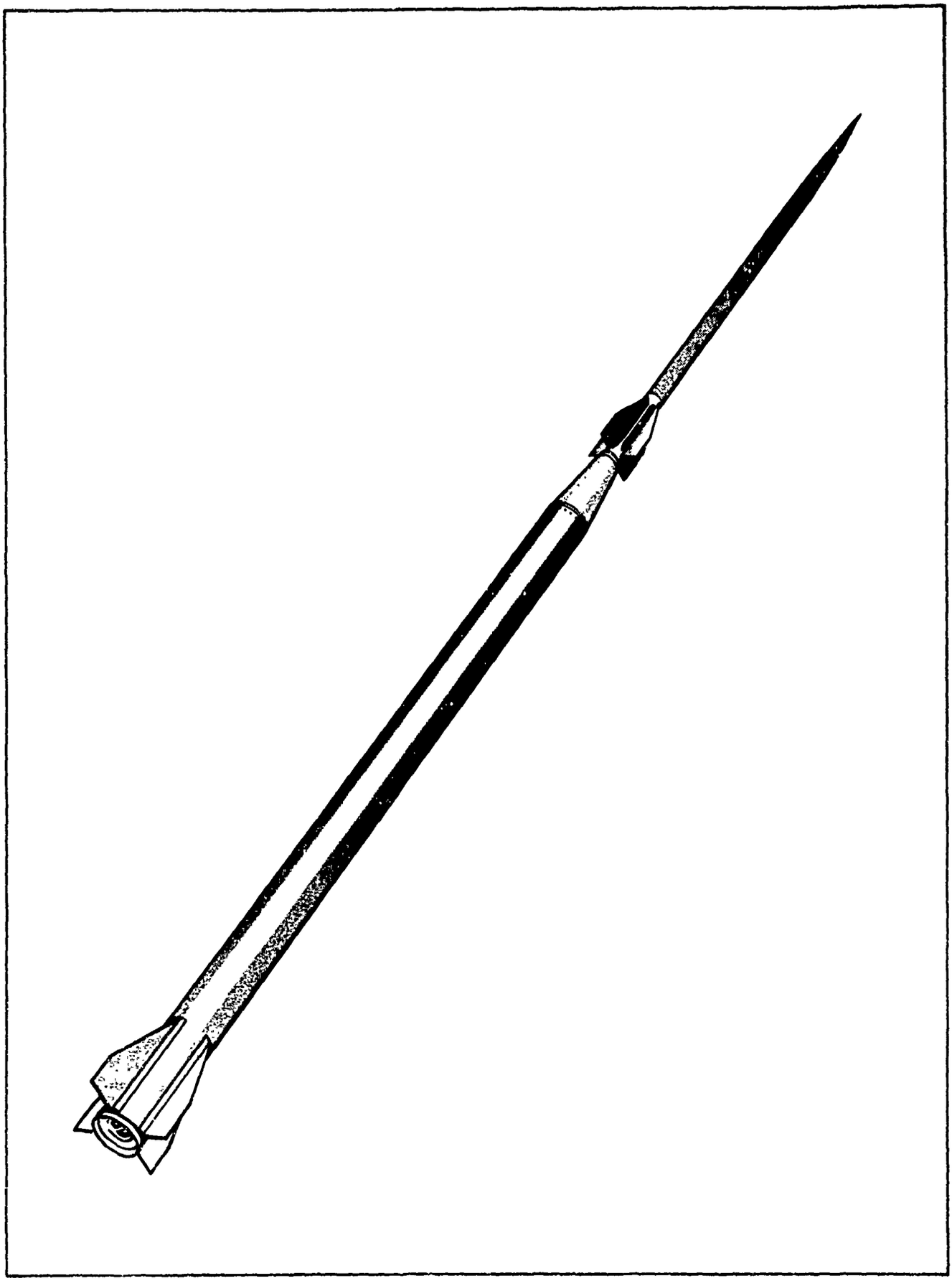

FIGURE 4.1 SUPER LOKI ROBIN DART

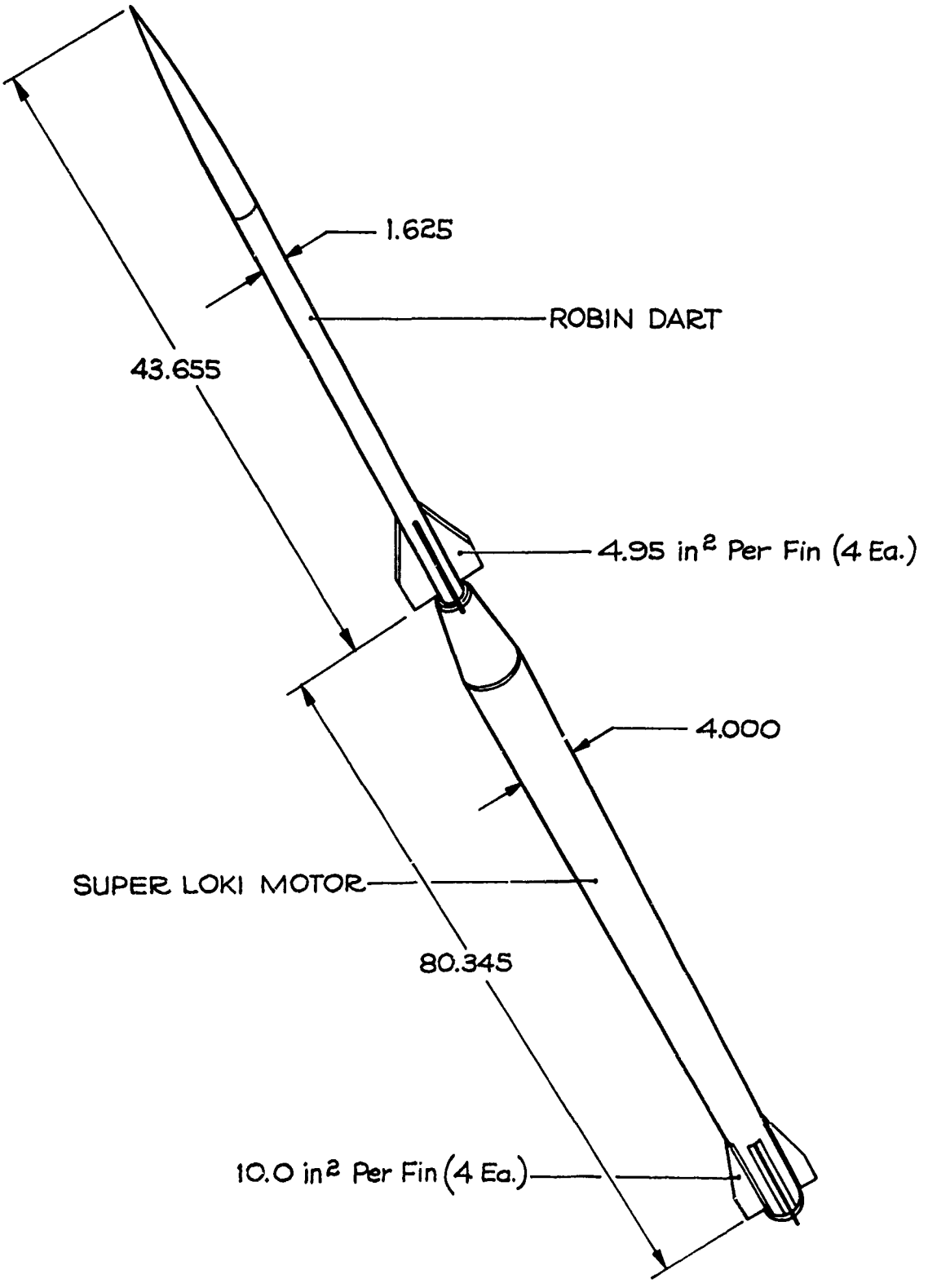

FIGURE 4.2 SUPER LOKI ROBIN DART VEHICLE

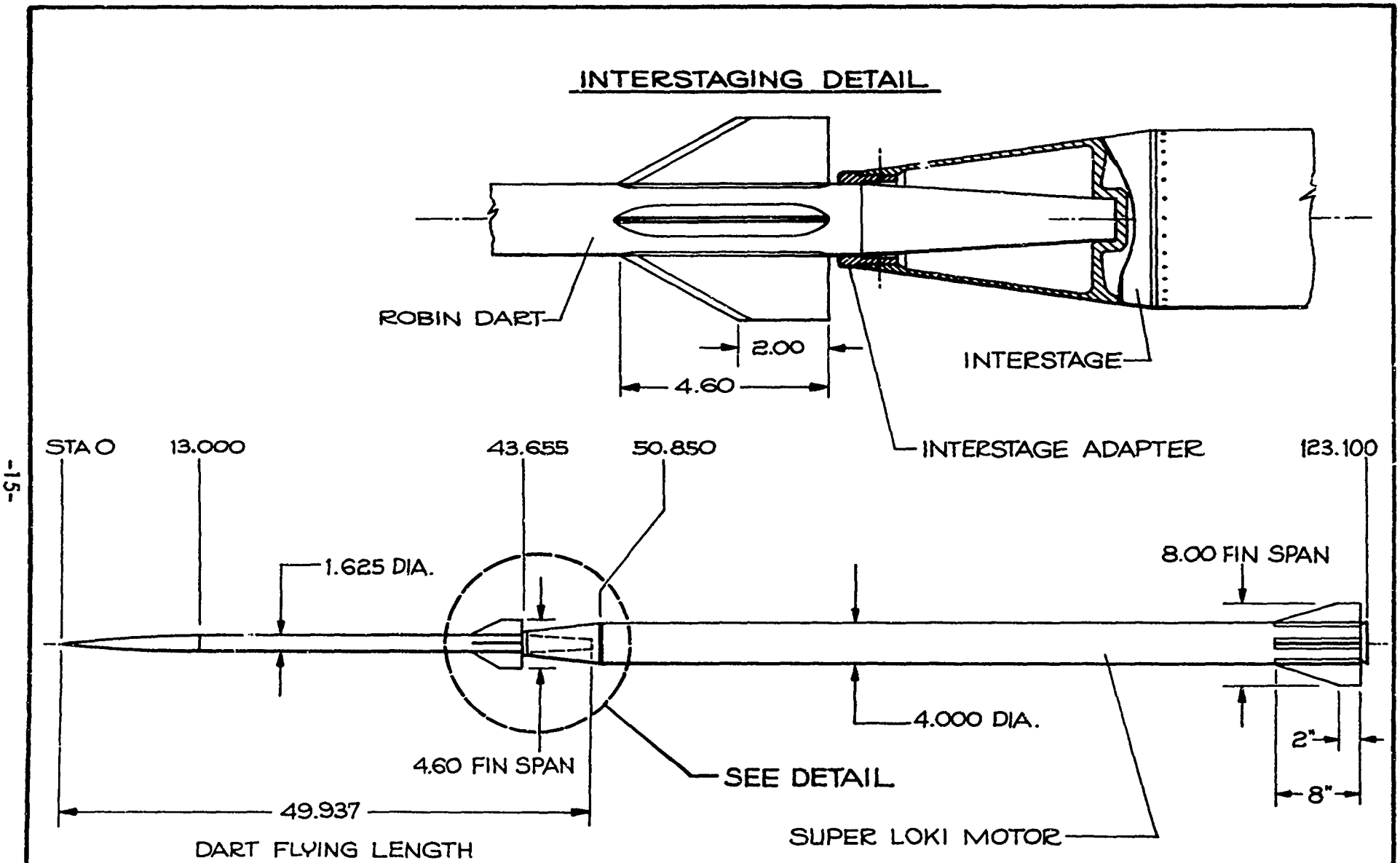

FIGURE 4.3 SUPER LOKI ROBIN DART VEHICLE CONFIGURATION

TABLE 4.1

SUPER LOKI ROBIN DART VEHICLE MASS PROPERTIES

Robin Dart:			
	Weight	13.50	lb
	Center-of-Gravity	34.5	inches from aft end of dart
	Pitch Moment of Inertia	0.450	slug/ft^2
Booster:			
	Loaded Weight	50.87	lb
	Expended Weight	13.36	lb
	Loaded Center-of-Gravity	33.70	inches from aft end of motor
	Expended Center-of-Gravity	33.50	inches from aft end of motor
	Load Pitch Moment of Inertia	5.37	slug/ft^2
	Expended Pitch Moment of Inertia	2.27	slug/ft^2
Vehicle:			
	Launch Weight	64.37	lb
	Burnout Weight	26.86	lb
	Launch Center-of-Gravity	46.6	inches from aft end of motor
	Burnout Center-of-Gravity	68.4	inches from aft end of motor
	Launch Pitch Moment of Inertia	15.06	slug/ft^2
	Burnout Pitch Moment of Inertia	7.79	slug/ft^2
Maximum Vehicle Acceleration.		153	g
Minimum Payload Acceleration		150	g

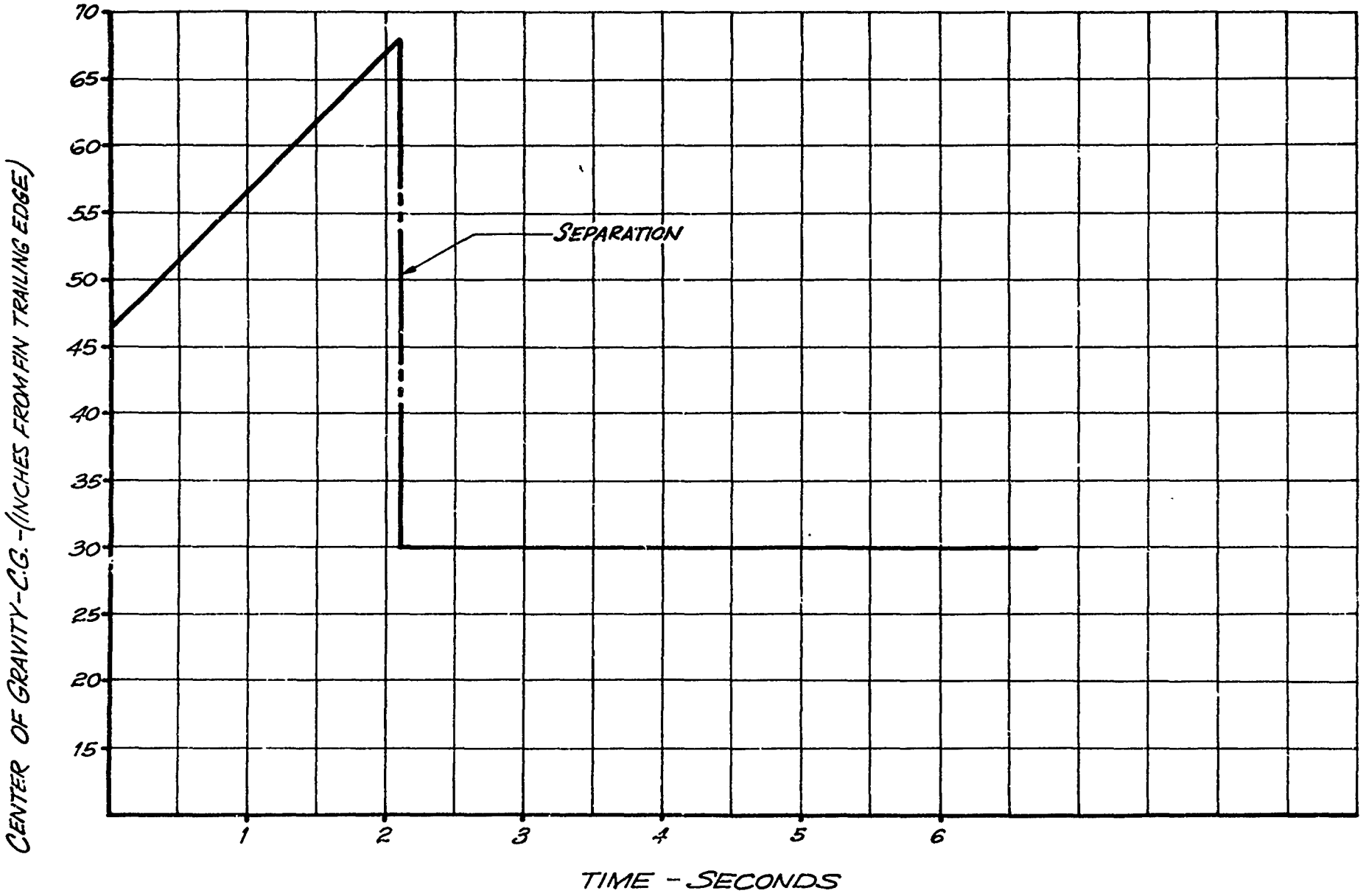

FIGURE 4.4 SUPER LOKI ROBIN DART C. G. VS TIME

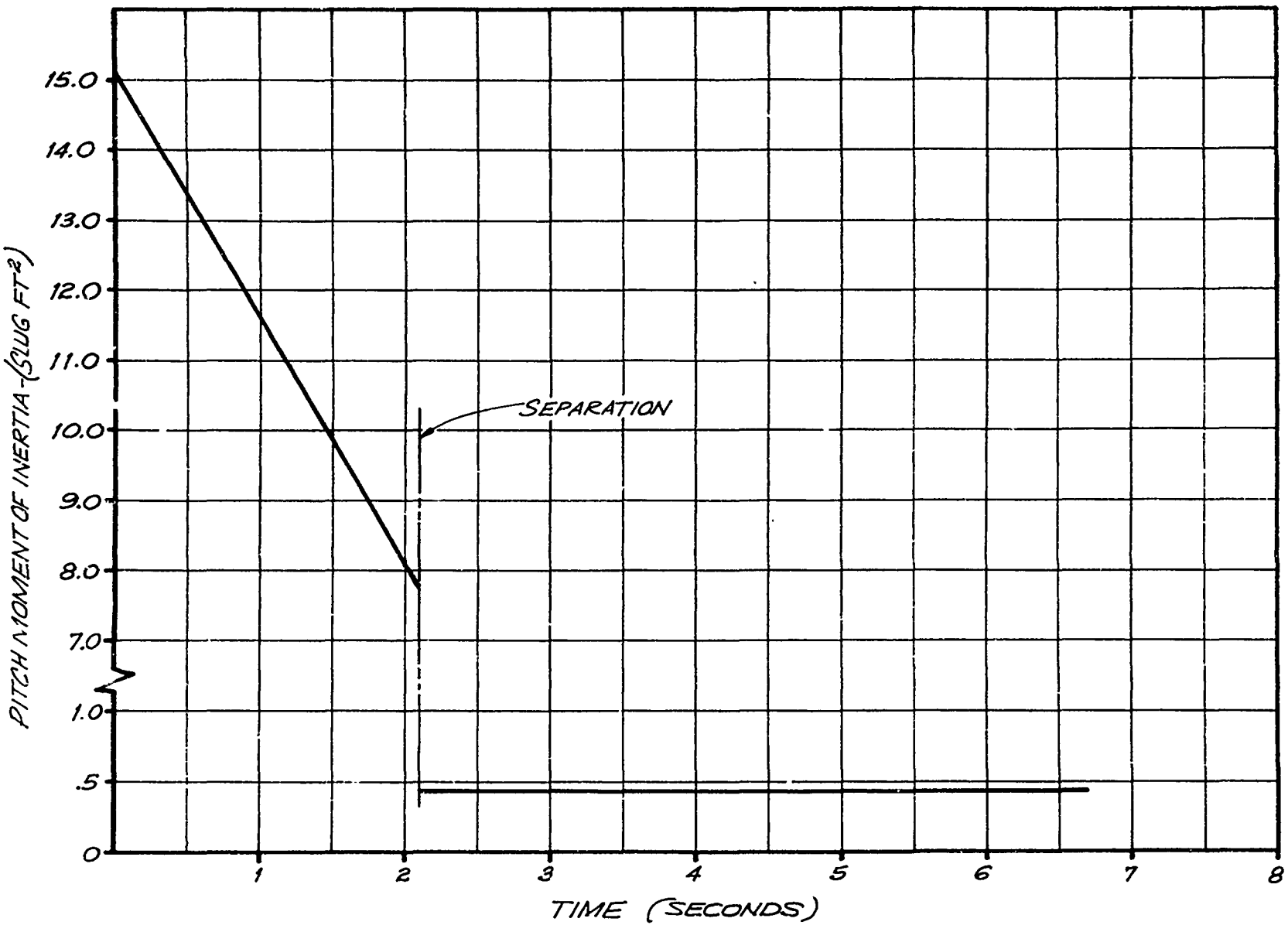

FIGURE 4.5 SUPER LOKI ROBIN DART PITCH MOMENT OF INERTIA VS TIME

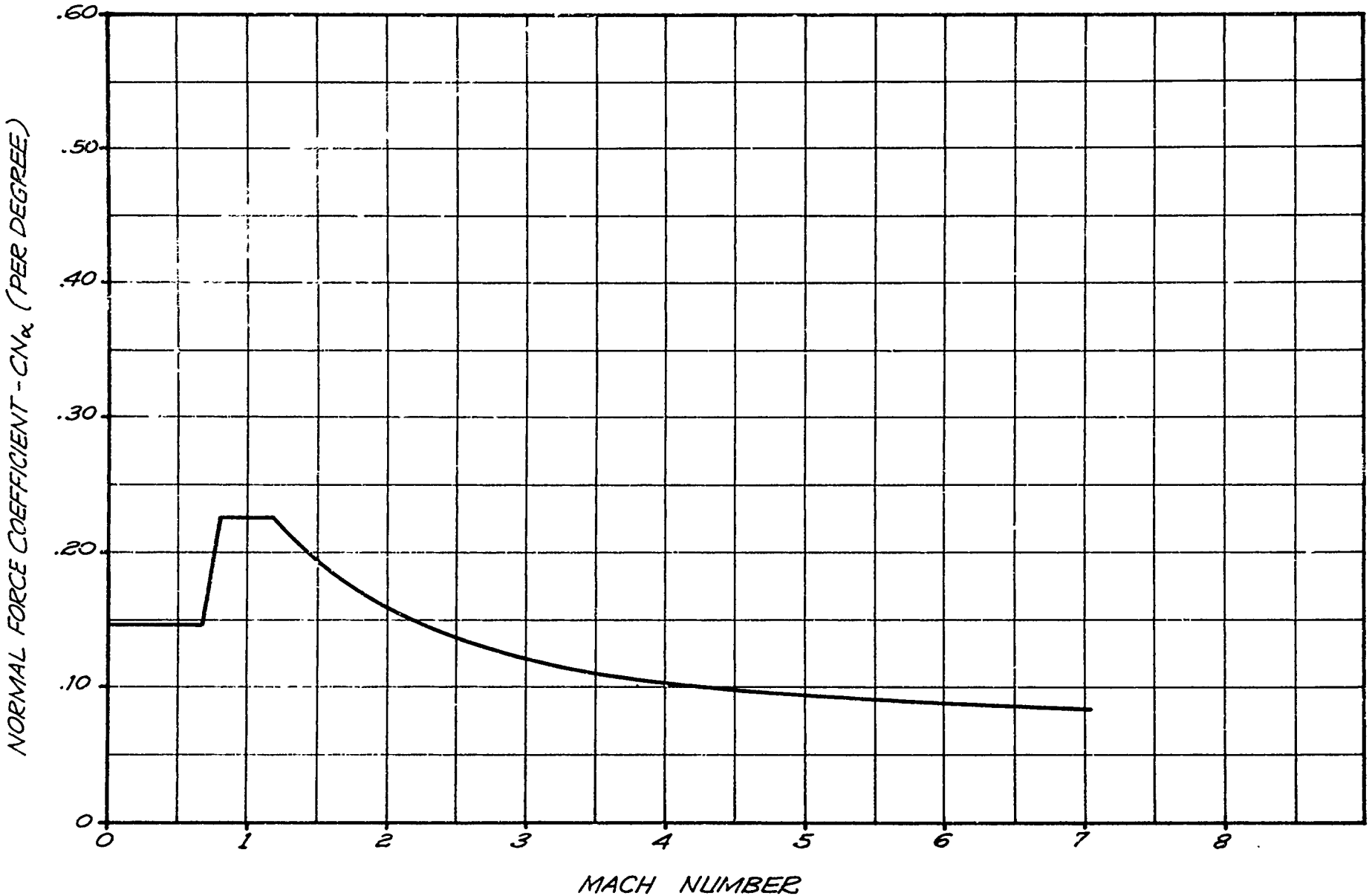

FIGURE 4.6 SUPER LOKI ROBIN DART CN_α VS MACH NO. - FIRST STAGE A_{REF} + 12.55 IN^2

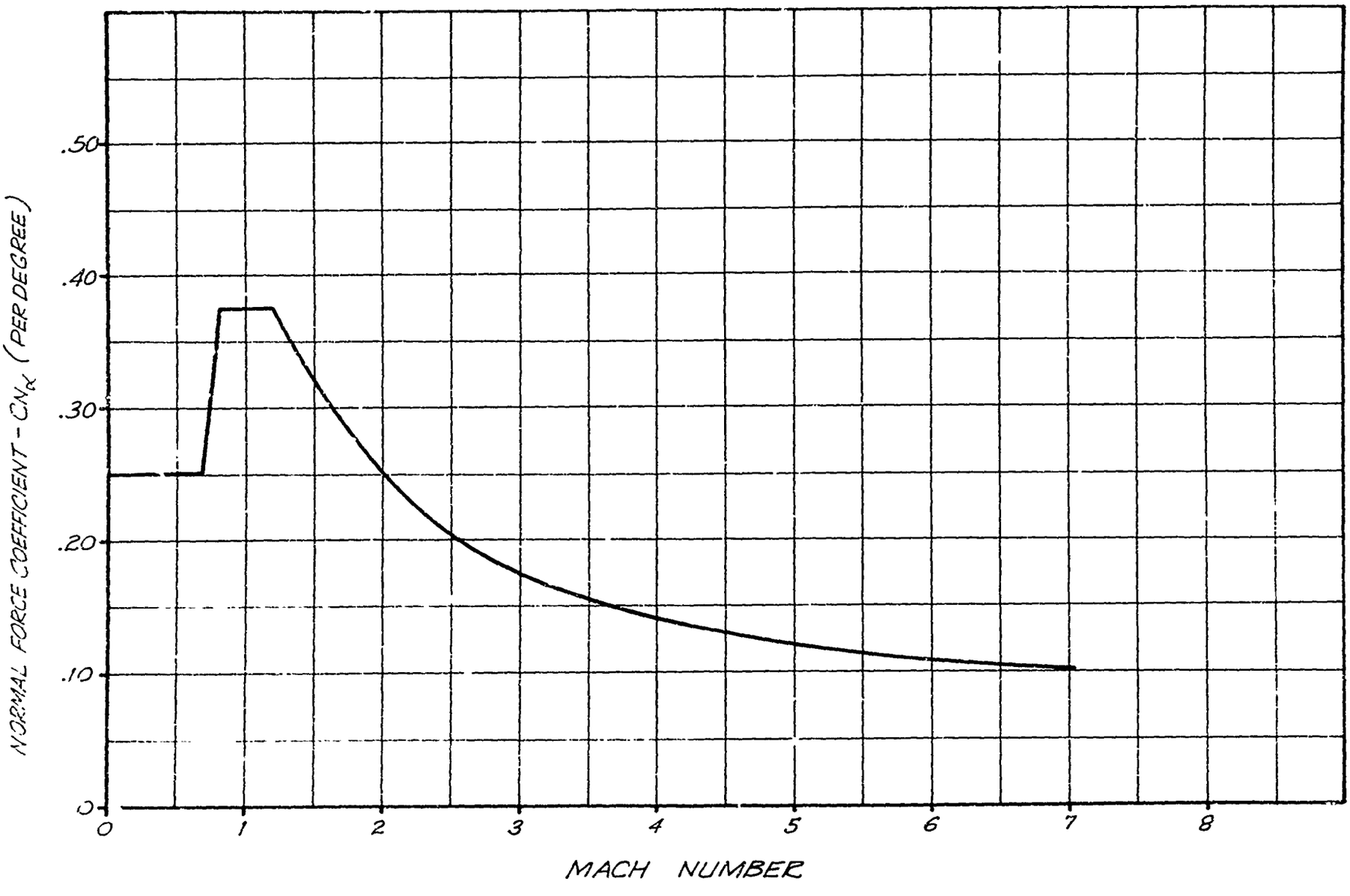

FIGURE 4.7 SUPER LOKI ROBIN DART CNα VS. MACH NO. - DART A_{REF} + 2.07 IN^2

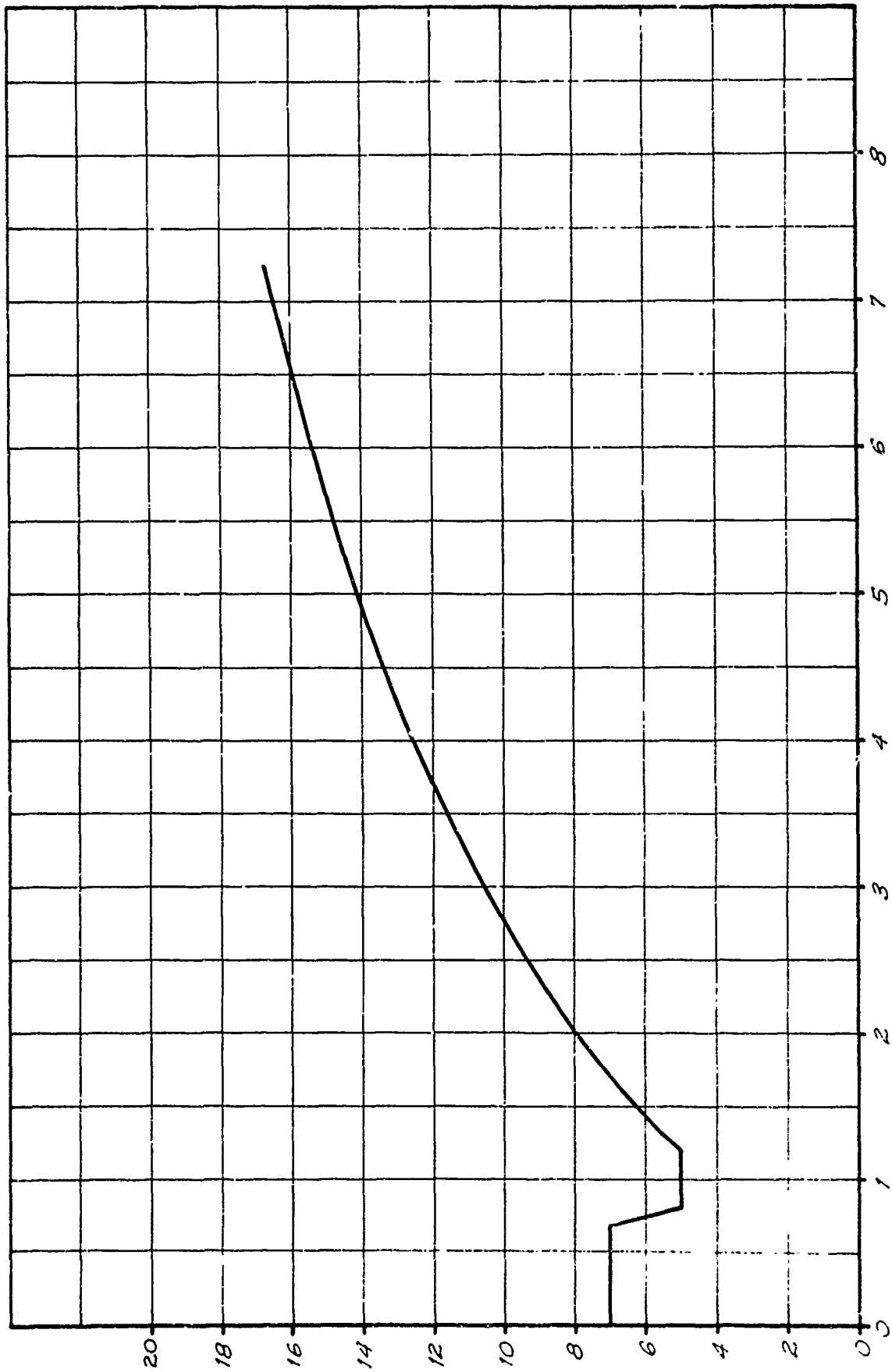

FIGURE 4.9 SUPER LOKI ROBIN DART CP VS MACH NO. - DART

TABLE 4.2

DRAG COEFFICIENT DATA

SUPER LOKI ROBIN DART VEHICLE

Super Loki Dart Vehicle - Two Stages
Reference Area (0.0920 ft^2)

Mach No.	C_D
0	0.400
0.50	0.420
0.80	0.430
0.81	0.930
1.40	0.930
1.50	0.880
1.75	0.770
2.00	0.682
2.25	0.620
2.50	0.570
2.75	0.533
3.00	0.500
3.25	0.470
3.50	0.440
3.75	0.420
4.00	0.397
4.25	0.380
4.50	0.360
4.75	0.345
5.00	0.331
5.25	0.320
5.50	0.310
5.75	0.300
6.00	0.290
7.00	0.260

Dart - Coasting
Reference Area (0.0107 ft^2)
Stage Weight (13.50 lb)

Mach No.	C_D
0	0.350
0.90	0.350
1.00	0.576
1.50	0.576
1.75	0.489
2.00	0.432
2.25	0.393
2.50	0.365
2.75	0.345
3.00	0.329
3.50	0.308
4.00	0.294
4.50	0.284
5.00	0.277
6.00	0.268
7.00	0.262
8.00	0.262

Expended Booster - Unstable
Stage Weight (12.30 lb)
Reference Area (0.0872 ft^2)

Mach No.	C_D
0	22.423
1.00	22.423
2.00	15.376
3.00	6.407
4.00	1.068
5.00	0.945
10.00	0.945

4.3 Dart Description

The Super Loki Robin Dart is shown in Figure 4.10. A cross-section view is presented in Figure 4.11. The dart consists of a steel ogive containing lead ballast, a cylindrical steel tubular body and an aluminum tail section which mates to the rocket motor interstage and to which are mounted four steel fins for dart aerodynamic stabilization. The tail section contains an electrically-initiated 145-second pyrotechnic delay and a 3.5 gm $BKNO_3$ pelletized payload separation charge.

The inflatable sphere payload and inflator assembly are packaged within a set of split staves within the dart body. The forward end of the staves terminate at the base of the ogive, and the aft end of the staves terminate at a two-stage payload ejection piston which is located just forward of the separation charge.

Prior to liftoff the dart tail is energized, and the pyrotechnic delay burns during upflight of the rocket and dart. Close to apogee the delay ignites the separation charge which creates a pressure behind the payload ejection piston. The inner core of the piston moves forward to strike the firing pin of the inflator delay. Subsequently, the outer piston is forced forward against the outer steel staves. This transmits the ejection load to the ogive which is attached to the dart body by means of three brass shear screws. These screws are sheared, and the entire payload assembly and the staves are ejected from the dart body at a speed of about 80 feet per second. Centrifugal force due to the vehicle spin forces the staves to separate from the payload as soon as they leave the constraints of the dart body. The forward end of the dart tube or body is slightly constricted on the inner diameter in order to stop the ejection piston within the dart tube. This is to trap the ejection charge hot exhaust gases and burning particles from damaging the sphere payload during deployment.

The sphere payload is packaged together with the inflator inside two sets of split staves. The outside set of staves are made from steel to transmit the ejection stroke loads. They are dimpled both outside and inside to provide a 0.030 inch air gap on either side. This is to reduce conductive heat transfer from the outer dart wall to the payload. In addition, shiny aluminum foil is bonded to the outside surface of the outer staves to reduce radiative heat transfer from the hot dart wall. The inner staves are made from a fiberglass plastic. They are covered on the outer surface with shiny aluminum foil to reduce radiative heat transfer and are lined with cork to reduce conductive heat transfer. The inflatable sphere is evacuated and vacuum-packed into the staves assembly. The assembly is then slid into the dart body.

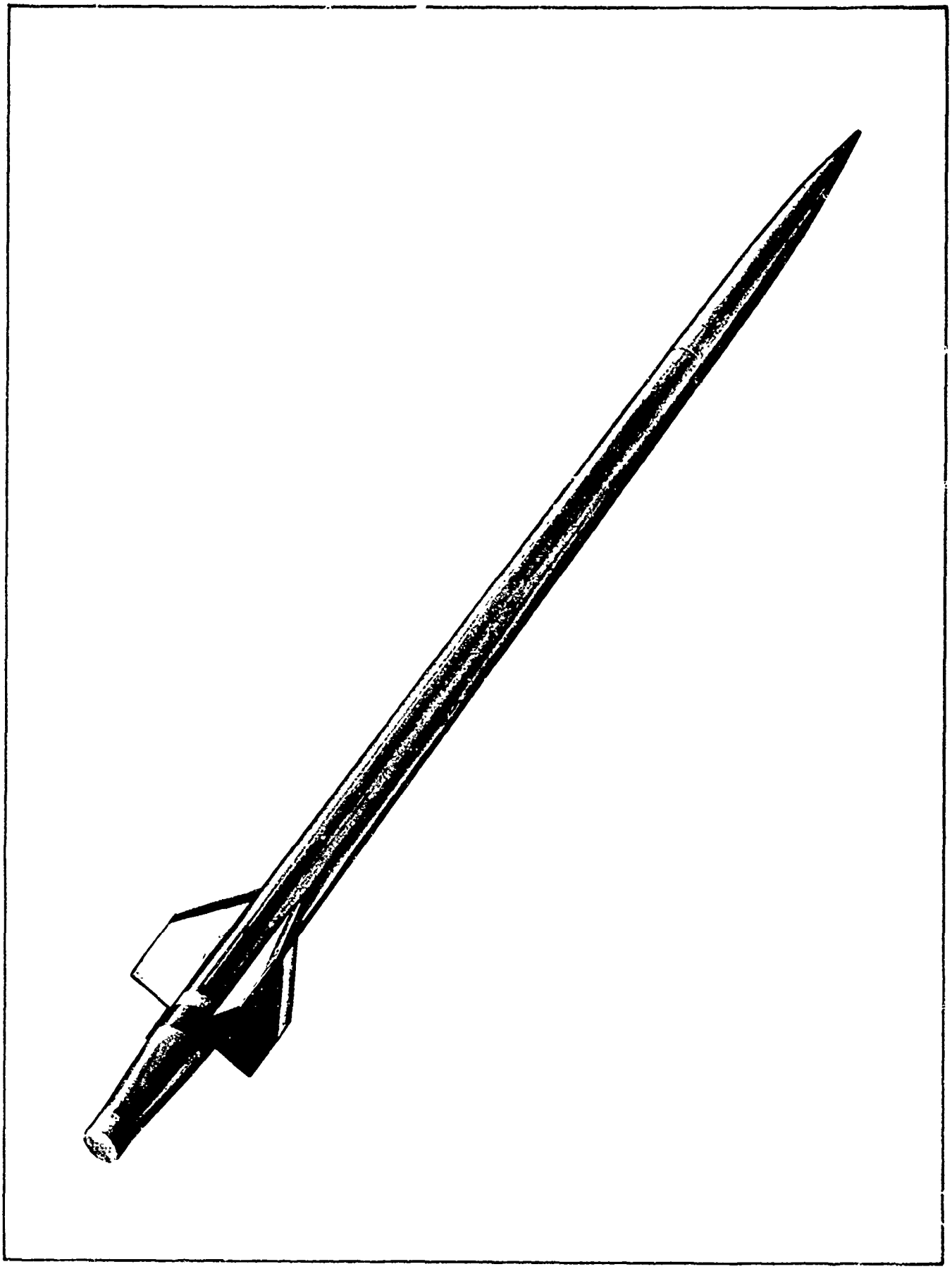

FIGURE 4.10 SUPER LOKI ROBIN DART

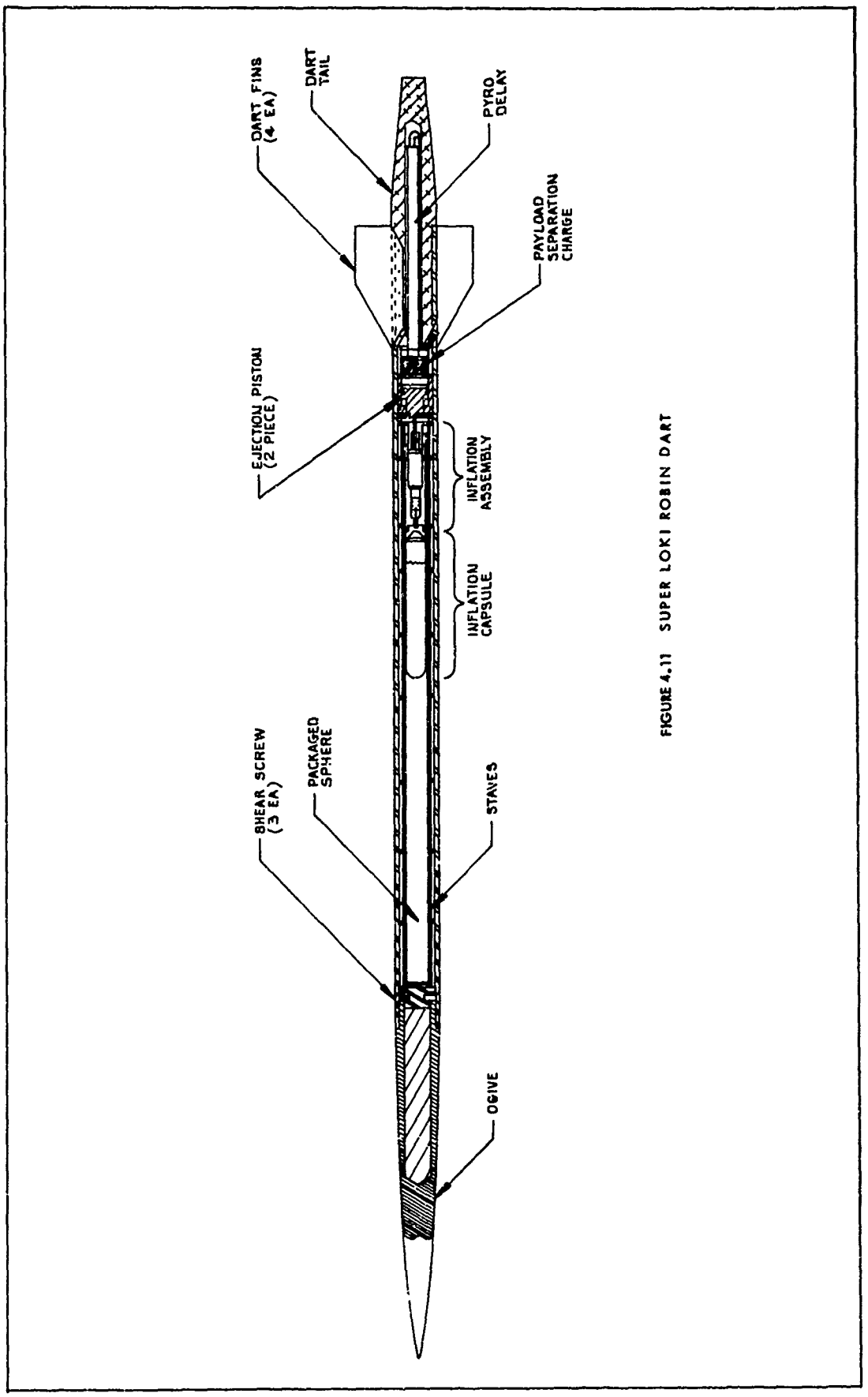

FIGURE 4.11 SUPER LOKI ROBIN DART

The outside surface of the dart is coated with a layer of an ablative material, Thermolag T-230. This material ablates at a temperature of 230°F and therefore limits the dart wall temperature to this level until it is consumed by the ablation process. The remaining aerodynamic heating pulse then causes a rise in the dart wall temperature above 230°F. A coating thickness of 0.070 inch was found to be required to maintain reliable sphere performance. As ablative coating thickness is reduced below this level, sphere deflation problems occur.

4.4 Payload Description

The Robin falling sphere payload is a 1-meter diameter inflatable spherical balloon. The balloon is made from 1/2 - mil Mylar which has been aluminized for radar tracking. After ejection from the dart at apogee, a capsule of isopentane inflatant is used to inflate the sphere to a superpressure equivalent to a 32 km altitude. The inflator mechanism has been designed to delay the initiation of inflation until six seconds after payload ejection. This has been done to protect the thin balloon skin from damage during the ejection process. The inflator also has a two-stage inflation feature to achieve a relatively slow and controlled inflation rate. Too rapid inflation can cause sphere damage.

Details of the inflator assembly are shown in Figure 4.12. A small port hole is constructed in the balloon surface at which point the inflator assembly is attached. The balloon material around this port hole is securely clamped between the balloon outer and inner plates in a leakproof joint. The major part of the inflator assembly resides within the balloon. The dart payload ejection piston inner core is fired forward during the initial phase of the ejection stroke. This inner piston strikes the inflator drive pin which in turn impacts the percussion delay firing pin into the delay. After six seconds the delay output charge is fired, and the gas pressure forces the piercing pin through the thin-wall section of the inflatant capsule. The vapor pressure of the inflatant forces the liquid out through a port channel in the piercing pin into a cavity in the inflator. A single port 0.025" diameter channel from this cavity leads out from the inflator into a 1/2-mil Mylar diffuser bag. The diffuser base has twenty 1/4-inch bleed holes, is 20 inches long and 4 inches in diameter. Thus, sphere inflation is accomplished at a controlled rate.

The major characteristics of the falling sphere payload are presented in Table 4.3.

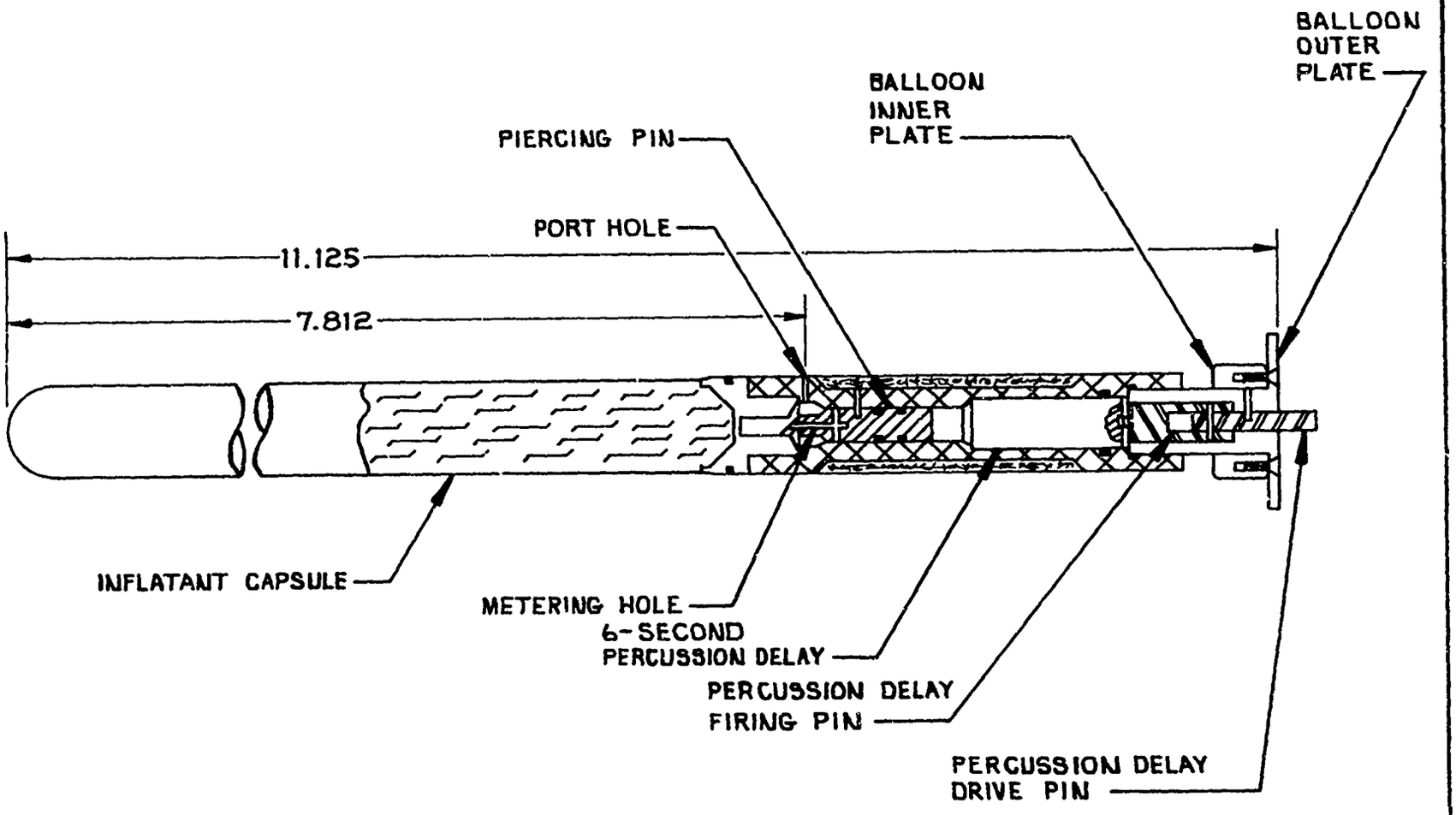

FIGURE 4.12 INFLATOR ASSEMBLY

TABLE 4.3

ROBIN FALLING SPHERE PAYLOAD MAJOR CHARACTERISTICS

Diameter	1 meter
Balloon Material	Aluminized 1/2-mil Mylar
Construction	20 gores
Sealing	0.5 inch heat pressure sensitive Mylar type
Inflatant	Isopentane
Inflatant Weight	19.16 gm
Balloon Weight	66.50 gm
Inflator Weight	82.50 gm
Total Sphere System Weight	167.73 gm
Radar Cross-Section ("C"-Band)	0.785 m^2
Design Deflation Altitude	32 km

5.

INSTRUMENT SYSTEM FINAL DESIGN

5.1 Introduction

The Super Loki Instrument Dart, as shown in Figure 5.1, consists of a 2.125-inch diameter dart second-stage with the Super Loki rocket motor. The dart carries a transponder rocketsonde payload to an altitude of 75 km where it is deployed on a Starute (balloon-parachute) decelerator. During its descent, the transpondersonde telemeters atmospheric temperature and position data, including slant range, to an AN/GMD-4 ground-station receiving set. This system eliminates the need for radar. In the case of a transmitter sonde it provides temperature and position data (without slant range) to an AN/GMD-1 ground set.

5.2 Vehicle Description

The Super Loki Instrument Dart is a two-stage vehicle which consists of the Super Loki rocket motor as the first or booster stage and a non-propulsive 2.125-inch diameter dart second stage. The vehicle configuration is shown in Figure 5.2, and detailed dimensions are included in Figure 5.3.

A summary of the vehicle mass properties is presented in Table 5.1. The vehicle center-of-gravity vs. time is presented in Figure 5.4, and pitch moment-of-inertia is presented in Figure 5.5.

The aerodynamic data for the vehicle are presented as follows:

Figure 5.6	$C_{N\alpha}$ vs. Mach No., First Stage
Figure 5.7	$C_{N\alpha}$ vs. Mach No., Dart
Figure 5.8	C_p vs. Mach No., First Stage
Figure 5.9	C_p vs. Mach No., Dart
Figure 5.10	C_p and CG vs. Mach No., First Stage
Figure 5.11	C_p and CG vs. Mach No., Second Stage Dart

The Super Loki Instrument Dart is stable during the two-stage propulsive flight at essentially a zero degree angle of attack. After dart separation at motor burnout, the dart coasts to apogee in a stable flight made at essentially a zero degree angle of attack in the sensible atmosphere. After rocket motor

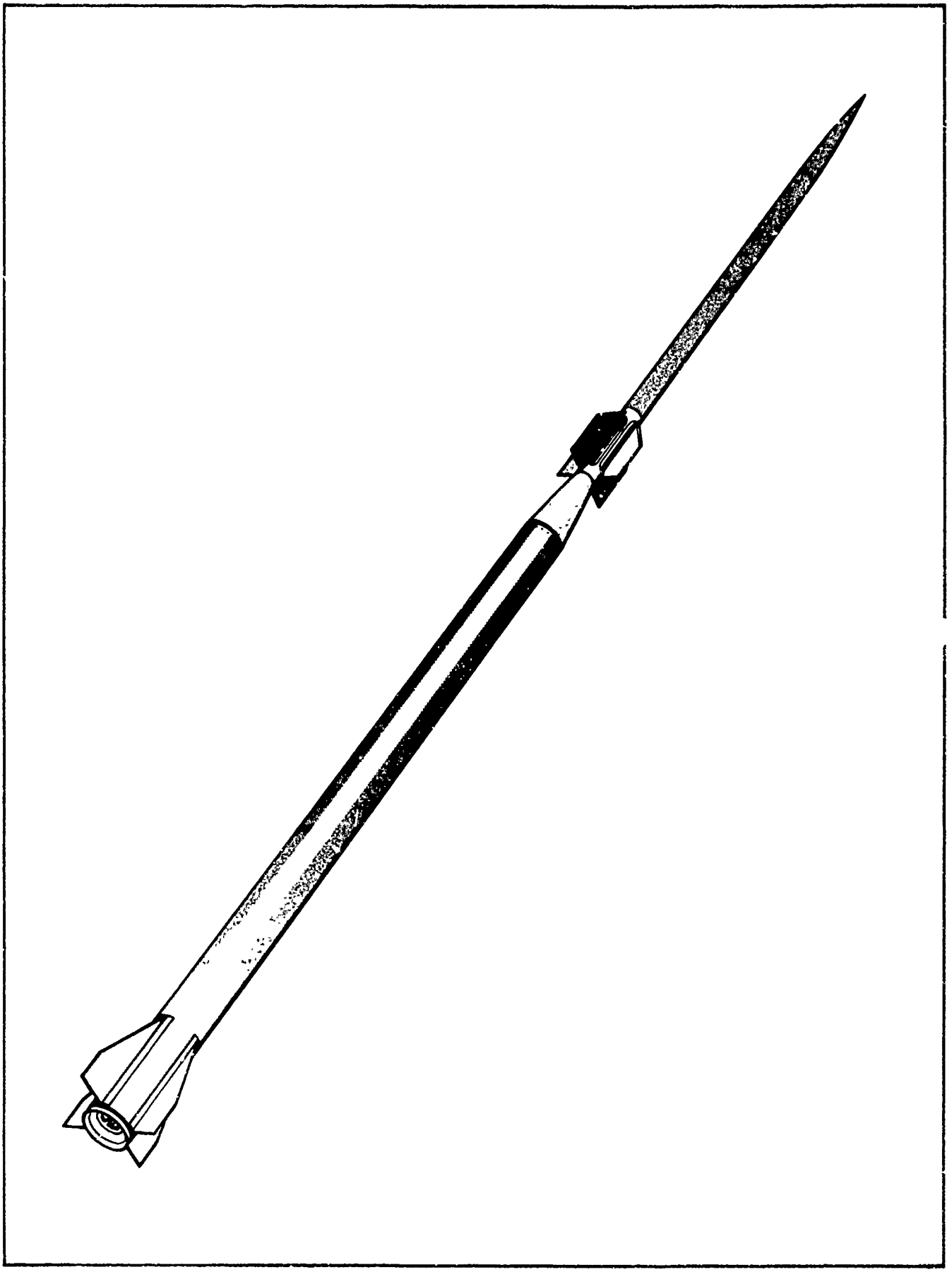

FIGURE 5.1 SUPER LOKI INSTRUMENT DART VEHICLE

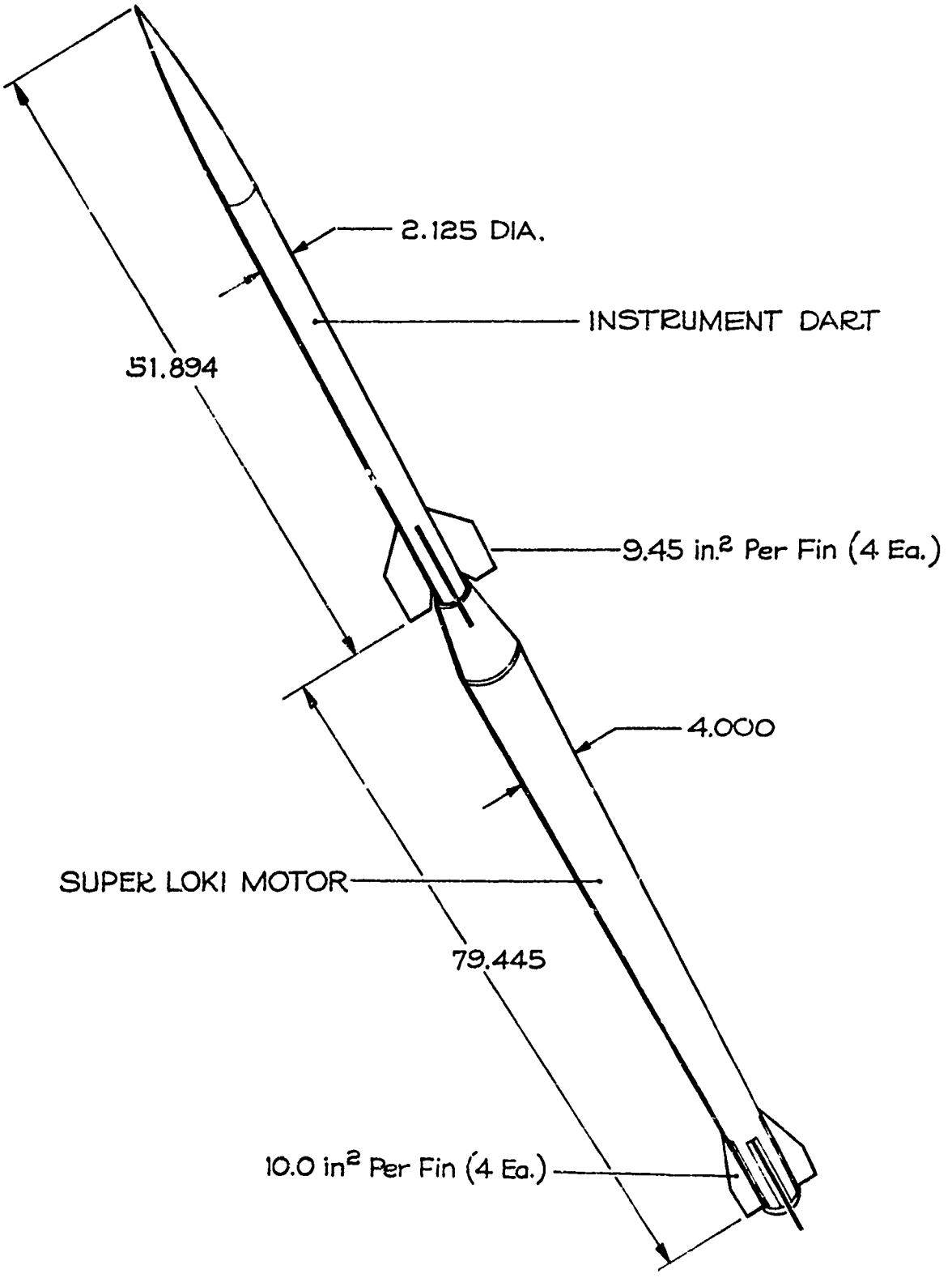

FIGURE 5.2 SUPER LOKI INSTRUMENT DART VEHICLE CONFIGURATION

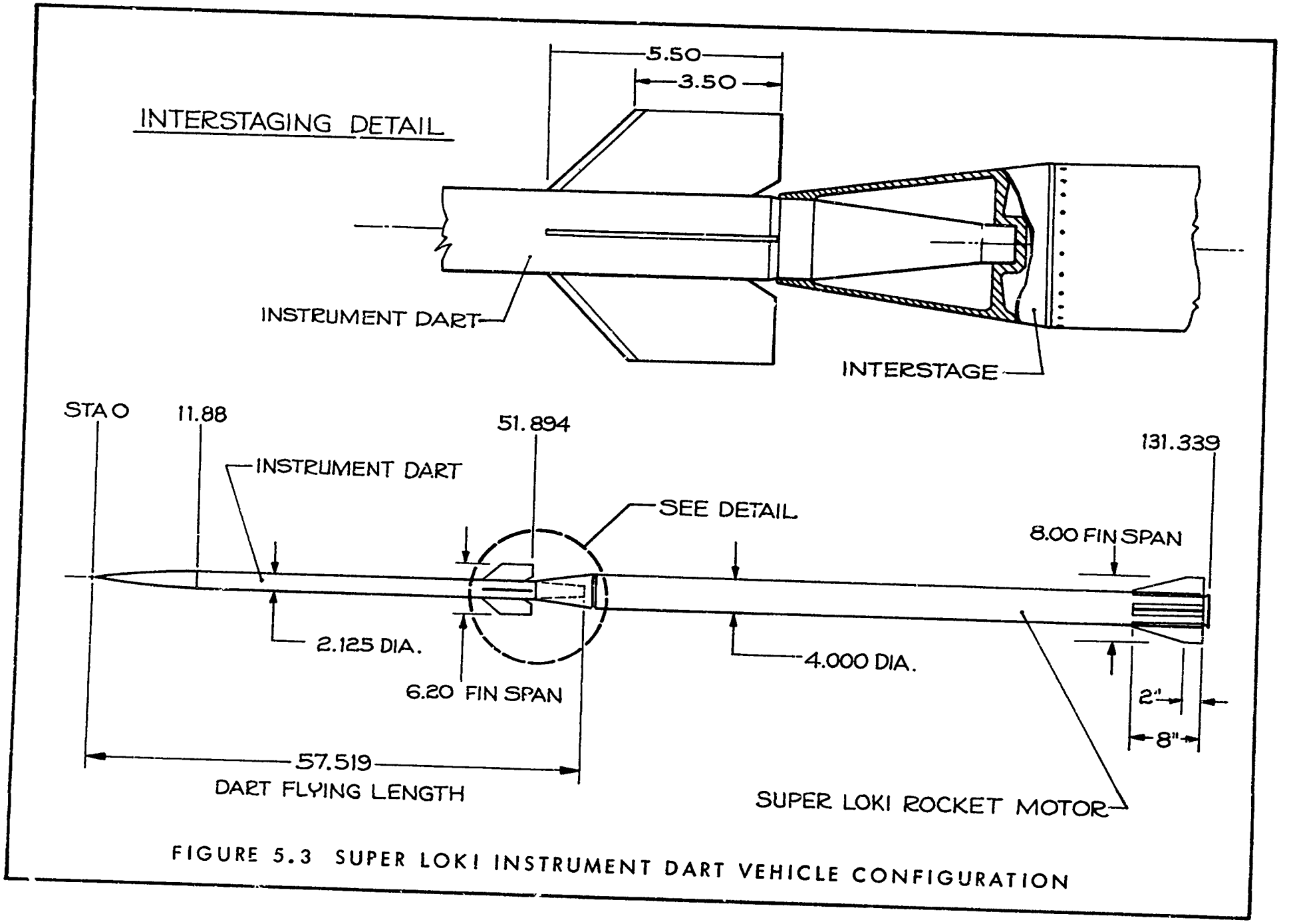

FIGURE 5.3 SUPER LOKI INSTRUMENT DART VEHICLE CONFIGURATION

TABLE 5.1

SUPER LOKI TRANSPONDER DART VEHICLE MASS PROPERTIES

Instrumented Dart:		
	Weight	18.25 lb.
	Center-of-Gravity	30.1 inches from aft end of dart
	Pitch Moment of Inertia	0.727 slug/ft^2
Booster:		
	Loaded Weight	50.20 lb.
	Expended Weight	12.69 lb.
	Loaded Center-of-Gravity	33.70 inches from aft end of motor
	Expended Center-of-Gravity	33.50 inches from aft end of motor
	Load Pitch Moment of Inertia	5.37 slug/ft^2
	Expended Pitch Moment of Inertia	2.27 slug/ft^2
Vehicle:		
	Launch Weight	68.45 lb.
	Burnout Weight	30.94 lb.
	Launch Center-of-Gravity	51.23 inches from aft end of motor
	Burnout Center-of-Gravity	74.41 inches from aft end of motor
	Launch Pitch Moment of Inertia	18.97 slug/ft^2
	Burnout Pitch Moment of Inertia	10.15 slug/ft^2
Maximum Vehicle Acceleration		135 g
Maximum Payload Acceleration		110 g

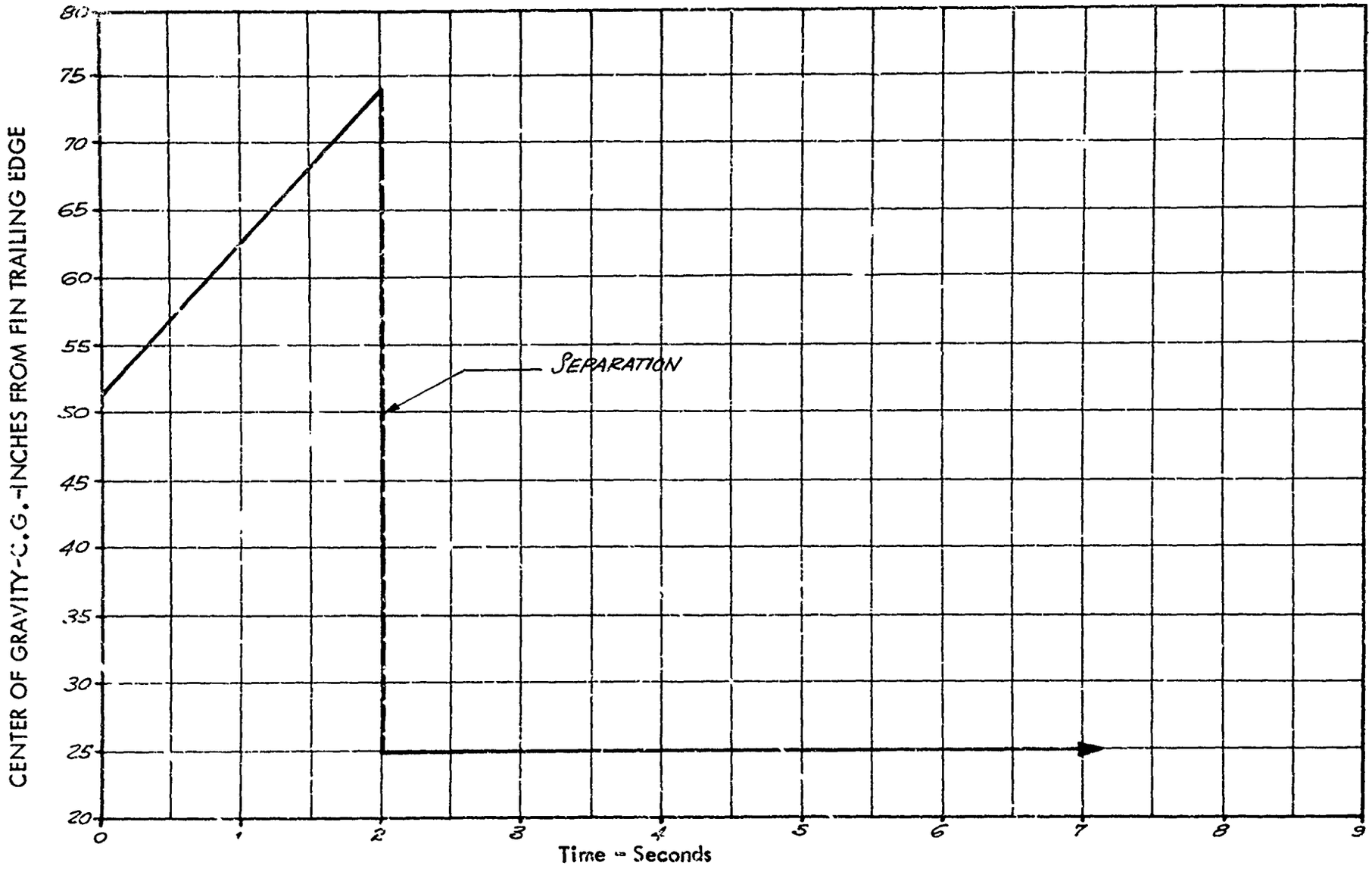

SUPER LOKI INSTRUMENT DART VEHICLE C.G. VS. TIME

FIGURE 5.4

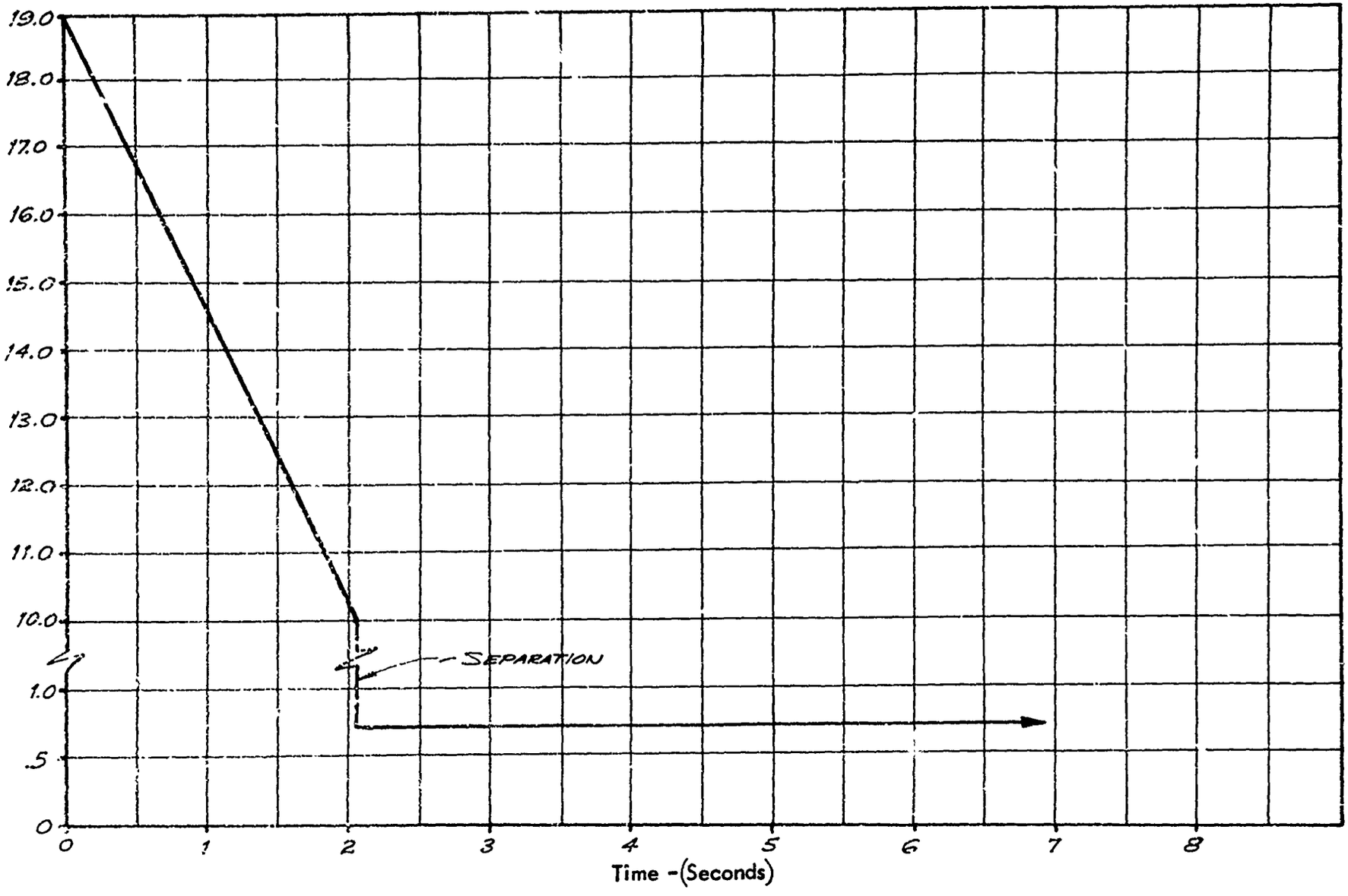

FIGURE 5.5 SUPER LOKI INSTRUMENT DART VEHICLE PITCH MOMENT OF INERTIA VS TIME

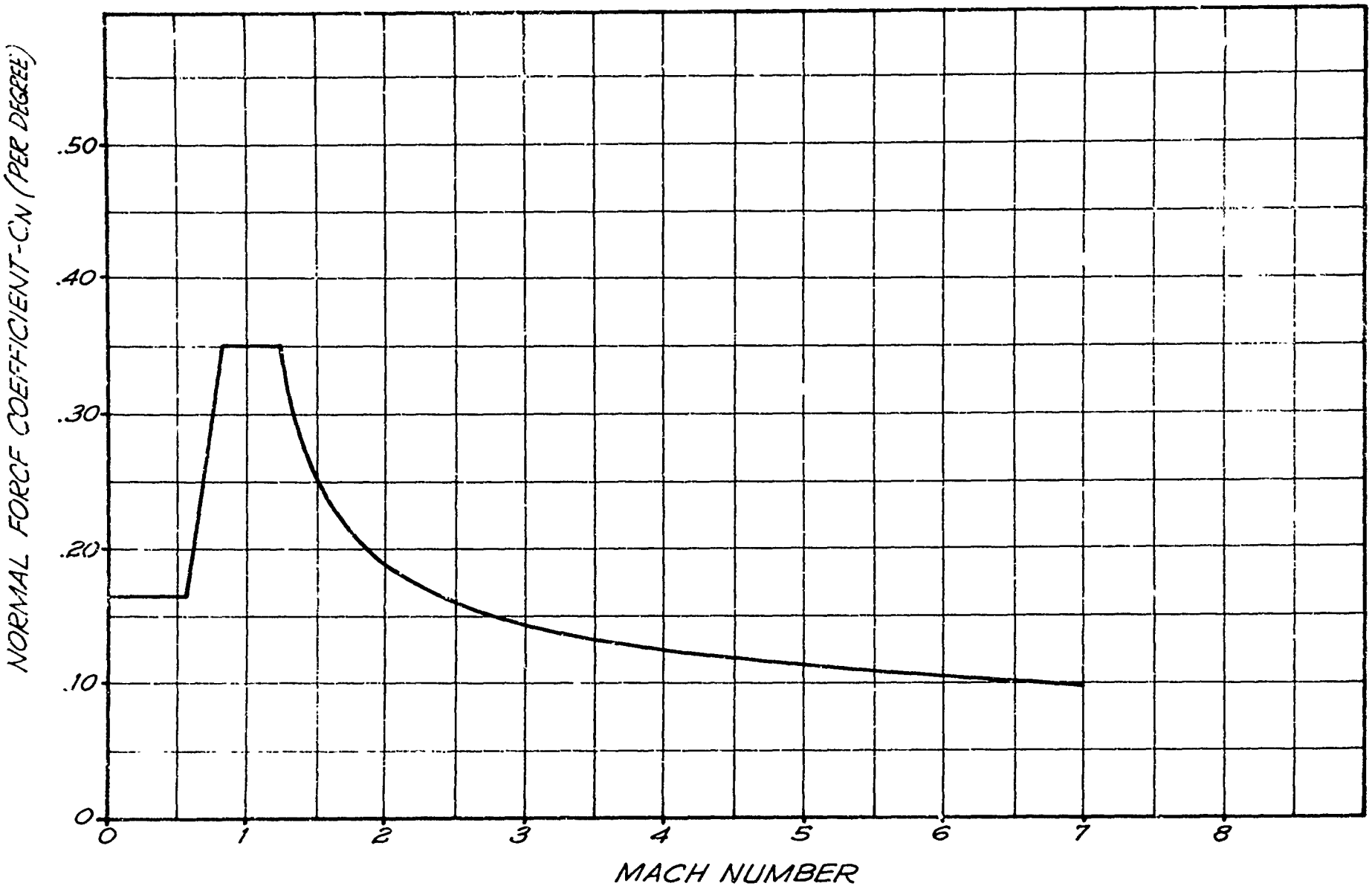

FIGURE 5.6 SUPER LOKI INSTRUMENT DART CN VS MACH NO
FIRST STAGE A REF. = 12.55 IN^2

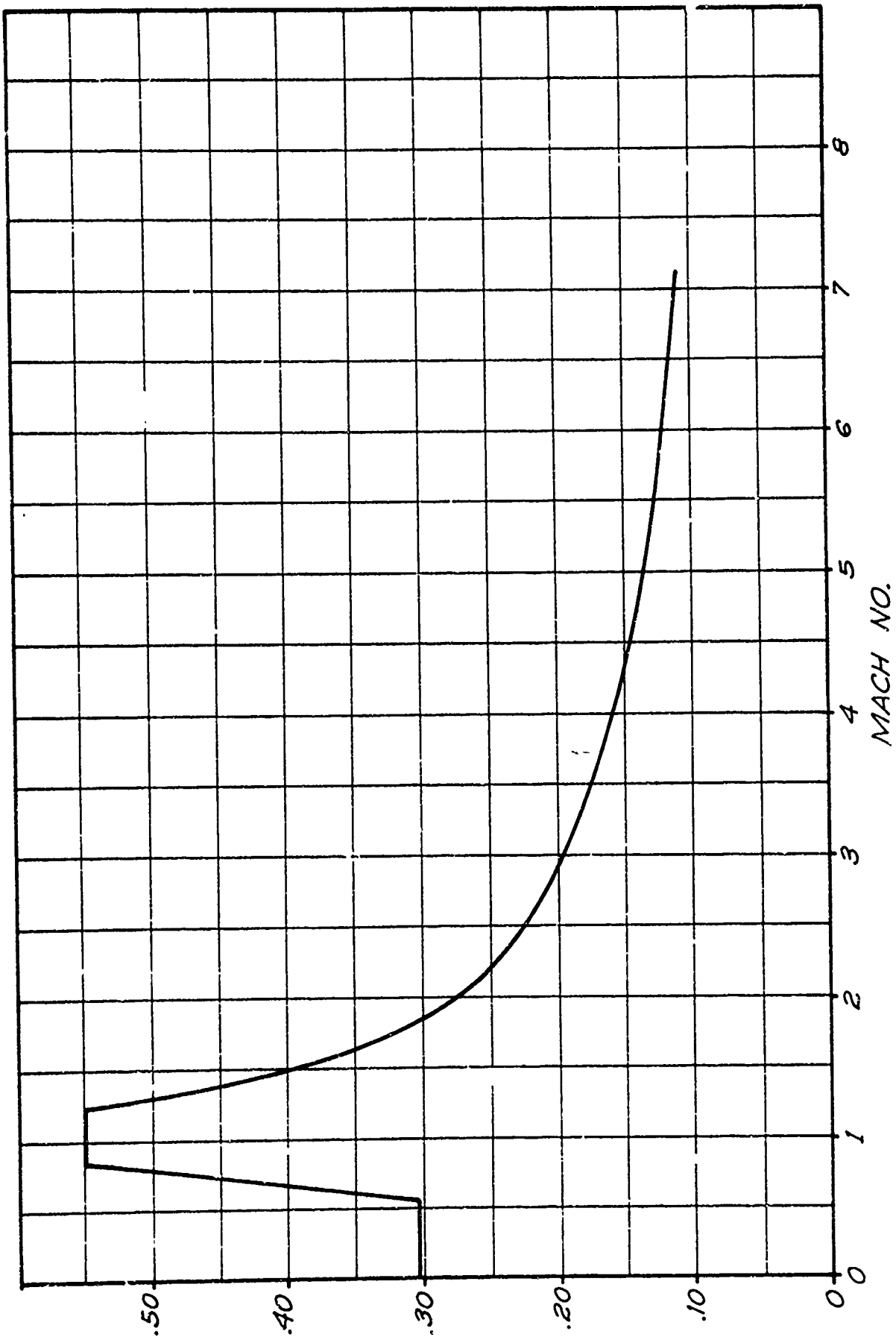

FIGURE 5.7 SUPER LOKI INSTRUMENT DART - CN VS MACH NO.
DART - 2ND STAGE A REF. = 3.54 IN^2

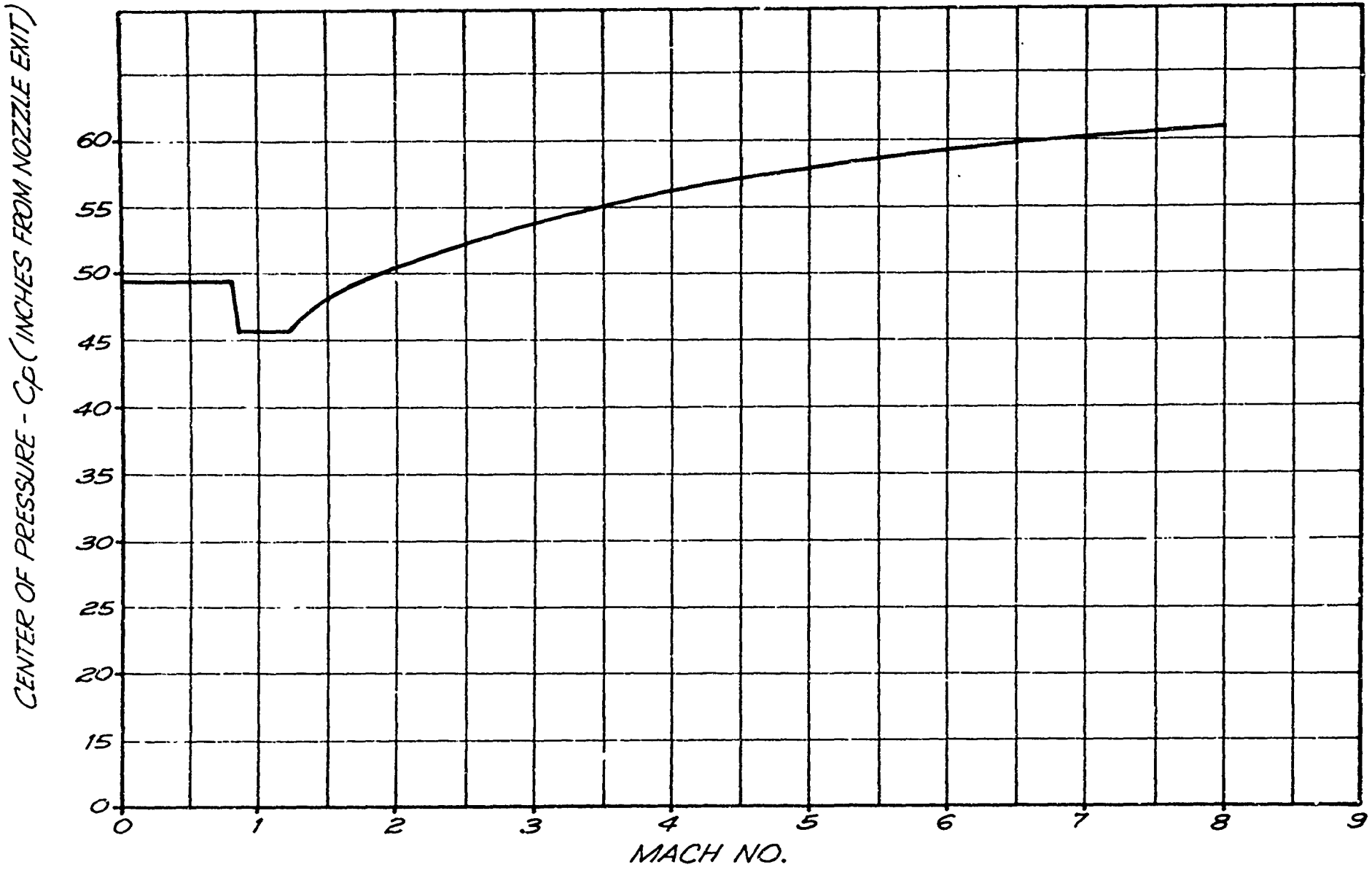

FIGURE 5.8 SUPER LOKI INSTRUMENT DART - CP VS MACH NO. 1ST STAGE

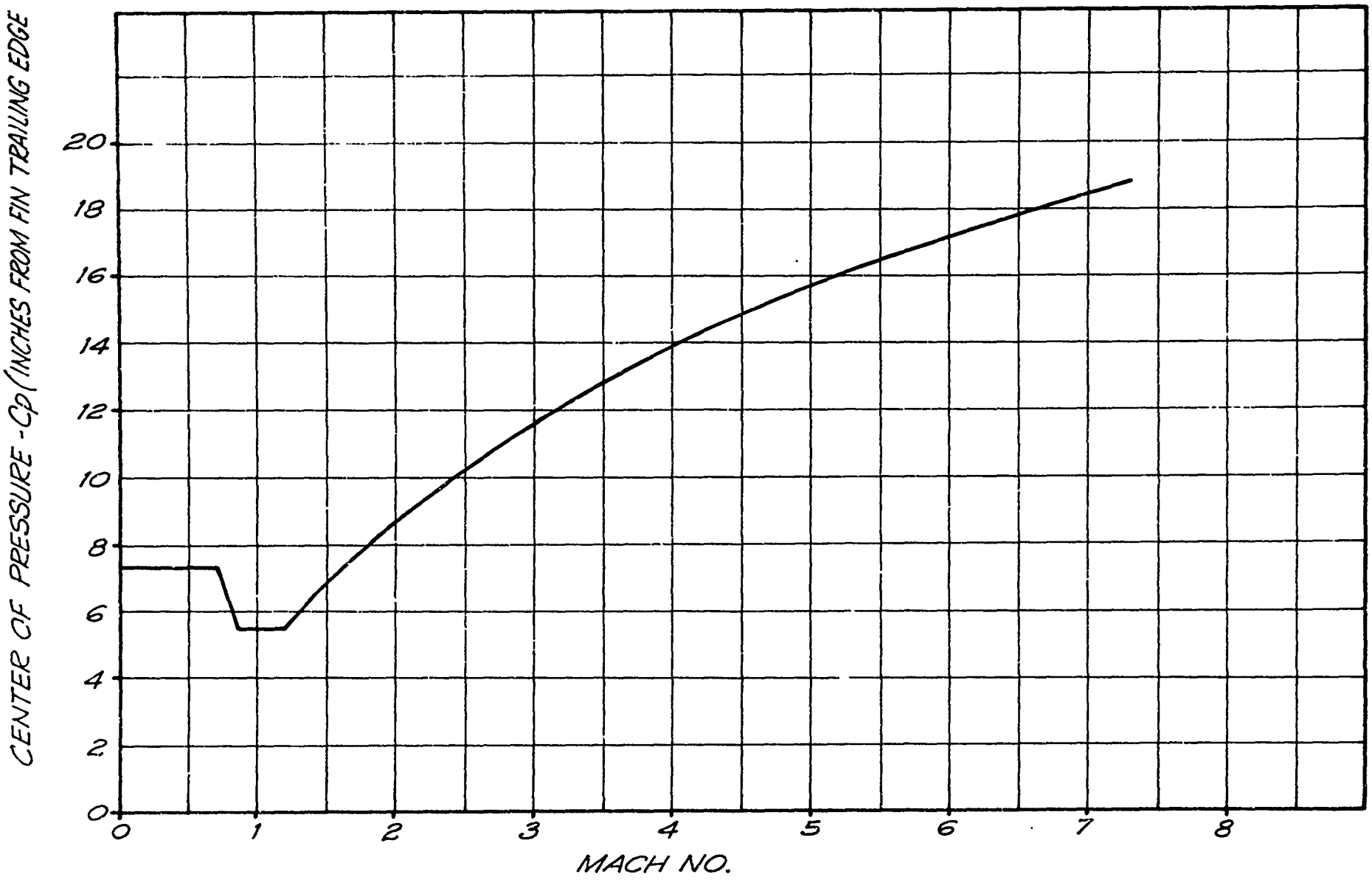

FIGURE 5.9 SUPER LOKI INSTRUMENT DART - CP VS MACH NO. DART - 2ND STAGE

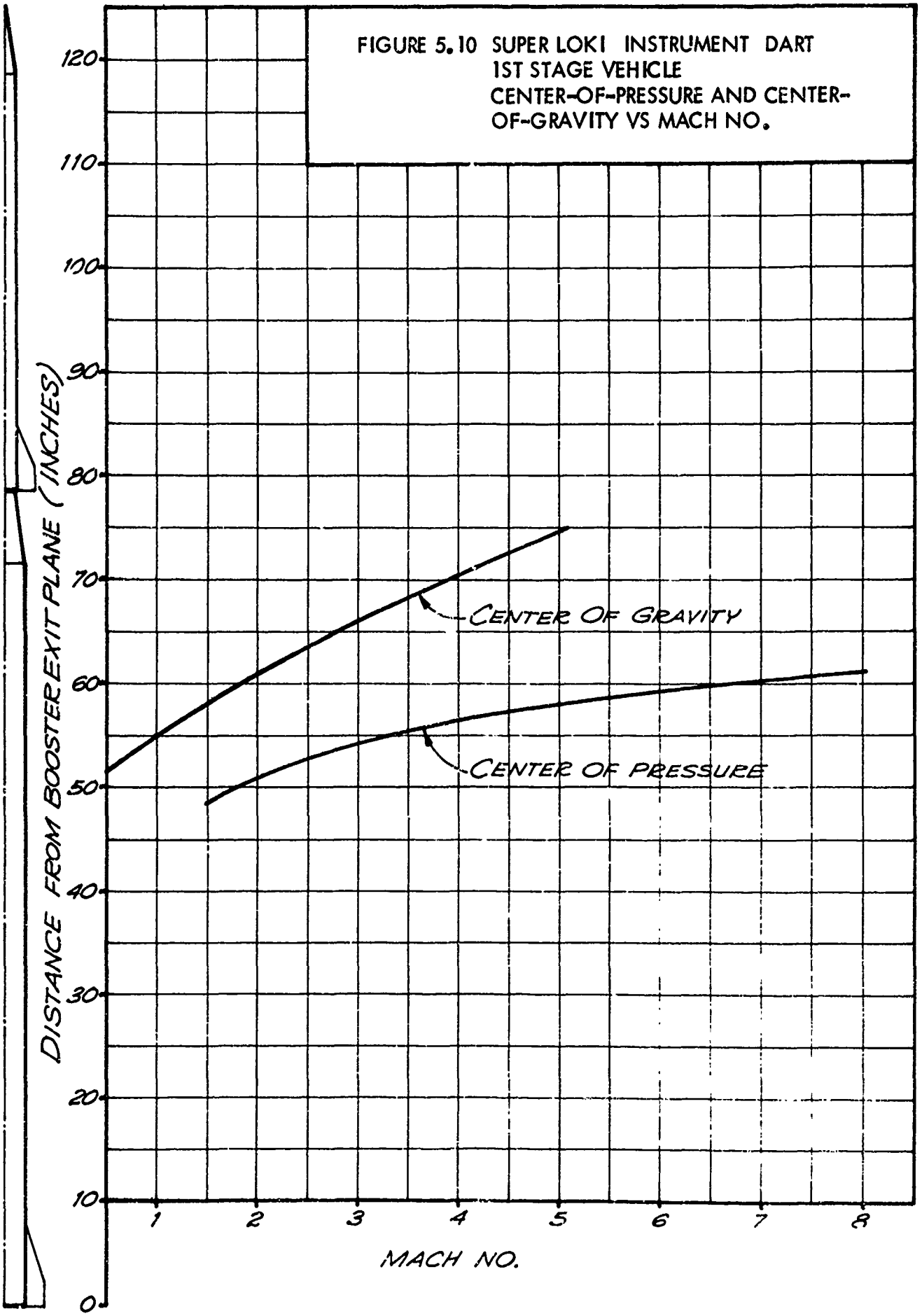

FIGURE 5.10 SUPER LOKI INSTRUMENT DART
1ST STAGE VEHICLE
CENTER-OF-PRESSURE AND CENTER-
OF-GRAVITY VS MACH NO.

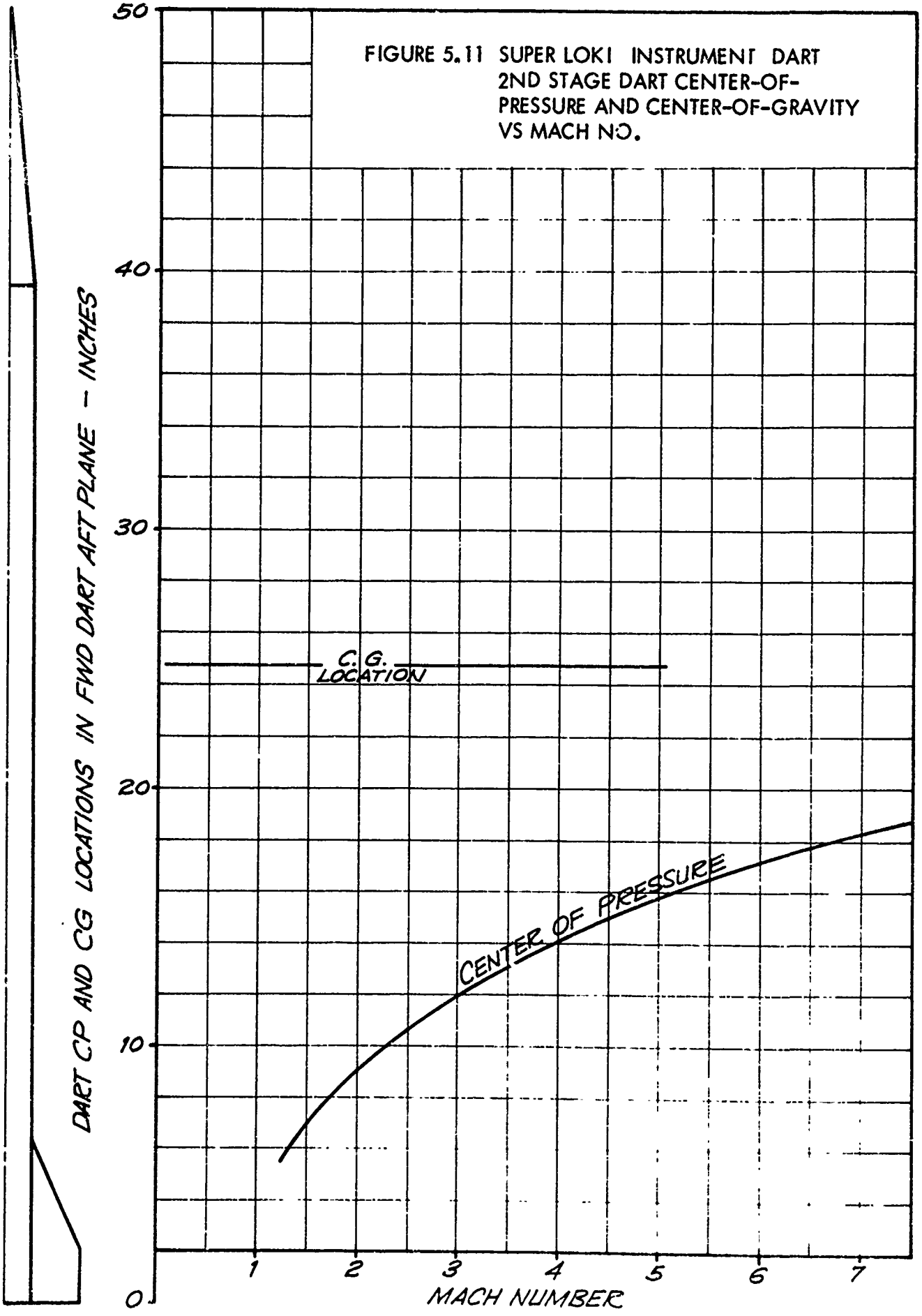

FIGURE 5.11 SUPER LOKI INSTRUMENT DART 2ND STAGE DART CENTER-OF-PRESSURE AND CENTER-OF-GRAVITY VS MACH NO.

burnout and stage separation, the expended booster becomes unstable and tumbles. Eventually the booster descends in a flat spin to impact at a relatively slow rate of speed. The drag coefficients for the various stage configurations are presented in Table 5.2.

5.3 Dart Description

The instrumented dart, as shown in Figure 5.12, for the Super Loki system consists of a steel cylindrical body with a steel ogive and an aluminum tail piece. The cylindrical body contains the payload which is packaged into split steel staves. The ogive is retained at the forward end of body with shear-screws which are sheared during payload expulsion out from the forward end of the dart. The tail piece contains an electrically-actuated 120-second pyrotechnic time delay and a small payload ejection charge. Four steel fins are roll-pinned into the dart tail for flight stability. The aft end of the dart tail is boattailed to reduce aerodynamic drag and to be used to mate the dart to the booster. A cross-section view of the dart is shown in Figure 5.13.

The instrument and Starute decelerator are packaged within two sets of split staves within the dart body. The forward end of the staves assembly terminate at the base of the ogive, and the aft end terminates at the payload ejection piston which is located just forward of the separation charge.

Prior to liftoff the dart tail is energized, and the pyrotechnic delay burns during upflight of the rocket and dart. Close to apogee the delay ignites the separation charge which creates a pressure behind the ejection piston. The piston is forced against the steel staves which transmit the load to the ogive base to effect separation. The entire payload assembly, the staves, and piston are ejected from the dart body at a speed of about 80 feet per second. Centrifugal force due to the vehicle spin forces the staves to separate from the payload as soon as they leave the constraints of the dart body. The instrument and the Starute decelerator are thus deployed. A pictorial view of payload ejection is shown in Figure 5.14.

The instrument staves are dimpled on the outside surface to provide an 0.032-inch air gap to the dart wall to restrict the conductive heat transfer to the instrument. They are also lined with an 0.031-inch layer of cork on the interior for the same purpose. A layer of aluminum foil covers the outside stave surface to reduce the radiative heat transfer from the dart wall.

The Starute staves are recessed 0.220 inches from the dart wall to provide an air gap for thermal insulation. They are covered with a layer of aluminum foil to reduce radiative heat transfer. Inner fiberglass plastic staves or liners are employed between the outer staves and the Starute for added thermal protection. The outer dart wall is black oxidized to provide an emissive surface for radiating heat energy.

TABLE 5.2

DRAG COEFFICIENT DATA

Super Loki Dart Vehicle - Two Stages
Reference Area 0.0920 ft^2

Mach No.	C_D
0	0.400
0.50	0.420
0.80	0.430
0.81	0.930
1.40	0.930
1.50	0.880
1.75	0.770
2.00	0.682
2.25	0.620
2.50	0.570
2.75	0.533
3.00	0.500
3.25	0.470
3.50	0.440
3.75	0.420
4.00	0.397
4.25	0.380
4.50	0.360
4.75	0.345
5.00	0.331
5.25	0.320
5.50	0.310
5.75	0.300
6.00	0.290
7.00	0.260

Dart - Coasting
Reference Area 0.0214 ft^2
Stage Weight 16.50 lb.

Mach No.	C_D
0	0.350
0.90	0.350
1.00	0.576
1.50	0.576
1.75	0.489
2.00	0.432
2.25	0.393
2.50	0.365
2.75	0.345
3.00	0.329
3.50	0.308
4.00	0.294
4.50	0.284
5.00	0.277
6.00	0.277
7.00	0.262
8.00	0.262

Expended Booster - Unstable
Stage Weight - 1163 lb.
Reference Area - 0.0872 ft^2

Mach No.	C_D
0	22.423
1.00	22.423
2.00	15.376
3.00	6.407
4.00	1.068
5.00	0.945
10.00	0.945

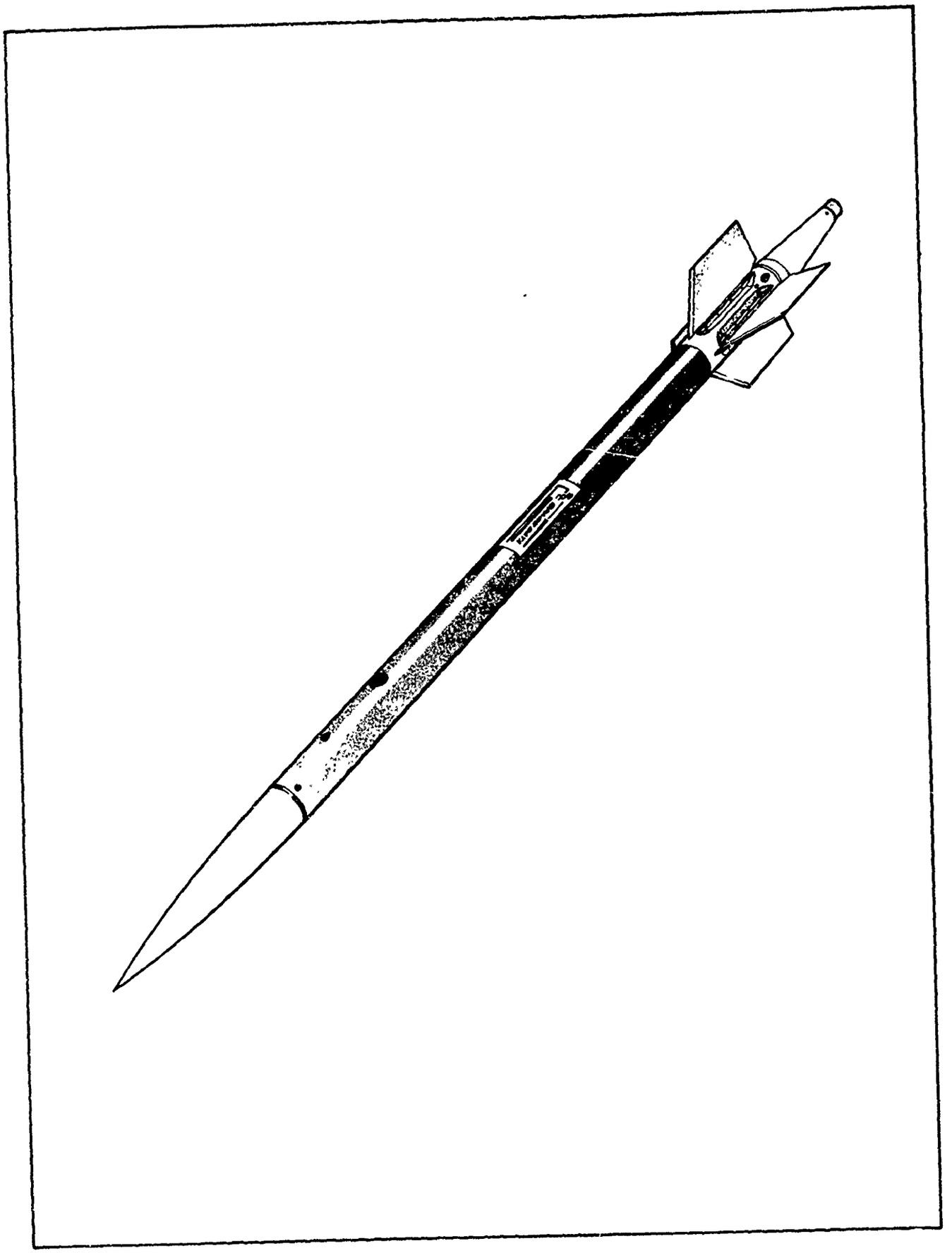

FIGURE 5.12 SUPER LOKI INSTRUMENTED DART

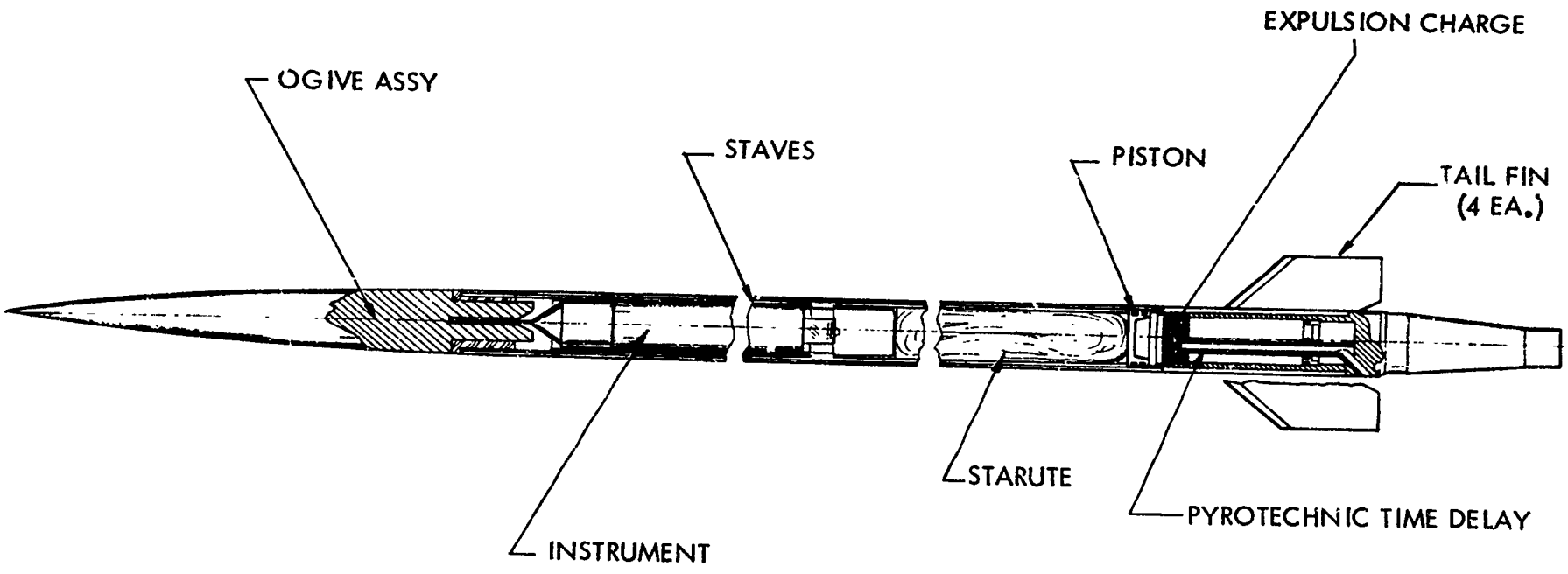

FIGURE 5.13 CROSS SECTION VIEW OF THE SUPER LOKI INSTRUMENT DART

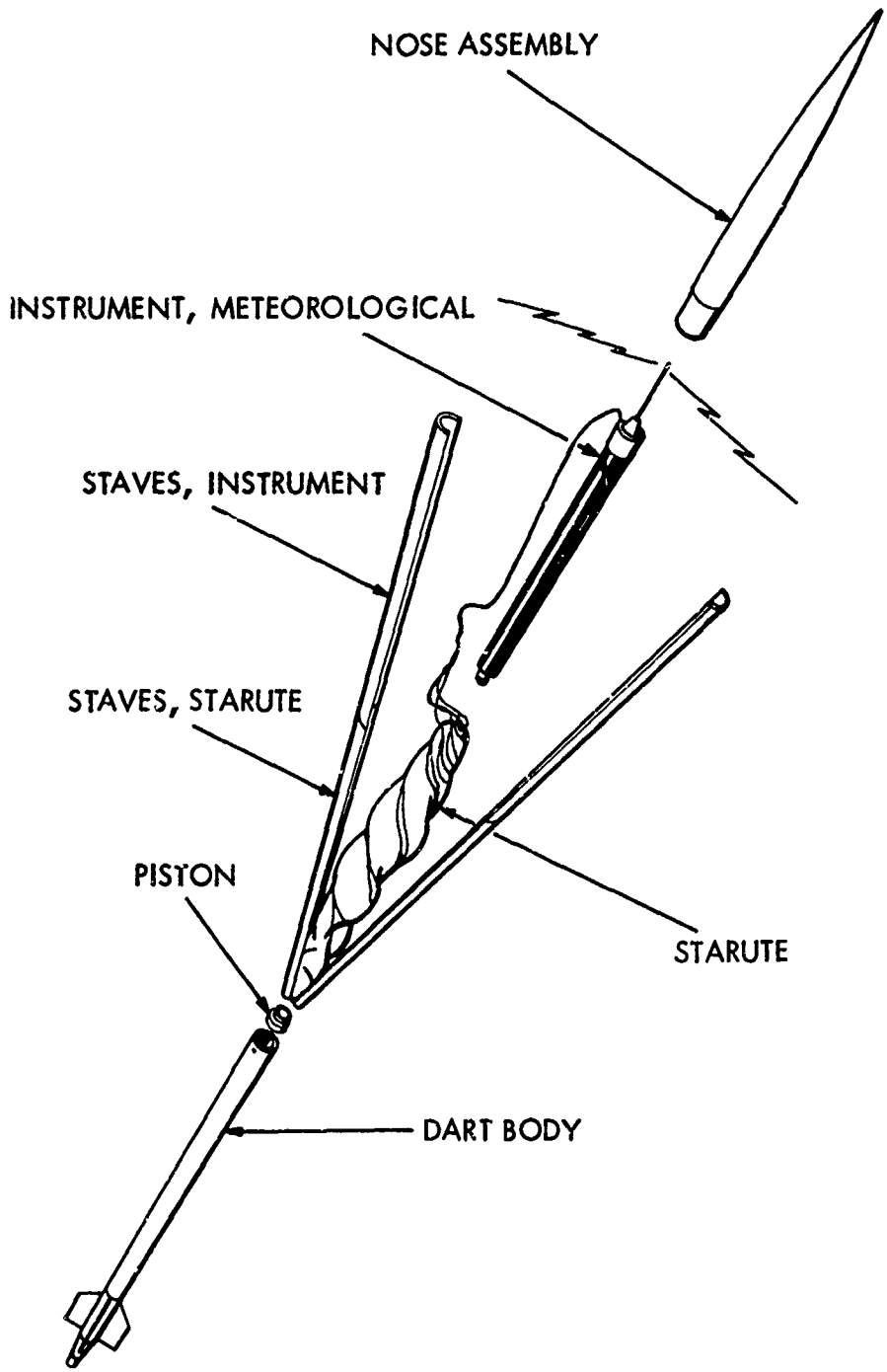

FIGURE 5.14 PICTORIAL VIEW OF PAYLOAD EJECTION

The air gap thermal protection techniques were used in this dart design in place of the more expensive ablative coating.

5.4 Payload Description

5.4.1 General

The payload consists of a transponder or transmitter instrument which is compatible with the AN/GMD-4 or -1 ground-station receiver and a 10-feet per side Starute decelerator.

5.4.2 Super Loki Starute

The Super Loki Starute, as shown in Figure 5.15, is a scaled-up version of the Loki 7-feet per side Starute. Major characteristics of the Super Loki Starute are presented in Table 5.3.

TABLE 5.3

SUPER LOKI STARUTE MAJOR CHARACTERISTICS

Side Length	10 ft
Material	1/4-mil Mylar
Weight	326 gm
Drag Area	100 ft^2
Drag Coefficient	0.875
Ballistic Coefficient with Instrument	0.020 lb/ft^2 1.030 lb
Height	80.50 in
Ram-Air Inlet Side	23.25 in
Suspension Lines Length	16.75 in

Upon ejection from the dart body, the Starute inflates initially by its own entrapped air, and inflation is maintained during its descent by ram-air flowing into an inlet located at the bottom the the envelope. The instrument payload is attached by means of suspension lines below the inlet. The burble fence located about the equator of the envelope is to provide attitude

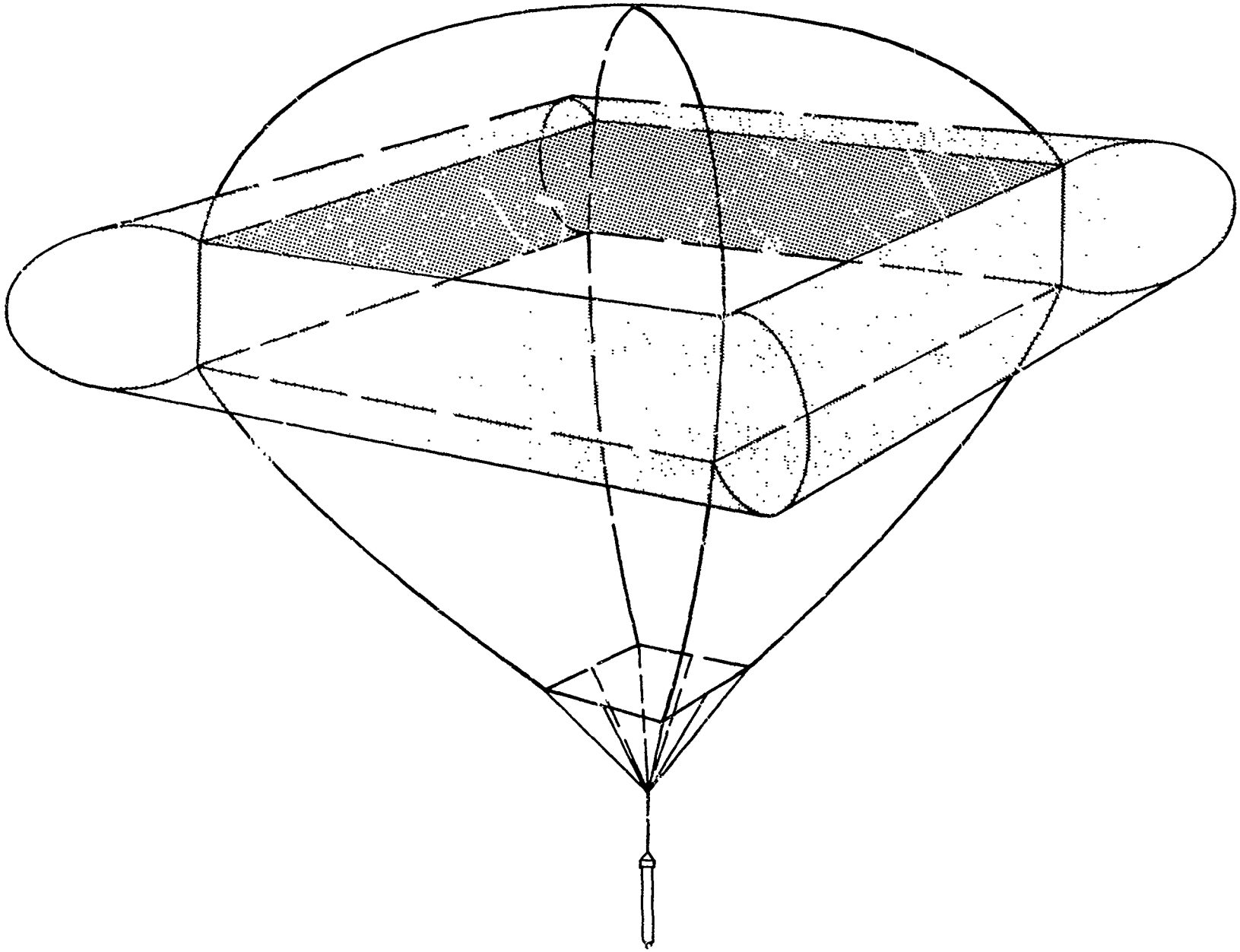

FIGURE 5.15 SUPER LOKI 10' STARUTE

stabilization and added drag area. Reinforced port holes are located between the envelope main body and burble fence and in the burble fence exterior. These port holes are to vent entrapped air during packaging and high altitude deployment and to vent the ram-air into and out from the burble fence to provide a positive inflation pressure without the possibility of overpressuring the envelope. The burble fence is constructed from aluminized Mylar to provide a radar target.

5.4.3 Transponder Instrument

The following sections, 5.4.3.1 through 5.4.4, are extracted from Reference 2.

5.4.3.1 General

The transponder instrument or rocketsonde is designed to be flown in the Super-Loki rocket vehicle to an apogee altitude of about 75 km where it is ejected and descends on a "Starute", or stable parachute, while transmitting meteorological data. It is tracked by an automatic ground-tracking station, Rawin Set AN/GMD-4, which demodulates the signals transmitted by the sonde to provide direct measurement of atmospheric temperatures, elevation and azimuth angles, and slant range. The angles and slant range are then used to compute wind velocity and the altitudes to which temperature and winds are assigned. It is this independent slant range measuring capability which distinguishes the transpondersonde from other types of rocketsondes in that high precision radars are not necessary to obtain the wind and altitude data as is necessary with the nontransponder rocketsonde systems. As a result, meteorological rocket soundings can now be conducted in areas of the world where tracking radars are not available or cannot be suitable scheduled.

The major assemblies of the transpondersonde are a 1680 MHz transmitter and antenna, an 82 KHz amplifier, a 403 MHz receiver and antenna, a meteorological data oscillator, a clock commutator, a DC/DC converter, a relay and "umbilical" connector, a 6.25 volt battery, and a temperature sensor and mount. Figure 5.16 is a block diagram depicting these assemblies. Physically the sonde measures 13 in. long, 1-5/8 in. in diameter, and weighs about 1 pound. Once assembled, the electronics are inserted into a cylindrical tube and encapsulated to provide both mechanical support and heat protection. The transmitter is located at one end of the tube with the 1/4 wavelength dipole antenna (about 2 in. long) protruding (as in Figure 5.17). The temperature sensor is mounted at the other end behind the battery pack. A circuit diagram is presented in Figure 5.18.

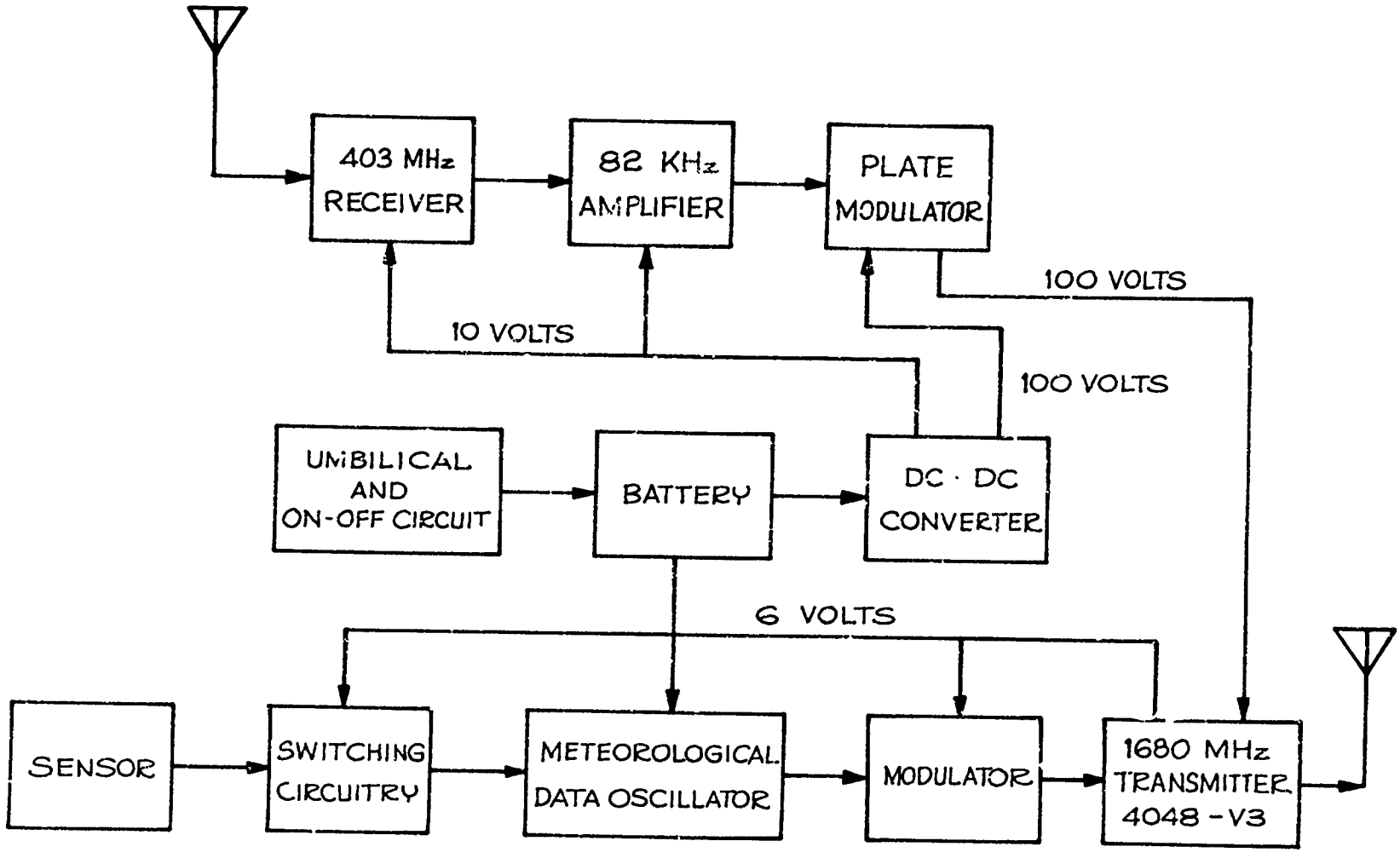

FIGURE 5.16 BLOCK DIAGRAM - SUPER LOKI TRANSPONDERSONDE, REF. 2

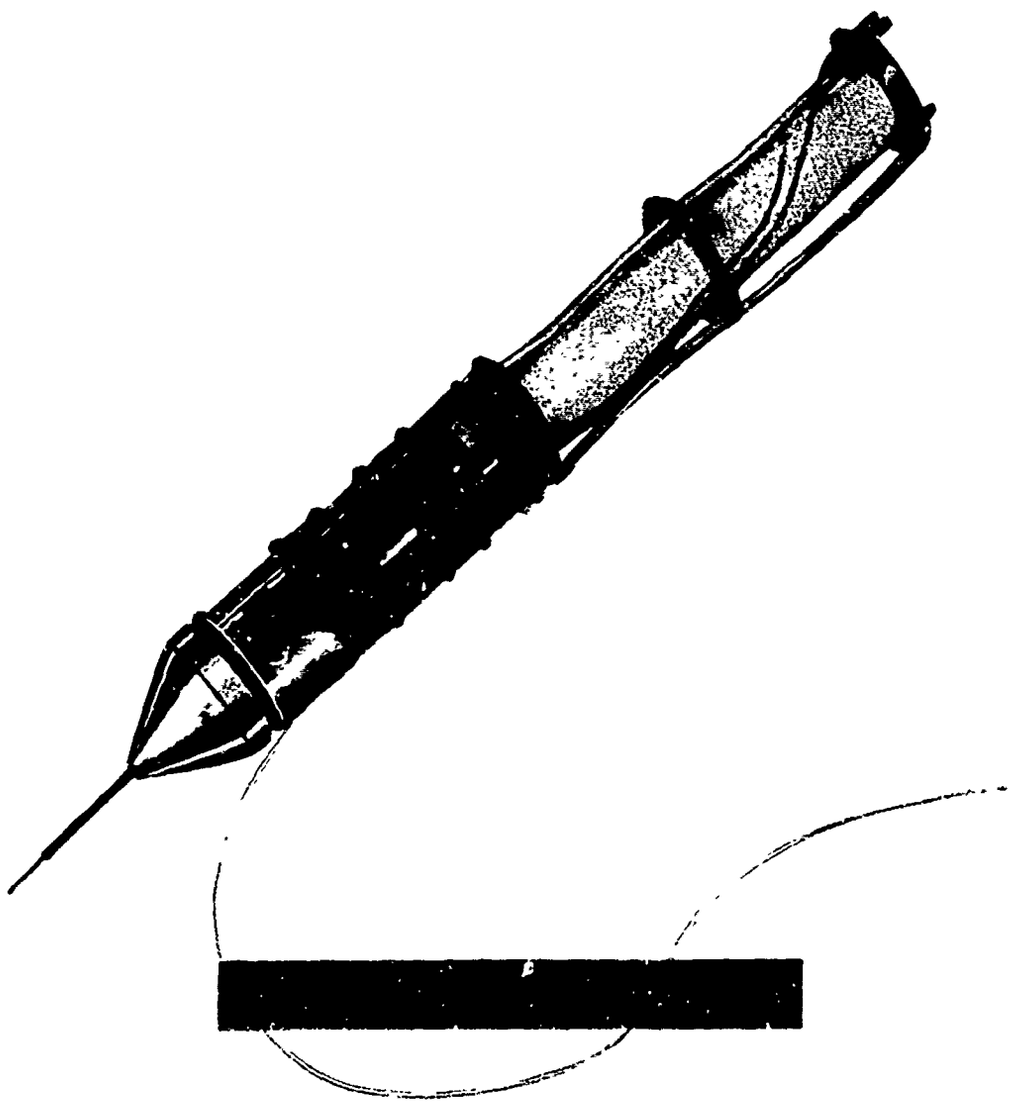

FIGURE 5.17 SUPER LOKI TRANSPONDERSONDE, REF. 2

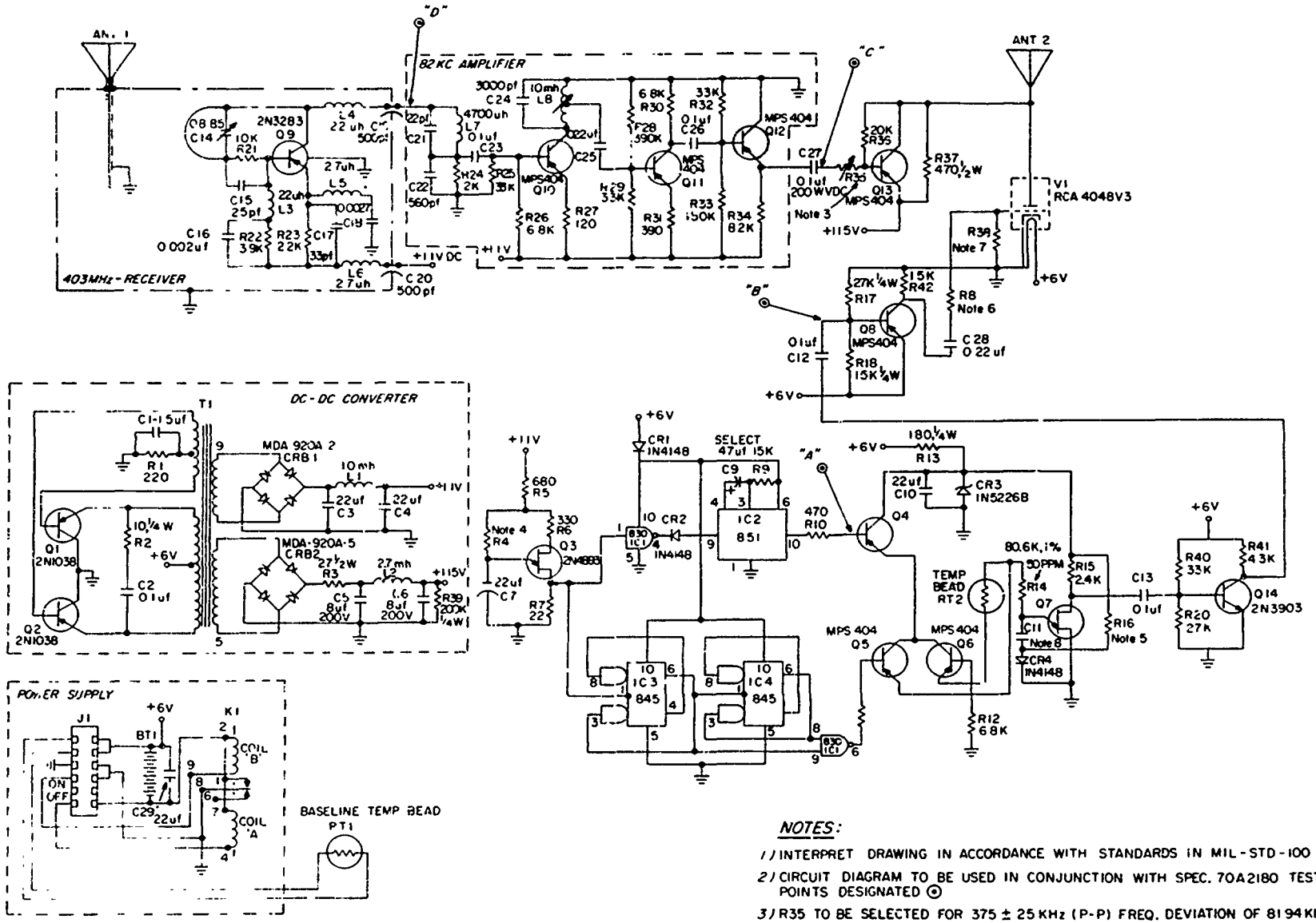

NOTES:

1) INTERPRET DRAWING IN ACCORDANCE WITH STANDARDS IN MIL-STD-100

2) CIRCUIT DIAGRAM TO BE USED IN CONJUNCTION WITH SPEC. 70A2180 TEST POINTS DESIGNATED ⊙

3) R35 TO BE SELECTED FOR 375 ± 25 KHz (P-P) FREQ. DEVIATION OF 8194 KHz RANGING SIGNAL WITH 400uv INPUT SIGNAL

4) R4 TO BE SELECTED FOR 5 ± 0.5 SEC. TIMING, ~180K OHMS

5) R16 MAY VARY FOR EACH TRANSISTOR(Q7) LOT, 1.5 TO 3K APPROX

6) R8 TO BE SELECTED FOR 350 KHz NOMINAL DEVIATION

7) R38 TO BE SELECTED FOR 30 ma PLATE CURRENT ON V1

8) C11 TO BE SELECTED FOR REFERENCE FREQ. 190 ± 15 KHz

FIGURE 5.18 CIRCUIT DIAGRAM TRANSPONDER, REF. 2

5.4.3.2 Transmitter and Antenna

The transmitter consists of a fundamental 1680 ± 20 MHz tunable RF cavity oscillator. It supplies approximately 400 milliwatts output and is FM modulated. The meteorological pulses FM modulate the grid with 200 ± 50 KHz negative peak-to-peak deviation. The 81.94 KHz ranging signal FM modulates the plate with 375 ± 25 KHz peak-to-peak deviation.

The transmitting antenna consists of a quarter-wave dipole stub and a conical ground plane. The antenna radiation pattern has a deep null along the cone axis, which is typical of dipole patterns. It radiates a linearly polarized wave. The combination of antenna pattern and polarization causes excessive signal dropouts at high elevation angles (70°), but has a relatively steady signal strength pattern below 70°.

5.4.3.3 Receiver and Amplifier

The receiver is a nominal 403 MHz single stage, self-oscillating, super regenerative type. It requires RF shielding to maintain oscillation due to the external capacitive and inductive effects at UHF frequencies. This type of receiver is characterized by its continuous oscillation frequency called the "quench" signal. This is a sawtooth type buildup and decay signal of about 1.5 Vpp and a 2.5 μsec period (400 KHz) which the 2N3283 (Q-9) stage generates. The period and amplitude of the sawtooth is determined principally by C-18 in the emitter circuit of Q-9. The quench frequency is lower than the carrier frequency (403 MHz) and higher than the ranging modulation frequency (82 KHz) to prevent interference between the signals.

As the detector goes in and out of self oscillation, the 403 MHz carrier signal, 82 KHz ranging signal, and 400 KHz quench signal comprise the components on the collector circuit of Q-9. The 403 MHz and 400 KHz signals are attenuated by two tuned stages of L - C filtering which allow only an 82 KHz signal to reach the 82 KHz amplifier. This 82 KHz amplifier consists of four MPS404 transistor stages. The first two stages (Q-10 and Q-11) provide the majority of the gain while the last two stages (Q-12 and Q-13) provide impedance matching to the transmitting tube.

5.4.3.4 Receiving Antenna and Lanyard

The receiving antenna consists of a center fed 1/4 wavelength dipole made up of a 50 ohm miniature coaxial cable. The total length is approximately 23 in., with 6-1/2 in. (1/4 wavelength) stripped back on one end. This end is physically attached to the lanyard. The other end is stripped back about 1/2 in. and fed through the top of the receiver "can". Here the two 1/2 in. leads are soldered to the bottom of the can and inductively coupled to the base of transistor Q-9. This results in a DC short circuit, but it provides satisfactory energy transfer at 403 MHz to transistor Q-9, while limiting the bandwidth to prevent radio frequency interference from other frequencies near 403 KHz.

5.4.3.5 Clock - Commutator and Meteorological Data Oscillator

The meteorological data oscillator (MDO) is commutated by a two-channel solid state commutator that provides temperature and reference data channels. The sequence provided by the commutator is of three temperature and one reference data periods. Each data period has an on-time of 4.5 seconds and an off-time, or blanking period of 0.5 seconds.

The clock commutator consists of a 0.2 Hz (one pulse every five seconds) clock, two 845 micrologic flip-flops (IC3 and IC4), one 830 dual two-point micrologic NAND gate (IC1), one 851 micrologic monostable multivibrator (IC2), and three switching transistors -- Q4, Q5, and Q6.

5.4.3.6 DC-to-DC Converter

With a 6-volt battery input, the converter supplies 115 VDC at 30 ma and 11 VDC at 15 ma. These supply the tube plate/82 KHz amplifier voltages and the receiver/82 KHz amplifier voltages respectively. The voltage supply for the MDO and transistor switches is provided from a 3.3 VDC Zener diode and dropping resistor from the 6-volt battery.

The nominal frequency of oscillation of the converter is 2.2 KHz and was so selected to minimize core losses and not interfere with the 82 KHz amplifier or the meteorological data (15-200 Hz). The primary and secondary winding outputs are square waves generated from the asymmetrical conduction of Q-1 and Q-2, which alternately create magnetic field hysteresis buildup and breakdown in the windings. The two square wave outputs are connected to two diode bridges (CRB1 and CRB2) which result in a DC voltage output which contains spikes due to the transistor switching times. These spikes are eliminated by π filters at the diode bridge output

5.4.3.7 Battery

The total instrument current drain is close to 1 amp, so a 1 ampere-hour battery is necessary along with a recharging capability. A group of five 1.25 VDC nickel cadmium cells connected in series to make a 1-3/4 in. diameter, 5 in. long, 8-ounce battery pack is used. When fully charged, the voltage output runs close to 7 volts and has a plateau above 6 volts for one hour at 1 amp current drain.

5.4.3.8 Mount and Sensor

The sensor consists of an aluminized 10 mil, 5 K-ohm (nominal) bead which is compatible with the sonde meteorological blocking oscillator. A 33 pf chip capacitor is attached in parallel with the bead thermistor to provide shunting which minimizes RF heating of the bead. The leads to which the bead is soldered are about 1 in. long.

A separate temperature sensitive bead is placed at the bottom of the sensor mount with two leads out to the umbilical connector. A meter, which displays the temperature this bead senses (in ^{o}C), is attached to the umbilical connector. This temperature is compared to the temperature sensed by the thermistor and they should agree within $3^{o}C$. In this manner, a baseline (or calibration check) capability is provided which gives assurance that the thermistor and electronics are operating properly prior to launch.

5.4.3.9 Remote Control Capability

A remote control box is utilized which has the following features:

a. It can turn the sonde ON and OFF through a cable attached to an "umbilical" connector (J1) in the sonde.

b. It can power the sonde externally.

c. It can recharge the sonde batteries.

When it is desired to power the sonde on its own batteries, relay K1 is activated by the remote control box and completes the ground to the 6 VDC battery.

The remote ON-OFF capability proved itself to be extremely valuable at the test ranges as in several instances long holds (more than 10 - 15 minutes) were encountered in the final countdown before launch. An operator did not have to leave the blockhouse, go to the launcher, lower the dart, and turn the sonde OFF. All he had to do was flip a switch at the blockhouse. Surprisingly, the umbilical connector attached to the dart survived the launches in good condition and was reusable.

5.4.3.10 Summary

A summary of the listing of the electrical specifications is presented in Table 5.4.

5.4.4 Transmitter Instrument

The transmitter system and dart are essentially identical to the transponder system except that the ranging receiver has been eliminated from the transponder instrument to yield the transmitter instrument. All of the other electronic parts and structures remain unchanged and a blank space is left in place of the ranging receiver so that the two instruments are interchangeable within the same dart hardware and vehicle configuration. The purpose of the transmitter system is to save the cost of the ranging receiver at launch sites where adequate tracking radar is available.

All of the aerodynamic, trajectory and vehicle parameters are identical for both the transponder and transmitter systems.

TABLE 5.4

ELECTRICAL SPECIFICATIONS - TRANSPONDERSONDE, Ref. 2

Transmitter	
Type	Tube RCA 4048V3
Power Output	100 Milliwatts (minimum)
Frequency	1670 - 1695 MHz (tunable)
Sensor Modulation	FM
81.94 KHz Range Signal Modulation	FM
403 MHz Receiver	
Tuning Range	400 - 406 MHz
Sensitivity	50 μv Minimum
50 db Bandwidth	392 - 415 MHz
81.94 KHz Amplifier	
Tuning Range	75 - 82 KHz
Modulation	375 KHz Peak to Peak (FM)
Type of Modulation	Plate
Commutator	
Sequence	T T T R, ...
Duration	5 seconds each
Channel Break	0.5 second
Meteorological Data Oscillator	
Reference Frequency	190 Hz
Pulse Amplitude	200 KHz Peak to Peak (FM)
Pulse Width	100 μsec
Calibration	22 Points
Type of Modulation	Grid
DC/DC Converter	
Input Voltage	6.25 VDC
Output Voltages	11 and 115 VDC
Current Drain	
Instrument	1 amp maximum
Tube Plate	30 milliamps
Size	13.25 in. long; 1.640 in. diameter
Weight	480 grams (nominal)

6.

LAUNCHER FINAL DESIGN

6.1 General

The Super Loki Launcher consists of a helical launch rail assembly mounted onto a base or pedestal. The launch rail assembly is similar for both the 1.625-inch and 2.125-inch darts with the only difference being the depth of the grooves to accept the two different dart fin spans. Two rails are therefore required to launch both sizes of dart systems.

6.2 Launch Rail Assembly

The launch rail assembly consists of four helical rails which complete approximately one-third of a revolution throughout the launch rail length. The launch rail assembly, as shown in Figure 6.1, consists of six cast aluminum sections which are bolted together to form a continuous 12 foot long rail assembly. The four internal rails are equally spaced and form four continuous helices throughout the 12 foot length. The edges of the rails are stepped to support the vehicle by the dart fins and the rocket motor nozzle ring. The outside diameter of the launch rail assembly is 10-1/4 inches.

The purpose of the launch rail is to impart and 8.5 rps spin to the vehicle by constraining the dart fins to a helical path during their travel along the launch rails. The aft end of the motor travels for 12 feet prior to its release from the launcher.

The Super Loki launch rail assembly can be mounted to any suitable launcher base by means of forward and aft mounting brackets. A launcher base specifically designed for this rail is shown in Figure 6.2.

A pullaway umbilical harness is provided with the launch rail assembly to retract the dart firing line during first motion of the vehicle.

6.3 Launcher Base

The Super Loki launch rail assemblies can be bolted to any suitable launcher base which is sufficiently sturdy to sustain a 4,000 lbf reaction load without significant deflection or vibration. Most launcher bases at existing missile ranges are more than adequate to support the Super Loki launch rail assemblies.

An attempt to launch theSuper Loki vehicles from the LAU-66/A Loki launcher pedestal and base resulted in altitude-horizontal range values equivalent to a reduction of launcher elevation angle of 3 to 5 degrees. After the launcher superstructure was rebuilt to a more rigid configuration, the pitch down effect was reduced to about 2 degrees.

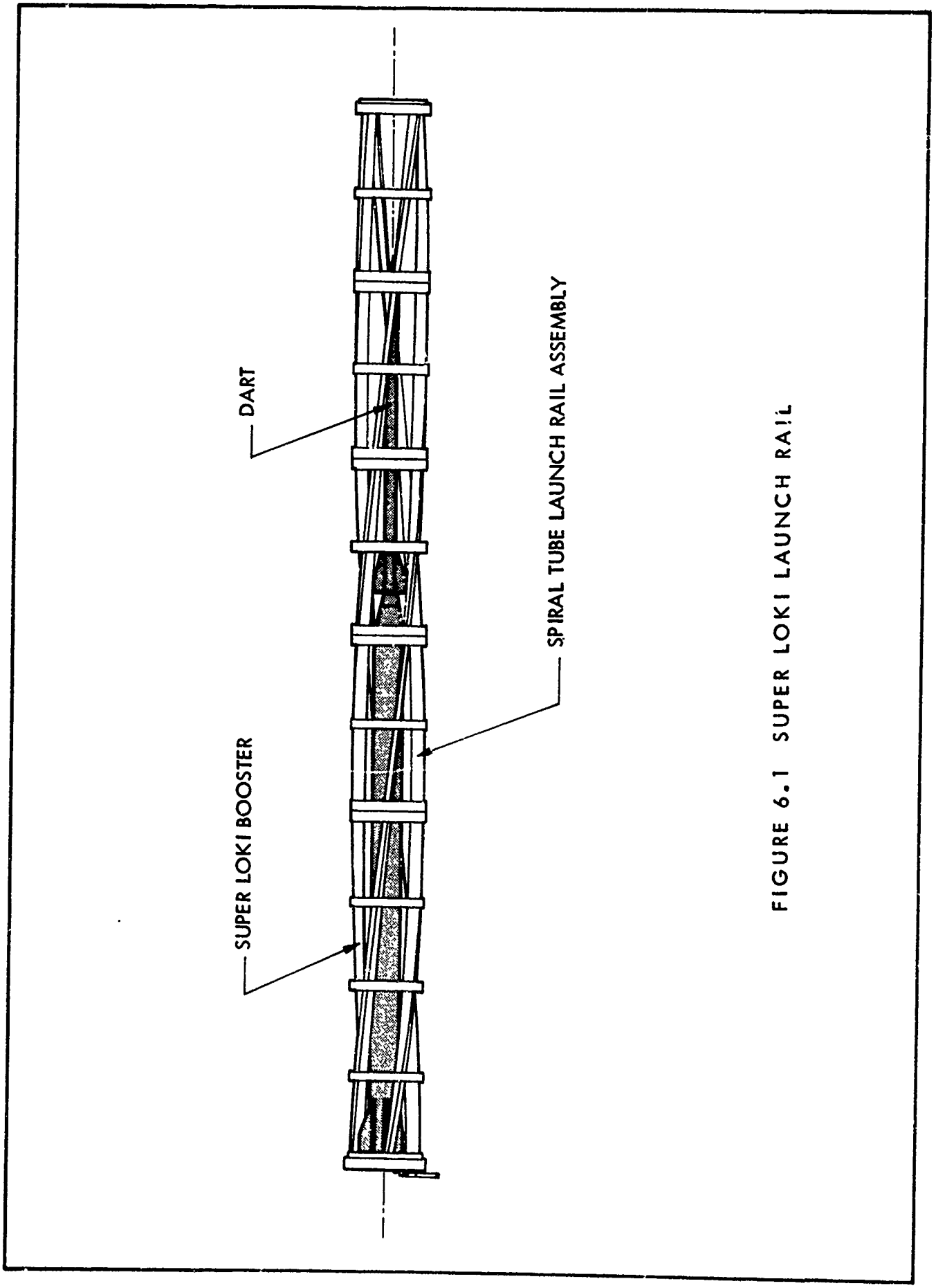

FIGURE 6.1 SUPER LOKI LAUNCH RAIL

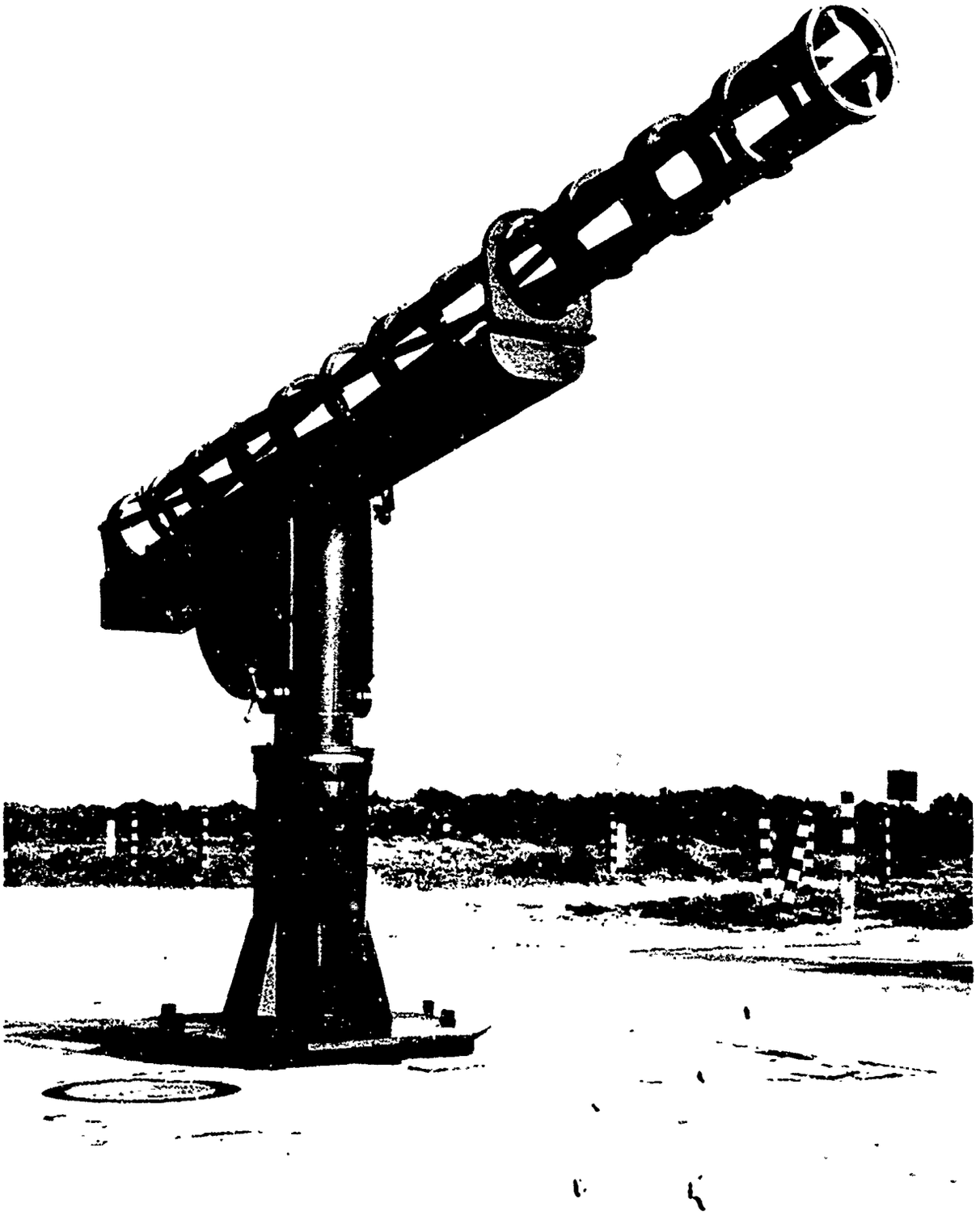

FIGURE 6.2 SUPER LOKI LAUNCHER

A program of LAU-66/A launcher pedestal and base analysis, testing and modification is currently being undertaken to completely eliminate this pitch down effect. Preliminary results of the analysis indicate that the vehicle pitch down may be due to a vibration resonance of the launcher base and pedestal combination with the rocket motor jet blast impingement on the ring bulkheads of the launch rail assembly during rocket travel along the rails. It appears that the standard LAU-66/A Loki Launcher base, pedestal and support assembly must be significantly stiffened to increase its natural bending frequency beyond the resonance region for the Super Loki system.

The LAU-66/A launcher was completely redesigned for the Super Loki Systems as shown in Figure 6.2.

7.

VEHICLE PERFORMANCE

7.1 General

A series of Digital computer trajectories have been run for both the Super Loki Robin Dart and Instrumented Dart vehicles. The results are presented in the sections which follow:

7.2 Instrumented System

A series of Super Loki Instrumented Dart trajectories have been run on a digital computer, and the results are presented as follows:

Table 7.1	Nominal Trajectory Summary, 80° QE
Figure 7.1	Dart Apogee Altitude vs Apogee Range for Various QE's
Figure 7.2	Dart Apogee Altitude vs QE
Figure 7.3	Dart Apogee vs QE
Figure 7.4	Dart Impact Range vs QE
Figure 7.5	Dart Altitude vs Range, 80° QE
Figure 7.6	Dart Altitude vs Time, 80° QE
Figure 7.7	Dart Velocity vs Time, 80° QE
Figure 7.8	Booster Apogee Altitude vs QE
Figure 7.9	Booster Impact Range vs QE
Figure 7.10	Booster Altitude vs Range, 80° QE
Figure 7.11	Booster Altitude vs Time, 80° QE
Figure 7.12	Vehicle Roll Rate vs time

TABLE 7.1

NOMINAL TRAJECTORY SUMMARY

SUPER LOKI INSTRUMENTED DART, 80° Q.E. SEA LEVEL LAUNCH

	Booster	Dart
Burnout Altitude (ft)	4,608	4,608
Burnout Range (ft)	864	864
Burnout Time (sec)	2.0	2.0
Apogee Altitude (ft)	6,680	236,670
Apogee Range (ft)	1,285	85,183
Apogee Time (sec)	6.0	121.5
Impact Range (ft)	1,330	170,679
Impact Time (sec)	97	244.1

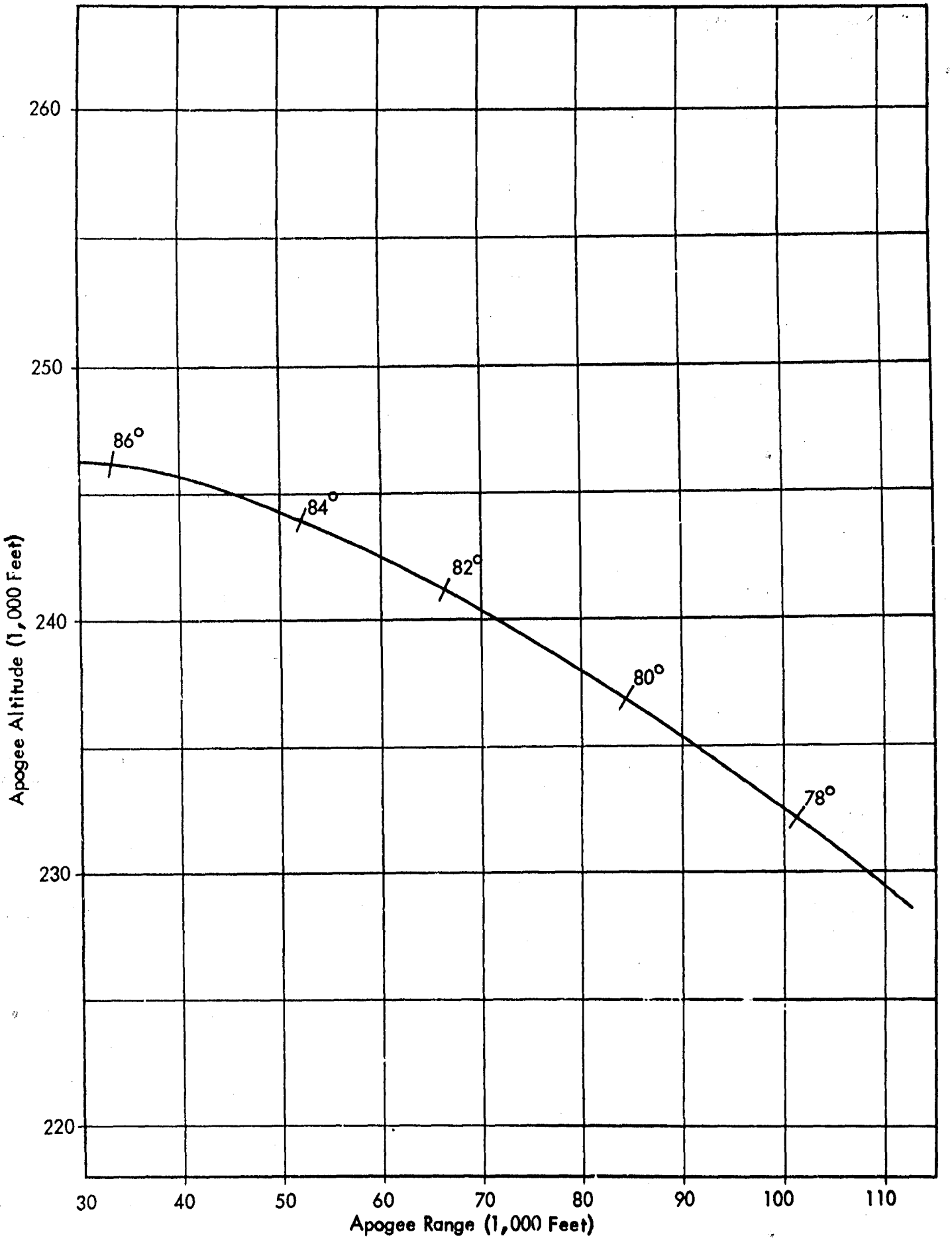

FIGURE 7.1 SUPER LOKI INSTRUMENTED DART
DART APOGEE ALTITUDE VS APOGEE RANGE
FOR VARIOUS QE's

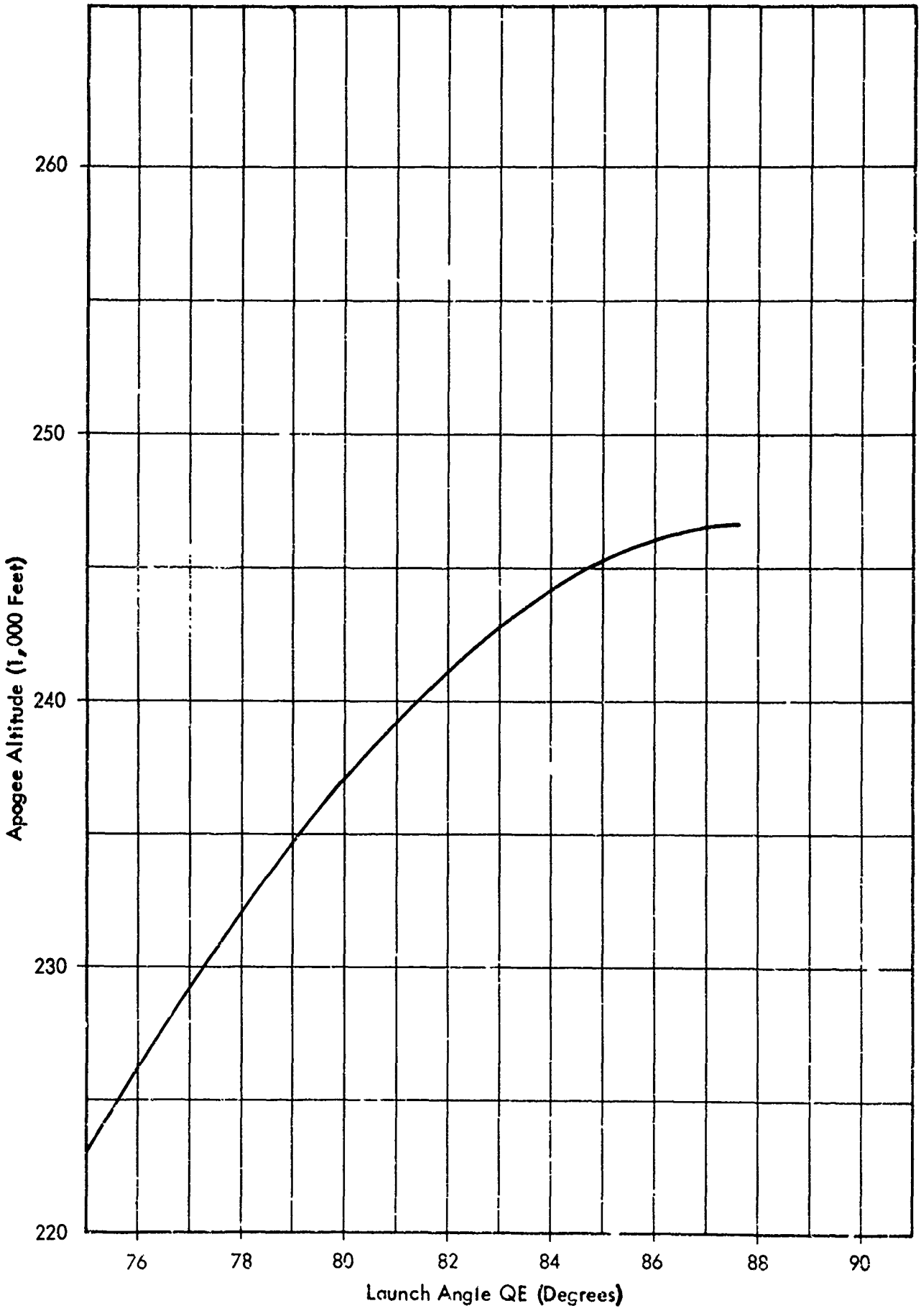

FIGURE 7.2 SUPER LOKI INSTRUMENTED DART
DART APOGEE ALTITUDE VS QE

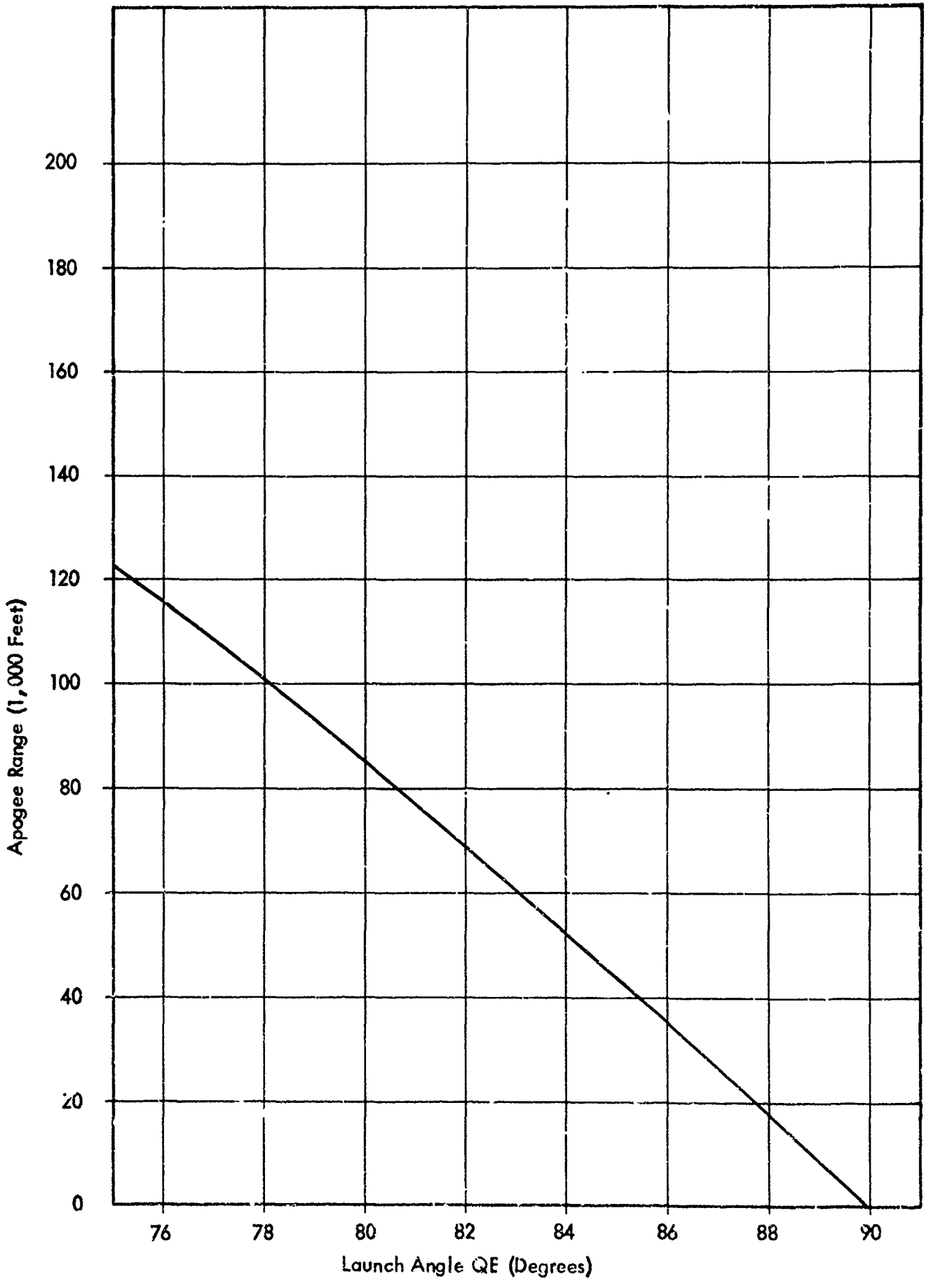

FIGURE 7.3 SUPER LOKI INSTRUMENTED DART
DART APOGEE RANGE VS QE

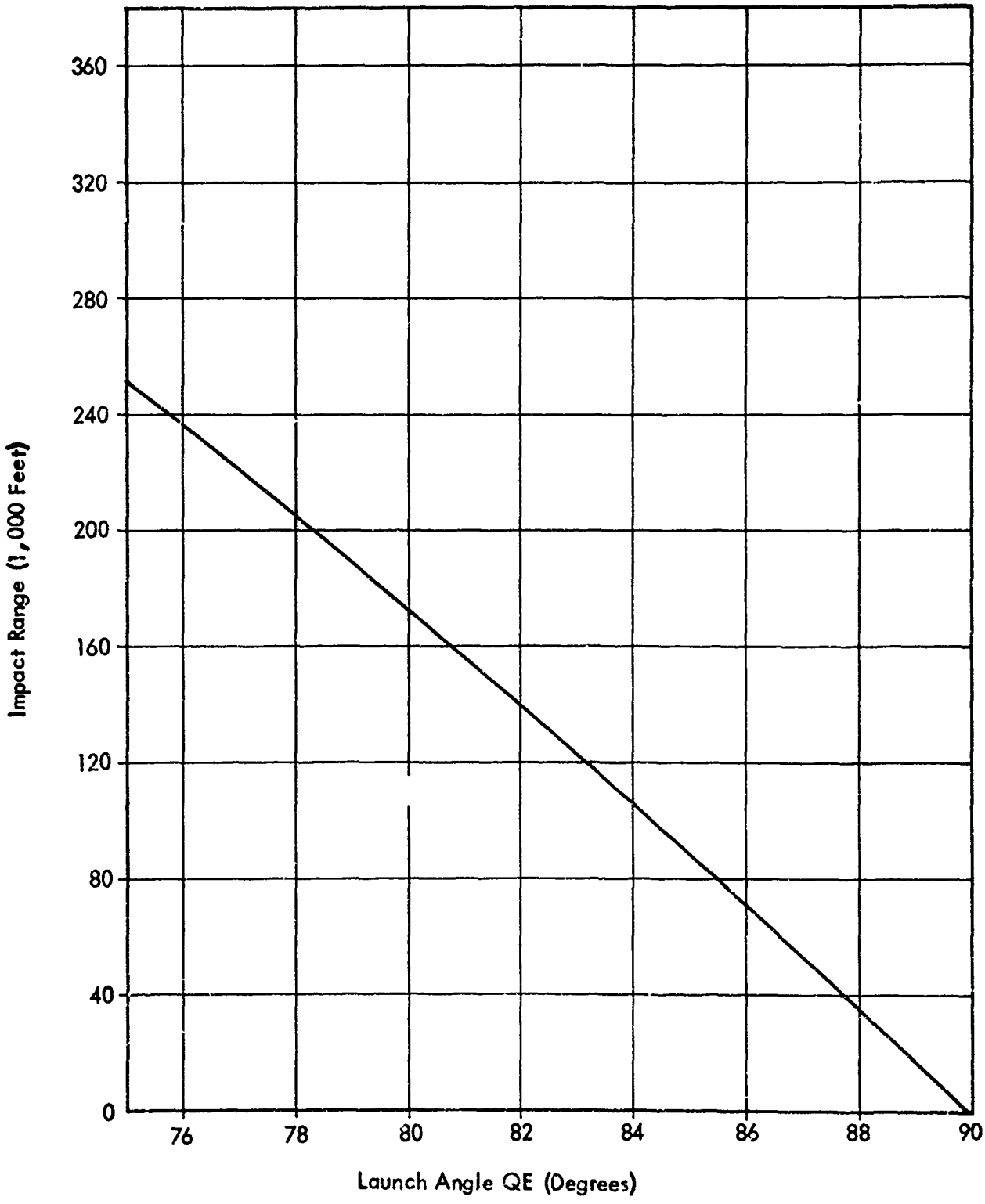

FIGURE 7.4 SUPER LOKI INSTRUMENTED DART
DART IMPACT RANGE VS QE

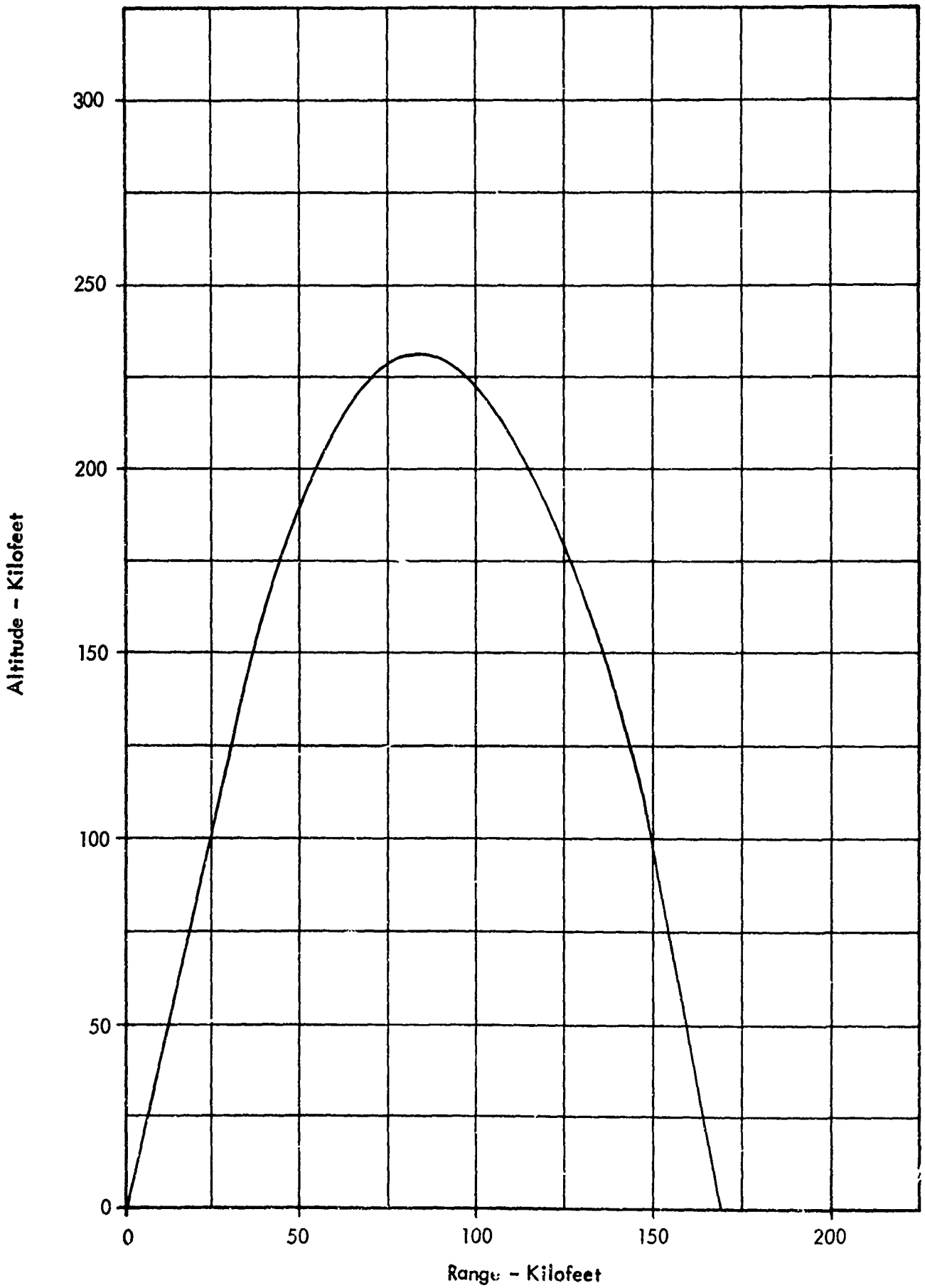

FIGURE 7.5 SUPER LOKI INSTRUMENTED DART
ALTITUDE VS RANGE 80° QE

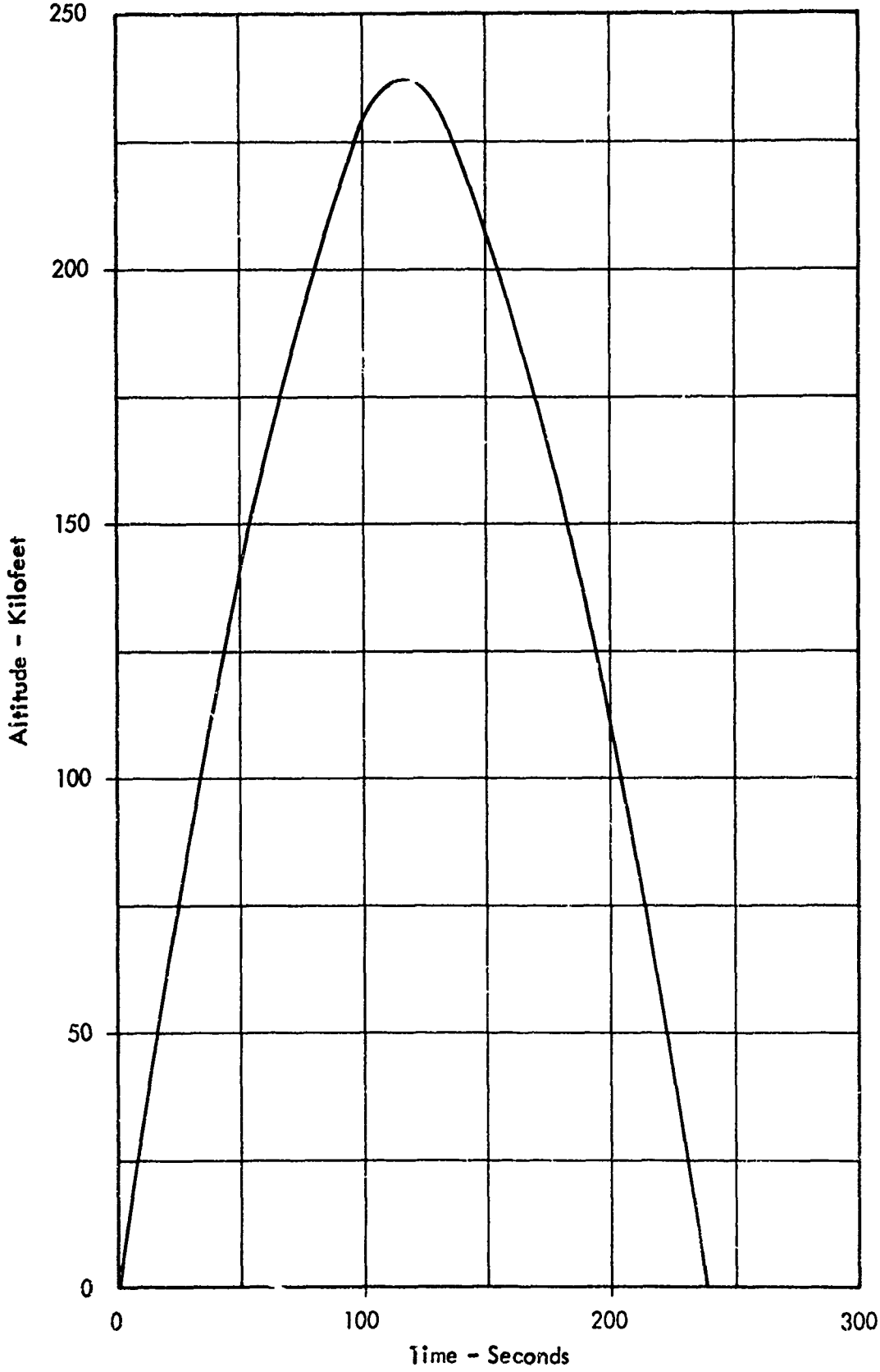

FIGURE 7.6 SUPER LOKI INSTRUMENTED DART
DART ALTITUDE VS TIME 80° QE

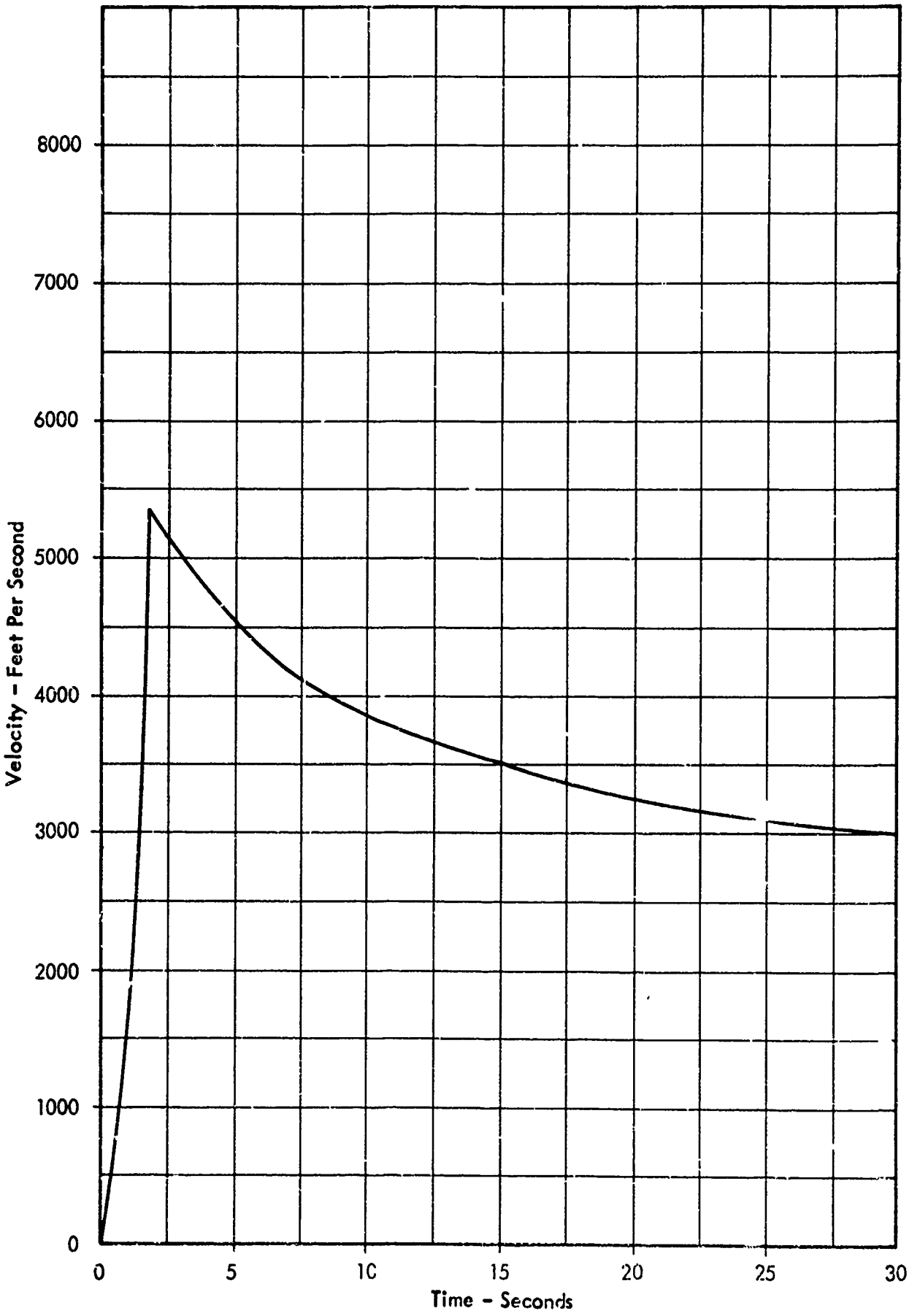

FIGURE 7.7 SUPER LCKI INSTRUMENTED DART
DART VELOCITY VS TIME 80° QE

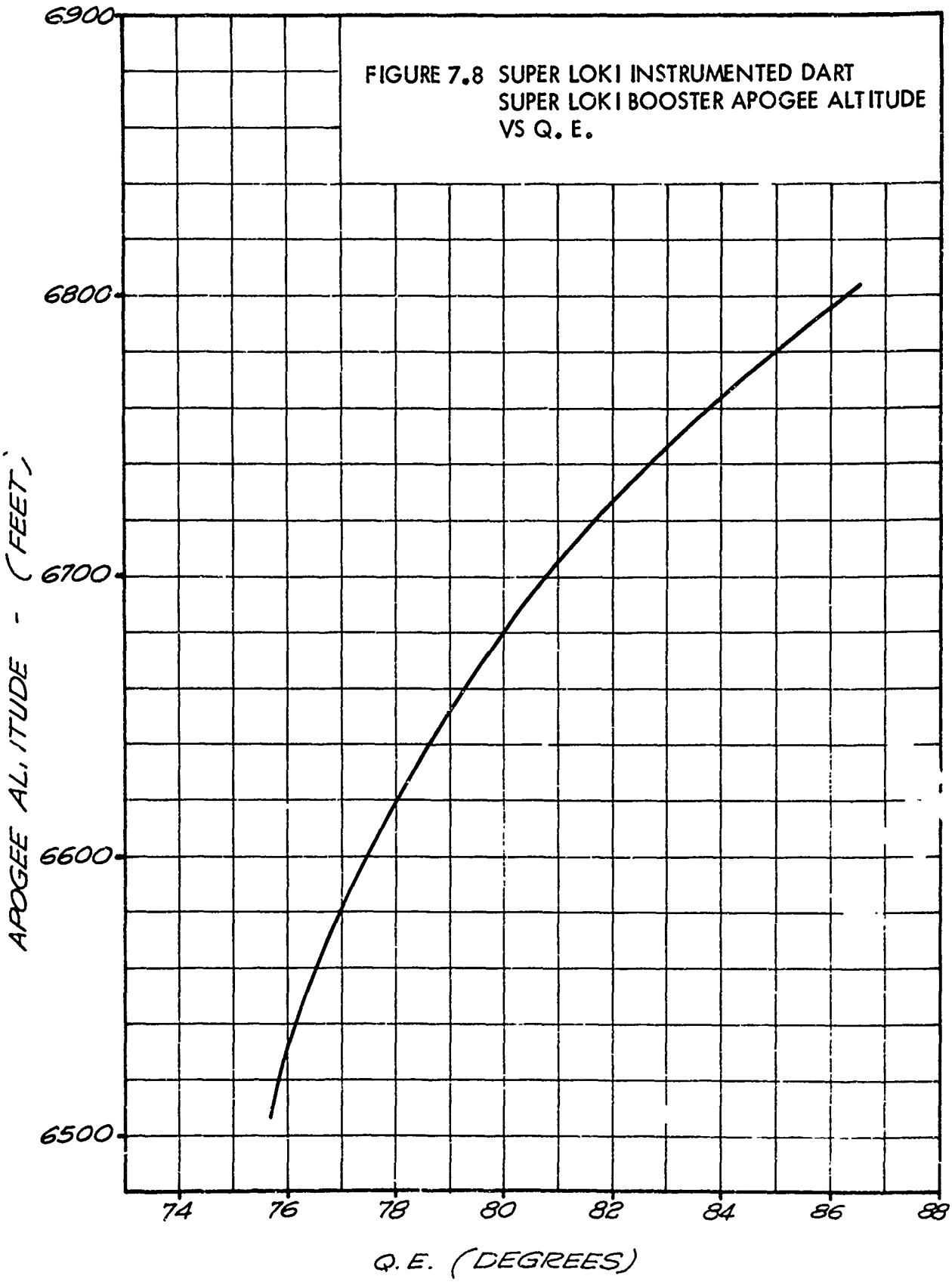

FIGURE 7.8 SUPER LOKI INSTRUMENTED DART
SUPER LOKI BOOSTER APOGEE ALTITUDE
VS Q. E.

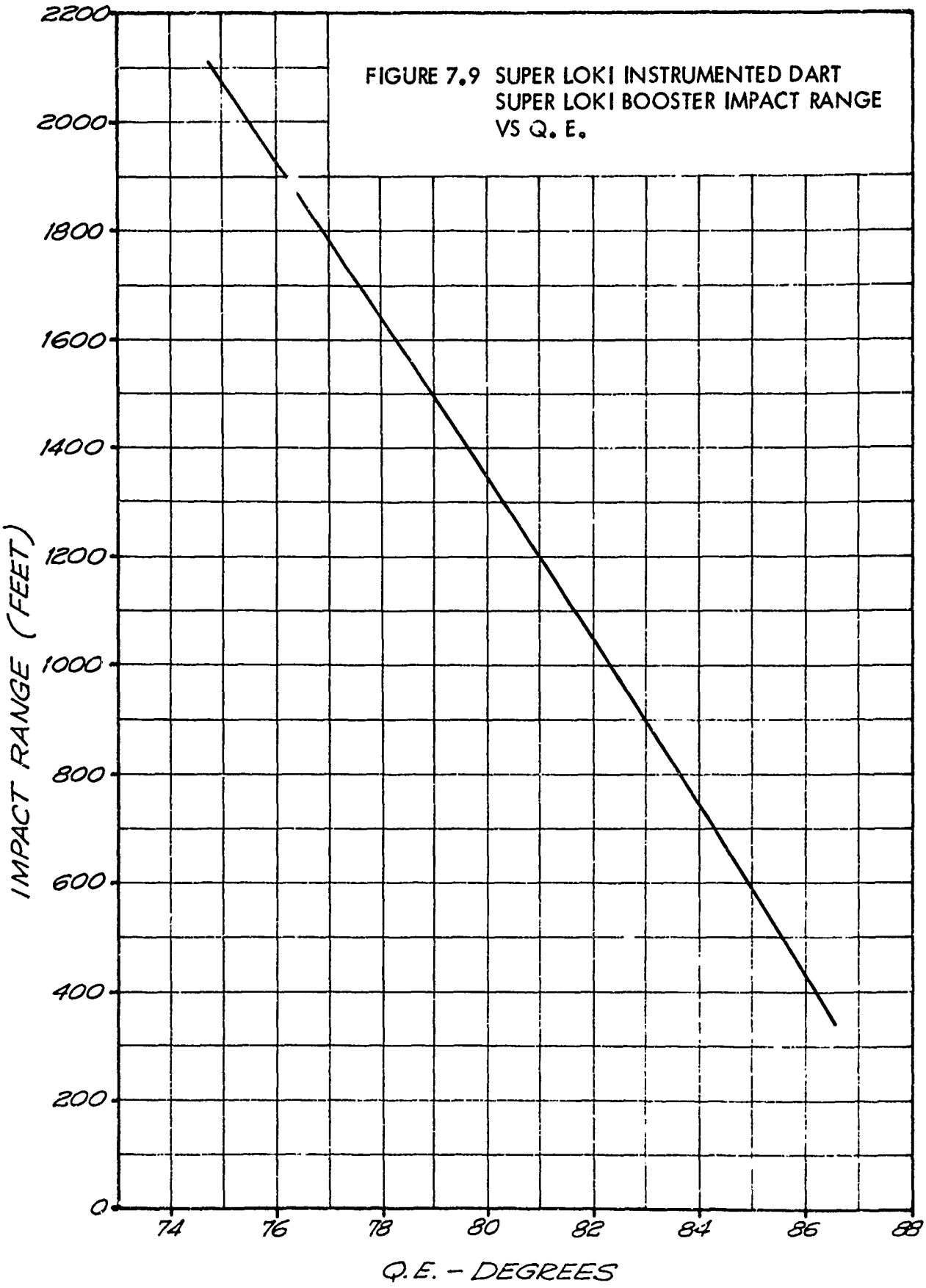

FIGURE 7.9 SUPER LOKI INSTRUMENTED DART
SUPER LOKI BOOSTER IMPACT RANGE
VS Q. E.

FIGURE 7.10 SUPER LOKI - BOOSTER
NOMINAL TRAJECTORY
80° Q. E. SEA LEVEL LAUNCH

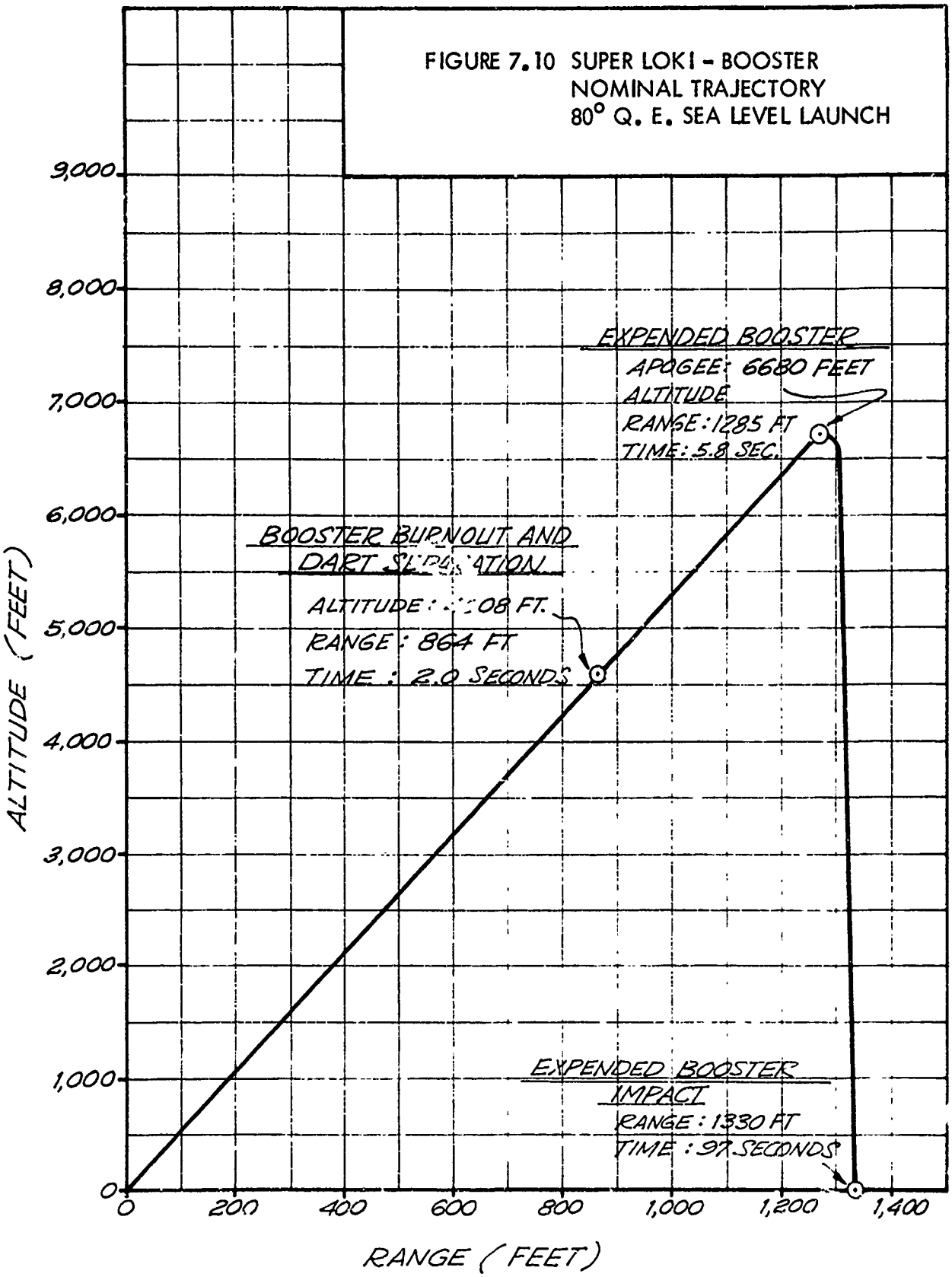

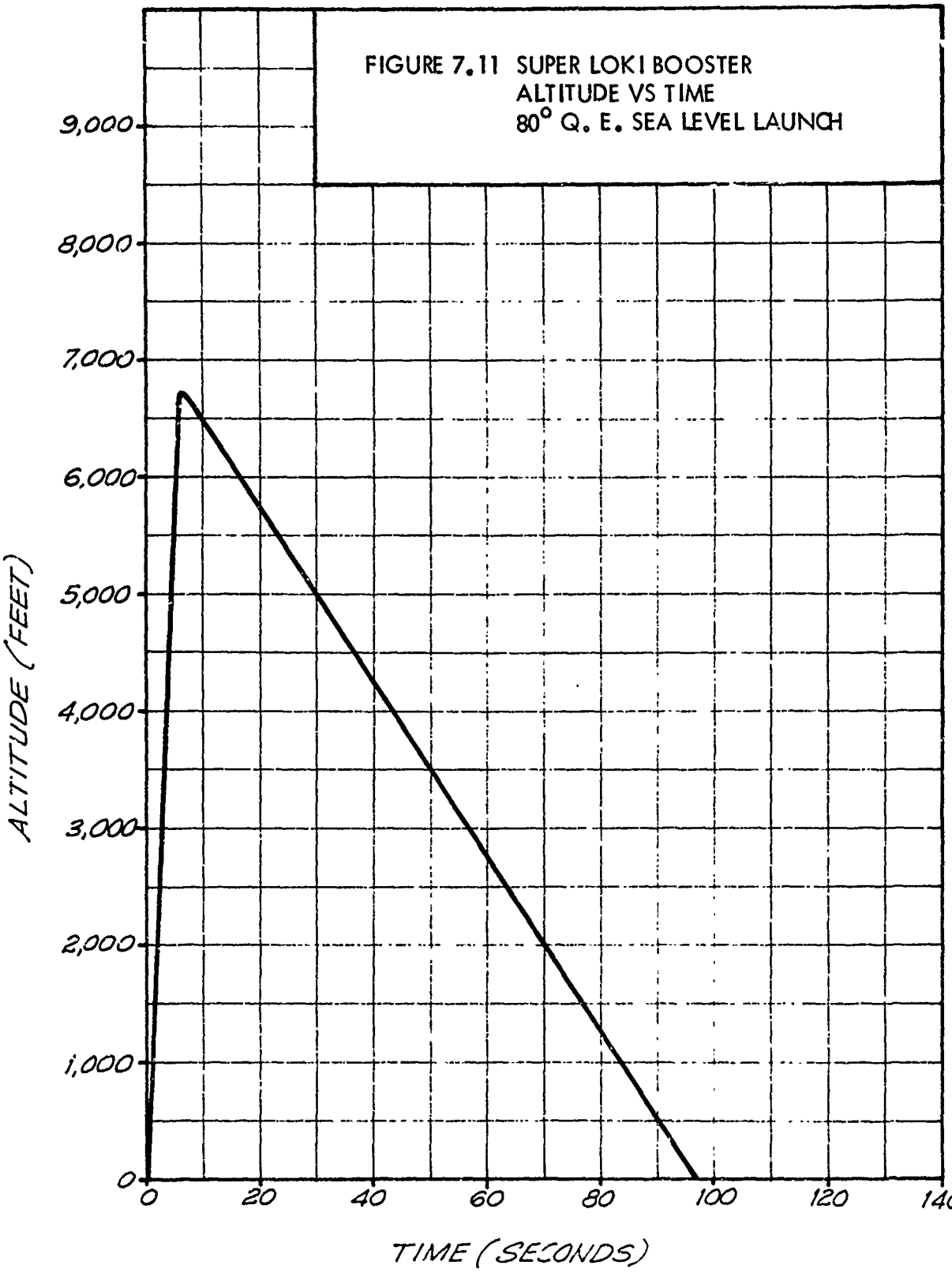
FIGURE 7.11 SUPER LOKI BOOSTER
ALTITUDE VS TIME
80° Q. E. SEA LEVEL LAUNCH
9,000
8,000
7,000
6,000
5,000
4,000
3,000
2,000
1,000
0
ALTITUDE (FEET)
0
20
40
60
80
100
120
140
TIME (SECONDS)

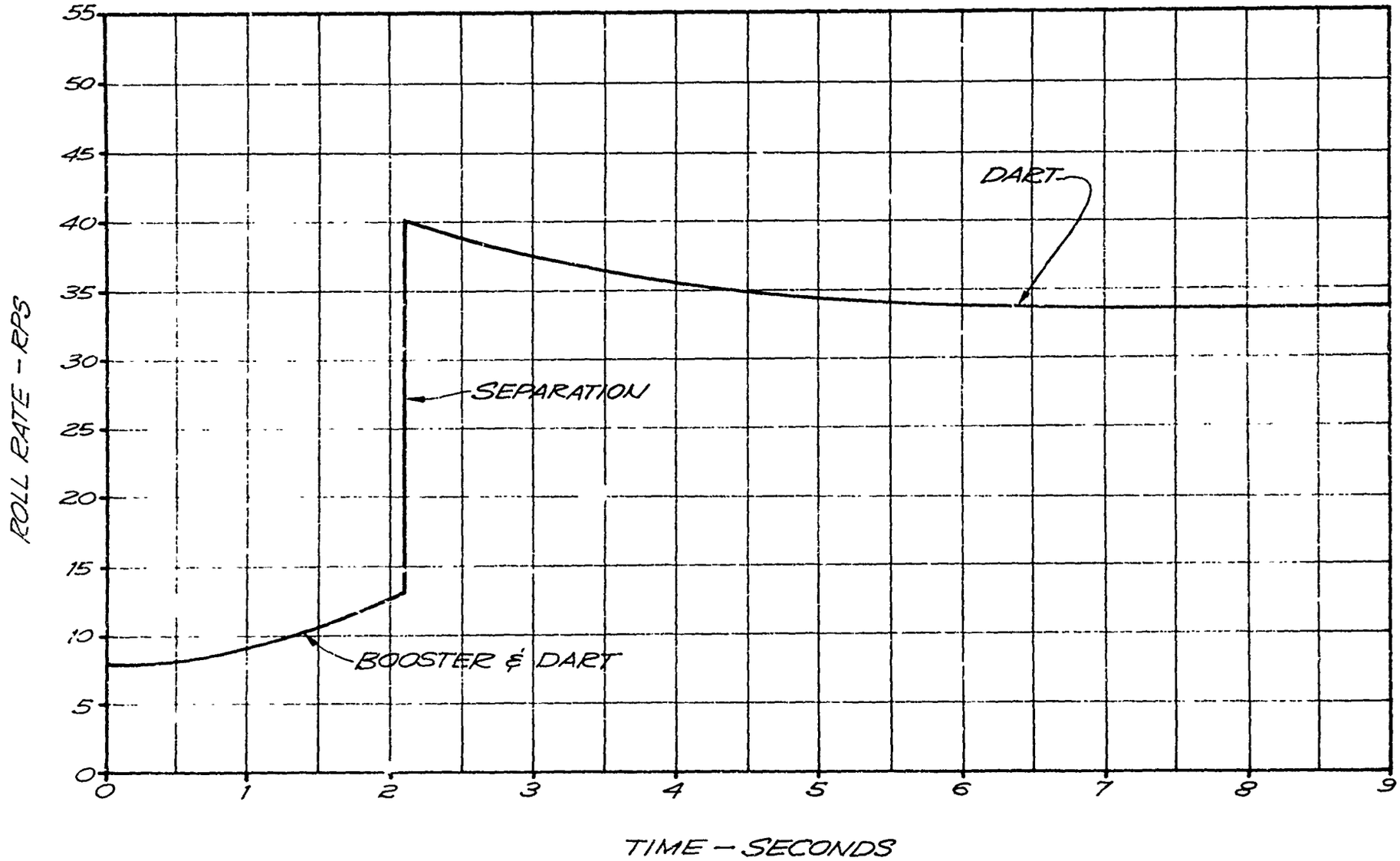

FIGURE 7.12 SUPER LOKI INSTRUMENTED DART ROLL RATE VS TIME

7.3 Robin System

A series of Super Loki Robin Dart trajectories have been run on a digital computer, and the results are presented as follows:

Table 7.2	Nominal Trajectory Summary
Figure 7.13	Apogee Altitude vs Apogee Range, Dart
Figure 7.14	Altitude vs Range, 80° QE, Dart
Figure 7.15	Altitude vs Time, 80° QE
Figure 7.16	Velocity vs Time, 80° QE, Dart
Figure 7.17	Altitude vs Range, Various QE's
Figure 7.18	Apogee Altitude and Impact Range vs QE, Dart
Figure 7.19	Altitude vs Range, 80° QE, Booster
Figure 7.20	Altitude vs Time, 80° QE, Booster
Figure 7.21	Apogee Altitude and Impact Range vs QE, Booster
Figure 7.22	Vehicle Roll Rate vs time

The dart trajectory is based upon stable dart flight prior to and after stage separation. The booster trajectory is based upon stable flight to the point of stage separation. After stage separation, the booster goes unstable and decelerates rapidly to a slow velocity. The booster then descends rather slowly in a flat spin.

7.4 Super Loki Starute

The Super Loki Starute has a ballistic coefficient of 0.020 lb/ft^2 with the transponder instrument which weighs 1.030 lb. The drag coefficient is $C_D = 0.875$ per reference area of 100 ft^2 (10 ft x 10 ft). From the normal deployment altitude of about 240,000 feet the descending Super Loki 10' Starute system remains subsonic and has a fairly constant drag coefficient. A typical descent rate profile is presented in Figure 7.23. The normal flight time from liftoff to descent to 80,000 feet is about 36 minutes.

TABLE 7.2

NOMINAL TRAJECTORY SUMMARY

SUPER LOKI ROBIN DART, 80° Q.E. SEA LEVEL LAUNCH

	Booster	Dart
Burnout Altitude (m)	5,176 ft	5,176 ft
Burnout Range (m)	978 ft	978 ft
Burnout Time (sec)	2.1	2.1
Apogee Altitude (m)	7,608 ft	372,000 ft
Apogee Range (m)	1,464 ft	137,000 ft
Apogee Time (sec)	6.1	154.5
Impact Range (m)	1,517 ft	275,000 ft
Impact Time (sec)	108	309

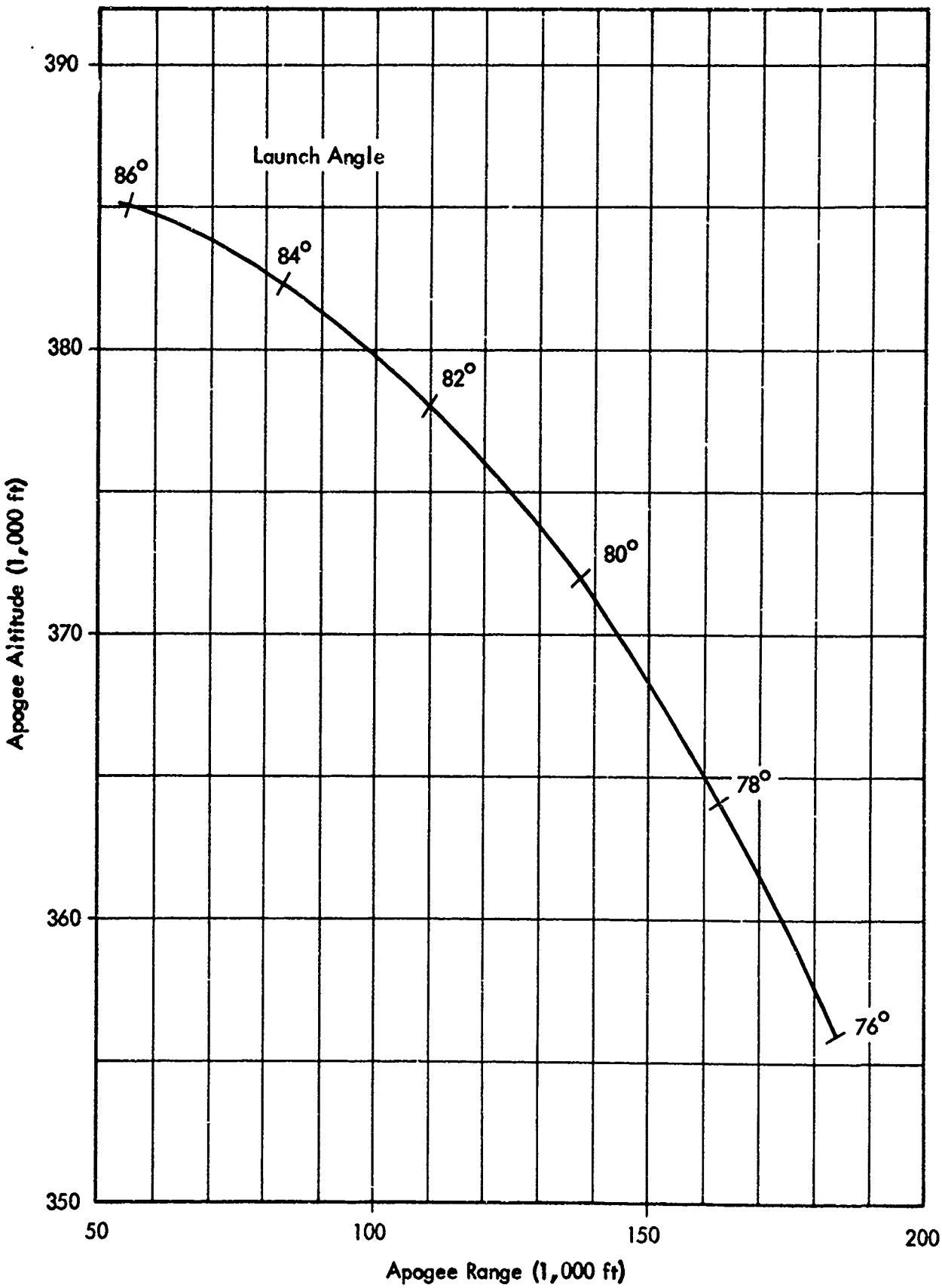

FIGURE 7.13 SUPER LOKI ROBIN DART
APOGEE ALTITUDE VS APOGEE RANGE

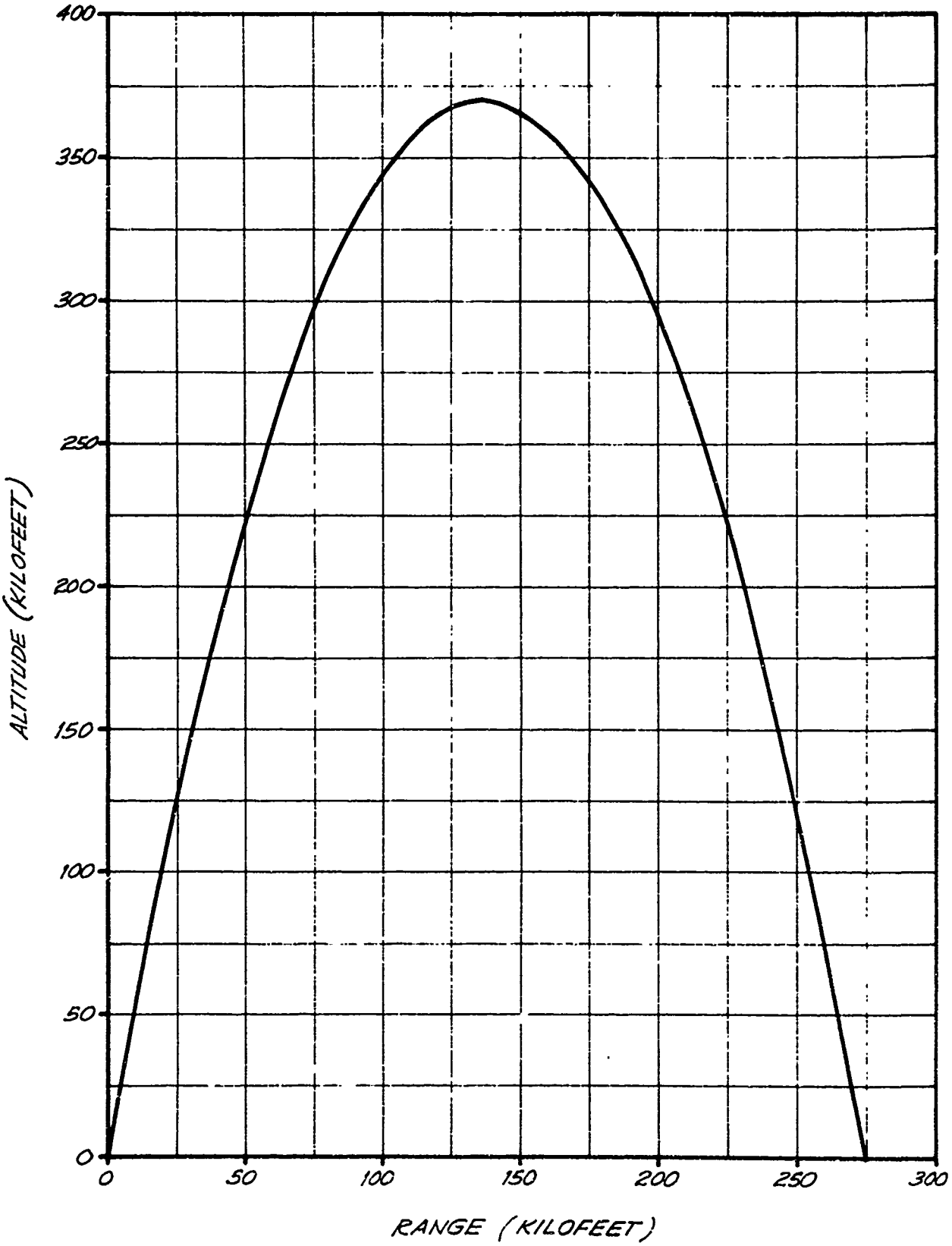

FIGURE 7.14 SUPER LOKI ROBIN D[illegible]LTITUDE VS RANGE 80° Q. E.

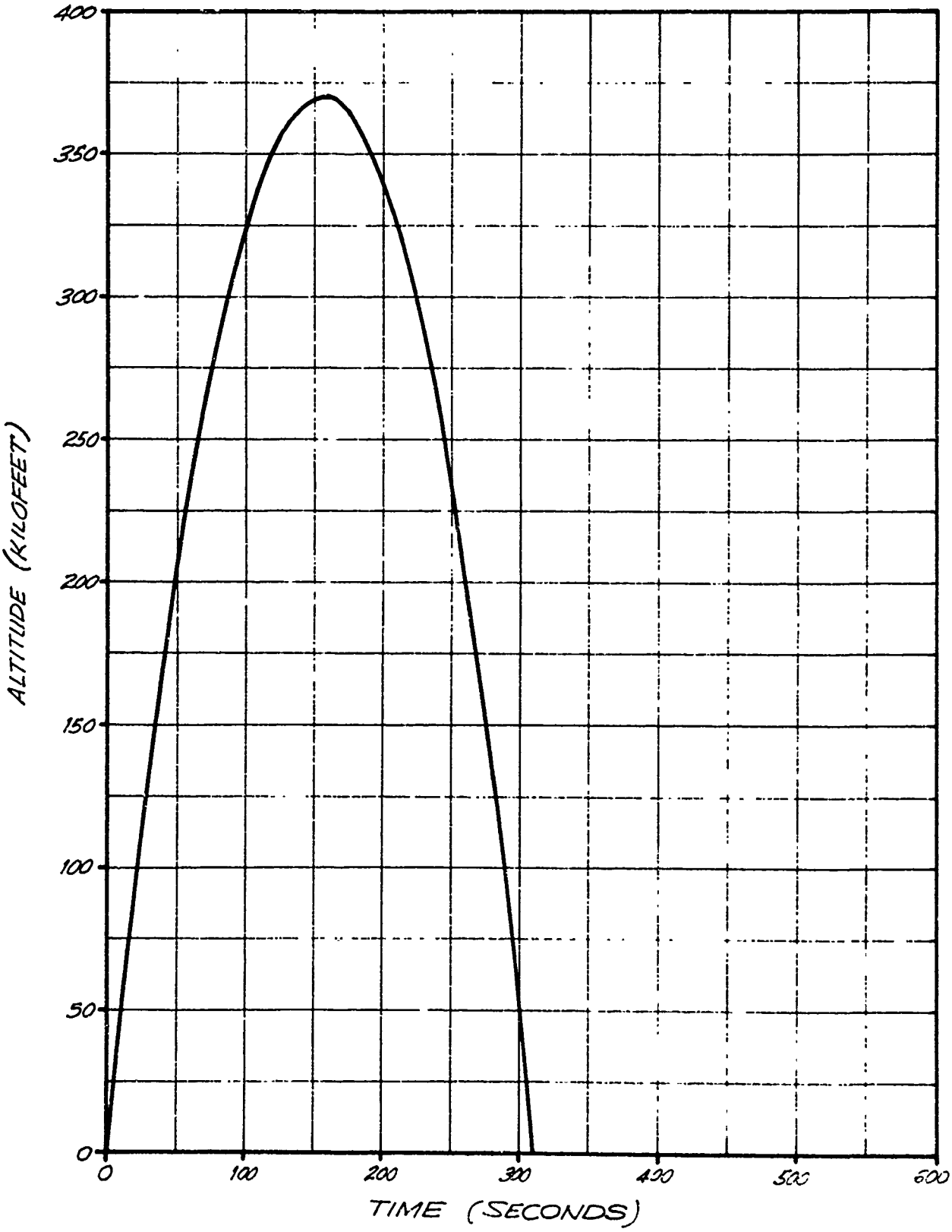

FIGURE 7.15 SUPER LOKI ROBIN DART ALTITUDE VS TIME

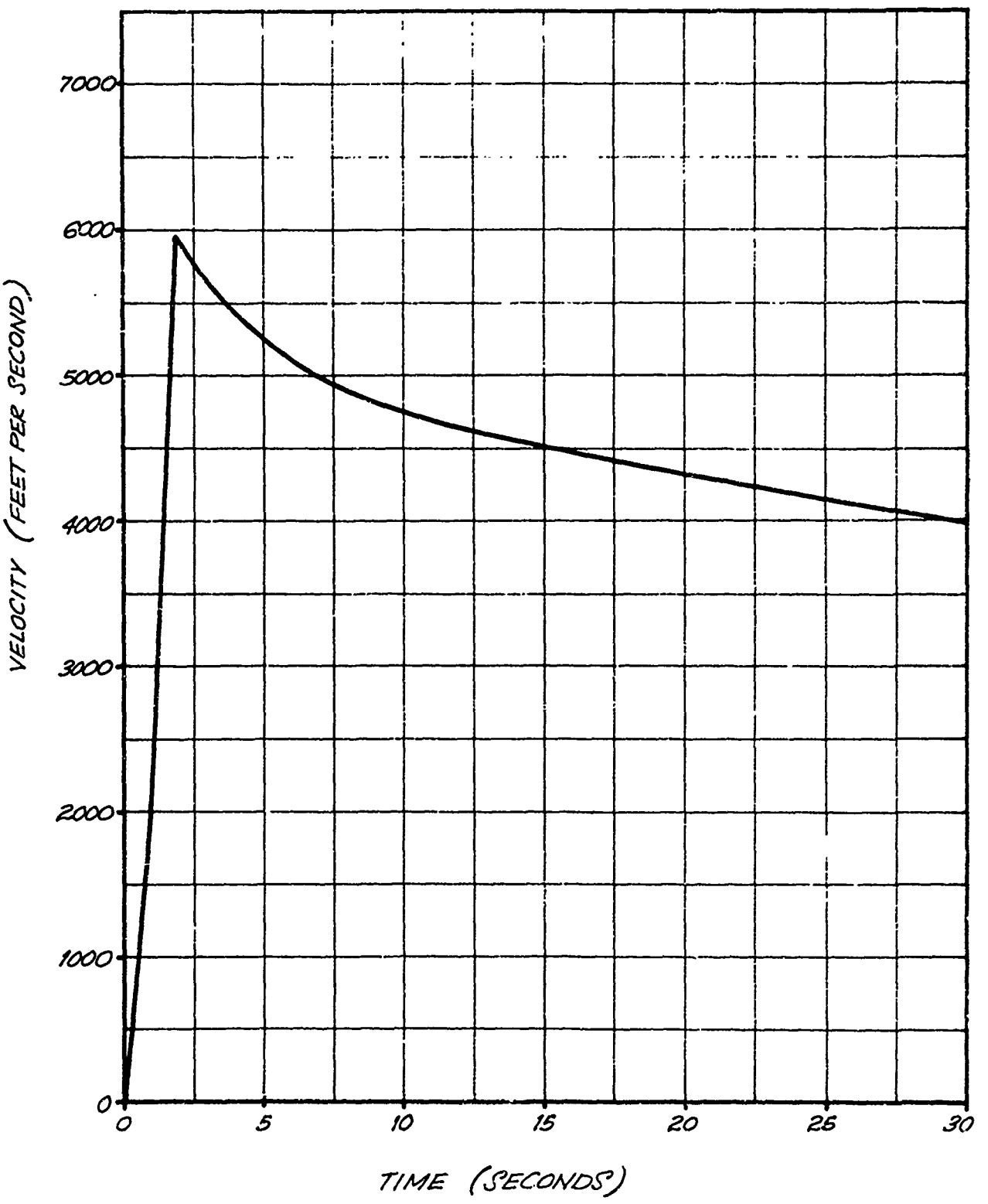

FIGURE 7.16 SUPER LOKI ROBIN DART VELOCITY VS TIME 80° Q. E.

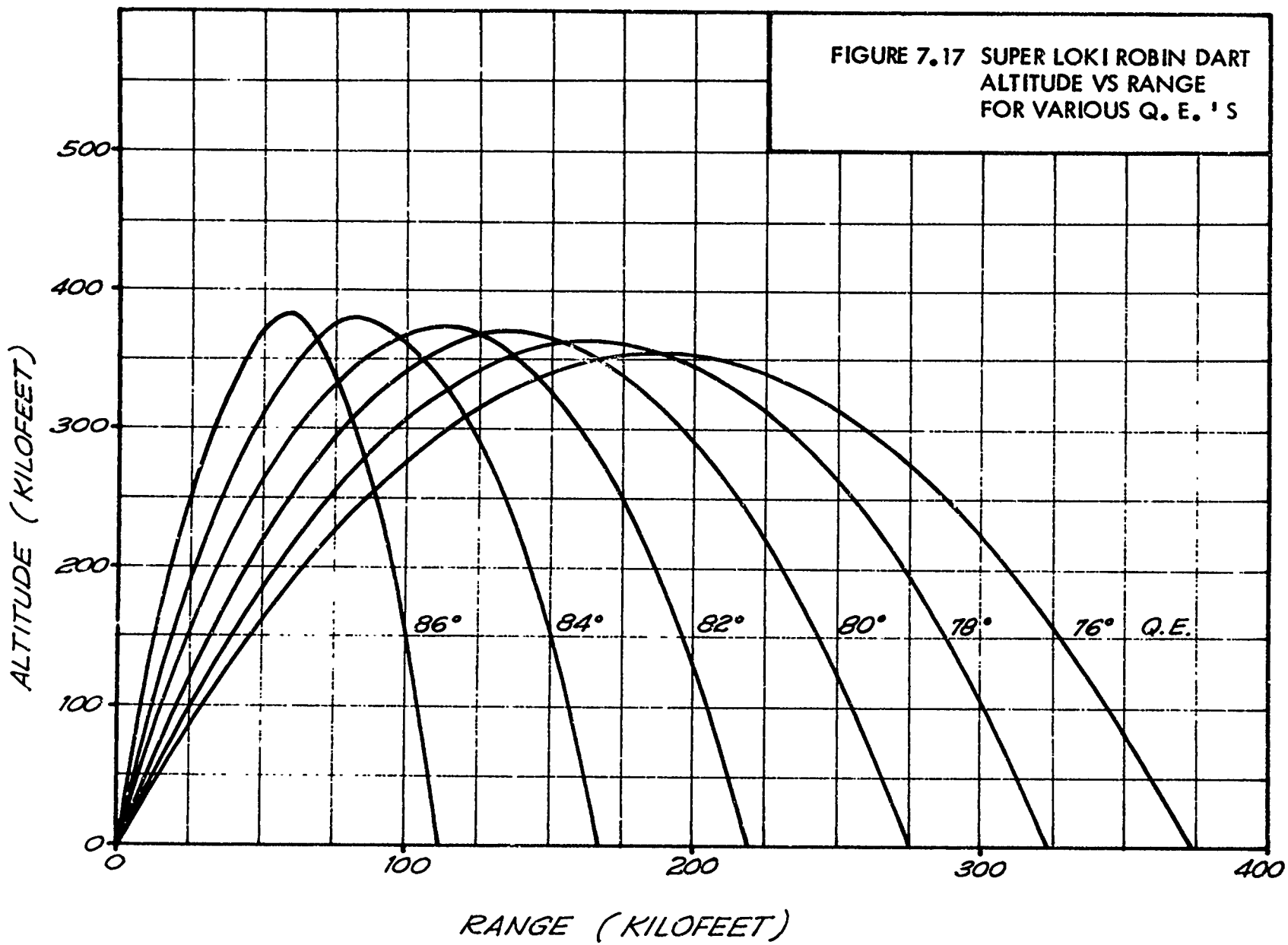
FIGURE 7.17 SUPER LOKI ROBIN DART
ALTITUDE VS RANGE
FOR VARIOUS Q. E. 'S
ALTITUDE (KILOFEET)
500
400
300
200
100
0
86°
84°
82°
80°
78°
76°
Q.E.
0
100
200
300
400
RANGE (KILOFEET)

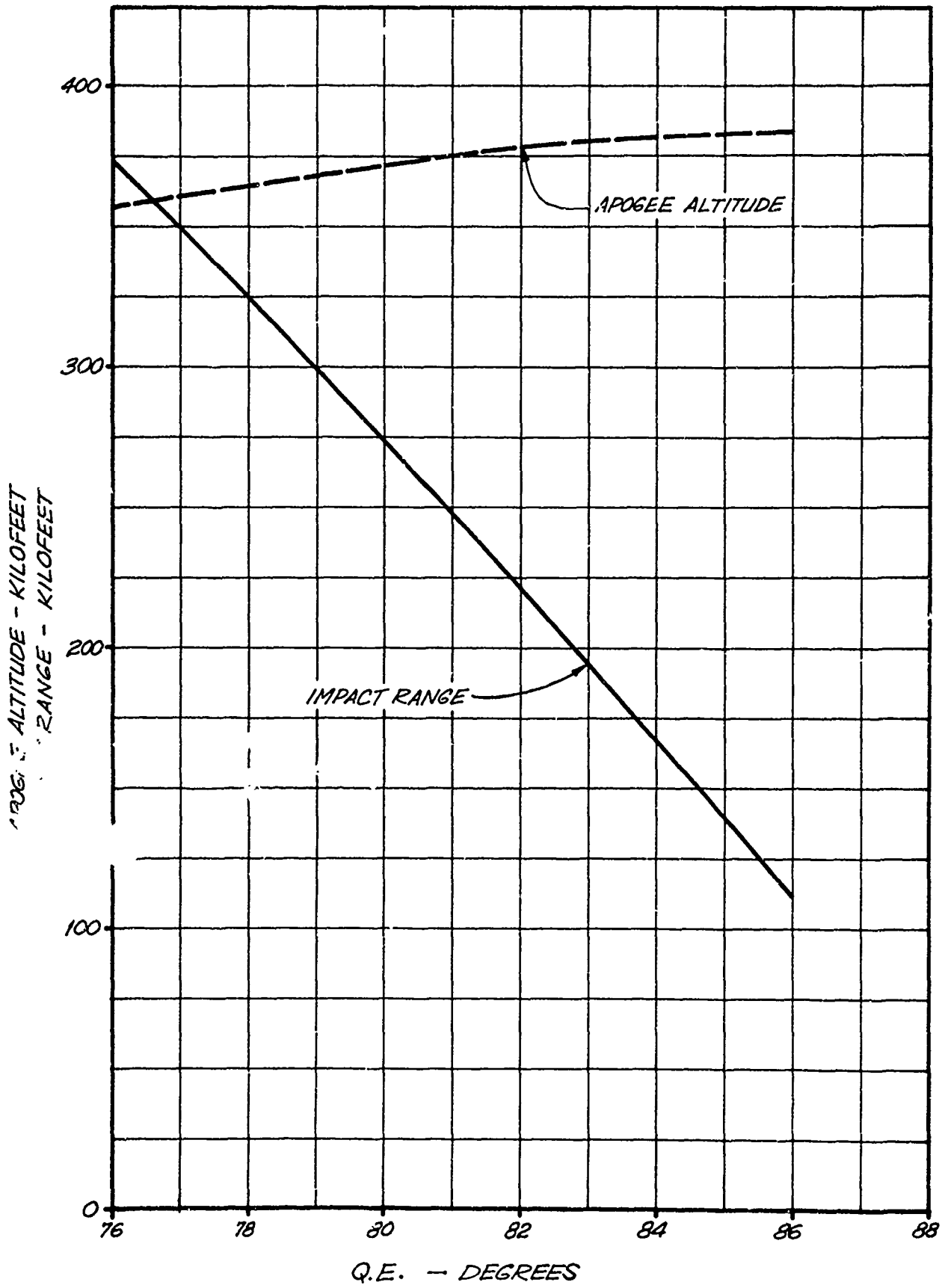

FIGURE 7.18 SUPER LOKI ROBIN DART APOGEE ALTITUDE & IMPACT RANGE VS LAUNCH ANGLE

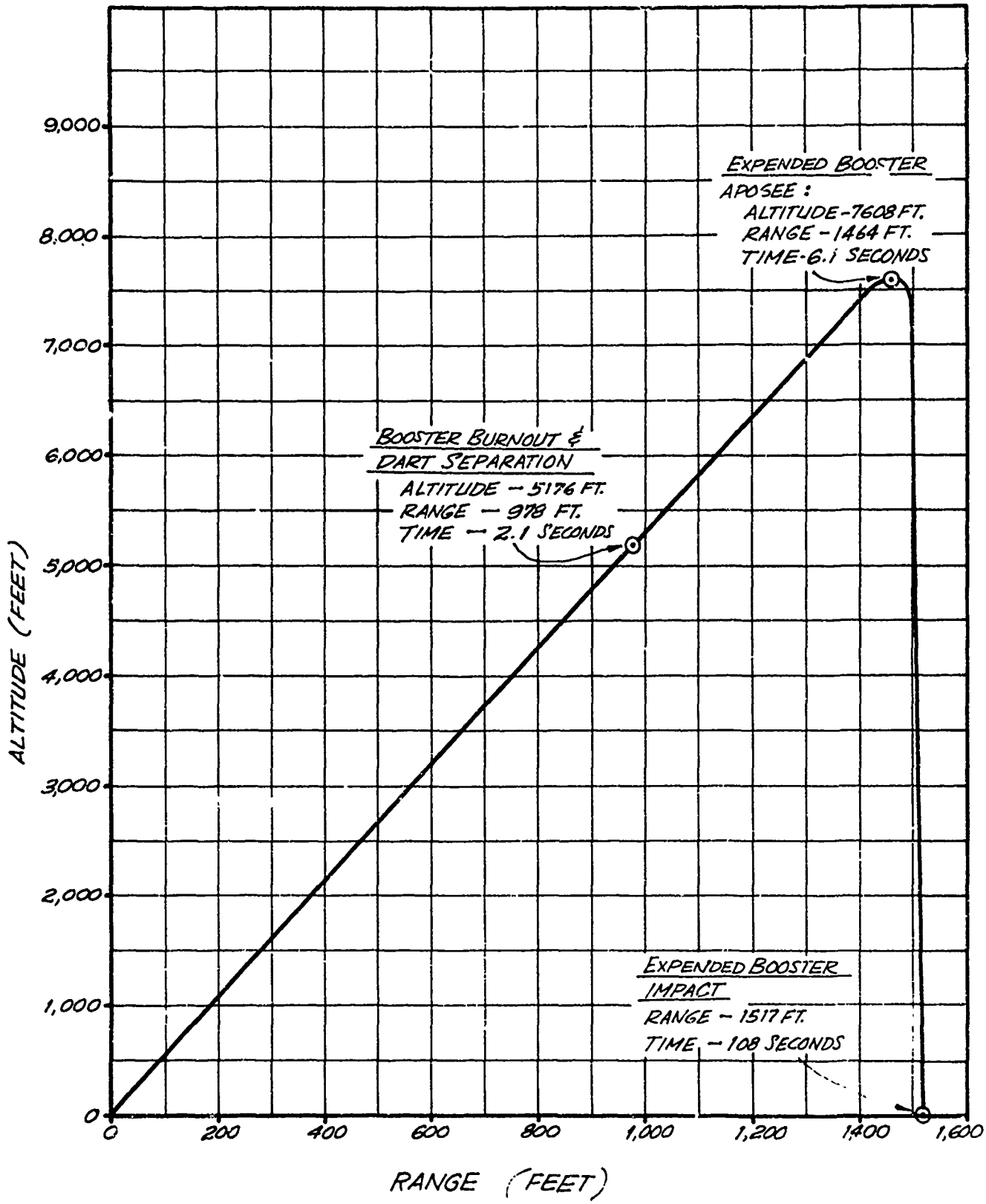

FIGURE 7.19 SUPER LOKI ROBIN BOOSTER NOMINAL TRAJECTORY 80° Q. E. SEA LEVEL LAUNCH

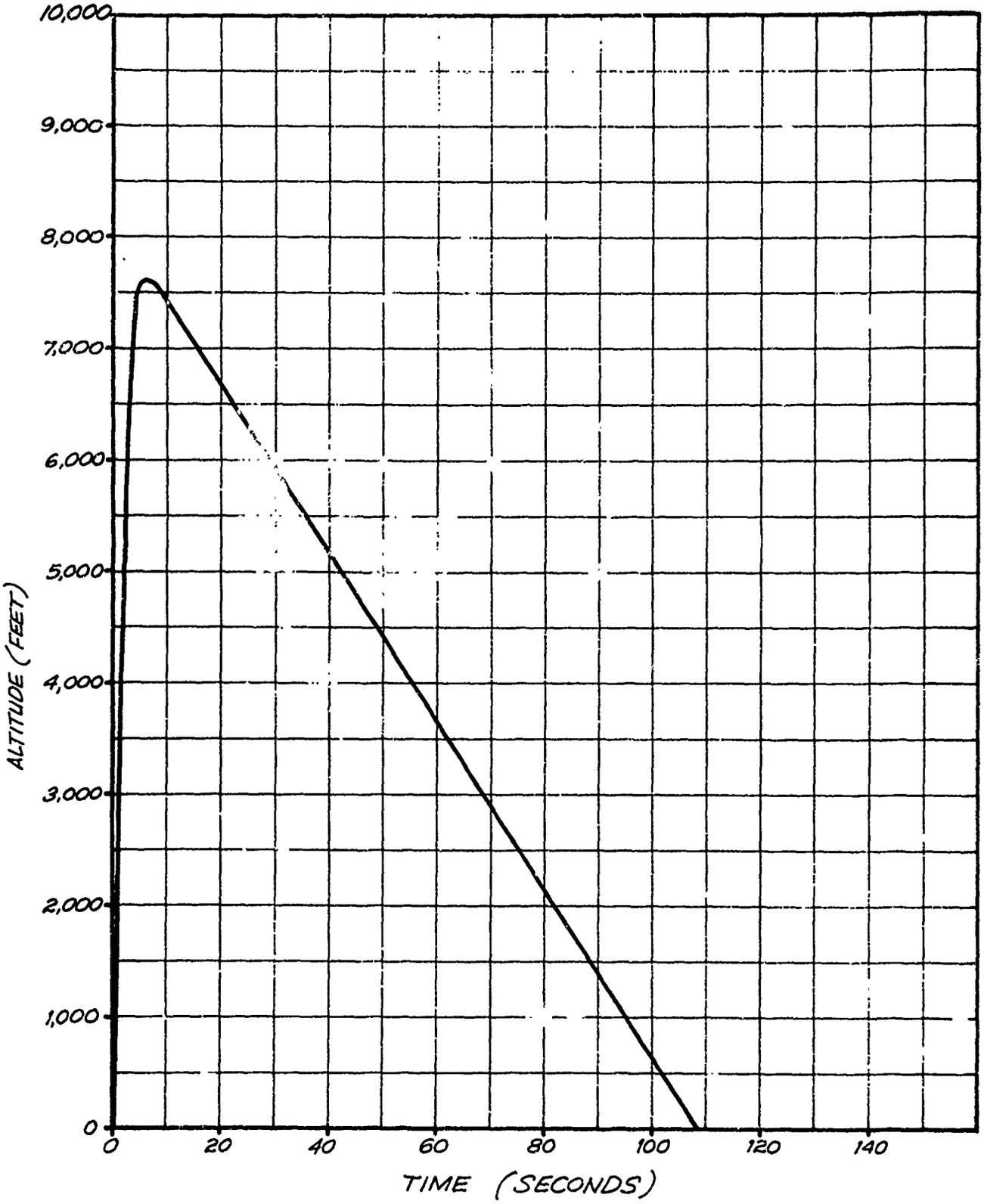

FIGURE 7.20 SUPER LOKI BOOSTER ALTITUDE VS TIME 80° Q. E. SEA LEVEL LAUNCH

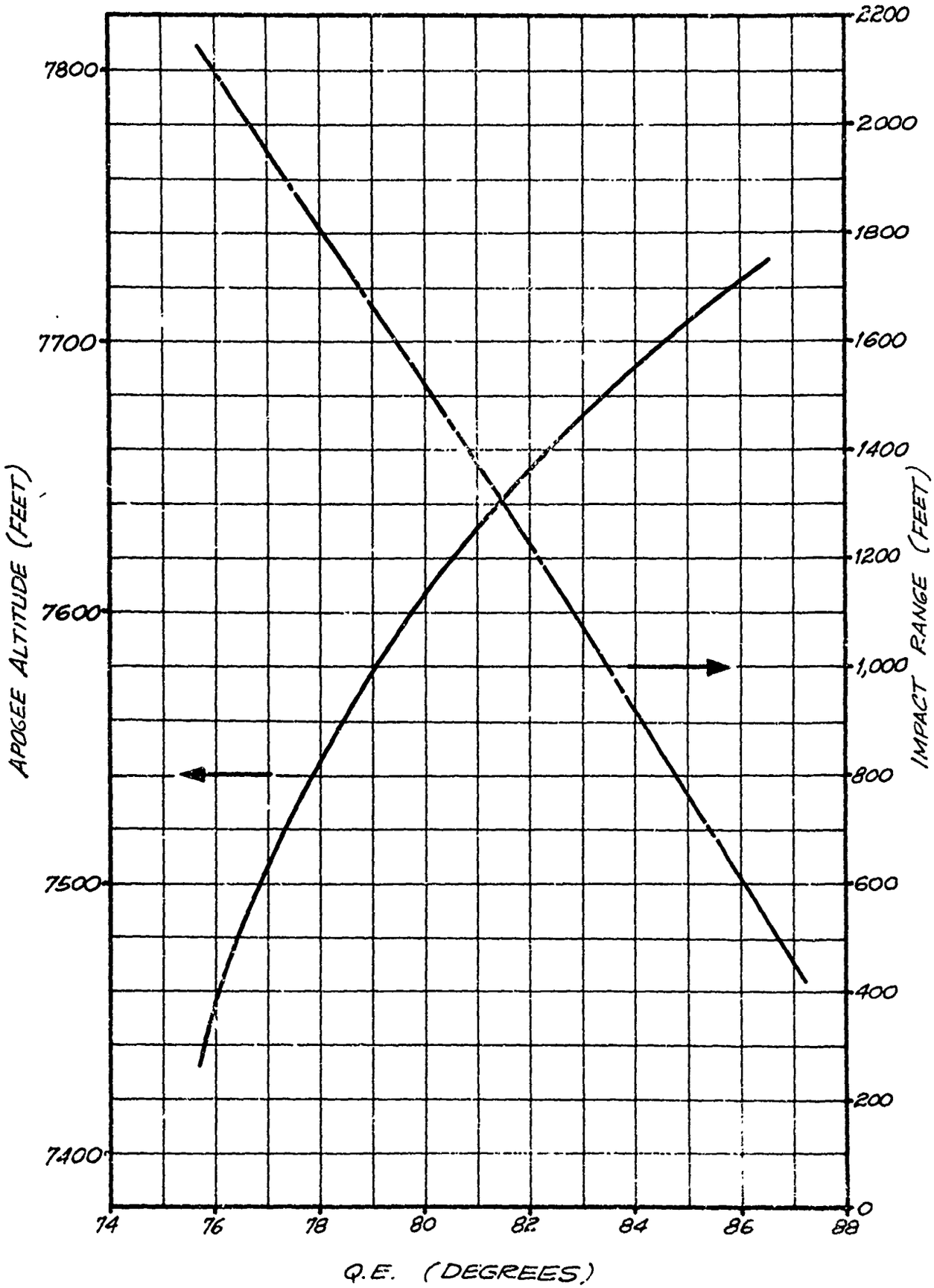

FIGURE 7.21 SUPER LOKI BOOSTER APOGEE ALTITUDE & IMPACT RANGE VS Q. E.

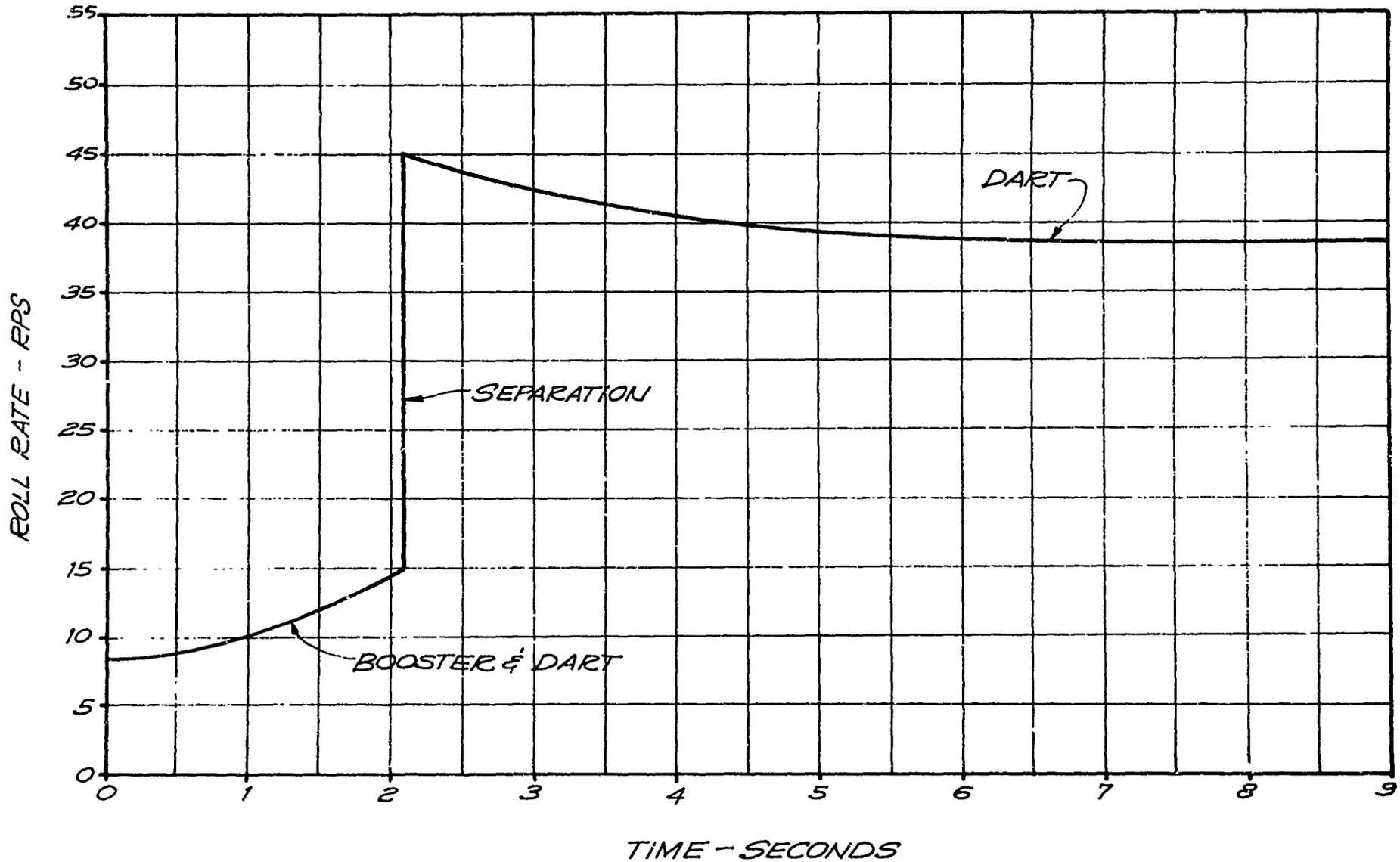

FIGURE 7.22 SUPER LOKI ROBIN DART ROLL RATE VS TIME

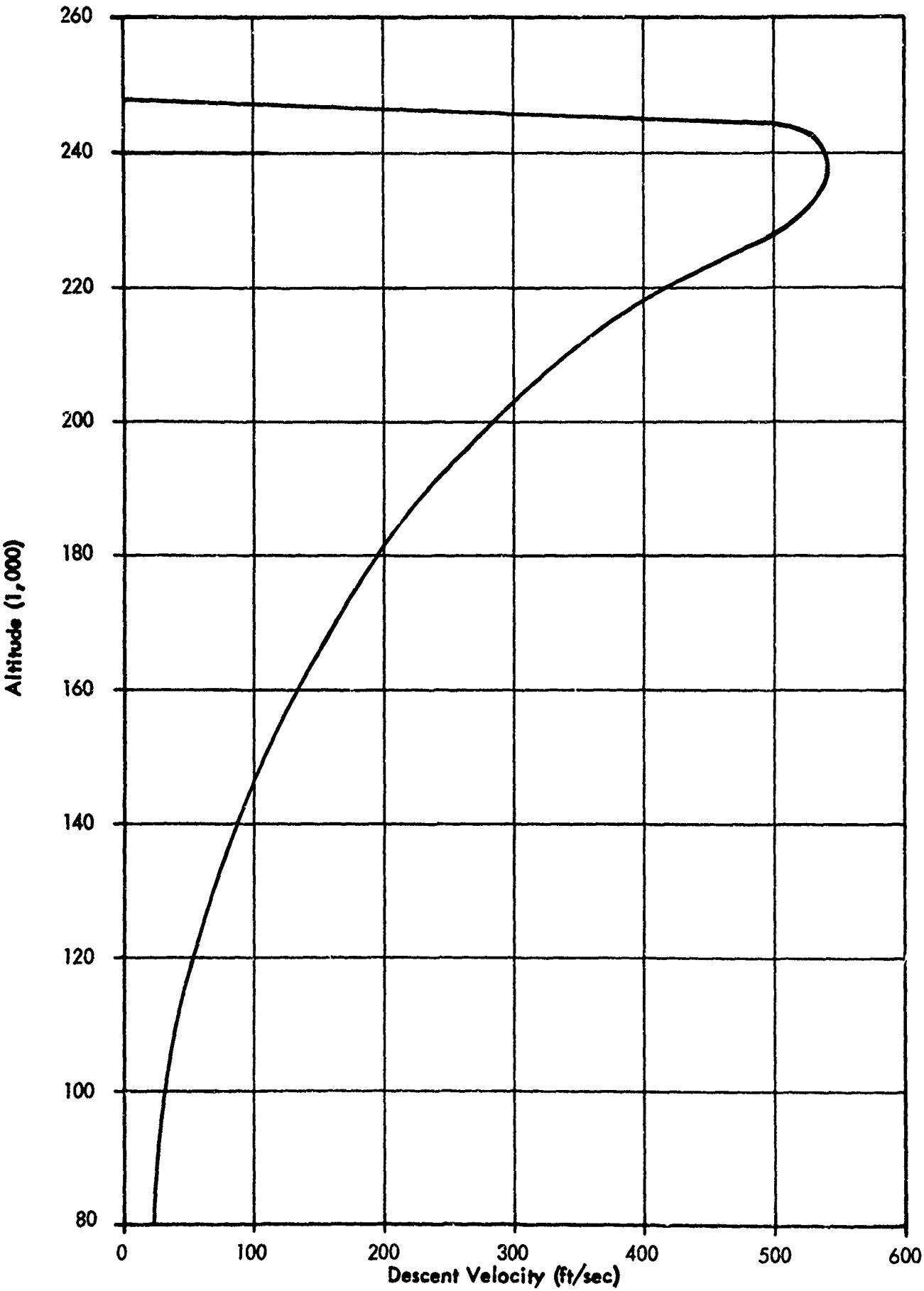

FIGURE 7.23 SUPER LOKI 10' STARUTE DESCENT RATE PROFILE WITH TRANSPONDER INSTRUMENT

7.5 Super Loki Robin

The Super Loki Robin falling sphere payload has a variable drag coefficient since it traverses a descent velocity profile from supersonic to subsonic speeds. Normally the sphere goes through the transonic speed range at about 70 km. The deflation altitude may normally vary from 28 km to 32 km. Higher deflation altitudes are cause for concern since they may be caused by a damaged and leaking sphere. This would indicate a loss of inflatant mass during descent and should be accounted for in the data reduction, Ref. 4. A typical sphere descent profile is presented in Figure 7.24.

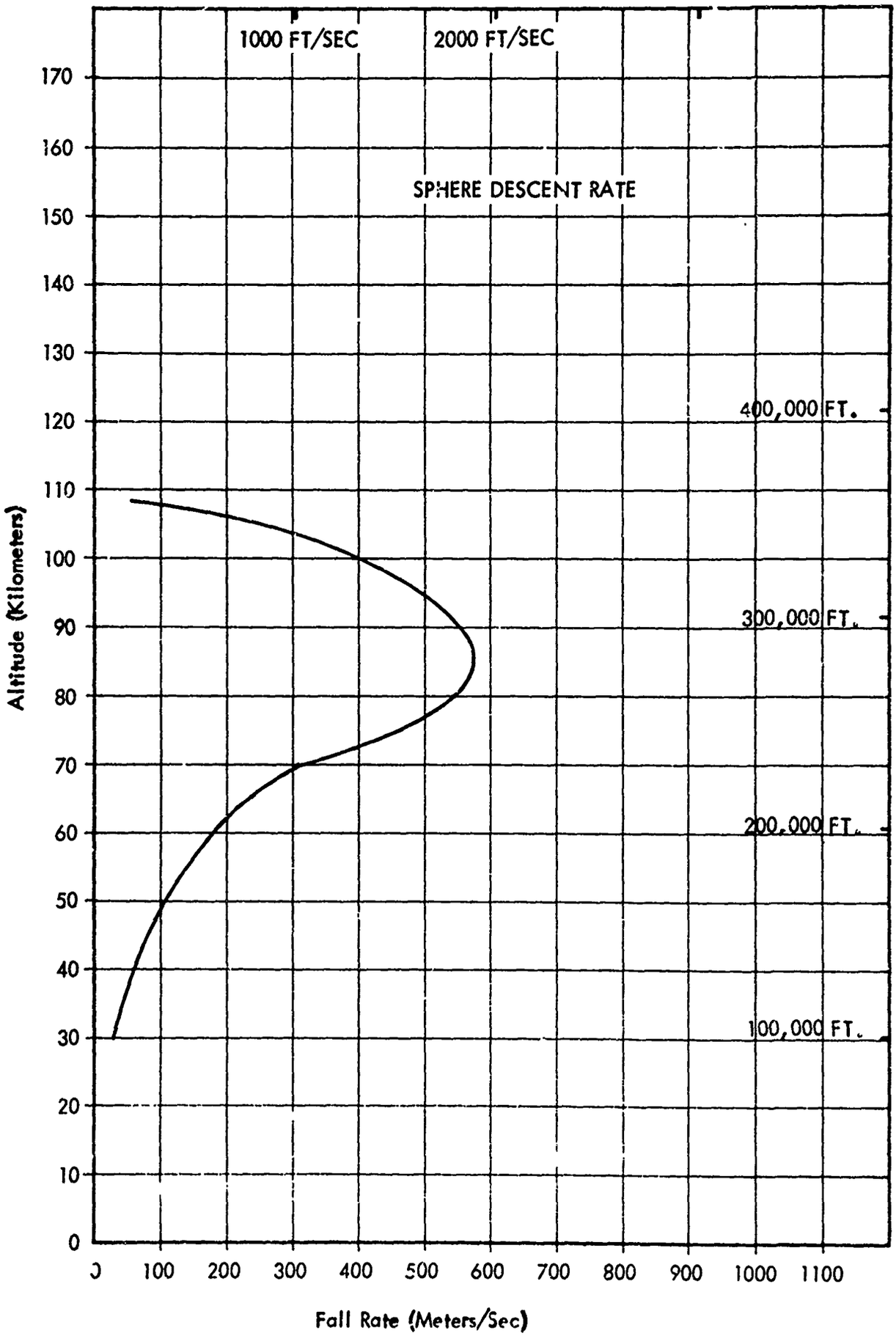

FIGURE 7.24 SUPER LOKI ROBIN

8.

RANGE SAFETY DATA

8.1 General

The range safety data presented here consists of vehicle wind-weighting information, vehicle impact dispersion estimates and ordnance data. This information is presented in the sections which follow.

8.2 Wind-Weighting Data

The wind-weighting data for both of the Super Loki vehicles are presented as follows:

Figure 8.1	Instrumented Dart Wind-Weighting Data
Figure 8.2	Instrumented Vehicle, Booster Wind-Weighting Data
Figure 8.3	Robin Dart Wind-Weighting Data
Figure 8.4	Robin Vehicle, Booster Wind-Weighting Data

8.3 Vehicle Impact Dispersion Data

Impact dispersion three-sigma radii for the instrumented dart and booster are presented in Table 8.1. Impact dispersion three-sigma radii for the Robin dart and booster are based upon the dart and booster having been wind-weighted.

8.4 Vehicle Ordnance Data

The vehicle explosives and electroexplosives ordnance data is presented in Table 8.3. The rocket motor is shipped as ICC Class B, and the dart tails are shipped as ICC Class C.

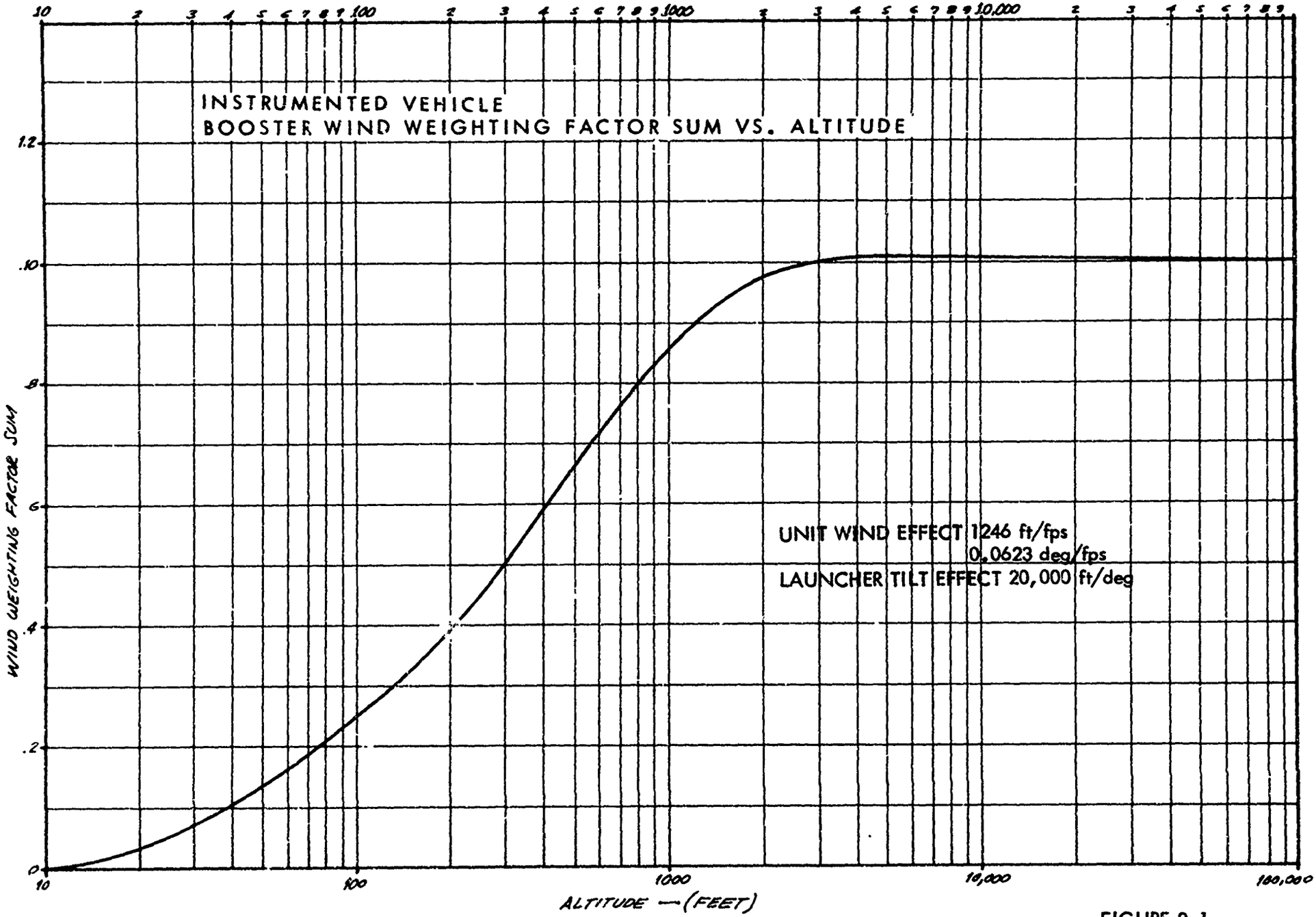
INSTRUMENTED VEHICLE
BOOSTER WIND WEIGHTING FACTOR SUM VS. ALTITUDE
WIND WEIGHTING FACTOR SUM
1.2
.10
.8
.6
.4
.2
0
UNIT WIND EFFECT 1246 ft/fps
0.0623 deg/fps
LAUNCHER TILT EFFECT 20,000 ft/deg
10
100
1000
10,000
100,000
ALTITUDE — (FEET)

FIGURE 8.1

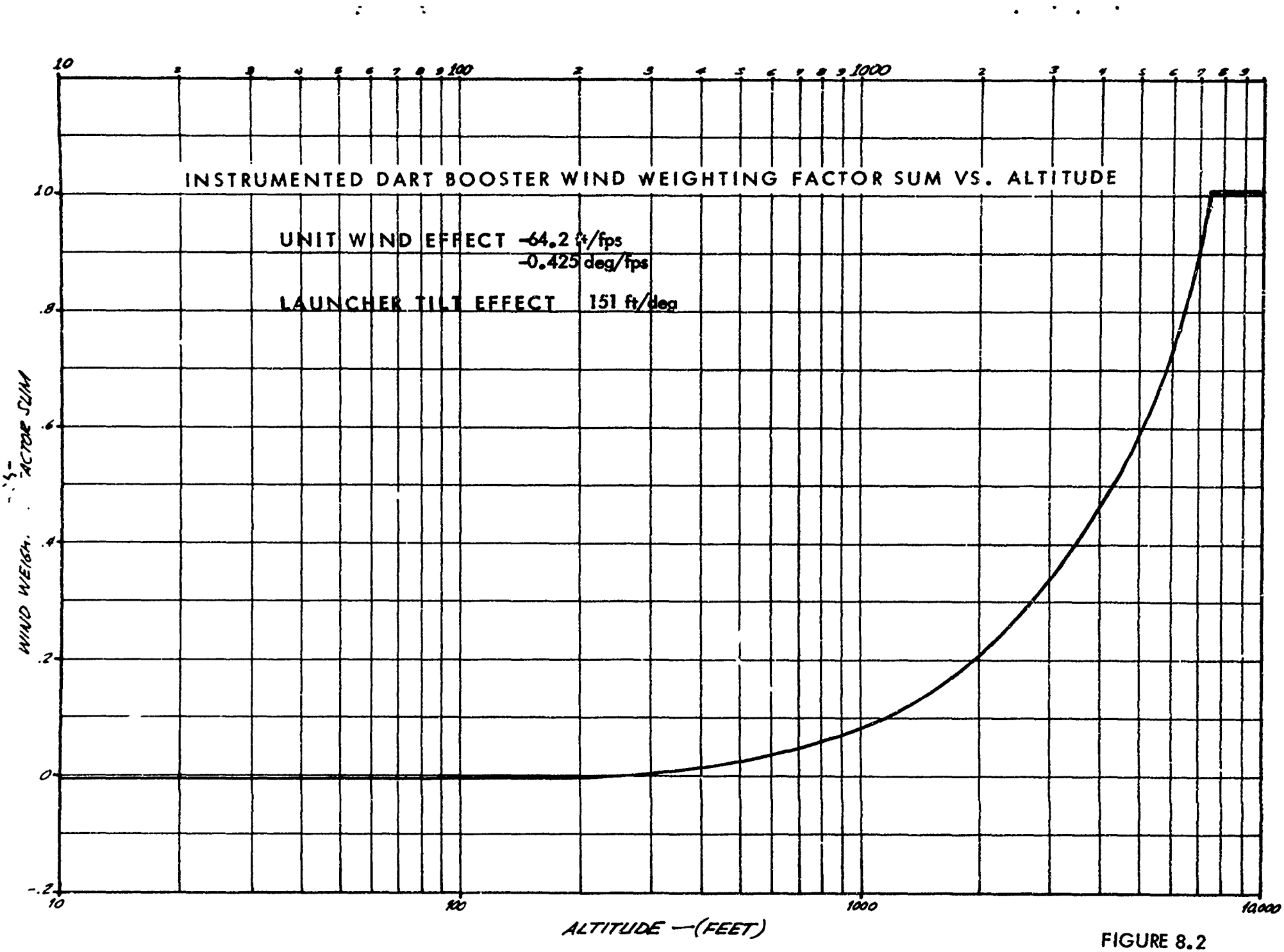
INSTRUMENTED DART BOOSTER WIND WEIGHTING FACTOR SUM VS. ALTITUDE
UNIT WIND EFFECT -64.2 ft/fps
-0.425 deg/fps
LAUNCHER TILT EFFECT 151 ft/deg
WIND WEIGH. FACTOR SUM
1.0
.8
.6
.4
.2
0
-.2
10
100
1000
10000
ALTITUDE —(FEET)

FIGURE 8.2

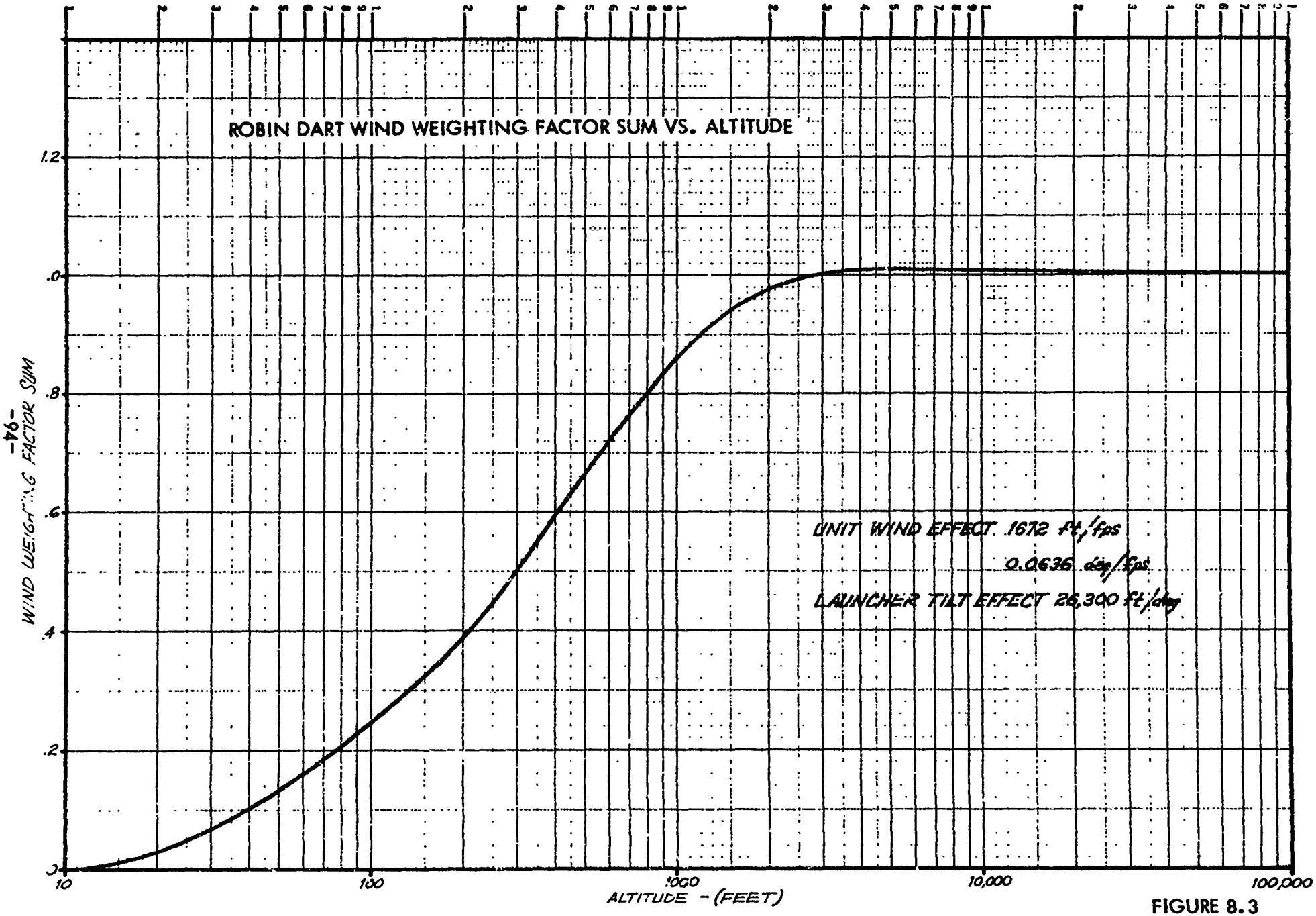
ROBIN DART WIND WEIGHTING FACTOR SUM VS. ALTITUDE
WIND WEIGHTING FACTOR SUM
1.2
1.0
.8
.6
.4
.2
0
10
100
1000
10,000
100,000
ALTITUDE - (FEET)
UNIT WIND EFFECT 1672 ft/fps
0.0636 deg/fps
LAUNCHER TILT EFFECT 26,300 ft/deg

FIGURE 8.3

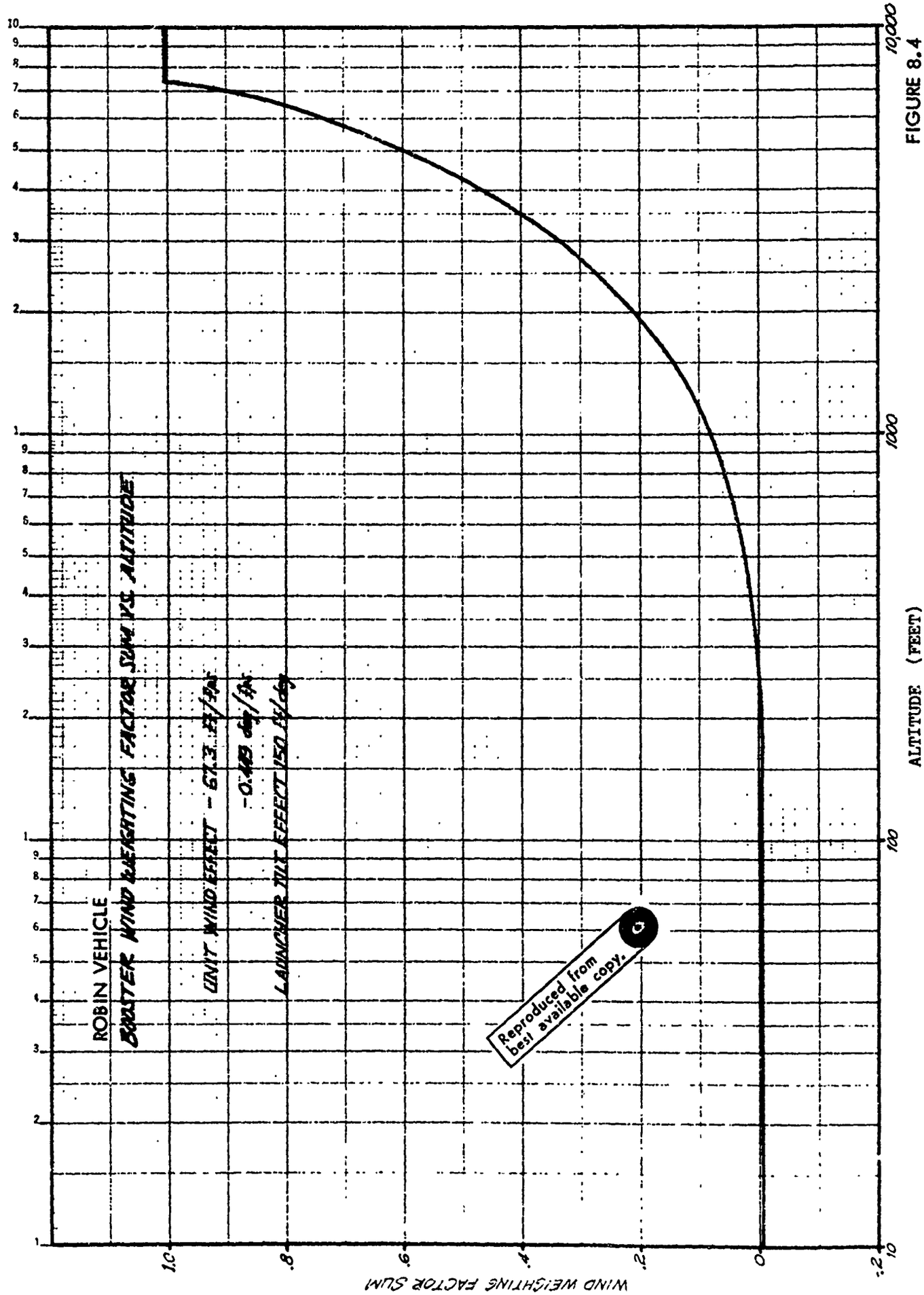
ROBIN VEHICLE
BOOSTER WIND WEIGHTING FACTOR SUM VS ALTITUDE
UNIT WIND EFFECT - 67.3 ft/sec
-0.43 deg/kt
LAUNCHER TILT EFFECT USA Style
WIND WEIGHTING FACTOR SUM
ALTITUDE (FEET)
Reproduced from best available copy.

FIGURE 8.4

TABLE 8.1

IMPACT DISPERSION DATA

INSTRUMENTED VEHICLE

Vehicle Stage	Dart	Booster
80° QE Impact Range	170,679 ft.	1330 ft.
Maximum Three-Sigma Impact Dispersion Radius	18,600 ft.	450 ft.

TABLE 8.2

IMPACT DISPERSION DATA

ROBIN VEHICLE

Vehicle Stage	Dart	Booster
80° QE Impact Range	275,000 ft.	1,517 ft.
Maximum Three-Sigma Impact Dispersion Radius	31,220 ft.	450 ft.

TABLE 8.3

ORDNANCE DATA

Item	Explosive		Electrical Squib Characteristics		
	Weight	Type	No-Fire	Resistance	All-Fire
Rocket Motor Propellant	37.20 lb	Polysulfide Ammonium Perchlorate	-	-	-
Rocket Motor Igniter	50 grams	Cupric Oxide Aluminum Powder	1 watt/1 amp 5-minutes each squib	1.15 ohms ±0.15 ohms each squib	5.0 amps each squib
Dart Payload Separation Device with Time Delay Transponder, 120 sec. Robin, 135 sec.	 8 grams 3.5 grams	Boron Potassium Nitrate	1 watt/1 amp 5-minute	-.05 ohms ±0.25 ohms	5.0 amp

9.

DEVELOPMENT PROGRAM

9.1 General

Note 4

Previous sections cover the final configurations that were developed under this contract. Under a separate effort, they are currently being put through Government qualification tests prior to their being produced for operational use.

In Sections 9, 10, and 11 the details of the development and many tests leading to these final configurations are discussed. Section 9 is a narrative of the many test sequences. While there were multiple and non-consecutive groups of reasons for each test, an attempt has been made to break the tests into four categories. It should be mentioned that any conclusion at any single point during test sequences are not necessarily final conclusions, but conclusions as of that particular point in time. They may be found modified as the program progressed.

The Super Loki development program consisted of the design, development, and flight testing of three different payload systems, two basic rocket vehicles and a number of new components. This development led to the final designs shown in Sections 3 through 8.

The vehicle analysis and design efforts in general followed along routine procedures of performance analyses, computer trajectories, stability analysis, dispersion and wind-weighting studies in addition to an assessment of aerodynamic heating and launch dynamics. No significant problems were encountered in the vehicle development program that were not eventually solved.

The Starute development entailed various fabrication studies and structural testing. A number of structural modifications were made during the course of the flight test program. Also a number of different radar reflectivity patterns were fabricated for flight evaluation to enhance the radar signal returns for remote launch sites with marginal radars.

Although the Robin 1-meter diameter inflatable sphere had been developed previously, significant development effort was expended on the design of a new inflator. This was to improve the reliability of the sphere inflation. Both aluminized spheres and spheres with internal corner reflectors were flight tested to evaluate the radar reflectivity patterns and data accuracies.

The transponder instrument was designed and developed as an in-house program at

AFCRL. The transmitter instrument was also designed and developed at AFCRL. The only significant instrument problems appeared to be physical antenna and suspension lanyard problems. A major cause for telemetry signal dropouts, and thereby problems in coarse ranging, was found to be Starute instability. This was eventually attributed to overheating damage of the Starute material during vehicle ascent.

The most significant problem in the development program was the severe aerodynamic heating of the dart vehicle and the subsequent overheating of the payloads. Both the Robin spheres and the Starutes are made from thin-film Mylar and are subject to failure when the become overheated. A cost reduction goal in the program was to eliminate the rather costly ablative coating as a means of coping with the aerodynamic heating problem. A great deal of effort was expended to provide other means for thermal protection of the payloads. The methods investigated included highly emissive dart exteriors, air gaps between the dart wall and the payload, high reflective surfaces on the payload staves and the use of various insulating materials. Ultimately, the twelve-foot Starute had to be reduced in size to ten feet to permit a sufficient air gap in the 2-1/8-inch diameter instrumented dart for reliable Starute performance. Since there was not sufficient space in the 1-5/8-inch diameter Robin dart for adequate thermal protection, the ablative coating had to be used. In fact, a relatively thick coating was found to be required for reliable Robin performance.

Although efforts in some of the problem areas continued through overlapping periods of the development program, a discussion of these problems, and the efforts to solve them, are separated into distinct topics in the following sections. First, however, a brief history of the development flight tests is presented.

9.2 Development Flight Tests

The development flight tests can be divided into four categories or groups in accordance with the overall purpose of each of the tests. Although all of the flights could be considered as systems development and evaluation, the vehicle development tests were carried out initially to establish the rocket vehicle design, performance and reliability. Once this was established, the major attention was directed toward flight evaluation, redesign and reliability improvement of the various payloads. Although minor vehicle problems become evident as the flight testing progressed, these problems were quickly resolved. The major problem area throughout the program was adequate thermal protection of the Starute decelerator and the Robin sphere. These problems were not finally resolved until the latter flight test series of the program. A summary of the flight test program is presented in the next sections.

9.2.1 Robin Vehicle Development Flight Tests

A summary of the initial flight tests which were devoted to the development of the rocket vehicle is presented in Table 9.1. A review of the flight tests is presented in the paragraphs which follow.

TABLE 9.1 FLIGHT TEST SUMMARY - VEHICLE DEVELOPMENT - 2 1/8" INSTRUMENTED DART

Flight Series	1	1	1	1
Fligh. No.	1	2	3	4
Date	7-23-69	7-23-69	7-24-69	7-24-69
Range	WTR	WTR	WTR	WTR
Test Purpose	Vehicle Development	Vehicle Development	Vehicle Development	Vehicle Development
Launch Elevation Angle (deg)	85.0	85.0	85.0	85.0
Vehicle Performance	Good	Good	Good	Good
Apogee Altitude (1,000 ft)	Late Radar	238 est	240 est	Late Radar
Deployment Time (sec)	Late Aq.	Late Aq.	Late Aq.	Late Aq.
Starute Size & Type	12'A	12'A	12' B	12'C
Starute Performance	Late Inflation, Unstable	Unstable	Good	Very Slow
Ballistic Coefficient (lb/ft^2)	.060 - .030	.017	.016	Suspect Radar Data
Sonde Type	Datasonde	Datasonde	Datasonde	Datasonde
Sonde Performance	Good; Dropouts	Good; Dropouts	Good	Good
Temperature Data	Internal	Internal	Internal	Internal
Comments	Signal dropouts indicate damaged Starute. Launcher slipped up 2° in elevation.	Signal dropouts indicate damaged Starute. Launcher slipped up 2° in elevation	Booster fins damaged by launch rail ring bulkheads.	

TABLE 9.1 FLIGHT TEST SUMMARY - VEHICLE DEVELOPMENT - 2 1/8" INSTRUMENTED DART (continued)

Flight Series	2	3	3	3
Flight No.	5	6	7	8
Date	9-25-69	11-3-69	11-3-69	11-5-69
Range	WTR	WTR	WTR	WTR
Test Purpose	Vehicle Development	Vehicle Development	Vehicle Development	Vehicle Development
Launch Elevation Angle (deg)	76.0	80.0	80.0	80.0
Vehicle Performance	*Unknown*	*Late Radar*	*Late Radar*	*Late Radar*
Apogee Altitude (1,000 ft)	No Track	Unknown	Unknown	Unknown
Deployment Time (sec)	Unknown	Late Aq.	Late Aq.	Late Aq.
Starute Size & Type	12' C	12' C	12'C	12' C
Starute Performance	*Unknown*	*Fair, Unstable*	*Sonde Separated*	*Sonde Separate*
Ballistic Coefficient (lb/ft^2)	Unknown	.022	---	---
Sonde Type	Datasonde	Datasonde	Datasonde	Datasonde
Sonde Performance	Unknown	Good; Dropouts	RAOB Interference	---
Temperature Data	Internal	CRL Mount	Internal	CRL Mount
Comments	Damaged Launch Rails	---	Sonde separated from Starute and splashed in 11.5 minutes.	Sonde separated from Starute and splashed in 7.5 minutes.

TABLE 9.1 FLIGHT TEST SUMMARY - VEHICLE DEVELOPMENT - 2 1/8" INSTRUMENTED DART (continued)

Flight Series	4	4*	4*	4
Flight No.	9	10	11	12
Date	1-14-70	1-15-70	1-15-70	1-15-70
Range	ETR	ETR	ETR	ETR
Test Purpose	Vehicle Development	Vehicle Development	Vehicle Development	Vehicle Development
Launch Elevation Angle (deg)	80.0	80.0	80.0	80.0
Vehicle Performance	Good	Good	Good	Low
Apogee Altitude (1,000 ft)	238	253	250 est	Low
Deployment Time (sec)	111	105	Unknown	Unknown
Starute Size & Type	12' C	12' C	12' C	12' C
Starute Performance	Good	Pieces Off	Pieces Off	----
Ballistic Coefficient (lb/ft^2)	.018	.018	.021	----
Sonde Type	Datasonde	Datasonde	Datasonde	Transponder
Sonde Performance	Good	Good; Some Dropouts	Good	----
Temperature Data	Internal	Internal	Internal	CRL Mount
Comments	Good Data, Internal Temp Max 75°C	2" Dia. Dart Good Altitudes. Starute Damage.	Booster Fins Hit forward launch rail. Good altitude. Starute Damage	Vehicle splash at 110 sec - No Data

* 2.00" diameter dart

TABLE 9.1 FLIGHT TEST SUMMARY - VEHICLE DEVELOPMENT - 2 1/8" INSTRUMENTED DART

Flight Series	5	5	5	6	6
Flight No.	13	14	15	16	17
Date	3-10-70	3-10-70	3-11-70	4-7-70	4-7-70
Range	ETR	ETR	ETR	ETR	ETR
Test Purpose	Booster Fin Launch Rail Spacing	Booster Fin Launch Rail Spacing	Booster Fin Launch Rail Spacing	Starute Thermal Protection	Starute Thermal Protection
Launch Elevation Angle (deg)	80.0	84.0	82.0	84.0	80.0
Vehicle Performance	Fair	Good	Fair	Good	Fair
Apogee Altitude (1,000 ft)	224	263	230	240	226
Deployment Time (sec)	103	103	111	117	117
Starute Size & Type	12' C	12' C	12' C	12' C	12' C
Starute Performance	Breakup, Early Splash	Breakup, Early Splash	Breakup, Early Splash	Good, No Pieces	Good, No Pieces
Ballistic Coefficient (lb/ft^2)	---	---	---	.015	.015
Sonde Type	Datasonde	Transponder	Transponder	Datasonde	Datasonde
Sonde Performance	Good; Dropouts	Good; Dropouts	Good; Dropouts	Good	Good
Temperature Data	Internal	Resistor	Resistor	Internal	Internal
Comments	Internal Temps extrapolated to above 100°C. Starute breakup.	Good vehicle perf., but Starute breakup.	Starute breakup.	Good Flight, Max internal temp 54°C.	Good Flight, Max internal temp 68°C.

The first flight test series consisted of four (4) similar 2-1/8-inch diameter dart systems launched at Vandenberg AFB on 23 and 24 July 1969. All four of the systems appeared to function satisfactorily in spite of launcher problems. In all cases booster burnout and dart separation appeared to be normal. Late radar acquisitions of only the descending payload do not permit an accurate determination of apogee altitude, however, extrapolations indicate an approximate payload apogee of about 240,000 feet with an 85-degree Q.E. Since the GMD did not obtain an uptrack on any of the flights, it is difficult to determine payload separation times.

Starute inflation appeared to be very late on the first flight where radar acquisition was also very late. The Starutes appeared to function properly on all of the other flights with $B = 0.017$ lb/ft^2.

In general, good atmospheric temperature profiles were obtained with the basic limitations being late acquisition by either the radar or GMD. On the first flight, however, 17 minutes of temperature data were lost due to rather rapid oscillations in signal strength. Two minutes of data were lost on the second flight for the same reason. The last two flights did not exhibit this fault. Initially this problem was believed to be correlated with sonde prelaunch turn-on time and the associated heating or a sonde antenna pattern problem. However, later in the program it was ascertained that this flight result was due to a damaged Starute which causes asymmetrical air flow. This air flow pattern forces the descending Starute into a rapid coning motion which results in signal droupouts due to the antenna null pattern.

Prior to the first launch, a grease lubricant was erroneously applied to the launcher elevation lock washer and quadrant. During the first flight, the launch moments caused a two-degree slip (increase) in the elevation setting. After this flight, the grease was discovered and it was wiped from the quadrant and lock washer. The second flight then caused a 0.6-degree slippage. After this quadrant and lock washers were thoroughly cleaned with a solvent and roughened with a file. No further elevation setting slippages occurred. A photograph of the rocket system in the launcher is presented in Figure 9.1.

The Super Loki expended boosters were recovered on the last two flights. Two adjacent fins on each of these boosters showed abnormal damage to the fin tips as though they had impacted with a ring bulkhead of the launch rail. This problem was analyzed as too great a tolerance in the inner diameter of the ring bulkheads, and the launch rail was returned for rework. The launch rail was received from VAFB, inspected and the problem was ascertained to be booster fin-launch ring bulkhead interference. Aluminum strips were bolted onto the

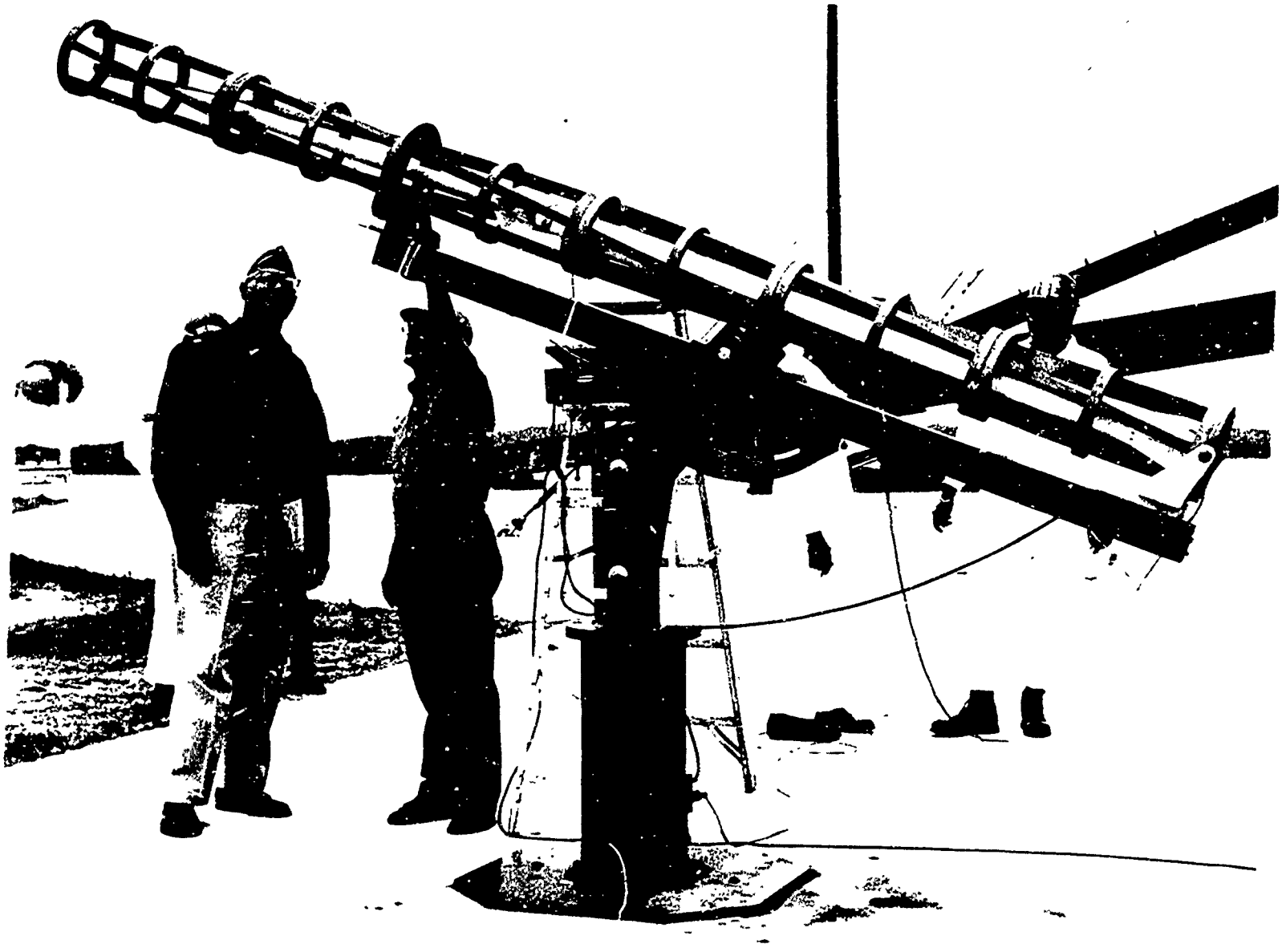

FIGURE 9.1 SUPER LOKI ROCKET VEHICLE IN STD. LAU-66 LOKI LAUNCHER AT VAFB (WTR).

launch rails to reduce the diametral clearance between the rocket motor and the launch rails so that booster fin clearance was assured. The launch rail was then returned to VAFB for the second series of flight tests. Four vehicle systems were fabricated and sent to VAFB for the second flight test series. These systems also contained the standard Datasonde instruments modified by the incorporation of a phenolic spacer about the instrument ground plane to eliminate the carrier signal droupouts which were prevalent during the first flight test series. High temperature thermistors were embedded into the sonde adapter rings to measure sonde skin temperature on two of the units. The other two units were to receive CRL thermistor mounts.

A Super Loki 2 1/8-inch dart system was launched at WTR during September, 1969 as flight 2-5, but neither radar nor GMD acquired a track. Vehicle performance is unknown. A post flight inspection of the launch site revealed damage to the forward end of one of the launch rails. The launch rail assembly was returned to Space Data for inspection. The launch rail adapters on the forward six-foot section were found to protrude about 1/16" above the rear rails. It is believed that the motor aft end bourelette impacted upon one of the stepped-up rail sections and retarded the vehicle spin. This in turn may have caused a booster fin to impact on the damaged portion of the launch rail. The cause of the launch rail tip bending is unknown at this time. An analysis of motion pictures taken during the launch did not reveal any indication of the damage, but did indicate that the vehicle was spinning immediately after launcher exit.

A launch dynamics analysis indicated that the booster spin rate could be sufficiently retarded after dart fin release so that a booster fin might impact against the launch rail. Thus, the alignment of dart fins to booster fins was altered on subsequent flights to allow for a greater safety margin in booster roll rate retardation.

The launch rail was modified by reboring inside diameter of the forward six-foot section for improved booster motor clearance. The booster fin span was also reduced by 1/8" per fin to permit adequate clearance from the launcher rail ring bulkheads. A vehicle stability analysis indicates an adequate static margin with the reduced booster fin area. See Figure 9.2.

Three vehicles were launched during November, 1969 at VAFB as Series 3. There are no reliable estimates of dart apogee from this series of flights since radar did not obtain an uptrack or a payload track within a reasonable period of time. The GMD generally picked up track from T + 25 seconds to T + 55 seconds and maintained track through payload deployment and descent. The only representative Starute data was from flight sequence 3-6 where radar track was available from about 220,000 ft. to 80,000 ft. The ballistic coefficient for this flight was about 0.023 to 0.020 lb/ft^2. This represents a faster fall rate than that attained for the first flight test series. During

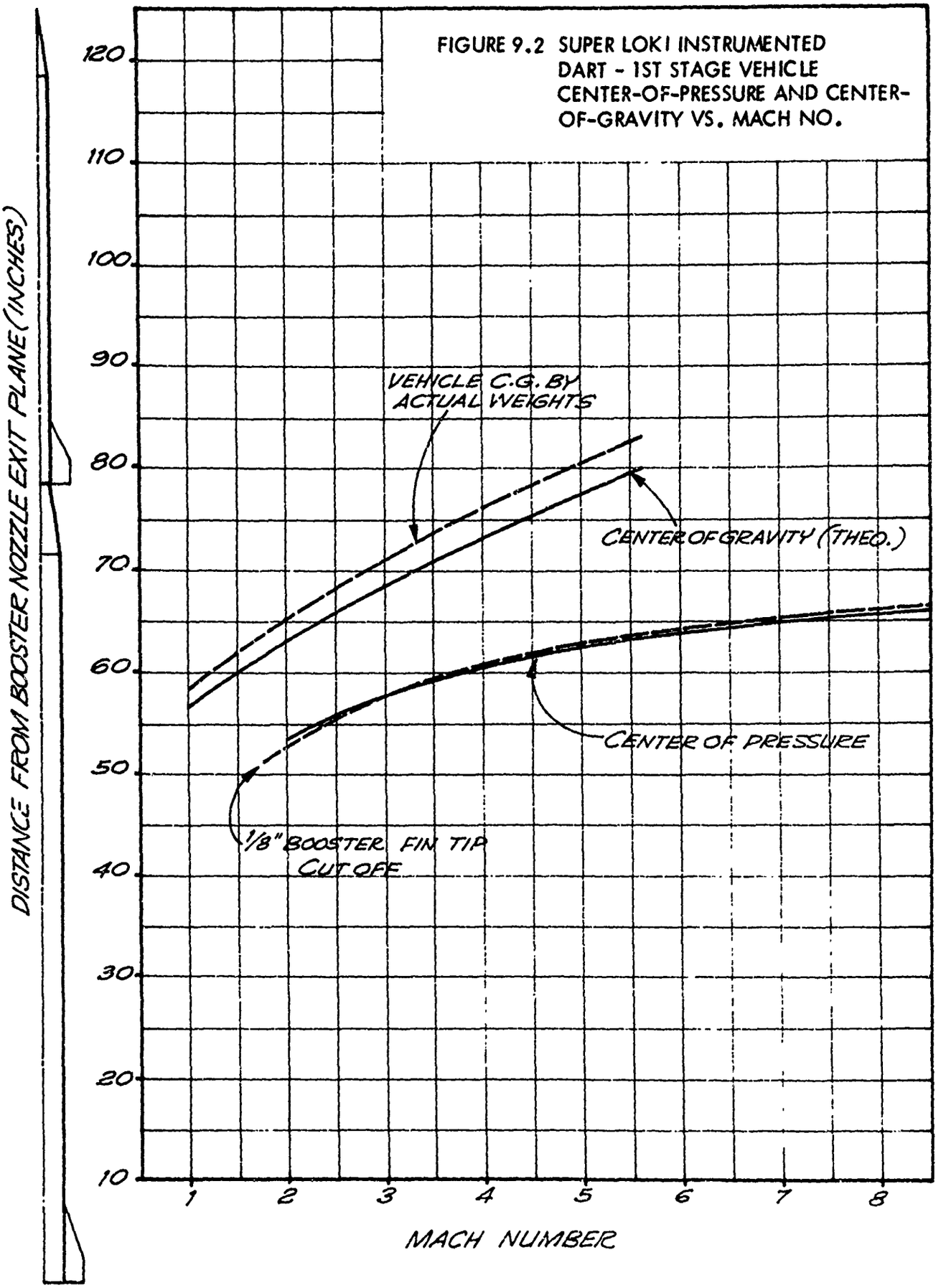

FIGURE 9.2 SUPER LOKI INSTRUMENTED DART - 1ST STAGE VEHICLE CENTER-OF-PRESSURE AND CENTER-OF-GRAVITY VS. MACH NO.

flights 3-7 and 3-8, it appeared that the instrument payload separated from the Starute during deployment. The sonde payloads splashed at T + 11.5 minutes and T + 7.5 minutes respectively, while radar still had a slowly falling target at a high elevation angle.

Internal temperature data was obtained on flight 3-7. The maximum temperature on the sonde's skin near spearation was + 32°C, which was + 19°C above the ambient atmospheric temperature at laucnch. Therefore, the aerodynamic heating temperature rise was no greater than 19°C.

A redesign and performance study was conducted during December, 1969, to improve the altitude capability of the Super Loki Instrumented Dart System. It appears that the 2 1/8-inch diameter dart reaches on apogee of about 235,000 feet, whereas an altitude of 250,000 feet is desired. Rocket motor redesign was not a practical way to improve altitude performance under the current program because of time and finances. The oxidizer content of the propellant could be increased, but this would cause a more brittle propellant which would not have the desirable properties at cold temperatures.

After completing a trajectory study, it was decided to reduce dart drag and weight by reducing the dart diameter to 2.000 inches. This should produce an altitude of 255,000 feet from an 80° sea level launch. Figure 9.3 presents a plot of apogee altitude vs dart weight for a two-inch diameter dart.

Detailed dart design was accomplished for the two-inch diameter dart during December, 1969. After consultation with CRL, it was decided to relieve the sonde diameter from 1.750 inches to 1.720 inches so that adequate thermal protection could be maintained. Dart tube wall thickness was reduced from 0.065 inch to 0.049 inch. This allows an 0.040 inch air gap and 0.016 inch thick asbestos stave lining for thermal protection. A column buckling stress analysis indicates a safety factor of 4 for this design for ambient temperature conditions. Aerodynamic heating of the steel dart tube will reduce this safety factor. The structural fidelity of this dart design must be determined by flight test, since the normal dart design safety factor has been appreciably reduced for this design.

Two 2 1/8-inch darts and two 2-inch darts were flown at the ETR during the week of 12 January 1970 as flight series 4. The expected altitude performance of about 236,000 feet for the 2 1/8-inch dart was verified during this series. At this point the program moved to ETR Cape Kennedy, Florida. The two-inch dart reached on apogee of slightly over 250,000 feet, thus satisfying the altitude performance requirement. The Starute was successfully deployed

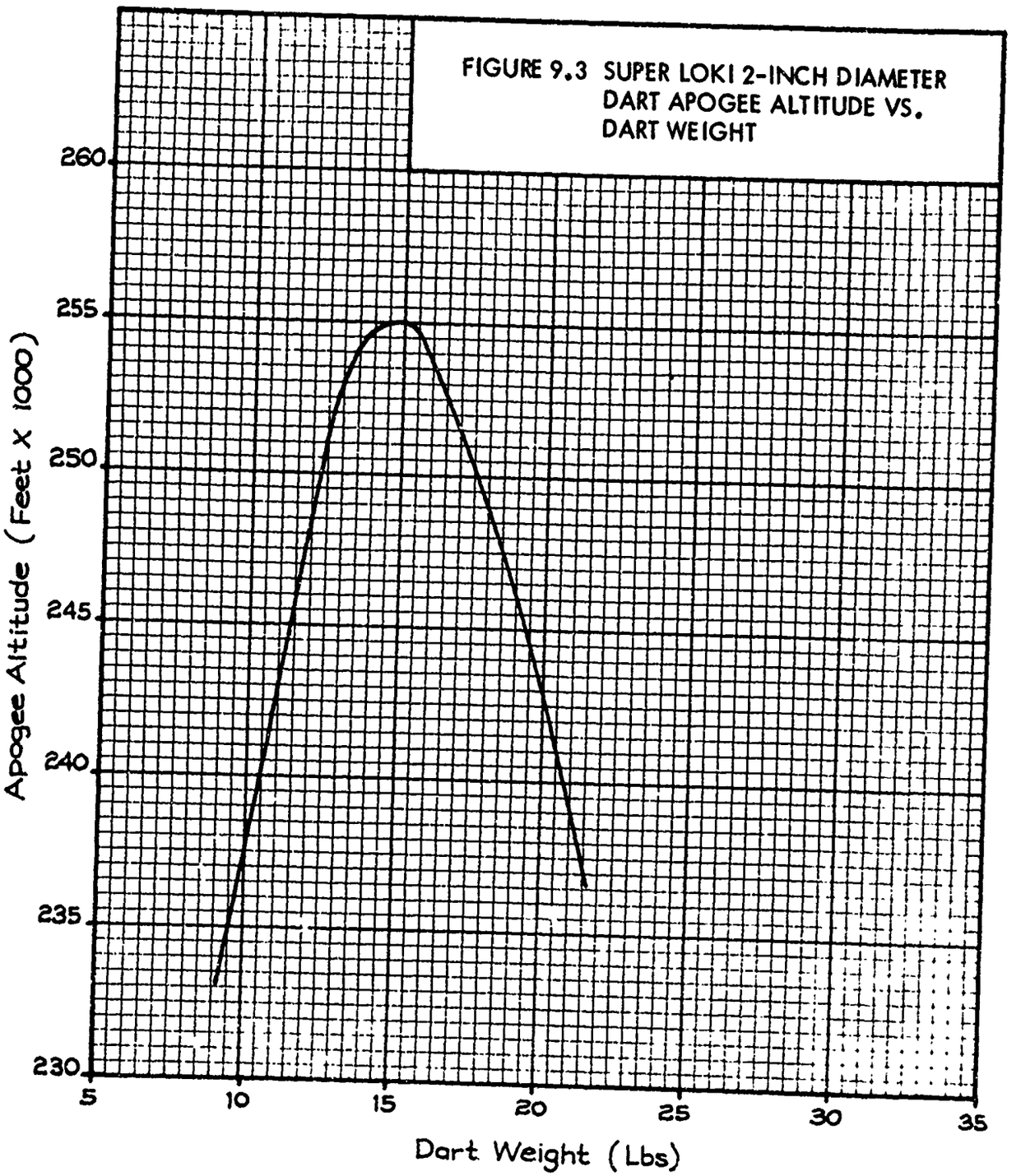

FIGURE 9.3 SUPER LOKI 2-INCH DIAMETER DART APOGEE ALTITUDE VS. DART WEIGHT

on three of the flights. Acceptable fall rates equivalent to about W/C_dA = 0.018 lb/ft^2 were achieved on two of these flights, while a faster than normal descent rate was observed, 0.021 lb/ft^2, for the third flight. On the radar target scope, occasional pieces of aluminized burble fence were noticed to tear off from the main target during descent for the second and third flights. The fourth flight apparently was low and splash occured before payload deployment.

The Datasonde instruments appeared to function satisfactorily, and internal temperatures were telemetered. The maximum temperatures for both dart designs appear to be on the order of 75°C. This was puzzling since the maximum temperature for a previous 2 1/8-inch dart flight at WTR was 32°C. It has been verified that the temperature sensors were located in the same position for the WTR flight test, but that asbestos paper was used between the thermistor and the stave wall in the WTR test. This probably accounts for the difference. From the ETR results, it appears that the thermal protection afforded by the two-inch dart is nearly as good as for the 2 1/8-inch dart.

On flight 4-11, the booster fins impacted upon the ends of the launch rail. This must have been due to friction on the rocket motor aft end after the dart fins had been released from the launch rails. This friction force creates a torque about the longitudinal axis of the vehicle which slows the dart spin rate. The cause of the friction was traced to the booster fin root pads which protruded about 0.015 inch above the motor bourelette. The white booster paint was cleaned from the launch rail prior to the final flight, and no evidence of booster fin impact was apparent for this final flight. The cause of the low altitude for flight 4 - 12 is not known.

Five flight units were fabricated and shipped to Cape Kennedy during February, 1970, although only three were flown. These units consisted of 2 1/8-inch diameter darts with one datasonde instrument. The booster fin tips were clipped 1/8 inch to accommodate the launch rail. The booster fin root pads were reduced in thickness to protect the booster fin impact problem. Also, the dart rotation alignment pin was moved to permit additional tolerance on the booster rotation slow-up side.

The fifth flight test series was conducted at Cape Kennedy during the week of 8 March 1970. Although the vehicles all functioned properly on all three flights, apparently the Starutes all failed. Pieces of the Starutes were observed to come off on the radar scope and extremely fast fall rates resulted in each case. Although the descenting telemetry signal strength was adequate for GMD tracking, the traces were scratchy. This indicates a nonstable descent

mode. Therefore, the problem during this flight test series was Starute failures. A second problem which became apparent during this flight series was the early payload ejection times of about 103 seconds. Apparently the vehicle performance and reliability was demonstrated to be satisfactory and no further evidence of launcher problems was found. The exceptionally high apogee altitude of flight No. 5-14 is puzzling, however, but no explanation has been found.

The Starute failure problem was subsequently investigated and has been attributed to aerodynamic heating of the dart causing excessive temperatures of the Starute. It has been hypothesized that excessive Starute temperatures inside the dart during vehicle ascent have caused the Mylar surfaces to become tacky and to stick together as thin Mylar film approaches the cold ambient atmospheric temperature. Then as the Starute descent velocity increases, the dynamic pressure causes pieces of the Starute material to tear.

The payload separation delay train time of 103 seconds causes ejection of the payload at about 5,200 feet below dart apogee for the 2 1/8-inch dart. Apogee time for this dart is about 122 seconds. A new delay was subsequently developed to give a 120-second delay time.

The staves temperature measured more than 85°C during vehicle ascent. See Figure 9.4. At 85°C the thermistor calibration went off scale and temperatures could not be determined above this level. Since the cool off curve was steeper than indicated on previous flights, it is expected that the thermistor was mounted more to the outer surface of the potting compound than the previous units. This may explain a portion of the apparently excessive temperature measurements as compared with previous flights.

Subsequent to the flight test series, a meeting was held at the Minnesota Plant of Space Data Corporation to review the starute failure problem and to inspect the Super Loki Starutes. It was ascertained that the 12-foot Super Loki Starute design had not been changed from the beginning of the program. Of course, material lots had changed, but existing physical property records indicated no significant differences. Potential changes in the Super Loki Starute design were discussed, i.e., thicker gage Mylar, altering inlet area and exhause port area, more reinforcing, etc., but it was decided to conduct two flight tests with thermal protection of the standard Super Loki Starute before embarking on a starute modification program. Subsequent to this meeting, a series of pressure burst tests were conducted with the results as follows:

a. Unit No. 618-04 (renumbered 618-25) Fabricated 2/69. Fabricated with extended skirt. One inch wide x 1/2 mil

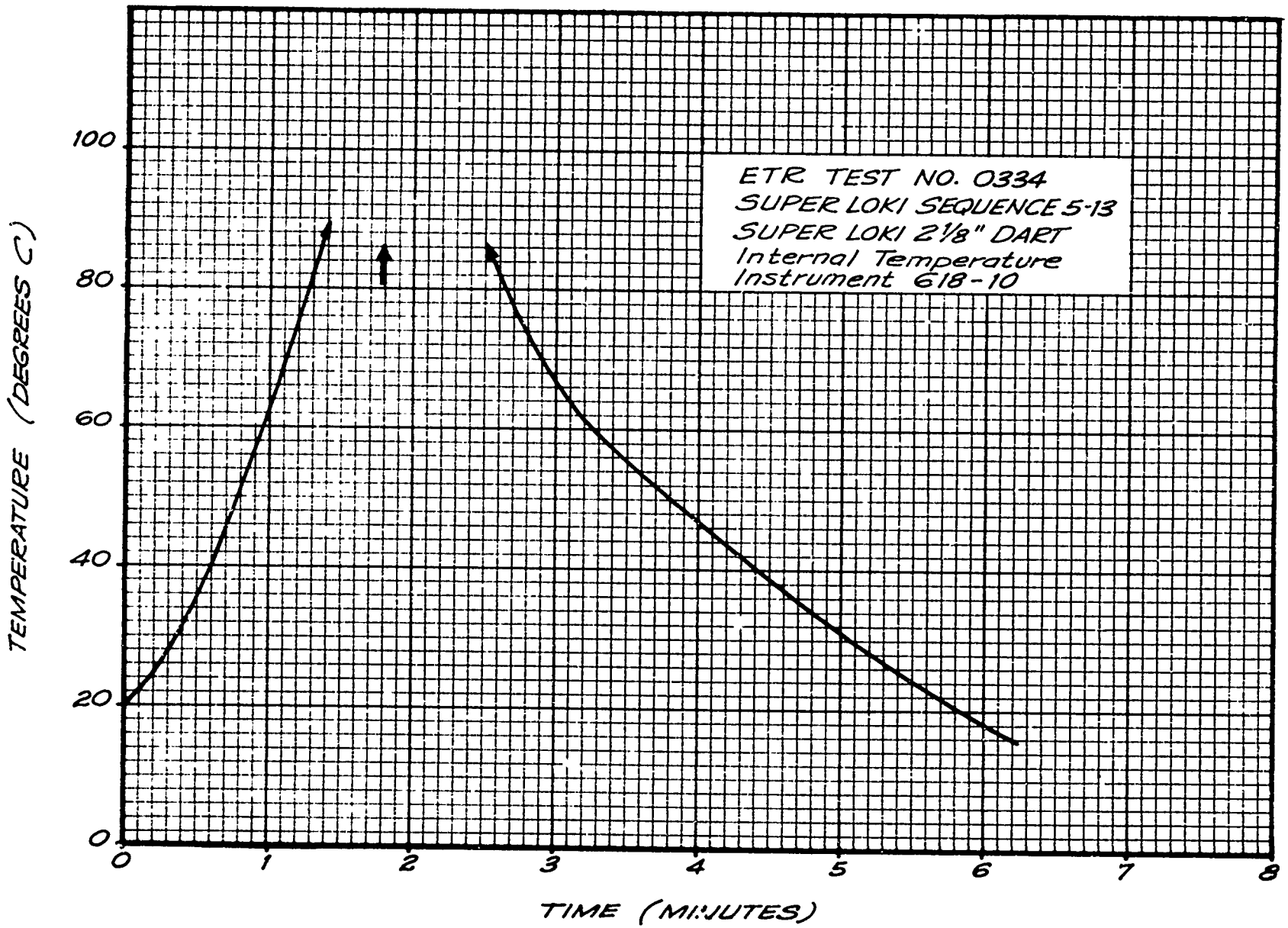

FIGURE 9.4 SUPER LOKI 2-1/8" DART INTERNAL TEMPERATURE VS TIME

tapes used to seal fence to main body gores. Seals not wiped with methylene chloride during fabrication.

Unit burst at 0.3 in. H_2O. Tape sealing burbie fence to main body gore peeled loose on one side.

b. Unit No. 618-19 Fabricated - 8/69
Standard fabrication with 1/2 mil x one inch wide tapes to attach fences to main body gores. Seal area wiped with methylene chloride.

Unit burst at 0.9 in. H_2O. Several holes in burst unit. Along one load tape from bottom of burble fence to apex On same side, main body gore halved along upper burble fence seal. Fence remained sealed to top section of main body gore. Separate holes at each corner adjacent to above load tape.

c. Unnumbered Unit Fabricated 3/19/70
Nonstandard construction in that "T" tape was used to seal burble fence to main body gores; 1/2 mil x 1 inch wide on outside with 1/4 mil x 1/2 inch wide on inside.

Unit burst at 1.3 in. H_2O - Principal tear on both sides of one load tape with secondary tears going in both directions from the "T" tape that intersected that load tape. Starute billowed up and beyond load tape during inflation past 0.6 inch H_2O.

i. is apparent that the more recently fabricated standard unit in Test B was significantly stronger than the old unit in Test A. Whether the difference is the methylene chloride wipe or aging of the older unit is not known. The double reinforced burble fence seam in Test C obviously is an improvement. It is interesting to note that current Loki 7-foot starutes were performing reliably at a burst strength of 0.6 inch H_2O in darts with adequate thermal protection.

Two 2 1/8-inch Datasonde darts were modified by incorporating a black emissive coating on the exterior, a shiny aluminum foil coating on the staves exterior and a 1/32-inch layer of cork on the starute staves interior in an attempt to thermally protect the standard 12-foot starutes. In addition, 120-second time delays were incorporated. These darts were sent to ETR for flight test.

Flight test series number 6 was conducted in early April to ascertain the aerodynamic heating protection effect upon starute reliability. Also the new 120-

second payload ejection delay was tested. The starutes in this series functioned properly as did the 120-second delays. This indicated that the system was ready for the CRL transponder instrument tests. Internal stave temperatures were measured on flights 6-16 and 6-17. These measurements were made of the internal metal stave temperature and are shown in Figure 9.5. The maximum temperature for flight 6-16 is 54°C and for flight 6-17 os 68°C. The only difference between these two flights was that a highly emissive paint, Nextel Black Velvet, was used on the 6-16 dart and a regular flat black paint was used. on 6-17. These temperatures are considerably lower than those found for flight 5-13 which had an estimated maximum dart staves temperature of over 130°C. This dart had no thermal protection beyond a small air gap between the inner dart wall and the payload staves.

Apogee altitude vs apogee range is plotted in Figure 9.6 along with the theoretical apogee data for the various launch QE's. All of the flights except 6-17 were launched at an 84° QE and the apogee's are in fact clustered about the theoretical 84° value. Therefore, the theoretical trajectory data appears to be valid. The effective QE results appear to be within about 1° which is a reasonable estimate on a one-sigma flight path angle dispersion. Flight 6-17 was launched at an 80° QE, but evidently achieved a lower effect angle trajectory. In general, the theoretical trajectories appear to be valid and the wind-weighing factors must be reasonable for such good agreement.

These last launches demonstrated sufficient reliability so that the remaining launches were set aside for payload development.

9.2.2 Transponder and Transmitter Systems Development Flight Tests

A summary of the flight tests which were devoted to the development of the transponder payload system is presented in Table 9.2.

Series 4 and 5 had shown promising results after preliminary transponder flights during four transponder flight tests conducted at ETR during April, 1970, as flight test series number 7. Although the vehicle and Starute performed satisfactorily on the first flight of this series, the sonde obviously dropped free from the deployed Starute. This problem was traced to a Dacron ribbon sonde suspension line which was placed in the split line between the instrument staves. Since this suspension line was in intimate contact with the inner dart tube wall, it is expected that temperatures on the order of 1000°F were experienced. This is well above the melting point of Dacron and similar organic substandes. The Dacron cables were replaced with steel cables for the remaining three transponder flight tests, and the systems performed reliably. Although the 1680 mc carrier and met data were adequately received at the ground station, the ranging signal

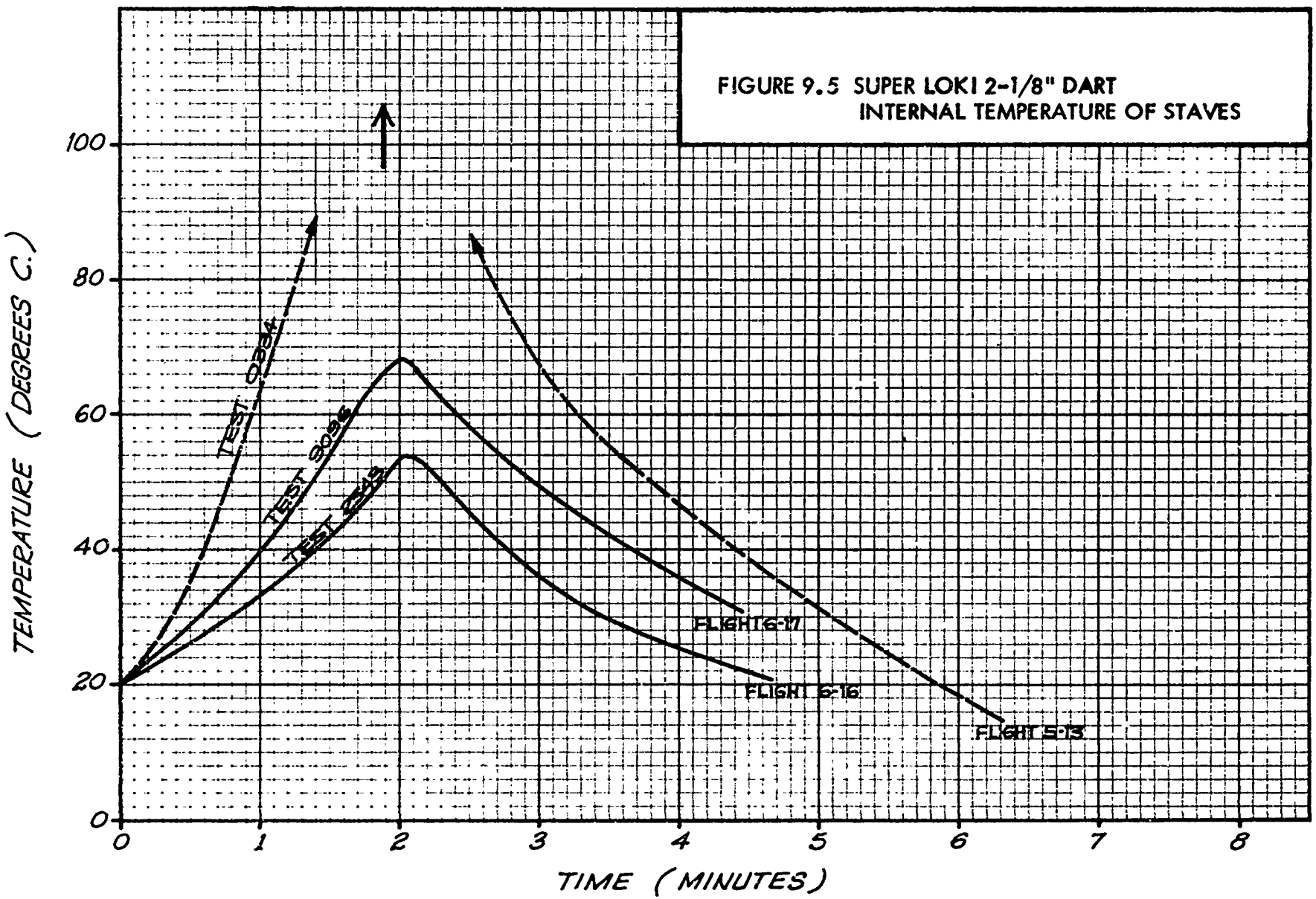

FIGURE 9.5 SUPER LOKI 2-1/8" DART
INTERNAL TEMPERATURE OF STAVES

FIGURE 9.6 APOGEE POSITION - SUPER LOKI 2-1/8" DART
84° Q.E. -- 100° AZ PREDICTED

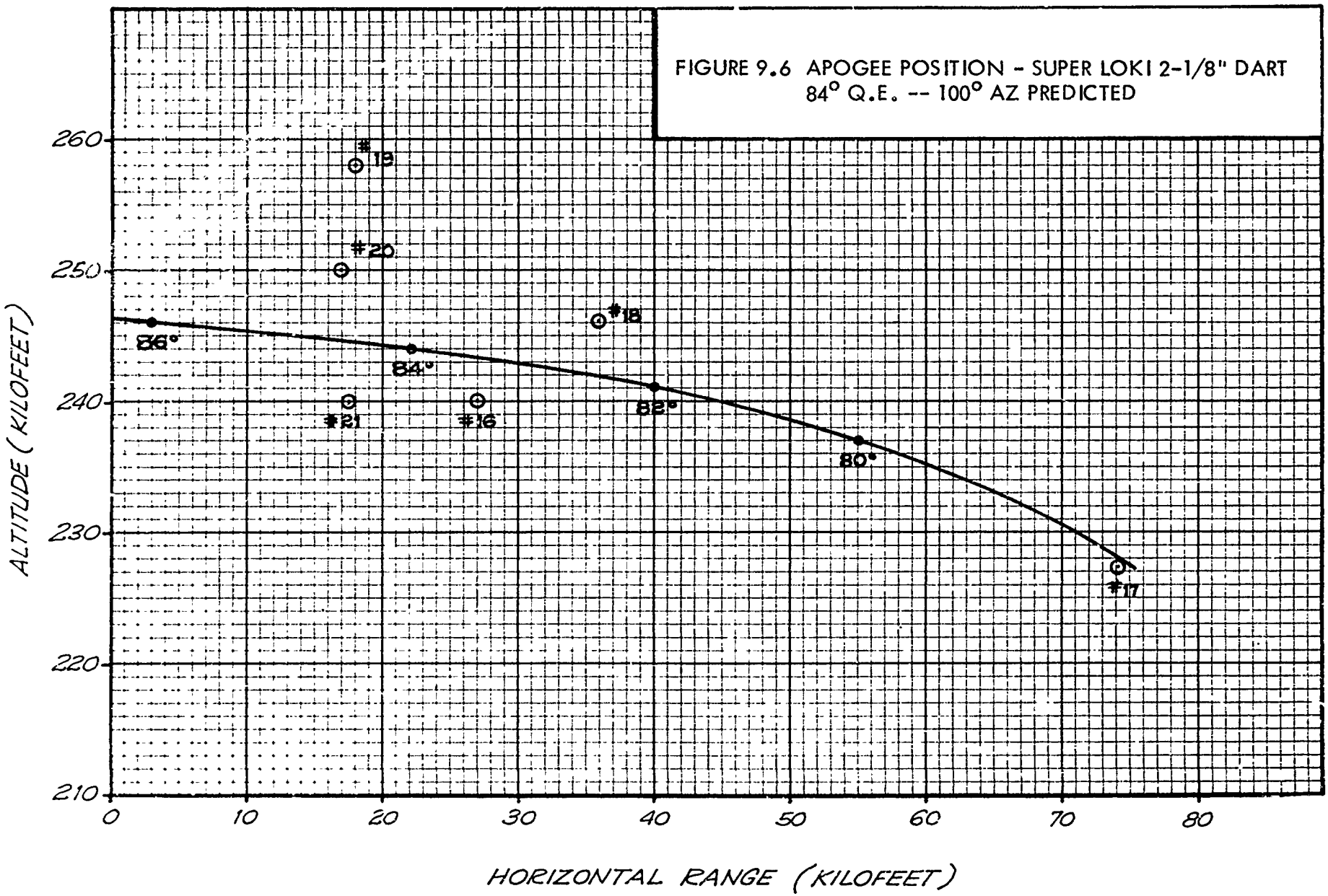

TABLE 9.2 FLIGHT TEST SUMMARY - TRANSPONDER SYSTEM DEVELOPMENT - 2 1/8' INSTRUMENTAL DART

Flight Series	7	7	7	7	8
Flight No.	18	19	20	21	22 M
Date	4-28-70	4-30-70	4-30-70	5-1-70	5-19-70
Range	ETR	ETR	ETR	ETR	ETR
Test Purpose	Development Transponder Steel cable	Development Transponder Steel cable	Development Transponder Steel cable	Development Transponder Steel cable	Development AMSS Sonde
Launch Elevation Angle (deg)	84.0	84.0	84.0	84.0	84.0
Vehicle Performance	Good	Good	Good	Good	Good
Apogee Altitude (1,000')	246	258	250	240	Late radar
Deployment Time (sec)	120	-	-	118	-
Starute Size & Type	12' C	12' C	12' C	12' C	12' C
Starute Performance	Good	Good	Good	Good	Good
Ballistic Coefficient	.010	.016	.016	.018	
Sonde Description	Sonde dropped off starute	Copper sleeve dipole antenna	Copper sleeve dipole antenna	Copper sleeve dipole antenna	Fair
Transmitter Performance	Good; dropouts	Fair	Good	Good	Weak; dropouts
Ranging Data	None	Weak	None	Fair	
Temperature Data	None	Resistor	Good	Resistor	
Comments	Dacron sonde cable melted	Weak and noisy ranging signal attributed to steel suspension cable.	Suspect output stage transistor shorted by steel suspension cable.	Suspect weak ranging signal due to steel suspension cable.	

TABLE 9.2 cont.

8	8	8	9	9	9	9	9
23 M	24 M	25 M	26	27	28	29	30
5-20-70	5-21-70	5-21-70	6-16-70	6-17-70	6-17-70	6-18-70	6-18-70
ETR	ETR	ETR	ETR	ETR	ETR	ETR	ETR
Amss sonde	Amss sonde	Amss sonde	Teflon suspension cable	Teflon suspension cable	Glass suspension cable	Teflon suspension cable	Teflon suspension cable
84	84	84	84	84	84	84	84
Good	Good	Good	Good	Good	Good	Good	Good
255		253	244	240	248	250	242
124		113	119	118			
12' C	12' C	12' C	12' C	12' C	12' C	12' C	12' C
Good	Good	Good	Good	Good	Good	Good	Good
			.017	.018	.017	.018	.016
			Datasonde	Transponder BBRC antenna	Transponder BBRC antenna	Transponder CRL antenna	Transponder CRL antenna
			Lost RF at ejection	Good	Good	Lost RF during uptrack	Good
				Good	Failed at deployment		Good
				Broken thermistor	Late cup off		Good
			Teflon cable held on datasonde	Teflon cable held on transponder	Good ranging signal on uptrack. Failed at deployment	Good teflon cable	Good flight

10	10	10	10	10	11	11	11
31	32	33	34	35	36	37	38
8-18-70	8-18-70	8-19-70	8-19-70	8-20-70	10-6-70	10-7-70	10-8-70
ETR	ETR	ETR	ETR	ETR	ETR	ETR	ETR
Development transponder	Development transponder	Development transponder	Development transponder	Development transponder	Development transponder	Development transponder	Development transponder
84	84	84	84	84	84	84	84
Good	Good	Good	Questionable	Low	Good	Good	Good
242	246	252	Late radar	135	239	234	255
118	120			118	118	119	116
12' C	12' C	12' C	12' C	12' C	12' C	12' C	12' C
Good 017	Good 018	Good 018	Pieces off at ejection	Broke up due to low apogee	2 pieces off; coning	Good	Good
CRL Antenna	CRL Antenna	CRL Antenna	Wrap Antenna		Fast		.018
Good high elev. d.o.	Good High elev. d.o.	Good High elev. d.o.	Cleaned up at end		CRL antenna	CRL antenna	CRL antenna
Good	Lost	Good			Good; dropouts	Good	Good
Good	Good	Good	Broken thermistor		Good; dropouts	Good	Good
				vehicle malfunction caused by improper alignment pin location	Good; dropouts	Good	Good
	White paint on dart	White paint on dart	White paint on dart		Good flight except for dropouts caused by damaged starute	Good flight	Good flight

11	11	12	12	13	13	13
39	40	41	42	43	44	45
10-8-70	10-8-70	11-19-70	11-20-70	2-9-71	2-10-71	2-11-71
ETR	ETR	ETR	ETR	ETR	ETR	ETR
Transponder	Development transponder	Transmitter	Transmitter	Production transponder	Production transponder	Production transponder
84	84	84	84	80	80	80
Good	Good	Good	Good	Unknown	Unknown	Good
242	238	257	253	Late radar	Late radar	234
113	118	122	121	Unknown	Unknown	121
12' C	12' C	12'	12'	12' C	12' C	12' C
Good	Good	Good	Good	Good	Good	Good
.018	.018	.019	.02+	.019	.019	.020
CRL antenna	CRL antenna	Transmitter	Transmitter	SDC Fabrication	SDC Fabrication	SDC Fabrication
Good	Good	Good	Good	Good	Good	Good
Good	Good	Good	Good	Good	Good	Noisy
Good	Good	----	----	Good	Good	Good
Good flight	Good flight	Good	Good	Good flight	Good flight	No coarse ranging signal too noisy

13	14	14	14	14	14	14
46	47	48	49	50	51	52
2-11-71	3-16-71	3-17-71	3-17-71	3-17-71	3-18-71	3-18-71
ETR	ETR	ETR	ETR	ETR	ETR	ETR
Production transponder	Production transponder	Production transponder	Production transponder	Production transponder	Production transponder	Production transponder
80	80	80	80	80	84	84
Good	Good	Good	Good	Good	Good	Good
235	Late radar	Late radar	240	Late radar	240	245
120	118	120	122	122	120	120
12' C	12' C	12' C	12' C	12' C	12' C	12' C
Good, sonde separated	Good	Good	Good	Pieces off	Good	Good
.010	.018	.018	.018	.019	.017	.017
SDC Fab	SDC Fab.	SDC Fab	SDC Fab.	SDC Fab.	SDC Fab.	SDC Fab.
Tumbling	Good	Good	Good	Lost at de-	Good	Good
Tumbling	Noisy, no coarse ranging	Good	Good	Transmitter off at deployment	Good	Good
Tumbling	Good	Good	Good	No ranging	Hot temps.	Good
Sonde lanyard failed at de-ployment	Rcvr noise may be due to sharp bend in coax.	Good flight	Good flight	Possible deploy-ment hang-up	Damaged thermistor, tumbling system at deployment	Good flight

15	15	15	16	16	16	17	17
56	58	59	62	64	65	68	69
4-27-71	4-28-71	4-28-71	6-16-71	6-16-71	6-17-71	8-10-71	8-10-71
ETR	ETR	ETR	ETR	ETR	ETR	ETR	ETR
Production transponder & starute reflectivity	" " "	" " "	Starute thermal protection	Starute thermal protection	Starute thermal protection	Reliability	Reliability
80	80	80	84	84	82	84	84
Fair	Good	Good	Good	Good	Good	Good	Good
224	242	250	250	245	239	255	244
			120	118	117	120	118
12' A	12' A	12' D	12' A	12' A	12' G	12' A	12' H
Good	Pieces off at 6 minutes	Breakup fast	Good	Good	Good	Good	Good
SDC Fab.	SDC Fab.	SDC Fab.	SDC Fab.	SDC Fab.	SDC Fab.	SDC Fab.	SDC Fab.
Good	Lost RF	Lost RF	Good	Good	Good	Good	Good
Good	Good for 4 min	Good for 4 min	Good	Good	Good	Good	Good
Good			Good	Good	Good	Good	Good
Good flight but slightly low	Starute damage caused dropouts. Payload tumbling may have caused transmitter & rcvr antenna damage no droupout by T + 10 min.	" " "	Good flight	Good flight	Good flight	Good flight	Good flight

17	17	17	19	19	19	19	19
70	71	73	76	77	79	80	83
8-11-71	8-11-71	8-12-71	10-12-71	10-12-71	10-14-71	10-14-71	10-15-71
ETR	ETR	ETR	ETR	ETR	ETR	ETR	ETR
Reliability	Reliability	Reliability	LAU-66/A launcher	LAU-66/A launcher	LAU-66/A launcher	LAU-66/A launcher	LAU-66/A launcher
84	84		84	84	84	84	84
Good	Good	Good	Low	Low	Good	Good	Low
242	253	254	220	220	235	232	210
117	111	110	111	115	115	113	124
12' A	12' A	12' A	12' H	12' A	12' A	12' H	12' H
Good	Questionable	Breakup	Good	Good	Variable	Good	Sonde dropped off
SDC Fab.	SDC Fab.	SDC Fab.	SDC Fab.	SDC Fab.	SDC Fab.	SDC Fab.	SDC Fab.
Good	Noisy	37 minutes to 80,000 feet	Weak	Erratic	Rapid dropouts	Good	Good
Good	Noisy	Aur. 02	Poor	Fair	Rapid dropouts	Good	Tumbling
Good	Hot temps.		Poor	Good	Rapid dropouts	Damaged thermistor	Tumbling
Good flight	Bad deployment, cup failed to release, tumbling payload.	Bad temps. due to tumbling	Launcher pitch down	Launcher pitch down	Possible starute problem		Sonde dropped off starute. Launcher pitch down.

was weaker and noisier than required to produce good coarse ranging. This was primarily attributed to a degradation in the 403 mc receiving antenna pattern due to the steel suspension cable. As a result of these flight tests, CRL began working on a substitute non-donductive cable.

During the month of May, 1970, a flight test series number 8 to evaluate the Motorola AMSS sondes was conducted at ETR. These flights indicated reliable vehicle and Starute performance. Apogee altitudes averaged about 254,000 feet an an actual 83.5° launch evelation angle. At an 80° QE this would reduce to 248,000 feet. Starute performance was in the range of β = 0.015-0.017 lb/ft^2. The payload loading into the darts was facilitated by a tighter Starute packaging and by the use of hose clamps. The instruments appeared to perform satisfactorily.

During the month of June, 1970, flight test series number 9 to test new sonde suspension cables and CRL transponder instruments was conducted at ETR. Five vehicles were launched through a new launcher, rail machined with grooves according to final design, and all were successful. Apogee altitudes were from 240,000 feet to 250,000 feet with effective launch angles of 80° $\pm$ 1° elevation. The Starutes all performed satisfactorily with ballistic coefficients β= 0.016 to 0.019 lb/ft^2. The sondes were slightly heavier than for previous series where β = 0.015 to 0.017 lb/ft^2. Both teflon and silica sonde suspension cables were successfully flight tested during this series. The transponder sonde suspension cables were oriented so that they fell into the narrow slot between the instrument staves rather than the wide slot. The future instrument staves are modified to rectify this problem.

The sonde results were not so good for this series. The r.f. frequency was lost on two flights, the ranging signal was lost on one flight, and the thermistor opened on a fourth flight. The fifth flight produced good results in spite of r.f. interference.

During August, 1970, a white coating was investigated to reduce the solar radiation heating on the dart payload prior to launch. A series of white epoxy paints were found with a low solar abosrptivity to infrared emissivity ratio, $\alpha s/\epsilon$ ir. Theoretically these paints should minimize the solar heating, i.e., wavelengths below 2.5 μ , and maximize the infrared cooling, i.e., wavelengths above 2.5 μ . Three types of white epoxy paints were tested for solar heating about midday in the sun at Phoenix on 12 August 1970. Steel panels 0.060 inch in thickness were painted with the sample paints with a black oxided panel used as a reference. Thermo-couples were attached to the panel back sides and the painted sides of the panels were placed facing upwards towards the sun. The temperatures were monitored with the results presented in Table 9.3. From

Table 9.3 Solar Radiation Heating Test - Test Panels

Surface Coating	Temperature, °C							
	Exposure Time (minutes)							
	0	5	10	15	20	25	30	45
Black Oxide	26	57	60	64	63	64	64	66
Catalac 443-3-1	26	38	39	41	41	42	42	43
Catalac 463-3-100	25	38	39	40	40	40	41	42
Catalac 443-1-500	25	38	39	41	41	42	42	43

the test results it appears that a near equilibrium temperature was achieved within five minutes from initial exposure. The very gradual creep upwards in temperature for all specimens was most likely due to increasing sun angles as the tests were initiated just prior to local noon. Within five minutes of exposure, the black oxide sample rose 31°C while all of the white samples rose only 12°C to 13°C. The white samples generally ran 23°C cooler than the black, and the variation among the white samples was negligible. A subsequent ground test conducted at Cape Kennedy also indicated a significantly greater temperature rise inside a black oxide dart coating as compared with a dart coated with the Catalac 433-1-500 white epoxy paint. The resulting temperature rise curve is presented in Figure 9.7. The temperature difference at the end of fifty minutes was 12°C. This temperature difference, of course, is a variable which depends upon the strength of the solar flux, i.e., time of day, geography, etc., and the ambient air temperature and ventilation velocity. In summary, it appears that the white epoxy paint coating is effective in reducing solar heating temperature rise to one-third for a black surface.

The tenth flight test series was conducted at ETR during the week of 16 August 1970 to test the latest transponder instrument design. The vehicle flights appeared to be satisfactory except for the 10-34 which went low due to field modifications. An old dart tail was used with the alignment pin causing the booster fins to lie in the old orientation, i.e., half way between the launcher rails. When this was discovered, a new notch in the interstage was cut to rotate the booster fins close to the off-side rails. It is obvious that the fins were placed to close to the off-side rails, since marks were found on them after the launch and the flight went low. The Starute appeared to perform satisfactorily in the first three flights, but failed in the fourth, 10-34. No reason for this failure has been determined. The white epoxy paint was used on three of the flight tests, 10-32, 33, and 34, with the latter flight resulting in the failed Starute. There is some question as to the possibility of the paint melting and flowing into the dart access holes causing damage to either the instrument of the Starute. The paint melts and decomposes at about 450°F, and blow torch tests have shown that it blisters, bubbles and then disappears in smoke leaving the underneath surface as original. The effect during flight is unknown.

During the month of October, 1970, five flights (11-36 thru 11-40) were conducted at ETR to further test the CRL transponder instrument. Vehicle performance was satisfactory for all flights as indicated by apogee altitudes ranging from 234,000 feet to 255,000 feet. The predicted QE's were all 84°, and the actual launcher elevation settings varied from 85° to 86° to allow for headwind components. Although Starute performance was generally acceptable, pieces were observed tearing loose on 11-36, and the fall rate varied from β = 0.040 psf at 220,000 feet to β = 0.019 psf at 120,000 feet. The damaged Starute evidently

coned rapidly in the higher altitude as indicated by rapid droupouts in the received carrier signal. The other Starutes appeared to function satisfactorily.

Since this flight test series was conducted, it has been discovered that a rubberized cork had been used to line at least one or more set of the Starute staves for this flight series (11-X) instead of the previously used pure cork. Rubber has a thermal conductivity of $k = 0.170$ Btu . hr^{-1} . ft^{-1} . F^{-1} while cork has a value of 0.025. Thus, rubber will conduct heat about seven times as fast as cork. The rubberized cork thermal conductivity is probably about four times as conductive as the previously used pure cork sheeting. Thus, we have hypothesized that the increased thermal conductivity of the rubberized cork probably led to the damaged Starute on flight 11-36. Subsequent flight tests, with the rubberized cork in the Starute staves having been replaced with pure cork, yielded good Starute flights.

The AFCRL transponder instrument performed quite well on all five flights. The carrier signal droupouts experienced during the high altitude portion of flight 11-36 is attributed to the Starute damage previously discussed.

The actual dart apogee data indicate that the effective launch elevation were within $\pm 1^{o}$ of the predicted QE. Thus, it appears that the published wind-weighting factors are reasonable. The booster impacts, however, ranged from 700 feet to 4000 feet from the predicted impact points, generally in a northeast direction. Although it appears that the booster wind-drift calculations had a directional bias, the large differences in the ranges indicate a fairly erratic behavior of the booster after dart separation.

The only significant problem over the last few flight test series has been Starute damage. A very high incidence of Starute failures occured up to flight 5-15 at which point high aerodynamic heating temperatures were deduced to be the problem. From flight 6-16 on, extra heat protection methods were employed, and the resulting Starute reliability became essentially 100% until flights 10-34, 10-35, and 10-36. It is believed that a rubberized cork was substituted for pure cork as Starute stave lining for these failed flights. Subsequent flights with the pure cork lining resulted in reliable Starute performance. Excessive heat transfer to the Starute material is a problem which requires vigilance in future production.

The first group of four transponder instruments fabricated at SDC were flight tested at ETR as series number 13. Although apogee altitude was not obtained for two of the flights, the remaining two flights resulted in apogees of about 235,000 feet. These are close to nominal, but slightly lower than desired. The apogee ranges appear to be nominal and so do the propellant weights. The Starutes appear to have functioned properly. The first two transponder instruments worked well, however, excessive converter noise was apparent during flight. The ranging signal on the third flight was excessively noisy, and coarse ranging could not be obtained. Although the Starute performed satisfactorily on the fourth flight, it appears that the sonde lanyard failed, and the sonde

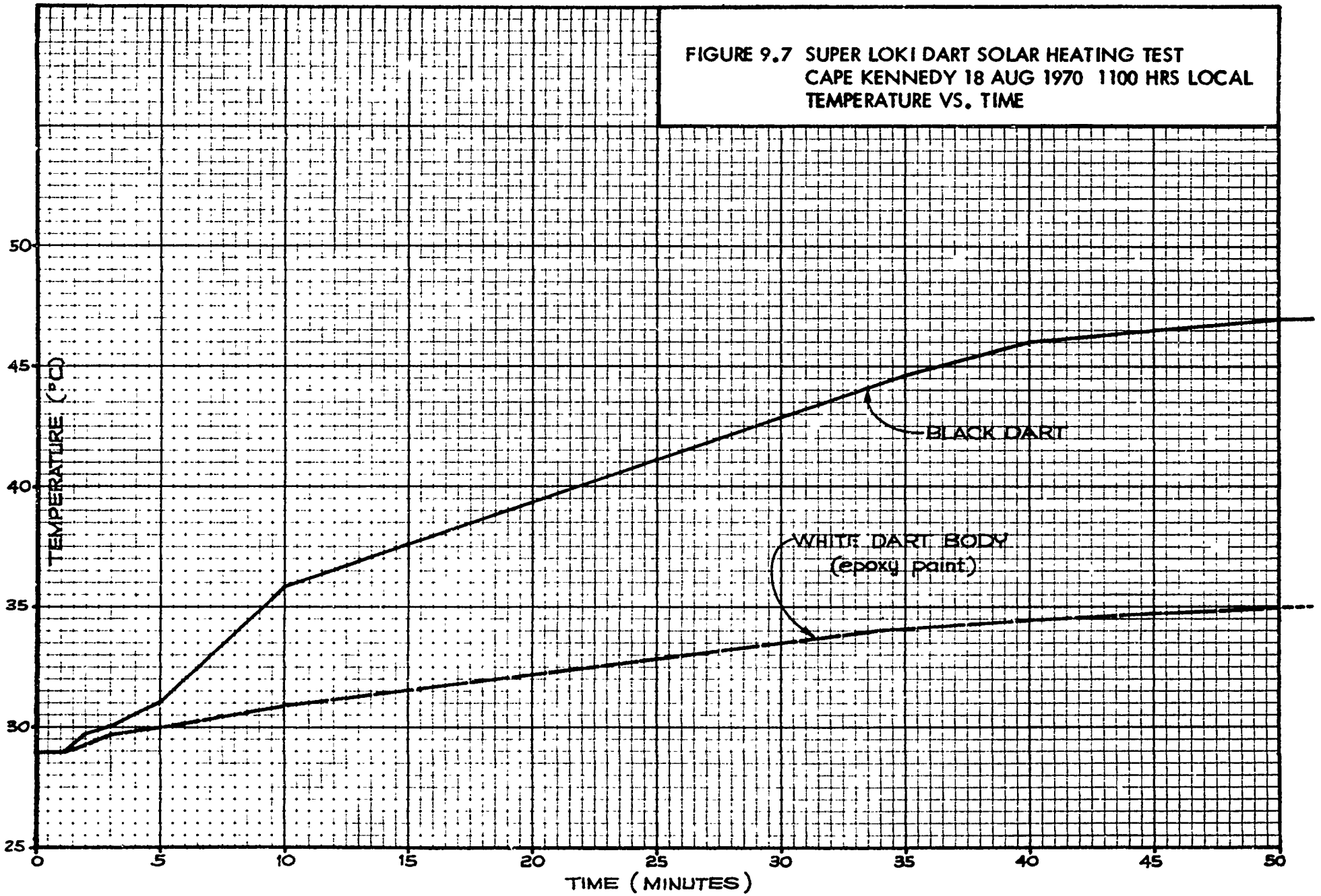
FIGURE 9.7 SUPER LOKI DART SOLAR HEATING TEST
CAPE KENNEDY 18 AUG 1970 1100 HRS LOCAL
TEMPERATURE VS. TIME
TEMPERATURE (°C)
TIME (MINUTES)
BLACK DART
WHITE DART BODY
(epoxy paint)
25
30
35
40
45
50
0
5
10
15
20
25
30
35
40
45
50

tumbled into a fast descent to impact. The lanyard failure was most likely due to the incorporation of paper tape which may have auto-ignited from aero heating and melted the teflon lanyard. The converter shielding can was deleted from these units and twisted leads were employed rather than coax. These factors may have been the cause of the excessive converter noise.

Six (6) transponder flight tests were conducted at ETR as series number 14 during the week of 14 March 1971. One (1) instrument was left over from the previous series, and the five new instruments included a shielding box for the converter and coax leads to reduce converter noise. The vehicles all appeared to have reached reasonable altitudes, although apogee data were not acquired for all flights. Of the six (6) flights, four resulted in good Starutes. Three (3) pieces came off the Starute during number 14-50, and the system fell slightly fast, $\beta = 0.019$ lb/ft^2. On this same flight, the sonde transmission stopped at 390 seconds, but the fall rate was good all the way. This flight resulted in warm temperature data most likely due to a damaged thermistor mount. In general, the sonde performances were good, with the exception of the transmitter, which failed at deployment.

Ground checks at ETR indicated that the old sonde from flight series number 14 (S/N 16) had converter noise of 1V pp, whereas the newer sondes ran from 0.20 to 0.40 V pp on internal power. Thus, the converter noise problem was solved.

By eliminating the ranging receiver from the transponder instrument, the transmitter instrument is derived. Otherwise the transmitter and transponder systems are identical. Initial fabrication and flight testing of the transmitter instruments was for flight series number 15 in which four transmitter sondes were flown along with three transponders. The transmitter flight test summary is presented as Table 9.4.

Seven (7) flight tests were conducted at ETR as series number 15 during the week of 26 April 1971. Reasonable vehicle altitudes were achieved for most of the flights. However, two flights resulted in apogees of only about 225,000 feet, which is considered as slightly low. The radar data for one flight showed an apogee of 277,000 feet and this is considered to be quite high. Four of the seven flights resulted in good Starute performance. On two of the flights, pieces were observed tearing off from the Starutes, however, descent rates were not catastrophic. Tumbling of the descending and deployed system was apparent for one of the flight tests. The sonde performances were generally good for this series with the exception of Starute induced signal droupouts, permature sonde turn-on well before launch, and excessive carrier frequency shifting from dart to free state. Two Starute configurations were flown during this test series in an attempt to improve radar cross-section.

The three problems which become evident during test series number 15 were Starute failure, sonde frequency shift and inadvertent turn-on of the sonde at the launch pad. A review of the heat transfer processes indicates that the dart heat pro-

TABLE 9.4 FLIGHT TEST SUMMARY - TRANSMITTER SYSTEM DEVELOPMENT - 2 1/8" INSTRUMENTAL DATA

Flight Series	15	15	15	15	16	16	16
Flight No.	53	54	55	57	60	61	63
Date	4-26-71	4-26-71	4-27-71	4-28-71	6-15-71	6-15-71	6-16-71
Range	ETR	ETR	ETR	ETR	ETR	ETR	ETR
Test Purpose	Production transmitter & starute reflectivity	Thermistor cup & starute reflectivity	Production transmitter & starute reflectivity	Production transmitter & starute reflectivity	Starute thermal protection	Starute thermal protection	Starute thermal protection
Launch QE (deg)	80	80	80	80	84	84	84'
Vehicle Performance	Good	Good	Good	Fair	Good	Good	Good
Apogee Altitude (1,000')	238	240	Late radar	226	247	247	248
Deployment Time (sec)	122	122	Late		119		117
Starute Size & Type	12' A	12' A	12' D	12' D	12' F	12' F	12' D
Starute Performance	Pieces off	Good	Good	Good	Good	Good	Good
Ballistic Coefficient (psf)	.020				.017		
Sonde Description	SDC Fab.	SDC Fab. Thermistor cup glued on	SDC Fab. q	SDC Fab.	SDC Fab.	SDC Fab.	SDC Fab.
Transmitter Performance	Noisy	Good	Good	Lost RF	Good	Good	Good
Temperature Data	Good	Good internal temps.	Good		Good	Good	Good
Comments	Starute deployment damage	Flight indicates that previous warm temps are due to damaged thermistor leads	Good flight	Sonde relay shorted at T-17 min	Good flight	Good flight	Good flight

17	23	23	24	24	24	24	24
74	95	96	97	98	99	100	102
8-12-71	3-16-o2	3-17-72	4-4-72	4-4-72	4-5-72	4-6-72	4-6-72
ETR	ETR	ETR	ETR	ETR	ETR	ETR	ETR
Starute thermal protection	10' starute & thermal protection	10' starute & thermal protection	10' starute & thermal protection	10' starute & thermal prot.	10' starute & thermal prot.	10' starute & thermal prot.	10' starute & thermal prot.
84	84	84	80	80	84	84	84
Good	Low	Low	Low	Low	Low	Low	Good
242	209	224	222	208	223	218	238
116	118						
12' H	10'	10'	10'	10'	10'	10'	10'
Good Good	Go	Good	Good	Unknow	Good	Good	Good
	.020	.020	.020	Questionable radar data	.020	.020	.021
SDC Fab.	SDC Fab.	SDC Fab.	SDC Fab.	SDC Fab.	SDC Fab.	SDC Fab.	SDC Fab.
Good	Good	Good	Lost RF	Lost RF	Good	Good	Good
Good	Possibly warm high	Good		G	Good	No modulation	Good
Good flight	Low. LAU launcher	Low LAU launcher	Low Mod LAU low prop. wgt.	Low Mod LAU low prop. wgt	Low Mod LAU low prop. wgt	Low General purpose launcher low prop. wgt. instrument was shorted out at launch pad	Good flight, general purpose launcher, medium prop. wgt.

tection may be marginal and this may still be the only Starute problem. Structural burst tests were conducted on two Starutes with results similar to previous data. Burst strengths are much higher than calculated dynamic pressure levels. The sonde frequency shift problem can most likely be eliminated by employing coax antenna cable leading from the RCA cavity oscillator tube to form the antenna system. In this design, the outer sheath of the coax is soldered to the outer sheath of the oscillator feed through and then to the sonde ground plane. The outer sheath is stripped from the coax at its end to form a dipole stub antenna from the inner conductor. A problem with this solution appears to be the difficulty in obtaining the specified frequency deviation for modulation once the above has been done. The inadvertent turn-on of the sondes appears to be due to the umbilical connector. This connector could be susceptible to shorting at the rear solder connections unless care is exercised in the fabrication of the connector board. This problem has not been encountered in later tests.

Dart heat protection techniques were studied in further detail, and redesign of the dart system was made for greater thermal protection of the Starute. The redesign consists of a black oxided dart outer wall with an electroless nickel plated inner wall, two sets (inner and outer) of Starute staves with an air gap between them. The outer staves are bright nickel plated steel with reduced dimple heights. The inner staves are 0.007 inch fiberglass with 0.012 inch fiberglass stand-off rings. The exteriors of these inner staves are coated with aluminum foil. Six dart systems with three transponders and three transmitters and various Starute designs were fabricated and flight tested at ETR during the week of 14 June 1971 as flight series number 16. The vehicle altitudes were all good and were much more consistent than in the previous series. The altitudes ranged from 239K feet to 250K feet. The Starutes all appeared to work well with nominal fall rates and no pieces reported to have torn loose. The three non-transponder and three transponder sondes all appeared to work satisfactorily although some of them which had been turned on early at the launch pad cut off after about 25 to 32 minutes of flight time. The converter noise for all these units was exceptionally low. Low power outputs resulted from the non-transponder antennas touching the ogives. These antennas were insulated and then worked satisfactorily. The umbilical connector inadvertent turn-on problems still occurred. Breakage of two thermistors occurred during shipping.

Since the vehicles, Starutes and sondes all worked quite well, the overall design was considered to be fairly well proven and finished. However, the umbilical connector and broken thermister problems were yet to be solved. In addition, the excessive frequency shift was still a problem.

Five transponders and one non-transponder instrument were flown at ETR during the August 1971 flight series number 17 with generally good results. The only problem appears to be Starute breakup in one flight and lesser damage in a second flight.

Photographs taken from a recovery aircraft showed a burble fence rupture on one side in 17-71. In these and other tests where radar reported pieces coming off, the overall fall rates were not catastrophically increased.

Five transponder dart systems for the October, 1971, flight test series number 19 were fabricated with three special Starutes. These special Starutes eliminate the bleed slot into each burble fence corner and incorporate bleed holes along each side of the main body into the fence and a set of bleed holes out of the fence. The October flight test series indicated rather weak transponder r.f. carrier signal strengths for the special transmitter tubes although the frequency shifts were somewhat reduced from the standard tube valves. Out of the five transponder flights, three had weak or erratic signal strengths and two had good signal strengths. One of the good signal strength units had a standard transmitter tube. Starute performance, in general, was good. However, it appeared that the sonde dropped off from an H model Starute on one flight and rapid transmitter droupouts on a second flight may have been caused by a faulty Starute. Low vehicle flights (220, 220, 235, 232, 210K feet at 84° QE) occurred during this series, and although the motor propellant weights were on the low side of specifications, the launcher base was suspect. Note that on this series the ETR Loki LAU launcher base was utilized instead of the previously used ETR "standard" launch base. The propellant weight variation should cause only a 10,000 foot decrease in apogee altitude. This was the first series that the LAU-66/A launcher base was used with the large 2 1/8-inch dart launch rail. The launcher base may be too flexible for the increased load. The thermistor on one flight appeared to have been damaged during deployment for warm temperatures were experienced.

Since marginal reliability of the Starute had been the most significant repeating problem throughout the development program, it was agreed that an extra safety margin must be build into the system to prevent Starute failures. A thorough analysis indicated that added thermal protection for the Starute was required. Redesign of the instrumented dart system was accomplished by scaling the Starute down to a 10 foot size, increasing the dart wall-to-wall staves air gap and increasing the wall thickness of the Starute staves.

Seven of the 10 foot Starute designs with the above added thermal protection design changes were flown at ETR with transmitter instruments in series numbers 23 and 24. All of these flights resulted in successful Starutes, and therefore, this latter design has been adpoted as final. Reference 1 was written while the 12 foot design was considered final.

Low apogee altitudes for the final two series has been attributed to below standard propellant weights and a slight elevation pitch down attributed to flexibility of the LAU-66/A launcher base. These problems are discussed in detail in a later section.

9.2.3 Robin System Development Flight Tests

A summary of the flight tests which were devoted to the development of the Robin falling sphere rocket system is presented in Table 9.5.

The first three flight tests of the sphere system were conducted during August at ETR during series number 17. The vehicles which were launched from a standard Loki LAU-66 launcher base, achieved the design apogees. However, the spheres were all bad. In two cases the sphere separation from the dart occurred prematurely at about 100 seconds rather than the design time of 135 seconds. It is believed that this did not contribute to the sphere failures, since the 100-second ejection would take place above 300,000 feet, and the sphere which was ejected at the proper time also failed. Both the aluminizer corner reflector spheres failed. The dart thermal insulation for this series consisted only of a 1/32-inch asbestos layer on the inside of the payload staves and a small air gap between the inner dart wall and the staves. This insulation was esentially the same design as employed with the Viper Dart and was successfully flown at WSMR on a previous Super Loki Robin Dart program sponsored by the Army. Although one of the darts was chilled with dry ice prior to launch in an attempt to reduce the effects of aerodynamic heating, this did not improve the situation since permature ejection and sphere failure occurred for this unit. It is believed that the dart warmed up to essentially ambient temperature prior to launch, since there was a short range hold after loading into the launcher.

Analysis of the August flight test data indicates that the sphere and premature payload separation were most likely due to aerodynamic heating. A redesign of the thermal protection for the sphere dart was then conducted. The pyrotechnic dealy was isolated from the dart tail to prevent autoignition of the delay output charge. Improved thermal protection for the sphere was made. One of the returned sphere darts was groundfired with ejection time and performance found to be nominal. A second returned dart was thermolagged and the delay train better insulated. This dart was flight tested at ETR on 10 September 1971 with an apogee of 340,000 feet at 80° QE. The payload ejection time was nominal for the pyrotechnic delay train which was better isolated thermally from the dart hardware. This indicated that the original delay problem (premature activation) was due to excessive heating. The sphere for this flight evidently was a failure from deployment on down. Although this dart was thermolagged to a layer thickness of 0.050 inch, the problem could still be aerodynamic heating.

A redesign of the thermal protection for the sphere dart was undertaken. The redesigned configuration consisted of an outer set of steel ejection staves dimpled inside and outside (0.030 inch each) with aluminum foil on the outside. A set of fiberglass inner staves was included with aluminum foil on the outside and 3/22-inch cork on the inside. The inner staves were rotated 90° with respect to the outer staves to prevent dart tube radiation through the gap regions. The

TABLE 9.5 FLIGHT TEST SUMMARY - ROBIN SYSTEM DEVELOPMENT - 1 5/8" SPHERE DATA

Flight Series	17	17	17	18	19	19	19
Flight No.	66R	67R	72R	75R	78R	81R	82R
Date	8-9-71	8-9-71	8-11-71	9-10-71	10-13-71	10-15-71	10-15-71
Range	ETR	ETR	ETR	ETR	ETR	ETR	ETR
Test Purpose	Initial evaluation	Initial eval.	Initial eval.	Insulated dart tail	Ablative coating	Ablative coating	No ablative coating
Stave Configuration	1 Air Gap	1 Air Gap	1 Air Gap	1 Air Gap	2 Air Gaps	2 Air Gaps	2 Air Gaps
Launch QE (deg)	80	80	80	80	84	84	84
Vehicle Performance	Good	Fair	Good	Fair	Good	Good	Good
Apogee Altitude (1,000')	370	352	370	340	370	Lute Radar	400
Deployment Time (sec)	100	135	102	130	129	Late radar	128
Sphere Design & Weight (gm)	aluminized 97.6	Corner reflector 112.2	aluminized 97.1	Corner reflector 112.2	aluminized 108.2	aluminized 103.8	aluminized 103.5
Inflator Design	Std. Capsule	Std. Capsule	Std. Capsule	Std. Capsule	Diffusor Long Capsule	Diffusor Long Capsule	Diffusor Long Capsule
Sphere Performance	Bad	Bad	Bad	Bad	Fair	Good	Bad
Deflation Altitude (1,000')	Deployment	Deployment	Deployment	Deployment	150	100	Deployment
Comments	Early expulsion and bad sphere suspect aeroheating	Bad sphere suspect aeroheating	Early expulsion and bad sphere suspect aeroheating	Proper ejection time. Bad sphere .050" thermolag	Early deflation .050" thermolag	Good sphere .050" thermolag	Bad sphere No thermolag

19	20	20	20	20	21	21	21
84R	85R	86R	87R	88R	89R	90R	91R
10-15-71	11-15-71	11-16-71	11-16-71	11-17-71		12-15-71	12-15-71
ETR	ETR	ETR	ETR	ETR	ETR	ETR	ETR
Ablative Coating	Medium ablative coating	Medium ablative coating	Medium ablative coating	Medium ablative coating	Medium ablative coating	Medium ablative coating	Medium ablative coating
84	84	84	84	84	84	84	84
Fair	Unknown	Good	Good	Unknown	Fair	Fair	Good
350	Late radar	372	370	Late radar	355	365	378
129	unknown	130	Late Radar	Unknown	133	Late radar	133
Aluminized 97.8	Aluminized 163.69	Aluminized 164.88	Aluminized 163.68	Aluminized 164.48	Aluminized .64.32	Aluminized 166	Aluminized 168
Special capsule	Delay/2-stg	Delay/2-stg	Delay/2-stg	Delay/2-stg	Delay/2-stg	Delay/2-stg	Delay/2-stg
Bad	Bad	Good	Good	Good	Good	Good	Bad
Deployment	Deployment	130	130	130	105	118	190
Bad sphere	Bad sphere	Good sphere	Good sphere	Good sphere	Good sphere	.035" thermolag good sphere	.035" thermolag bad sphere

21	22	22
92R	93R	94R
12-16-71	1-11-72	1-12-72
ETR	ETR	ETR
Medium ablative coating	Heavy ablative coating	Heavy ablative coating
84	84	84
Fair	Good	Good
345	Late radar	370
131		
Aluminized/168	aluminized/167	aluminized/165
Delay/2-stg	Delay/2-stg	Delay/2-stg
Bad	Good	Good
Deployment	98	105
.035" thermolag bad sphere	.070" thermolag good sphere	.070" thermolag good sphere

inflation capsule was redesigned to a small diameter to accommodate the added thermal protection thickness. An inflation diffuser system was included in some of the flight series 19 units. The diffusor design consists of an outer cylinder about the capsule and a small 9-inch diameter thin film balloon with holes about the outer cylinder. Thus, the inflation takes place in three steps: (1) Capsule to cylinder, (2) Cylinder to small balloon, and (3) Small balloon to Robin. This design should permit a slower inflation rate.

Four Robin flights were conducted during flight series number 19 in October. Two of the flights were with an inflation diffuser and thermolag. These resulted in good spheres. An inflation diffuser without a thermolagged dart resulted in a bad sphere as did the redesigned capsule with thermolag.

The Robin inflation system was redesigned to the final configuration. A six-second pyro delay timer was incorporated within the Robin inflator which used an 0.020-inch hole to meter the inflatant after the capsule is pierced. Thus, inflation takes place after the balloon clears the ejected hardware debris after deployment. The 9-inch diameter was replaced with a single tubular thin-film diffuser about 4 inches x 18 inches. Five units of this design were fabricated and flight tested in thermolagged darts during November.

Three Robin flight systems were fabricated for flight series number 21 which was carried out by range personnel at ETR during December, 1971. These systems were of the same basic design as for series number 20, two orifices .040 inch. However, it was discovered that various tolerances were not the same and had too large an ejection charge. Although the rocket vehicles all performed satisfactorily, the Robin spheres all failed. Redesign efforts were initiated and two additional units were fabricated for flight tests in January, 1972, as flight series number 22. The modifications include retention of the outer staves at the forward end by the ogive, a reduction in inflation orifice size and the incorporation of a spacer in the aft end of the dart to take up tolerance slack internally.

Two Robin darts were flown as flight series number 22 in January. These darts had a similar configuration as for flight series numbers 20 and 21, except that (1) The forward end of the outer staves were retained by the ogive, (2) There was a reduction in the inflation orifice size to one 025 inch, and (3) A spacer was incorporated at the aft end of the staves to take up slack and the thermolag coating was increased to 0.070 inch. Both of these units performed satisfactorily down to collapse altitude of about 32 km or less. Since the series #22 Robin darts performed satisfactorily, further design efforts were halted and the Robin system will be qualified in this configuration.

9.3 Vehicle Performance Analysis

During the development program up to flight series number 19, the vehicle performance had generally been quite good. The instrumented darts had reliably achieved altitudes from 235,000 feet to 260,000 feet. The Robin darts had reliably achieved altitudes from 350,000 feet to 400,000 feet. However, concurrent with flight series number 19, the instrumented dart vehicle performance dropped significantly to altitudes from 208,000 feet to 238,000 feet. The reasons for this decrease in performance is the subject of this section.

Since the loss in vehicle performance occurred at the same time the LAU-66/A launcher base was first used for the Super Loki instrumented dart flights, the launcher base was suspected. Plots of apogee altitude vs apogee range indicated a fairly close cluster of the apogee points about the launch QE (+ 1 degree) for the previous flights which utilized the large general purpose (GP) launcher base. However, there appeared to be a 4-to-5 degree loss in flight path angle when the LAU launcher base was used. This amounts to about a 7,000 foot altitude loss for the instrumented darts. Subsequently, the superstructure of this base was stiffened and the QE loss was reduced to 2-to-3 degrees. This is equivalent to an altitude loss of about 5,000 feet. Since the altitude losses incurred were on the order of 20,000 feet to 30,000 feet, it became obvious that another factor was involved. This was subsequently found to be an increased rocket motor inert weight due to excessive liner and a reduction in propellant weight.

A detailed analysis of the altitude loss factors is presented for the later flight test series in Table 9.10. It can be seen that only about a $\pm$ 2,000 foot altitude variation due to QE effect occurs with the GP launcher. The altitude loss becomes -1,600 feet to -10,400 feet with the LAU launcher. This establishes the fact that there is a launcher effect. Further, it is seen that the liner weight is about 0.50 lb., and the propellant weight average is about 37.70 lb. for the series number 16 units which produced altitudes on the order of 245,000 feet. For the series number 19 units, the liner weight average was increased to about 0.90 lb., and the propellant weight average was reduced to 37.09 lb. The resulting altitudes were on the order of 223,000 feet. This amounts to a loss of about -10,000 feet after allowance is made for the QE loss. Series numbers 23 and 24 resulted in altitude losses on the order of -20,000 feet after QE loss allowances. For these motors the liner weights were up to essentially 1.00 lb., and the propellant weights were down to an average of about 36.70 lb.

The theoretical variation in altitude for the 2 1/8-inch diameter instrumented dart is + 10,605 feet for 1 lb. of propellant and -10,852 feet for 1 lb. of liner. Generally, there is a good correlation between liner weight and propellant weight,

TABLE 9.10 SUPER LOK' 2 1/8" DART PERFORMANCE

Flight	Date	Launcher	Motor #	Prop Wgt (lb)	Liner Wgt (lb)	Pred QE (deg)	Act QE (deg)	Ap Alt (K')	theo	Ap Rng (K')	Δ QE (deg)	QE Loss Alt (K')	Motor Loss Alt (K')
24-101	4-6-72	GP	255	37.19	0.73	84.	84.2	238	244	48	+0.2	+0.4	- 7.5
24-100	4-6-72	GP	230	36.53	1.11	84.	82.8	218	242	57.6	-1.2	-2.4	-22.0
24-99	4-5-72	LAU Mod	228	36.43	1.09	84.	80.9	223	238	75	-3.1	-6.2	-24.20
24-98	4-4-72	LAU Mod	234	36.35	1.11	80.	77.4	208	230	100	-2.6	-5.2	-25.96
24-97	4-4-72	LAU Mod	233	36.69	0.93	80.	77.9	222	231	99	-2.1	-4.2	-18.5
23-96		LAU	249	36.86	0.98	84.	81.8	224	240	68.4	-2.2	-4.4	-14.7
23-95		LAU	216	36.50	84	84.	83.2	209	243	84	-0.8	-1.6	-22.7
Q-1	1-10-72	LAU	237	37.02	0.70	84.	82.0	235	241	69	-2.0	-4.0	-11.2
Q-2	1-10-72	LAU	238	37.08	0.70	84.	79.2	225	235	89	-3.8	-7.6	- 9.9
19-76	10-12-71	LAU	208	36.77	1.12	84.	80.0	222	237	81	-4.0	-8.0	-16.7
19-77	10-12-71	LAU	209	36.93	1.10	84.	78.8	217	234	91.5	-5.2	-10.4	-13.2
19-79	10-14-71	LAU	205	37.45	0.73	84.	79.7	235	236	87	-4.3	-8.6	- 1.8
19-80	10-14-71	LAU	175	37.55	0.70	84.	79.9	232	236	84	-4.1	-8.2	+ 0.4
19-83	10-15-71	LAU	218	36.75	1.17	84.	80.0	210	237	81	-4.0	-8.0	-17.1
17-68	8-10-71	GP	165	37.35	0.70	84.	84.3	255	244	51	+0.3	+0.6	- 4.0
17-69	8-10-71	GP	166	37.20	0.65	84.	84.5	244	244	48	+0.5	+1.0	- 7.3
17-70	8-11-71	GP	170	37.10	0.78	84.	84.6	242	244	45	+0.6	+1.2	- 9.5
17-71	8-11-71	GP	171	37.65	0.75	84	84.2	253	244	51	+0.2	+0.4	+ 2.6
17-73	8-12-71	GP	173	37.40	0.70	84.	84.2	254	244	51	+0.2	+0.4	+ 2.8
17-74	8-12-71	GP				84.	83.2	242	243	58	-0.8	-1.6	
16-60		GP	152	37.59	0.52	84.	84.3	247	244	48	+0.3	+0.6	+ 1.3
16-61		GP	150	37.77	0.52	84.	83.3	247	243	60	-0.7	-1.4	+ 5.3
16-62		GP	149	37.84	0.51	84.	84.0	250	244	52	0	0	+ 6.8
16-63		GP	136	37.79	0.50	84.	84.6	248	245	46	+0.6	+1.2	+ 5.7
16-64		GP	137	37.94	0.51	84.	84.4	245	245	48	+0.4	+0.8	+ 9.0
16-65		GP	157	37.65	0.74	82.	82.0	239	241	69	0	0	+ 2.6
Average of near nominal performance				37.53 lb.	0.63 lb.								

since an increased liner volume takes up propellant volume space. Propellant density is 0.063 lb/in^3, and liner density is 0.050 lb/in^3. Therefore, the tradeoff is about 1.26 lb. of propellant for each pound of liner. Therefore, a motor with one pound less propellant than the nominal should cause the instrumented dart a 19,245 foot reduction in altitude below the nominal.

A theoretical analysis was conducted to describe the launch dynamics. The launch velocity profile is described in Table 9.11. The dart fins release from the launch rails at 100 ms after travelling 5.45 feet. The linear velocity is 128 fps, and the spin rate is 6.05 rps. The booster exits from the launcher at 145 milliseconds after travelling 12.00 feet. The booster exit velocity is 190 fps, and for a well-behaved system the spin rate should remain at about 6.0 rps. Therefore, the booster should rotate through 98.0 degrees after dart fin release, and the rail helix angle should cause the rail position to rotate 111.2 degrees to the same point to the forward end of the launcher. Thus, for a nominal launch the booster fin lag should be 13.2 degrees as compared with the launch rails. A lag of 36 degrees would be required for booster fin-launch rail interference, as indicated in Figure 9.8. It appears that the nominal design has sufficient safety factor for booster fin rail interference unless there is a catastrophic slow-up of the booster spin rate after dart fin separation.

As a result of the above analysis and early flight test results, a design modification was made to offset the booster dart rotational alignment by 13 degrees by relocating the dart anti-roll pin. Thus, the booster fins should end up halfway between the launch rails at the forward end of the launcher during booster exit. This creates an extra allowance for booster spin slow-up during launch.

After the launcher pitch-down effect was discovered when launching the Super Loki instrumented darts from the standard LAU-66/A Loki launcher, the top support assembly was reconstructed to a heavier and stiffer configuration. This was accomplished by employing a twin-tubular beam assembly with thicker and stiffer sidewall plates. This launcher modification reduced the pitch-down effect to 2° to 3°. A stress and dynamics analysis were performed for the modified LAU-66/A launcher which resulted in a 2° to 3° pitch-down in flight QE. The results of the analysis are as follows:

SUMMARY OF LAU LAUNCHER STATIC DEFLECTIONS	
COMPONENT	STATIC DEFLECTION
Baseplate	12.27×10^{-3}
Concrete Pad Bolts	0.21
Fixed Column Bolts	0.93
Fixed Column Footing	0.14
Fixed Column Bending	29.52
Rotating Column Bending	13.29
Total	36.36×10^{-3} deg.

TABLE 9.11

SUPER LOKI LAUNCH PROFILE

Milliseconds	Distance (ft.)	Velocity (fps)
0	0	0
5	0	0
10	0	2
15	0	6
20	0	11
25	0	18
30	0	26
35	0	34
40	0	41
45	0	49
50	1	56
55	1	64
60	1	71
65	2	78
70	2	85
75	2	93
80	3	100
85	3	107
90	4	114
95	5	121
100	5	128
105	6	135
110	6	142
115	7	148
120	8	155
125	9	162
130	10	169
135	10	176
140	11	183
145	12	190
150	13	197
155	14	204
160	15	211
165	16	218
170	17	225
175	18	232
180	20	239
185	21	246
190	22	253
195	23	261
200	25	268

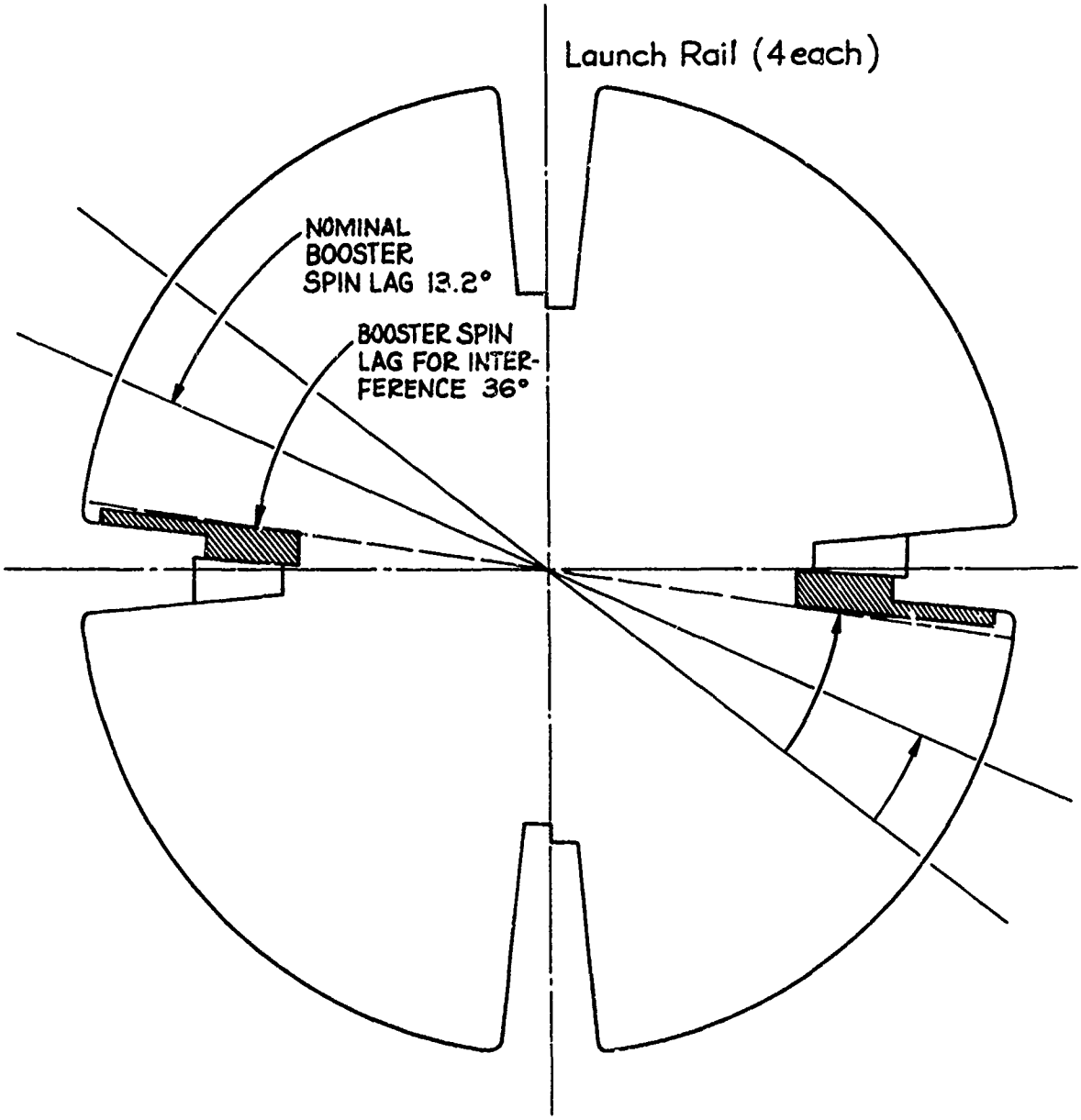

FIGURE 9.8 BOOSTER FIN ROTATION

Thus, it appears that the most flexible members of the modified LAU launcher are the baseplate, fixed column and inner rotating column.

Equivalent launcher stiffness 1.782×10^9 lbf. in^2.

FIRST MODIFIED LAU LAUNCHER, NATURAL BENDING FREQUENCIES		
Superstructure Weight (lb)	f_n 1st Mode (cps)	f_n 2nd Mode (cps)
100	97	621
200	69	439
300	56	357

As the rocket motor travels up the launch rail, the jet blast impinges upon the various ring bulkheads at a rate which increases with rocket velocity. The equivalent forcing function frequency profile is shown in Figure 9.9. This jet impingement frequency is in the same general region as the estimated natural first mode bending frequency of the launcher base and pedestal assembly. Therefore, a resonant bending vibration could be set up in the launcher base and pedestal during the rocket travel along the launch rail. The vibration amplitude magnification factor would grow to be 10 X and greater through the resonant region along the launch rail from a point one foot before to a point one foot after the resonant station. The vibration amplitude and velocity at the forward end of the launch rail is 3.58 times the angular deflection and deflection rate of the pedestal assembly.

The estimated static bending deflection of the launcher would cause less than a +0.130-degree pitch up of the vehicle. Therefore, the most likely cause of the 2-to-3 degree pitch down of the vehicle is a pitch plane vibration of the launch rail due to a resonant bending of the launcher base and pedestal assembly. The vibration amplitudes and rates at the forward end of the launch rail can be from 35 to 100 times the static deflection amplitudes of the launcher base and pedestal during the rocket aft end travel through one foot on either side of the resonant launch rail station.

The maximum jet impingement impulse probably occurs at the forward mounting bracket (Station 8') due to the relatively large area of the bracket. This probably occurs when the rocket motor aft end is at Station 9' to 10' due to the expansion geometry of the jet plume. By increasing the stiffness of the launcher base and pedestal, the natural bending frequency of the launcher can be increased above that of the rocket system. This should eliminate the vehicle pitch down problem.

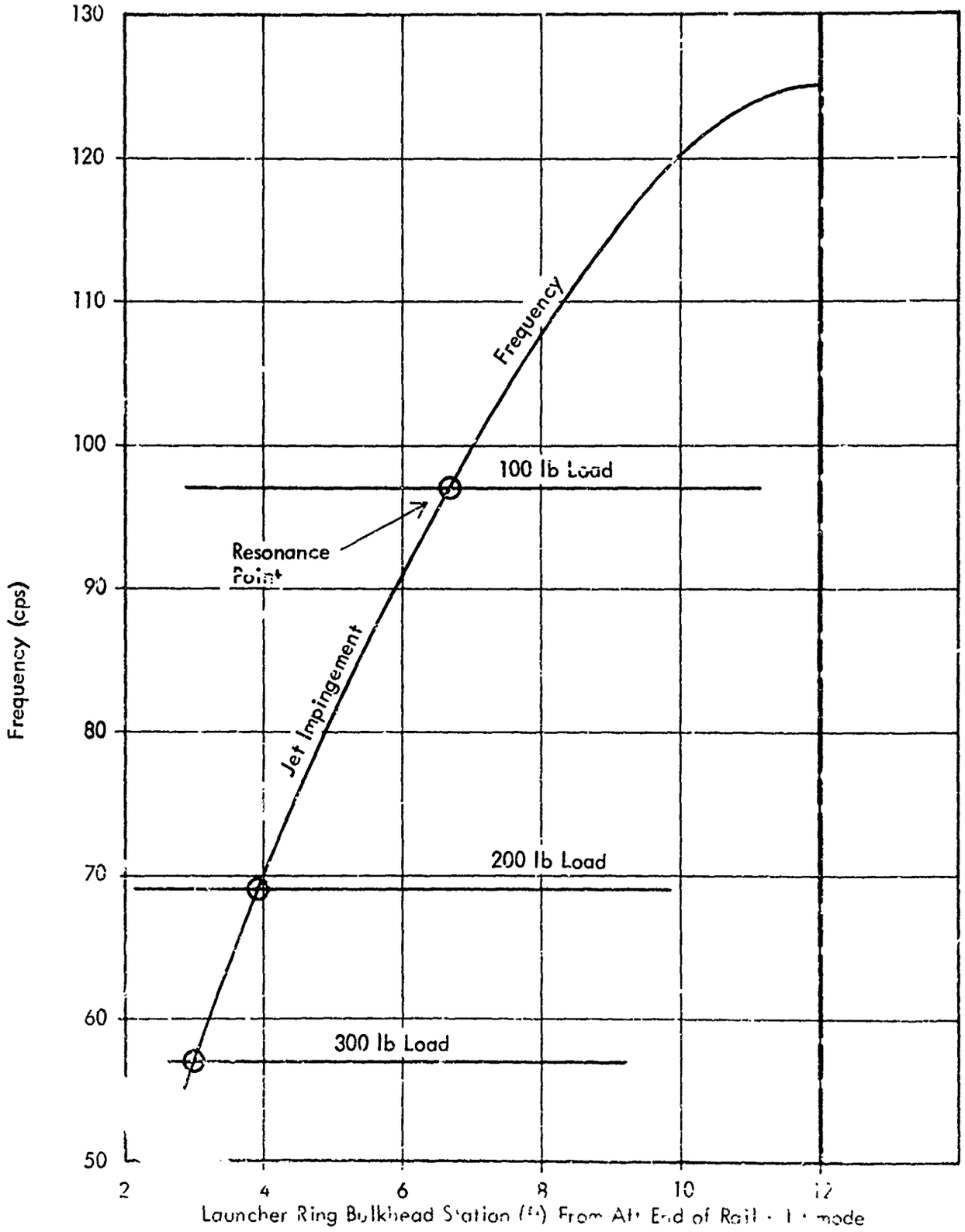

FIGURE 9.9 LAUNCHER VIBRATION RESONANCE

Static loading testings were performed on the launcher to experimentally determine the most flexible components. Stiffening can generally be accomplished by increasing the wall thickness of the various components and in some cases their size. The second modification using larger structures throughout was subsequently made as shown in Figure 6.2 under a later effort. This proved to reduce the pitch-down to a negligible value.

9.4 Payload Ejection Test

A payload ejection ground test for the 2 1/8-inch diameter instrumented dart was conducted during July, 1969. A 10-gram charge of boron potassium nitrate was calculated to give the desired payload separation velocity and maintain the peak acceleration below 200 g. To confirm the theoretical calculations, a ground ejection test was conducted by anchoring the dart at a 45-degree angle from the horizontal and firing a simulated payload and ogive through a ballistic (parabolic) trajectory. Separation velocity was determined by impact range and chamber pressure was monitored with a fast response pressure gage. The results of the ground ejection test are presented in Table 9.12. The chamber pressure profile is shown in Figure 9.10 and the relationship between impact range and initial velocity is shown in Figure 9.11.

Since the dart tube and tail are anchored in place and are not free to move, the ground ejection test is not completely representative of the flight performance conditions. In flight the dart tube and tail are accelerated in the opposite direction from the ogive and payload. This results in a greater separation velocity with a lower acceleration profile than for the ground test conditions. If the separation charge energy is assumed to be the same for both ground and flight test, flight test separation velocities can be calculated using the laws of conservation of energy and momentum as -

$$m_1 V_o^2 = m_1 V_1^2 + m_2 V_2^2 \text{ and}$$

$$m_1 V_1 = m_2 V_2$$

where

m_1	=	mass of forward components
m_2	=	mass of rearward components
V_o	=	ground test eject velocity
V_1	=	eject velocity of forward components
V_2	=	eject velocity of rearward components

assuming the weights of Table 9.13

m_1	=	0.340 slug
m_2	=	0.220 slug
V_o	=	317 ft/sec

TABLE 9.12

SUPER LOKI DART (2 1/8") GROUND

EJECTION TEST DATA

Ejection Charge	10 gm $BKNO_3$ 2A Pellets
Launch Angle	45°
Impact Range	317 feet
Ejection Velocity	100 fps
Pressure Trace:	

Time (ms)	Pressure (psig)
0	0
1	500
2	670
3	770
4.5	800
6	785
8	710
10	650
12	585
14	520
16	470
18	420
20	380
22	350
24	310
25	290
28	260
30	240

Maximum Pressure	800 psig @ 4.5 ms
Exis Pressure	240 psig @ 30 ms
Piston Area	3.050 in^2
Initial Free Volume	6.323 in^3
Stroke Length	26 in.
Payload Weight	11.0 lb
Dart Tube & Tail Weight	5.5 lb
Final Volume	79.0 in^3
Pressure for 200 g in a Static Test	738 psig
Ground Test Max. Acceleration	217 g

TABLE 9.13

ACTUAL SUPER LOKI DART WEIGHTS (2 1/8")

FLIGHT TEST SERIES #1

Ogive	6 lb 14 oz	6.875 lb
Dart Tube	4 lb 3.5 oz	4.218 lb
Dart Tail	2 lb 13.5 oz	2.845 lb
Instrument Staves	14 oz	0.875 lb
Starute & Staves	2 lb 3.5 oz	2.218 lb
Starute	517.8 gm	-
Sonde	428.5 gm	0.945 lb
Ejection Charge, etc.	100 gm	0.220 lb
Total Dart Weight		18.196 lb
Actual Dart Weight		18.25 lb

Forward Ejection

Ogive	6.875 lb
Instrument Staves	0.875 lb
Starute & Staves	2.218 lb
Sonde	0.945 lb

Rearward Ejection

Dart Tube	4.218 lb
Dart Tail	2.845 lb
	7.063 lb

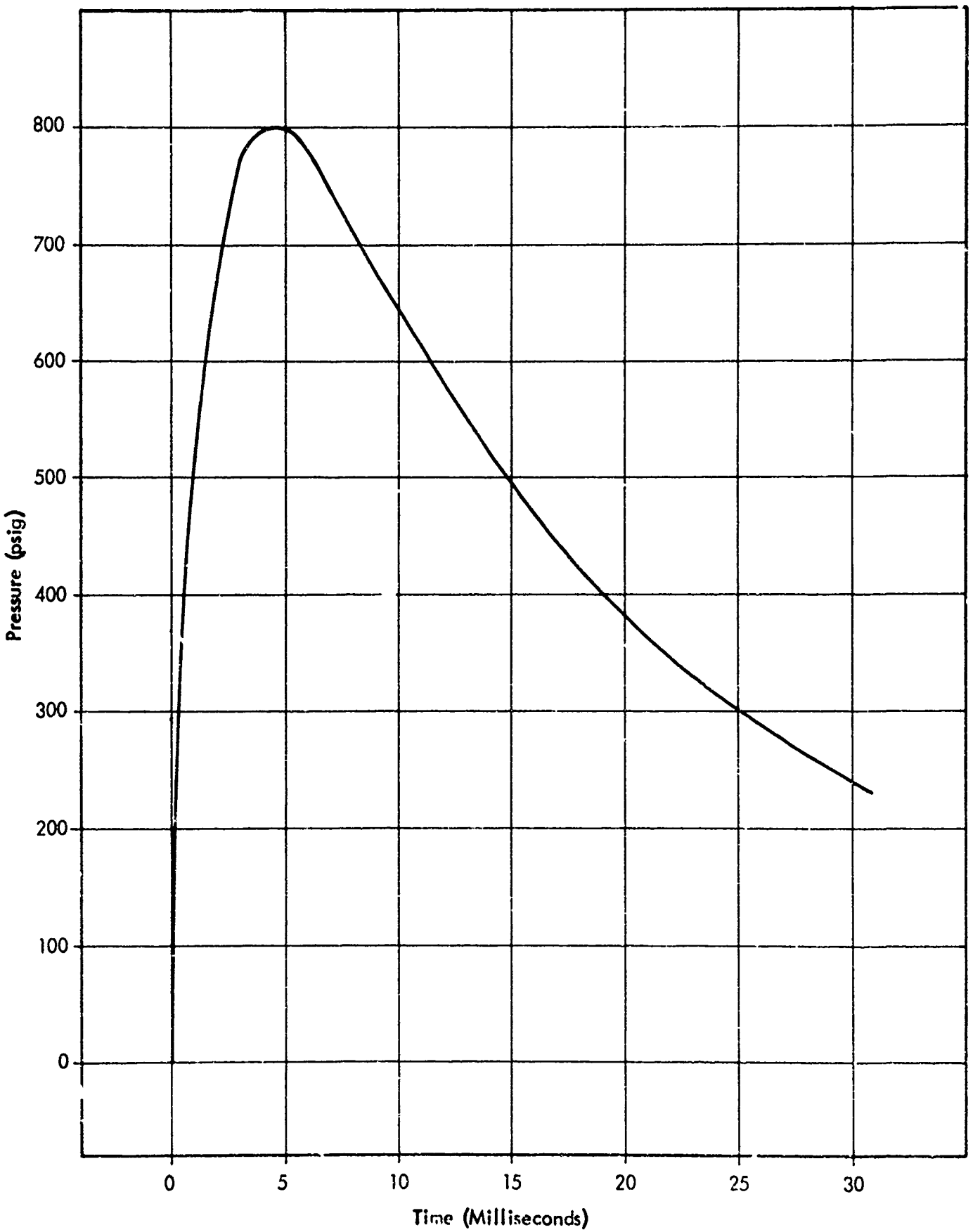

FIGURE 9.10 EJECTION TEST CHAMBER PRESSURE

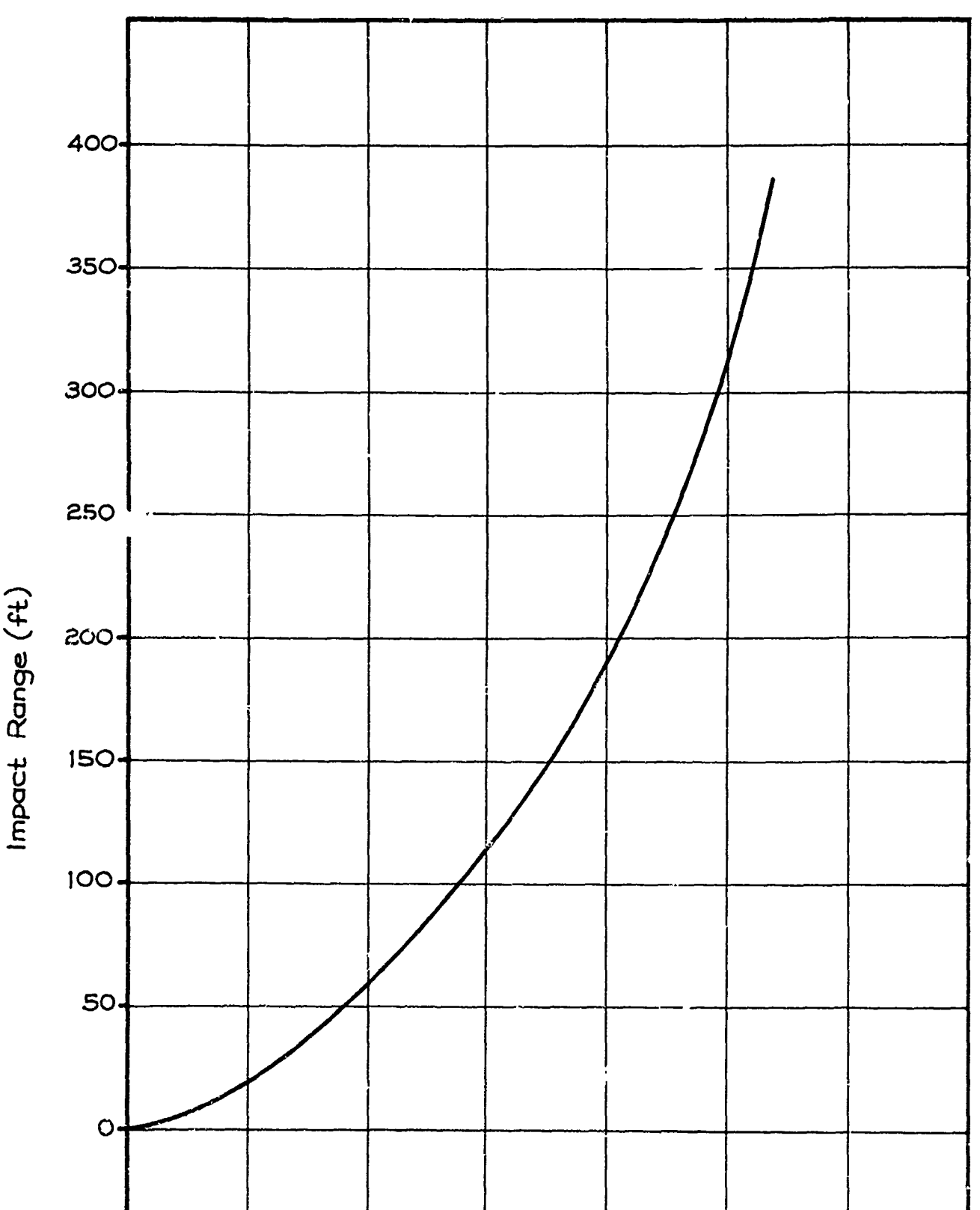

FIGURE 9.11 EJECTION TEST IMPACT RANGE VS INITIAL VELOCITY

then

$$V_1 = 198.7 \text{ ft/sec}$$

$$V_2 = 307.1 \text{ ft/sec}$$

Therefore, the theoretical separation velocity during a flight test is $V_1 + V_2 = 505.8$ ft/sec. The acceleration profile will be less than the ground test value, because the forward and rearward ejecting components will increase the chamber volume at a faster rate during a flight ejection and thereby reduce the chamber pressure vs time curve. This value is difficult to calculate.

It appears that the 10 gram separation charge is satisfactory and this is the value which has been selected for the initial flight test series for the 2 1/8-inch dart.

9.5 Starute Performance Review

The Super Loki Starute is essentially a scale-up in size from the standard Loki 7-foot Starute. The initial Super Loki Starute was sized to 12 feet in order to provide as slow a descent rate as possible in the higher altitude regions and still be able to be packaged into the 2 1/8-inch diameter instrumented dart. Although some limited success was achieved with this Starute size early in the flight test program, the reliability was not good. After a good deal of structural modifications and ground-testing, it was finally determined that aerodynamic heating was causing the Mylar film to stick together, and upon deployment, to rip apart. This was also found to be the case with the Loki 7-foot Starute and Viper Robin failures during the same time period.

Although improvements were subsequently made in the thermal protection of the Super Loki 12-foot Starute by means of air gaps, IR reflective coatings and cork insulation, the flight reliability still appeared to be erratic from one flight series to the next. Again, many flights, pieces reported but no large increase in fall rate.

Finally, a complete aerodynamic heat transfer analysis was performed for the existing configurations flown in the flight series numbers 15 through 19. It was found that although the radiant heat transfer was negligible, the heat conducted across the small air gap between the staves and the dart wall was appreciable. The results of the heat transfer analysis are presented in the following section. As a result of this analysis, it was decided to either use an ablative coating on the dart body or to reduce the size of the Starute to permit an appreciable air gap between the dart wall and the Starute staves. AFCRL chose the latter alternative to keep the system cost to a minimum.

The Starute was redesigned to the 10-foot side dimension, the staves were redesigned to a heavy wall for a thermal heat sink and a smaller diameter to provide a large air gap to the dart wall. This configuration was successfully flown in flight series 23 and 24 with good results.

An historical review of the Super Loki Starute performance is presented in Table 9.14. It can be seen that the Starute performance was poor prior to the incorporation of thermal protection modifications starting with series 6. Although the reliability was significantly improved by these modifications, the overall failure rate was approximately 20% as judged by telemetry signal dropout patterns. The Starute breakup rate was about 12% during this period. After the redesign to the 10-foot Starute and the large air-gap, all of the units performed satisfactorily. The ballistic coefficients for the various Starutes are presented in Table 9.15. The descent rate curves are presented in Figure 9.12.

9.6 Aerodynamic Heat Transfer Analysis

9.6.1 General

Aerodynamic heating of the dart outer wall is quite severe since the dart traverses the lower atmosphere at relatively high velocities. Aerodynamic heating input pulse conditions for the 2 1/8-inch diameter instrumented dart and the 1 5/8-inch diameter Robin dart are presented in Table 9.16 for an 80° QE launch. These conditions indicate that the aerodynamic heating input rate is both severe enough and sufficiently long in duration to cause a significant increase in dart wall temperature. Since the heating environment of the smaller 1 5/8-inch diameter Robin dart is so severe and the payload packaging volume so limited, it was decided to use an ablative coating for this dart. Therefore, the aerodynamic heating analysis was directed principally at the larger 2 1/8-inch diameter instrumented dart which travels in a somewhat less severe environment and has some diametral space available for thermal protection.

Flight experience has shown that the first and most critical problem due to aerodynamic heating is the failure of the Mylar payload devices such as Starutes and inflatable spheres. These devices appear to fail in less severe aeroheating environments than do the electronic instrument payloads. Laboratory testing indicates that Mylar starts to shrink at 125°C, becomes tacky at 135°C and disintegrates at 145°C. Thus, it is important to keep such devices below 100°C.

The aerodynamic heating first causes the dart outer wall to rise in temperature by direct conduction from the hot boundry layer to the steel wall. As the dart wall rises in temperature, it radiates heat from its outer surface to space and from its inner surface to the payload stave. Also, heat is transferred across the air

TABLE 9.14 SUPER LOKI STARUTE FLIGHT TEST SUMMARY

	Flight No.	Comments	B (psf)
	1-1	Late Inflation - dropouts	.060 - .030
	1-2	Good - some dropouts	.017
	1-3	Good - good signal - very few dropouts	.016
	1-4	Questionable radar data or tracking piece	
	2-5	No radar nor GMD track	
	3-6	Good-fair signal - some dropouts	.025 - .020
	3-7	Radar Tracking Slow Piece - GMD splash 11.5 min	
	3-8	Radar Tracking Slow Piece - GMD splash 7.5 min	
	4-9	Good - good GMD signal	.018
*	4-10	Medium Fast Fall Rate - pieces off signal strength erratic	.030 - .020
*	4-11	Medium Fast Fall Rate - pieces off signal dropouts	.030 - .020
	4-12	Low	
	5-13	Fast Fall Rate - Starute breakup	
	5-14	Fast Fall Rate - Starute breakup	
	5-15	Fast Fall Rate, Starute breakup	
**	6-16	Good - good signal	.015
	6-17	Good - good signal	.015
	7-18	Slow Starute-Sonde Lanyard Melted	.010
	7-19	Good Starute - good signal	.016

7-20	Good Starute - interference	.016
7-21	Good Starute - good signal	.018
8-22	Good starute - fair signal - some dropouts	
8-23	Good starute - good signal	
8-24	Good starute - good signal	
8-25	Good starute - good signal	
9-26	Good starute - bad sonde	.017
9-27	Good Starute - good carrier	.018
9-28	Good starute - good carrier	.017
9-29	Good starute - bad sonde	.018
9-30	Good Starute - good signal	.016
10-31	Good Starute - good signal	.017
10-32	Good Starute - good carrier	.019
10-33	Good Starute - good signal	.018
10-34	Late Radar - Starute breakup	
10-35	Low flight	
11-36	Pieces Off-Severe Dropouts	.040 - .020
11-37	Good Starute - good signal	.025 - .018
11-38	Good Starute - good signal	.018
11-30	Good Starute - good signal	.018
11-40	Good Starute - good signal	.018
12-41	Good Starute - good signal	.018
12-42	Good Starute - good signal	.02
13-43	Good Starute - good signal	.019
13-44	Good Starute - good signal	.019

	13-45	Good Starute - noisy signal	.020
	13-46	Good Starute - sonde drop off	.010
	13-47	Good Starute - good signal	.018
	13-48	Good Starute - good signal	.018
	14-49	Good Starute - good signal	.018
	14-50	Pieces Off- lost RF at deployment	.019
	14-51	Pieces off - Good signal	.017
	14-52	Good Starute - good signal	.017
	15-53	Pieces off - dropouts	.020
	15-54	Good Starute - good signal	.018
	15-55	Good Starute - good signal	.017
	15-56	Good Starute - good signal	.018
	15-57	Good Starute - lost RF	.018
	15-58	Pieces off - lost RF	.027 - .02
	15-59	Pieces off - lost RF	
	16-60	Good Starute - good signal	.017
	16-61	Good Starute - good signal	.02
	16-62	Good Starute - good signal	.018
	16-63	Good Starute - good signal	.016 - .017
	16-64	Good Starute - good signal	.019
	16-65	Good Starute - good signal	.018
	17-68	Good Starute - good signal	.016
	17-69	Good Starute - good signal	.017
	17-70	Good Starut - good signal	.016
***	17-71	Questionable - hot temps. cleared up	.018
	17-73	Breakup	.020
	17-74	Good Starute - good signal	

19-76	Good Starute - weak signal	.02
19-77	Good Starute - erratic signal	.018
19-79	Questionable data - rapid dropouts	.018
19-80	Good Starute - good signal	.02
19-83	Good Starute - sonde dropped off	
23-95	Good Starute - good signal	.020
23-96	Good Starute - good signal	.020
23-97	Good Starute - lost RF	.020
23-98	Questionable data - lost RF	-
23-99	Good Starute - good signal	.020
24-100	Good Starute - good signal	.020
23-102	Good Starute - good signal	.021

* 2,000" dia. dart

** Started Heat Protection Modifications

*** Recovery Pilot Reported Hole in Side of Starute

**** Start of new 10' Starute Design with added Thermal Protection

TABLE 9.15 STARUTE SYSTEMS BALLISTIC COEFFICIENTS

Starute System	Ballistic Coefficient B (psf)
Loki 7' Starute/Datasonde	0.030
Super Loki 10' Starute/Xponder	0.020
Super Loki 12' Starute/Xponder	0.018

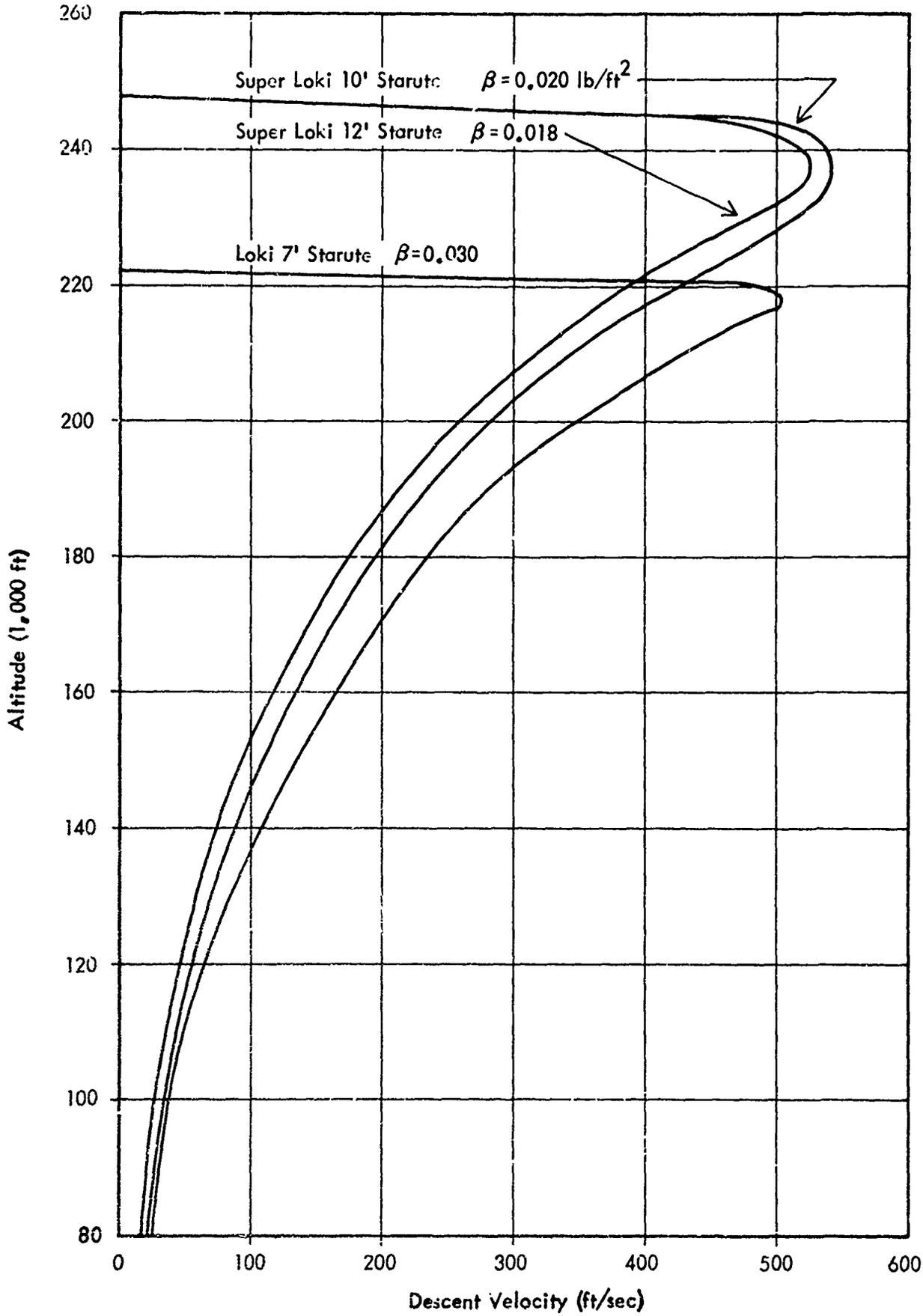

FIGURE 9.12 STARUTE DESCENT RATES

TABLE 9.16 AERODYNAMIC HEATING INPUT PULSE CONDITIONS

FOR THE

SUPER LOKI DARTS 80° QESL

	Flight Time (sec)	Altitude (ft)	Mach No.
2 1/8" Diameter Dart:			
Start Heat Pulse	1.4	1,787	3.0
Maximum Heat Pulse	2.0	4,455	4.9
End Heat Pulse	18.1	67,818	3.5
1 5/8" Diameter Dart:			
Start Heat Pulse	1.3	1,650	3.0
Maximum Heat Pulse	2.0	4,871	5.4
End Heat Pulse	23.1	102,856	4.2

gap between the dart wall and the payload stave by conduction. The stave steel wall will then start to rise in temperature and transfer heat to the payload through intervening air gaps and/or insulation layers primarily by conduction. Therefore, the overall heat transfer to the payload is a complex problem of multilayered radiation and conduction under dynamic conditions. For the ensuing analysis, this problem was broken down into discrete sub-analyses to obtain a gross estimate of payload heating and to locate potential sources of thermal protection. The results of these analyses are presented in the following sections.

9.6.2 Dart Wall Temperature

The dart wall temperature-time profile is extremely important in determining the heat transferred inwardly to the payload since it is the only direct driving force or heat source. Since the payload is retained for 120 seconds at which time deployment is affected, this temperature source is important for that length of time. Estimate dart wall temperatures are plotted against time in Figure 9.13 for various external dart wall emissivities. It can be seen that a high external dart wall emissivity will permit significant cooling of the dart wall by radiation to space. Thus, with a highly emissive outer surface, considerably less heat will be transferred inward to the payload.

Various surface finishes were evaluated with an infrared spectrophotometer, by laboratory heating rate measurements and from handbook valves for surface emissivity. The results are presented in Table 9.17. Even though the black paints have the highest emissivity, the black oxide finish was selected. It was believed that the black paints would blister and disintegrate under the high aerodynamic heating temperatures. The inner surface of the dart tube wall was plated with electroless nickel to prevent rusting and maintain a reasonably low emissivity to reduce radiation inward.

9.6.3 Stave Temperature

The stave temperature rise depends upon the radiative heat transfer from the dart inner wall, the conductive heat transfer across the air gap and the heat sinking capability (heat capacity) of the stave itself. A minute amount of heat transfer into the Mylar film payload will cause it to raise to the stave temperature level, hence heat loss inward from the staves is an insignificant factor in determining their transient temperature response.

A heat transfer analysis was performed to investigate the effects of dart wall exterior emissivity, stave wall exterior emissivity, air gap thickness, stave weight and initial dart wall temperature upon stave temperature. A single air gap, single stave configuration was investigated in addition to a double stave, double air gap configuration. The analysis and results are presented as follows:

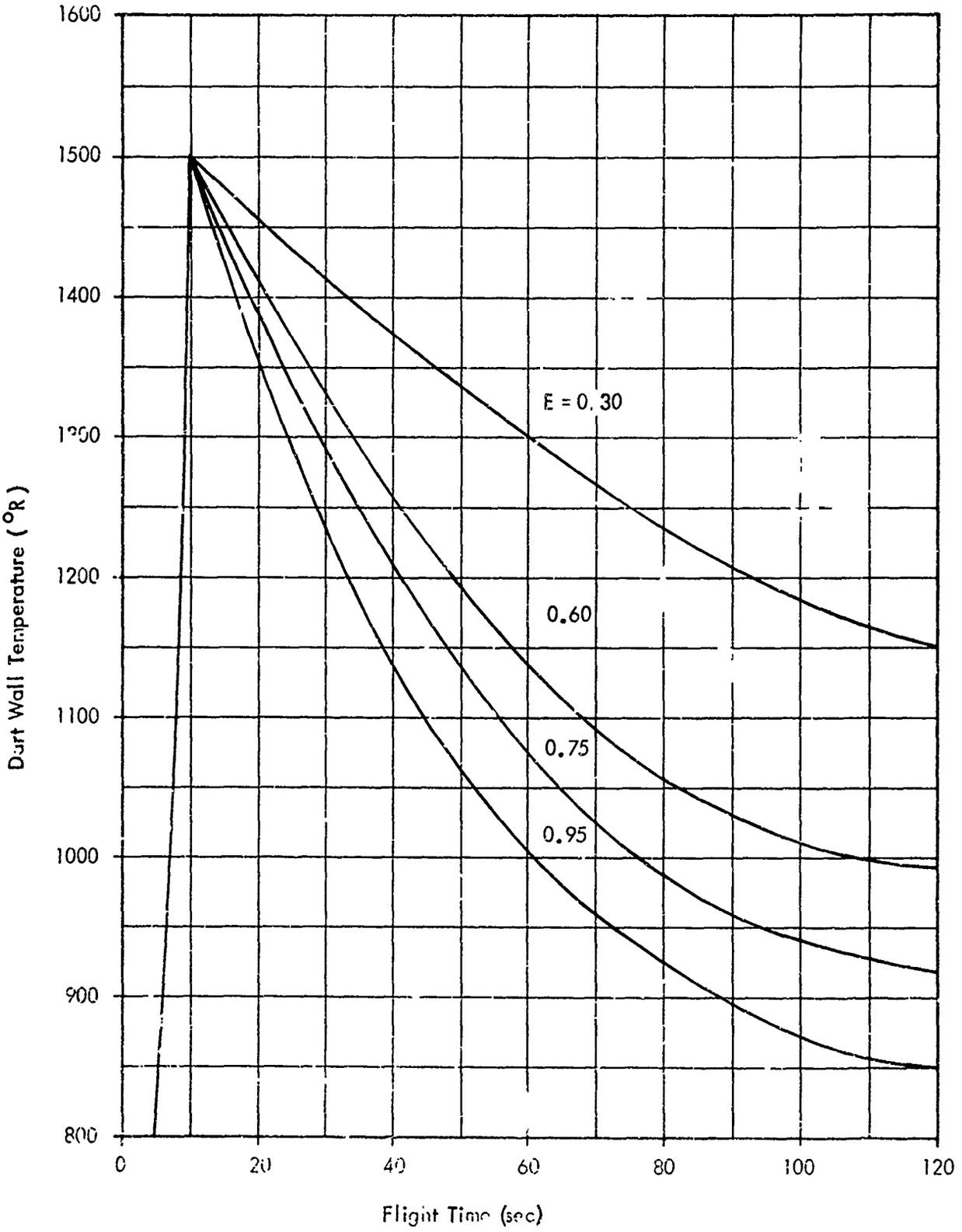

FIGURE 3.13 DART WALL TEMPERATURE FOR VARIOUS EXTERNAL SURFACE EMMISSIVITIES

TABLE 9.17 SURFACE FINISH EMMISSIVITIES

λ - 3 to 40 μ

Sample	Emmissivity, E
Aluminum, mystik tape	0.22
Aluminum Foil, Reynolds Wrap	0.05
Black Oxided Steel	0.69
Copper Plate, Shinny	0.18
Cadmium Plate, Type II	0.25
Cadmium Plate, Type I	0.38
Passivated Stainless Steel	0.65
Bright Nickel	0.30
Electroless Nickel	0.30
Mild Steel	0.24
Nextel Black Velvet Paint	0.98
Cat-a-lac Flat White Paint	0.90
Cat-a-lac Flat Black Paint	0.90

A heat transfer analysis was performed to investigate the effects of dart wall exterior emmissivity, stave wall exterior emmissivity, air gap thickness, stave weight and initial dart wall temperature upon stave temperature. A single air gap single stave configuration was investigated in addition to a double stave double air gap configuration. The analysis and results are presented as follows:

Configuration I. Single Stave, Single Air Gap

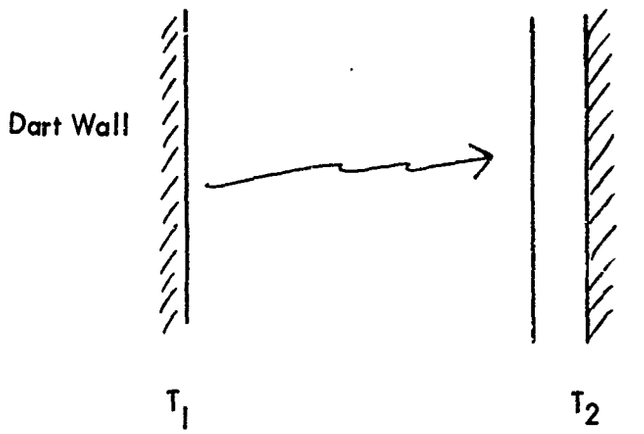

$$\Delta T_2 = \frac{\dot{q}_{12} \cdot \Delta t}{C_2 W_2} \text{ stave} \quad ; \quad \Delta T_1 = \frac{\dot{q}_{12} \cdot \Delta t}{C_1 W_1}$$

$$\dot{q}_{12} = \frac{kA}{x}(T_1 - T_2) + \sigma A \frac{1}{1/E_1 + 1/E_2 - 1}\left(T_1^4 - T_2^4\right)$$

where

T_1 = dart wall temperature

T_2 = stave temperature

k = conductivity across air gap

A = surface area

x = air gap thickness

σ = Boltzmann constant

E_1 = inner dart surface emissivity

E_2 = outer stave surface emissivity

$\dot{q}_{12}$ = heat transfer rate from dart wall to staves

C_2 = specific heat of staves

W_2 = weight of staves

C_1 = specific heat of dart wall

W_1 = weight of dart wall

Let $K_1 = \frac{kA}{x}$

$K_2 = \sigma A \left[\frac{1}{1/E_1 + 1/E_2 - 1}\right]$

$K_3 = \frac{At}{C_1 W_1}$

$K_4 = \frac{At}{C_2 W_2}$

Various conditions were run for this single stave, single air gap configurations, and the resulting stave temperature profiles are plotted in Figure 9.14. The cases are described as follows:

Case 1.

$X = 0.0445"$ or $0.003708'$

$C_1 = C_2 = 0.10\ B \cdot lb^{-1} \cdot R^{-1}$

$W_1 = 2.649\ lb/ft^2$

$W_2 = 1.426\ lb/ft^2$

$A = 1\ ft^2$

$k_{air} = 4.068 \times 10^{-6}\ B \cdot ft^{-1} \cdot sec^{-1} \cdot R^{-1}$

$T_{10} = 1500^\circ R$

$T_{20} = 530^\circ R$

$E = 0.60$ for black oxided dart exterior

$E_1 = 0.30$ for electroless nickel dart interior

$E_2 = 0.05$ for aluminum foil stave exterior

$T_1 = T_{10} - K_3\ \dot{q}_{12}$ - radiation loss to outside

$K_1 = 1.0970 \times 10^{-3}\ B \cdot sec^{-1} \cdot R^{-1}$

$K_2 = 2.127 \times 10^{-14}\ B \cdot sec^{-1} \cdot R^{-4}$

$K_3 = 37.75\ sec \cdot R \cdot B^{-1}$

$K_4 = 70.13\ sec \cdot R \cdot B^{-1}$

Radiation Heat Transfer	10%
Conduction Heat Transfer	90%
Maximum Dart Temperature	$460^\circ F$

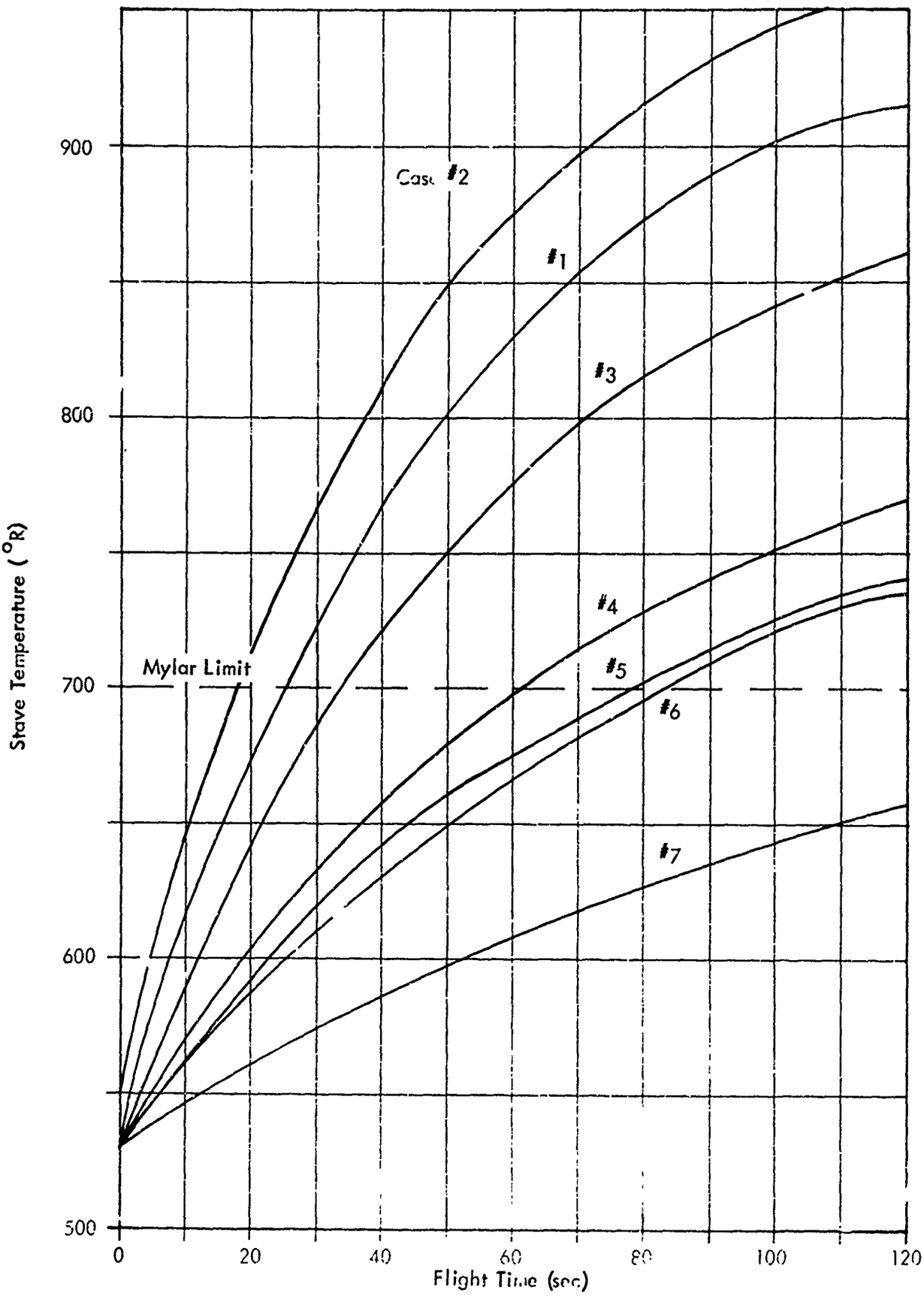

FIGURE 9.14 STAVE TEMPERATURE - SINGLE STAVE/SINGLE AIR GAP

Case 2. Same as Case 1 except:

E_2 = 0.30 electroless nickel stave exterior

K_2 = 8.382×10^{-14} $B \cdot sec^{-1} \cdot R^{-4}$

Radiation Heat Transfer 28%

Conduction Heat Transfer 72%

Maximum Stave Temperature 505°F

Case 3. Same as Case 1 except:

T_{10} = 1300° R initial dart wall temperature

Radiation Heat Transfer 5%

Conduction Heat Transfer 95%

Maximum Stave Temperature 402°F

Case 4. Same as Case 1 except:

W_2 = 2.852 lb double stave weight

K_4 = 35.06 $sec \cdot R \cdot B^{-1}$

Maximum Stave Temperature 311°F

Case 5. Same as Case 1 except:

X = 0.119" or 0.0099 larger air gap

K_1 = 4.056×10^{-4} $B \cdot sec^{-1} \cdot R^{-1}$

K_2 = 2.127×10^{-14} $B \cdot sec^{-1} \cdot R^{-4}$

K_3 = 37.75 $sec \cdot R \cdot B^{-1}$

K_4 = 70.13 $sec \cdot R \cdot B^{-1}$

Maximum Stave Temperature 281°F

Case 6. Same as Case 1 except:

X = 0.200" or 0.01667' larger air gap

E = 0.30 reduced external dart wall emissivity

K_1 = 2.440×10^{-4} $B \cdot sec^{-1} \cdot R^{-1}$

K_2 = 3.852×10^{-14} $B \cdot sec^{-1} \cdot R^{-14}$

Maximum Stave Temperature 285°F

Case 7. Same as Case 1 except:

X = 0.165" larger air gap

W_2 = 2.852 lb double stave weight

K_1 = 2.958×10^{-4} $B \cdot sec^{-1} \cdot R^{-1}$

K_2 = 3.852×10^{-14} $B \cdot sec^{-1} \cdot R^{-14}$

K_3 = 37.75 $sec \cdot R \cdot B^{-1}$

K_4 = 35.06 $sec \cdot R \cdot B^{-1}$

Maximum Stave Temperature 198°F

Thus, with a single air gap configuration, the Mylar temperature limit of about 700°R (240° F) is exceeded prior to deployment time in all of the above cases except number 7. The first case represents the configuration flown earlier in the program with marginal reliability. The main differences in case 7 are a large increase in the air gap thickness and an increase in the weight of the staves to provide a greater heat sink.

Configuration 2. Double Staves, Double Air Gap

The double staves, double air gap configuration was analyzed by using two sequential and independent solutions of the equations presented for configuration heat transfer. A similar series of cases were calculated from the double systems. The resulting temperature profiles and heat transfer rates indicated that for a given available space or path length that the double stave system was only slightly better than the single stave system. The double stave system reduced the radiant heat

transfer rates which were already quite small, but increased the larger conductive heat transfer rates above that for a pure air gap. The overall differences for the practical cases studies were found to be negligible.

9.6.4 Stave Insulation

Although asbestos had originally been used to insulate the electronic payload and the decelerator payloads from the stave temperatures, it was found that cork was a much better insulator. The thermal conductivity of cork is about 0.025 B . hr^{-1} . ft^{-2} . F^{-1} dt. and for asbestos this value is 0.096. Thus, cork was considered as an inner layer for both the instrument and Starute staves. However, calculations indicated that for a small thickness of cork and the relatively long rocket vehicle coast time prior to deployment, very little would be gained. A heating experiment was performed to verify the conduction calculations. A thin layer (0.062") of cork was placed against a constant temperature heat source and a thermocouple was placed against the opposite side of the cork layer. The temperature rise time data, as shown in Figure 9.15, verify the calculations that over a 120-second period a thin layer of any insulating material is not at all effective in reducing the temperature rise. Figure 9.16 indicates that for the 120-second flight time to deployment a relatively thick layer of cork would be required to appreciably drop the temperature below that of the staves.

9.6.5 Summary

A summary of the heat transfer analysis is listed as follows:

a. A high value for the exterior surface emissivity of the dart is important to rid the dart body of its accumulated heat by means of radiation to space.

b. For the most recent 12-foot Starute stave configuration with clean aluminum foil, 90% of the heat transfer is by conduction across the air gap and 10% is by radiation. If the staves become oily, temperature increases by 50°F, and radiation comprises 30% of the heat transfer.

c. By increasing the air gap from 0.044" to 0.120" the stave temperature is reduced from 385°F to 211°F.

d. Stave mass or weight affects stave temperature drastically. By doubling the weight of the staves, the temperature can be reduced by 145°F.

e. Although a double stave, double air gap system reduces radiation heat transfer, conduction transfer is increased. For equivalent gap sizes, the double stave system is not an improvement.

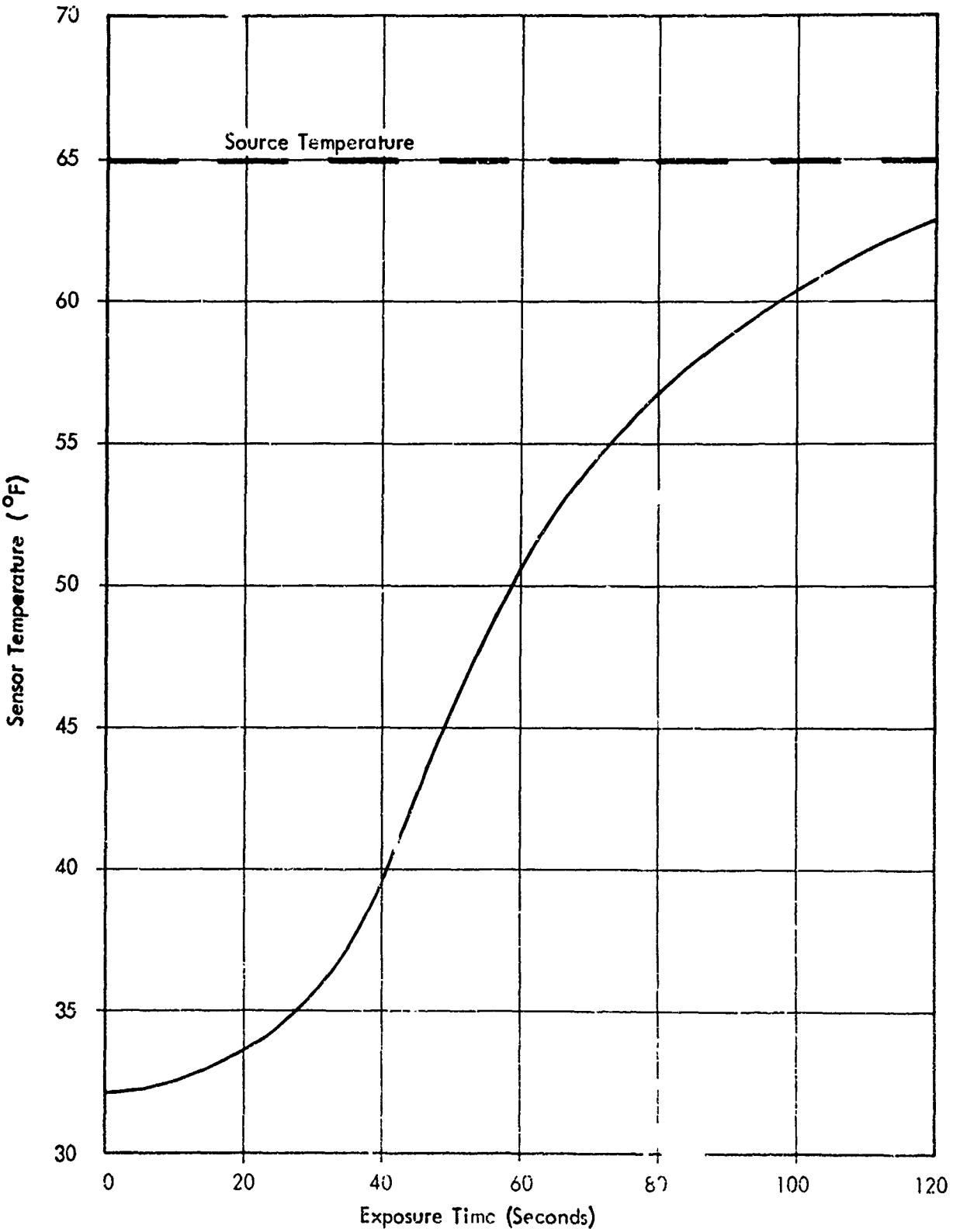

FIGURE 9.15 THERMAL CONDUCTION EXPERIMENT
0.062 LAYER OF CORK

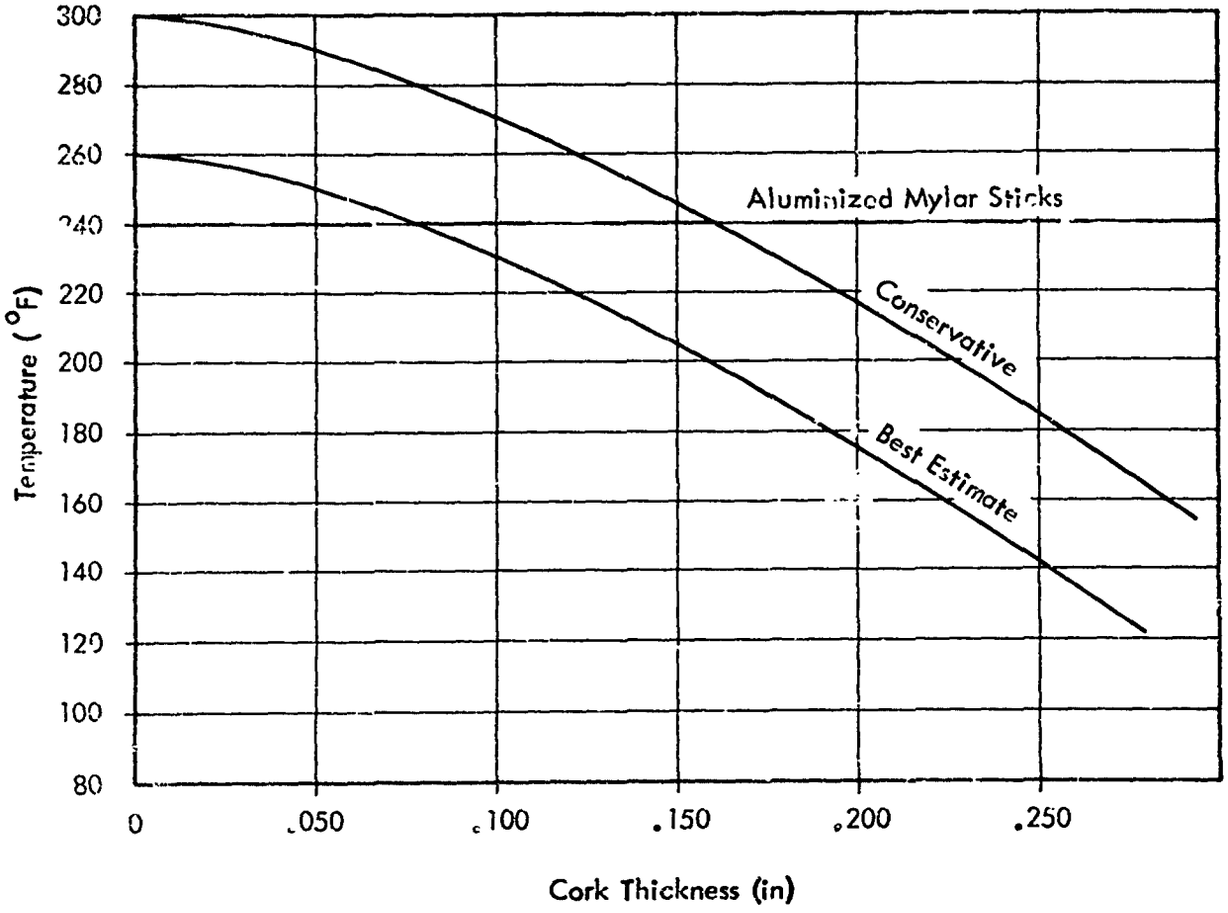

FIGURE 9.16 CORK INNER BOUNDRY TEMPERATURE VS CORK THICKNESS FOR 120 SECOND TIME PERIOD

9.7 Robin Falling Sphere Payload Performance

9.7.1 Flight Summary

A summary of the Robin falling sphere payload flight performance is presented in Table 9.18. It can be seen that none of the flights with less than a 0.050-inch thickness of ablative coating were fully successful. A 0.070-inch coating thickness is probably required for good reliability although the sample size is small. It also appears that improved reliability is achieved with the delay two-stage inflation design. The configuration used in the last flight series, number 22, has been adopted as the final design.

The descent velocity profile for the final design sphere is shown together with the previous lighter weight sphere velocity profile in Figure 9.17. The descent times for the final design sphere are presented in Figure 9.14.

9.7.2 Reliability Problems

Reliability problems with the falling sphere payloads have been failure to inflate, deployment bursting and premature deflation, i.e., above the deflation design altitude. Malfunction of the inflation capsule could be the cause of failures to inflate although entrapped air should cause sphere inflation down to about 70 km altitudes. The new inflator design should eliminate capsule failure problems. Deployment bursting is no doubt due to leaking inflatant capsules. The free inflatant can cause such a rapid overpressure at deployment as to shock the Mylar membrane of the sphere into fragmentation. Again, the new inflator design should eliminate this problem.

Premature deflation remains as a serious problem in the Robin system not only because of the loss of data below the inflation altitude, but also because the data may be biased above. This can be due to inflatant leaking from the sphere and reducing sphere mass during descent while the internal pressure is still adequate to maintain inflation. (This is discussed in the next section.) Premature deflation can be caused by pinhole leaks, burnholes, abrasion damage, seam failures or rips in the sphere material. The new delay two-stage inflator should help to eliminate these problems. A second mode of failure is due to the overheating of the Mylar sphere material which causes softening and sticking together of the packaged unit. Upon deployment and inflation, the sticking pieces probably rip apart and cause some damage to the sphere skin. This has been the most probable mode of failure and premature deflation for most of the previous flights. The solution is an adequate coating of ablative material on the dart vehicle.

A series of sphere burst tests were carried out during the development program to validate the adequacy of the design. The sphere diameters increased on the order of 2.00 cm (2%) from bare inflation to the burst pressure which was on the order 55 mb. Since normal operating superpressures are on the order of only about 10

TABLE 9.14 SUPER LOKI ROBIN FLIGHT TEST SUMMARY

Flight Series	Inflator Design	Ablative Coating Thickness (ins)	Deflation Altitude (1,000 ft)
17-66R	Old capsule	none	Deployment
17-67R	Old capsule	none	Deployment
17-72R	Old capsule	none	Deployment
18-75R	Old capsule	0.050	Deployment
19-78R	Diffusor	0.050	150 Bad
19-81R	Diffusor	0.050	100 Good
19-82R	Diffusor	none	Deployment
20-84R	Special capsule	0.050	Deployment
20-85R	Delay	.050	Deployment
20-86R	Delay	.050	132 Fair
20-87R	Delay	.050	126 Fair
20-88R	Delay	.050	130 Fair
20-89R	Delay	.050	105 Good
21-90R	Delay	.035	118 Fair
21-91R	Delay	.035	190 Bad
21-92R	Delay	.035	Deployment
22-93R	Delay	.070	98 Good
22-94R	Delay	.070	105 Good

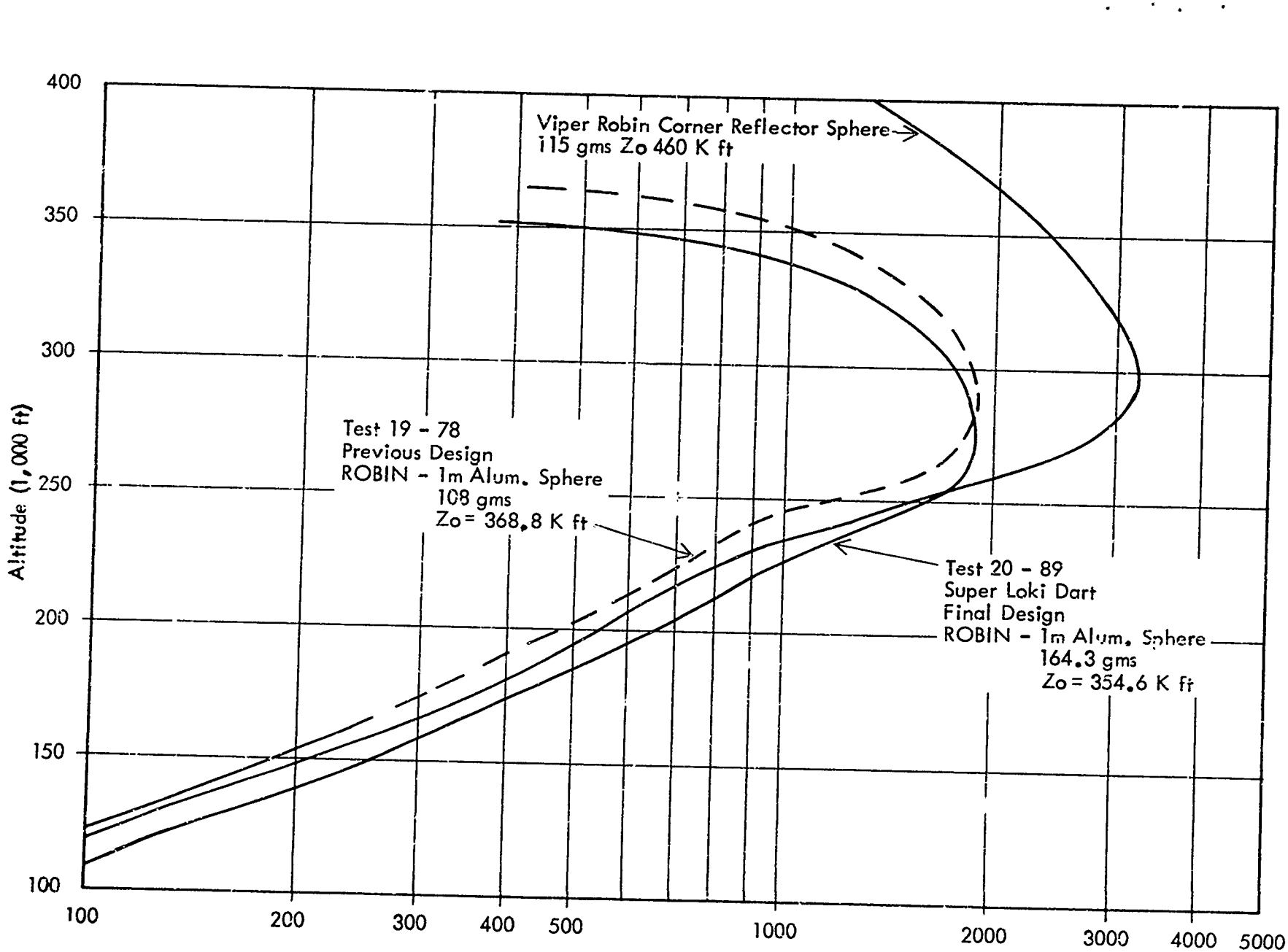

FIGURE 9.17 ROBIN FALLING SPHERE PAYLOAD DESCENT PROFILES

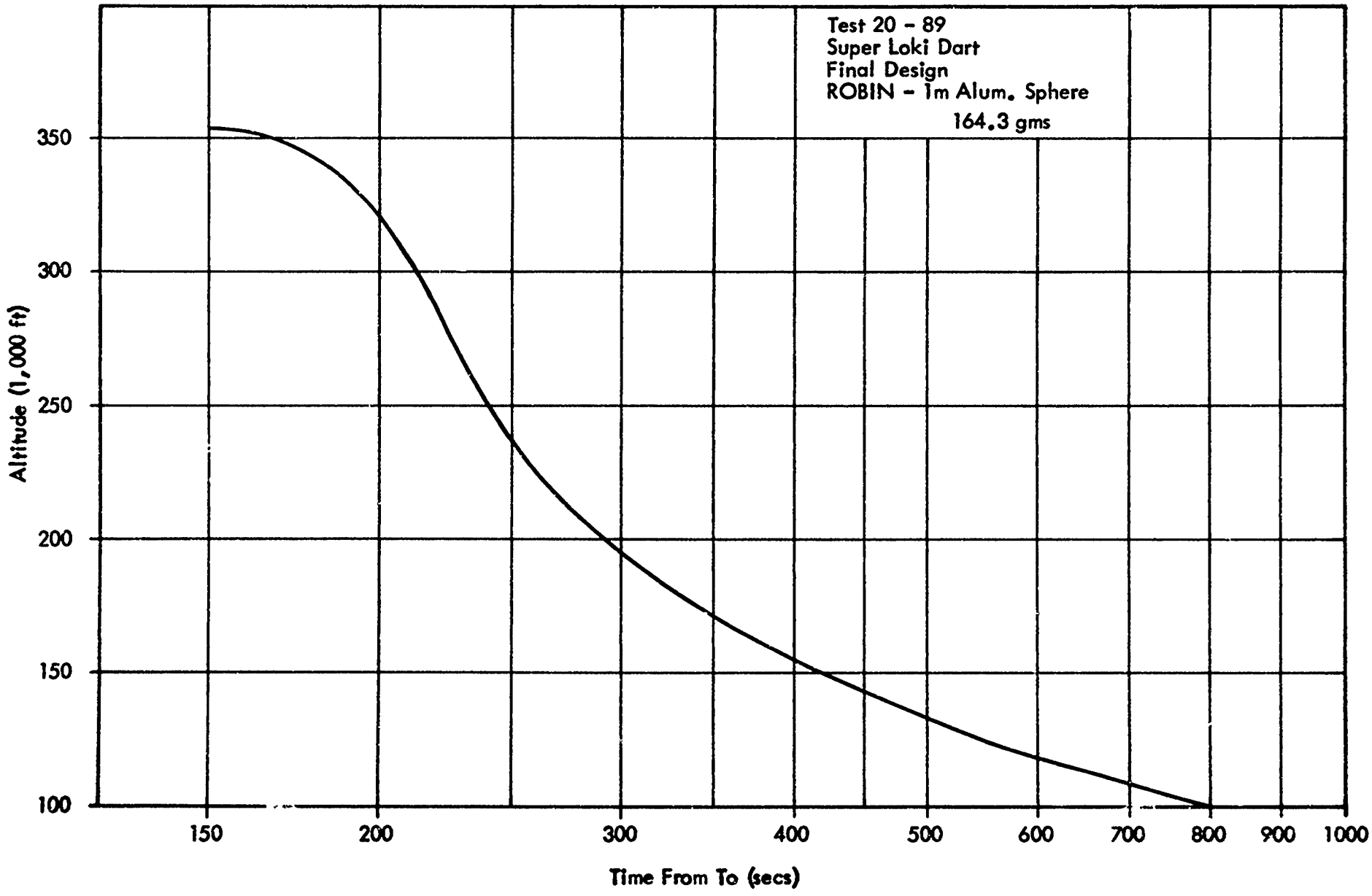

FIGURE 9.18 DESCENT TIME PROFILE FOR FINAL DESIGN SPHERE

to 12 mb, the deviation in sphere diameter due to pressure changes should be only about 0.43 cm or 0.43% for the sphere going from high altitude inflation to low altitude deflation. The real unknown in this estimate is the gas temperature vs time profile inside the sphere, although Reference 4 does produce some numbers.

9.7.3 University of Michigan Density Correction Method

The University of Michigan, Reference 4 or the NASA Symposium, has proposed a density computation correction to be used when a premature sphere deflation occurs. Their method assumes that premature deflations are caused by small pinhole leaks which cause a gradual escape of the inflatant during sphere descent. Thus, as the flight progresses, there is a continual loss of sphere mass which should be taken into account in the data reduction routine. The proposed method is described as follows:

Assumption: A pinhole type leak which causes a mass loss of isopentane inflatant during sphere descent. Sonic nozzling is assumed.

Correction Method: The mass, m, of inflatant at time, t, is given by:

$$m = m_i \cdot e^{-\alpha}$$

where $\alpha = \frac{t - t_d}{t_c - t_d} \ln \frac{P_i}{P_c}$

m_i = initial mass of inflatant

t_d = deployment time

t_c = collapse time

P_i = initial internal pressure

P_c = collapse pressure

Robin Capsule:

Capsule Volume	40.87 cm^3
Inflatant	Isopentane ISO - C_5H_{12}
Molecular Weight	72.1
Specific Gravity	0.625
Sphere Volume	523.6 liters

Standard Atmosphere Model 30°N Lat:

Period	T(°K)	P(%Std)	(mb)	P/P_{STD}
July 30 km	232	+ 8%	1.293×10^{1}	1.275×10^{-2}
40 km	255	+ 12%	3.215×10^{0}	3.174×10^{-3}
Jan 30 km	227	- 2%	1.173×10^{1}	1.157×10^{-2}
40 km	250	Std	2.871×10^{0}	2.834×10^{-3}
30 km		Std	1.197×10^{1}	1.181×10^{-2}

Inflatant Weights:

19.21 gm
19.19
19.04
19.10
19.20
19.18
19.25
19.18
19.22
19.03

Average 19.16 gm

19.04 - 19.25 gm

Expected Collapse Altitudes:

$$P_c = \frac{nRTc}{V}$$

$$n = \frac{W}{M}$$

$$= \frac{19.04}{72.1} \qquad \frac{19.25}{72.1}$$

$$= 0.2641 \qquad 0.2670$$

$$R = 0.082$$

$$V = 523.6 \text{ L}$$

$$P_c = \frac{0.082}{523.6} nT_c$$

Assume vapor temperature is same as atmospheric temperature:

Inflatant Quantity	Pressure (atm)			
	30 km		40 km	
	Cold (227° K)	Hot (232° K)	Cold (250° K)	Hot (255°K
19.04 gm	9.389×10^{-3}	9.594×10^{-3}	1.034×10^{-2}	1.055×10^{-2}
19.25 gm	9.492×10^{-3}	9.701×10^{-3}	1.045×10^{-2}	1.066×10^{-2}

The standard atmospheric pressure profiles are plotted in Figure 9.19 along with the expected internal sphere vapor pressures for the various extremes in atmospheric conditions. Collapse should occur at the intersection of the two curves. The most probable point is about 31.8 km with a tolerance of about $\pm$ 0.5 km. This is based upon the assumption that the internal inflatant vapor temperature is at the ambient atmospheric temperature. If the vapor temperature was maintained at a warmer level, i.e., by a warm inflator heat source or by solar radiation, then collapse altitude would be at a lower altitude.

Mass Correction Equation:

$$m_i = 19.16 \text{ gm}$$

$$P_i = 9.54 \times 10^{-3} \text{ atm}$$

$$t_d = 135 \text{ sec}$$

$$m = 19.16\, e^{-\frac{t - 135}{tc - 135} \cdot \ln \frac{9.54 \times 10^{-3}}{Pc}}$$

Where t is time from launch (sec)

tc is collapse time from launch (sec)

Pc is collapse altitude pressure (atm)

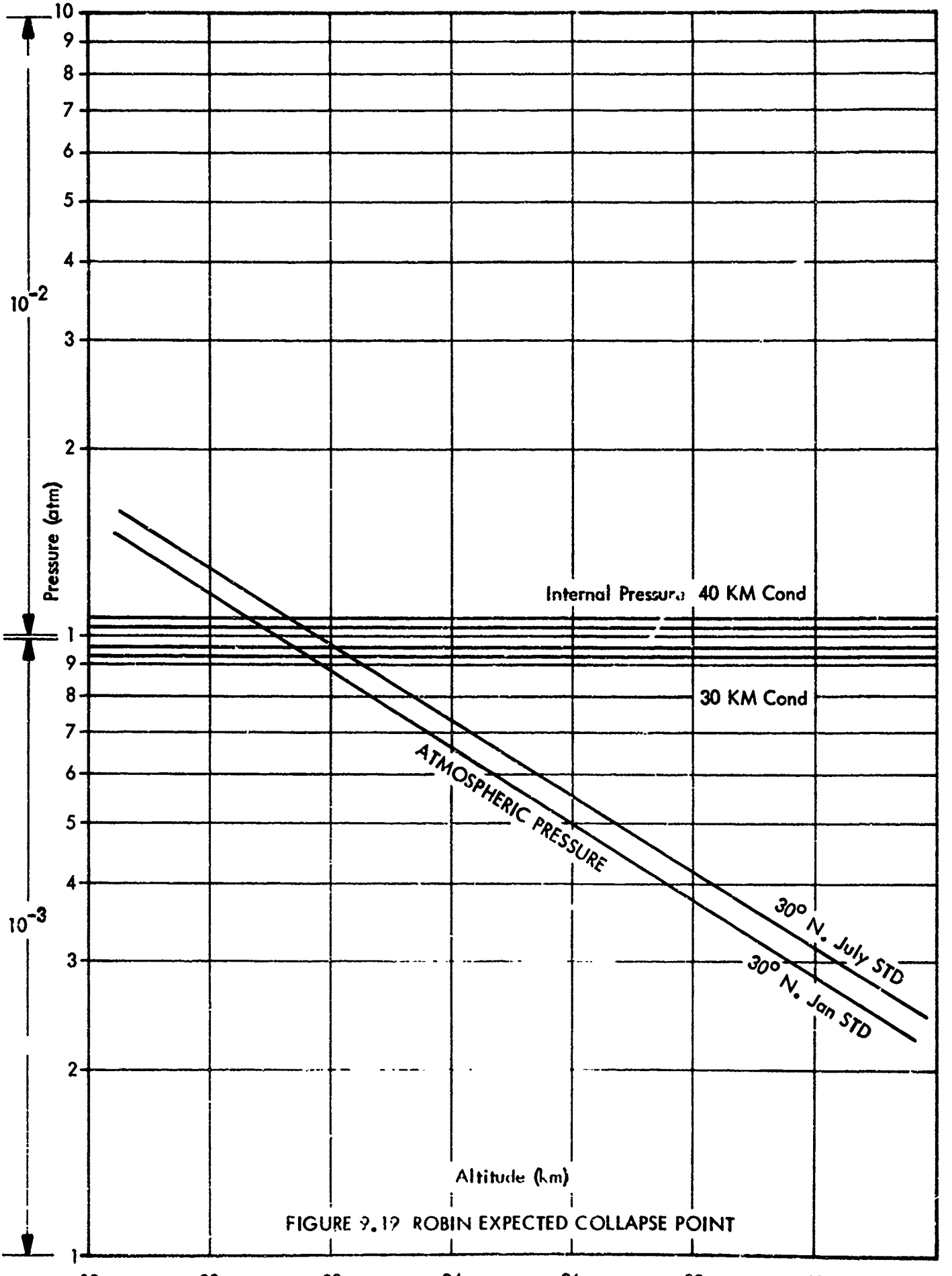

FIGURE 9.19 ROBIN EXPECTED COLLAPSE POINT

The mass of inflatant, m (gm), remaining in the sphere is given by the above espression. The density calculation routine in the Robin program may be modified by AFCRL to incorporate this term.

9.8 Transponder and Transmitter Development

The transponder instrument (and transmitter) was developed at AFCRL as an in-house program. See Reference 2. The primary considerations in the design of the transpondersonde were compatibility with both the Rawin Set AN/GMD-4 and the Super Loki Dart vehicle. The 1680 MHz transmitter tube was preferred to a solid state version because of cost and frequency stability problems. As a result, it became necessary to incorporate a DC-to-DC converter in the sonde to supply the plate voltage (115 VDC) to the tube and 11 VDC to the receiver. A solid state commutator proved to be very satisfactory in this sonde. A nickel cadmium battery was chosen to provide adequate capacity and shelf life along with a recharging capability.

Both transmitting and receiving antennae had to be extremely limited in size and shape due to the payload volume of the vehicle. Thus, the standard radiosonde cone and dipole arrangement transmitting antenna was chosen. Adequate signal strength has been obtained with this antenna, but the same problem of high elevation angle signal dropout is still present. A relatively major redesign effort would be necessary to solve this problem. The 403 MHz receiving antenna was also limited in configuration primarily by space limitations although two designs were tested: a wrap-around type and a coaxial center fed 1/4 wavelength dipole. The coaxial antenna was chosen because it presented less RF interference with the transmitting tube. It is physically attached to a lanyard which attaches the sonde to the parachute (Starute) and has performed well during the flight tests.

The need for a remote on/off capability resulted in a relay inside the sonde with an external "umbilical" cable which is also used to charge the batteries and to run the instrument on external power. A protective cup, similar to the one used in the standard Loki Dart system was designed to protect the thermistor and mount. This cup falls off after ejection. The sonde suspension lanyard is located above the sonde center of gravity such that the inclination angle of the sonde exposes the bead for optimum atmospheric temperature sensing. This avoids contamination of the air flow around the bead. Heavier gauge ground leads are strung from the battery along the length of the sonde to provide good electrical grounds and add to the structural strength. It was found that soldering two of these ground leads to the 403 MHz receiver shielding reduced the DC-to-DC converter noise spikes present in the modulating signals.

Four different materials were tested for the lanyard: nylon, fiberglass, wire, and teflon. Of the four, only teflon proved satisfactory. The nylon lanyard literally melted under the high temperatures of a flight ascent. The fiberglass lanyard was marginally acceptable in that it was flown successfully, but we observed that it broke if bent in a sharp angle. However, the use of fiberglass was curtailed, since it was felt this may occur to a certain number out of a large production lot. A wire lanyard was flown to get some flights where the sonde was known to have stayed attached to the Starute, but it interfered with the RF signals because it is a conductor close to the transmitting tube. Therefore, teflon was recommended for use as the lanyard.

A summary of ten typical transponder Super Loki flight test results is presented in Table 9.15. High precision tracking C-Band radars were used on every flight to verify performance. Rawin Set AN/GMD-4 was also used on every flight since it has a "coarse ranging" capability (Reference 5). These tests were performed at the Air Force Eastern Test Range, Cape Kennedy Air Force Station, Florida. The absolute mean error, algebraic mean error, and standard deviation have been computed for altitude, slant range, and elevation and azimuth angles. The altitude accuracies are dependent on both the slant range and elevation angle. For this reason, the 82 KHz range preset procedure becomes critical since it directly affects the final ranging resolution on any given flight. Also, proper alignment of the GMD pedestal is important since the elevation angle also enters into the altitude computations.

A typical flight slant range may go from about 80,000 yards near apogee down 45,000 yards at test termination at 26,600 yards altitude (the GMD-4 measures slant range in yards). Thus, when an average range of 60,000 yards is used, the absolute mean error of 176 yards yields about a 0.29 percent ranging system accuracy as compared with radar. The fact that the algebraic and absolute mean errors are close in magnitude indicates that a ranging bias remains constant for any given flight once the 82 KHz preset is obtained. This is why the preset error should be minimized, since it determines the magnitude of the bias even though the minute-to-minute slant range change compares very favorably with radar.

TABLE 9.15 SUMMARY OF TRANSPONDER FLIGHT DATA

REFERENCE 2

		Absolute Mean Error				Algebraic Mean Error				Standard Deviation			
Flight No.	No. Obs.	Altitude (ft)	Slant Range (yds)	El. Angle (deg)	Az Angle (deg)	Altitude (ft)	Slant Range (yds)	El. Angle (deg)	Az Angle (deg)	Altitude (ft)	Slant Range (yds)	El. Angle (deg)	Az Angle (deg)
1	81	717	327	0.63	0.18	-182	-327	+0.65	-0.03	1060	413	0.25	0.31
2	79	462	244	0.70	0.44	+ 80	-207	+0.61	-0.26	712	150	0.53	0.51
3	77	856	157	0.70	0.55	+745	+ 47	+0.66	-0.37	1055	278	0 37	0.84
4	75	437	258	0.13	0.07	-400	-258	-0.01	-0.58	313	36	0.15	0.07
5	76	202	81	0.12	0.08	+179	- 58	+0.06	-0.05	174	114	0.10	0.14
6	72	538	284	0.28	0.14	- 31	-185	+0.13	0	886	230	0.36	0.24
7	73	341	34	0.19	0.13	+133	- 15	+0.03	-0.01	374	64	0.22	0.15
8	79	418	170	0.53	0.30	+122	-170	+0.52	+0.01	475	51	0.36	0.35
9	79	448	101	0.50	0.41	+212	-100	+0.43	-0.23	508	45	0.45	0.55
10	79	413	104	0.50	0.43	+224	-103	+0.44	-0.18	462	57	0.37	0.84
Average		483	176	0.43	0.27	+108	-138	+0.35	-0.17	602	150	0.32	0.40

10.

RADAR EVALUATION OF VARIOUS STARUTE AND ROBIN FALLING SPHERE TARGETS

10.1 Introduction

Problems encountered in radar tracking the PWN-8B 7' Starute at remote sites with low powered radars prompted the investigation of various reflectivity patterns for the Super Loki 12' Starute. Various patterns of the metalized mylar construction were fabricated and flight tested with the 2/8" diameter Super Loki dart system at Cape Kennedy in order to determine an optimum radar cross-section pattern. The radar AGC records were subsequently analyzed, and radar cross-sections were determined for the various configurations. Comparisons among the various configurations were made to select the best overall radar target configuration. Subsequently, since it was found to be necessary to finalize on a 10' Starute design, this is also included in the comparison.

A comparison between the Robin aluminized sphere and the corner reflector sphere has also been made.

10.2 Starute Configurations

The Super Loki 12' Starute configurations investigated in the radar reflectivity flight tests are as follows:

A. Standard Configuration, Metalized Burble Fence
B. Same as A.
C. Same as A.
D. Metalized Fence and One Pair of Adjacent Gores.
E. Metalized Crown Only.
F. 1-meter Corner Reflector Metalized Only.
G. Metalized Crown and Burble Fence.

The standard Starute construction is shown in Figure 10.1. The various reflectivity patterns are indicated in Figures 10.2 through 10.6.

A number of additional reflectivity configurations were previously investigated for the 7' Loki Starute. Configuration D was found to be superior for long range tracking. This is most likely due to the increased focusing power of the convergent view of the metalized gore pattern at low elevation angles. This occurs when looking through the clear gores to the inside of the opposite reflective gore surfaces. Since configurations A through C have been standard and configuration D was previously found to be superior in the Loki program, these designs in addition to the new ones F, G and H, were included, in the Super Loki evaluation. The 10' Starute with the

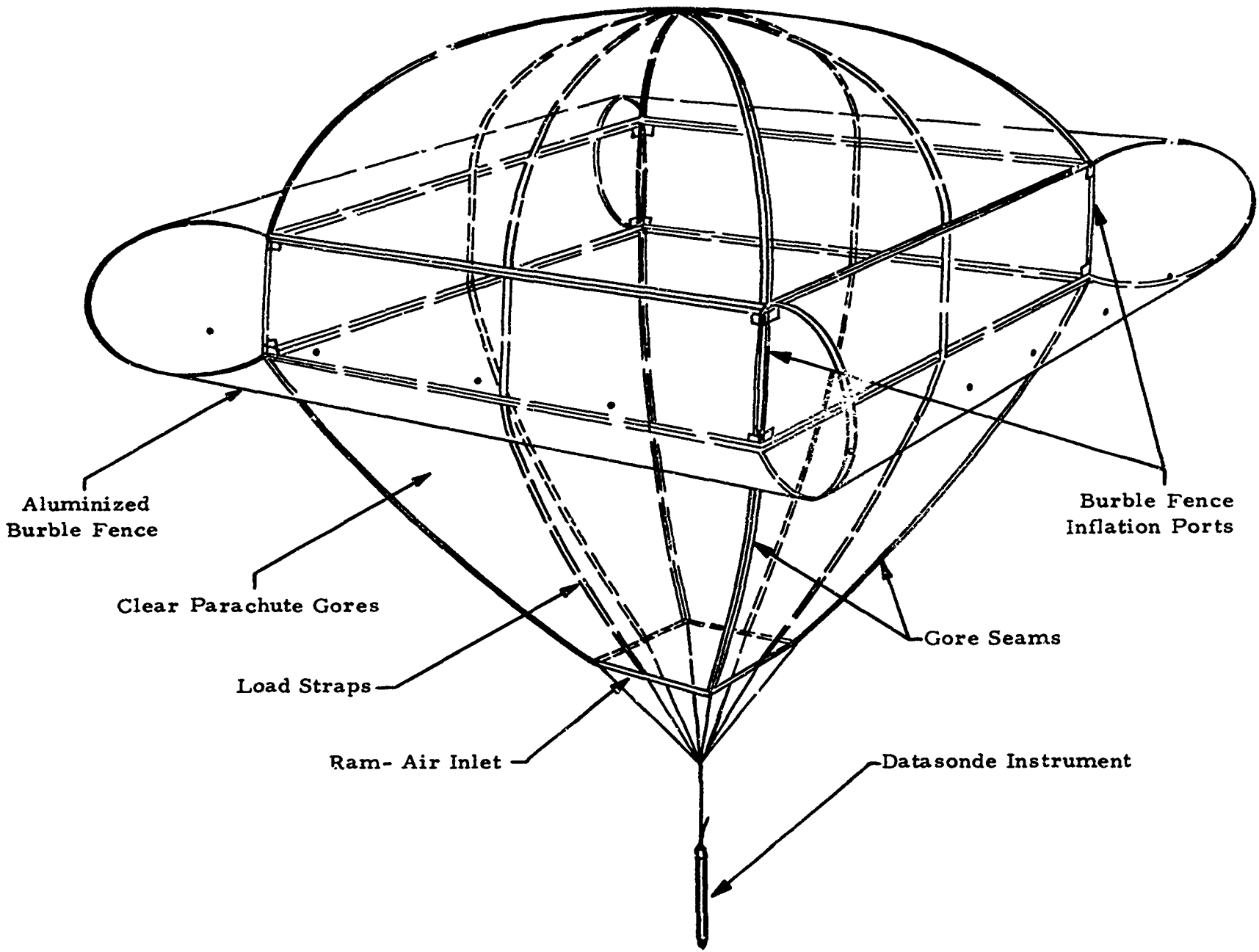

FIGURE 10.1 STARUTE CONSTRUCTION

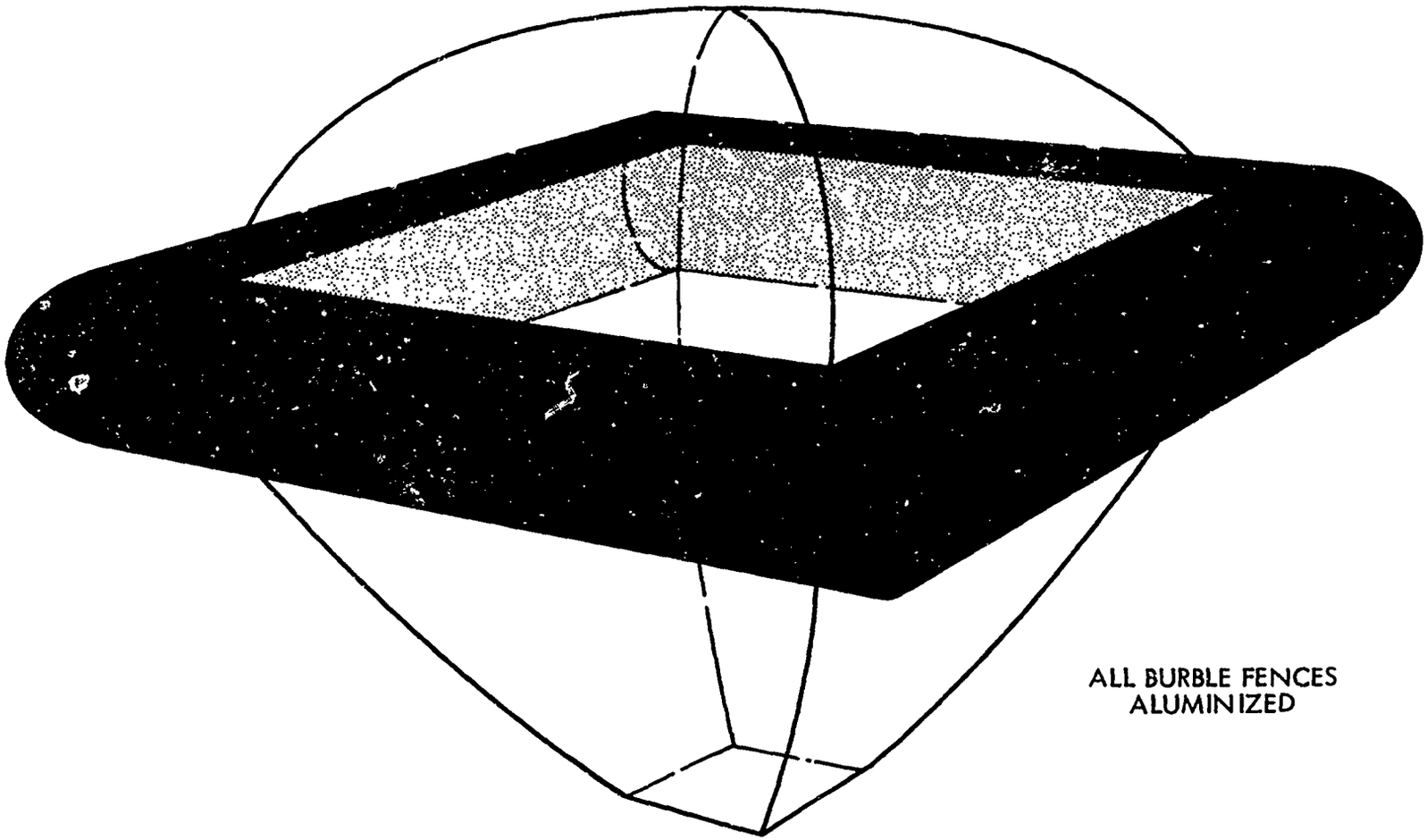

FIGURE 10.2 STARUTE CONFIGURATIONS 'A', 'B', AND 'C'

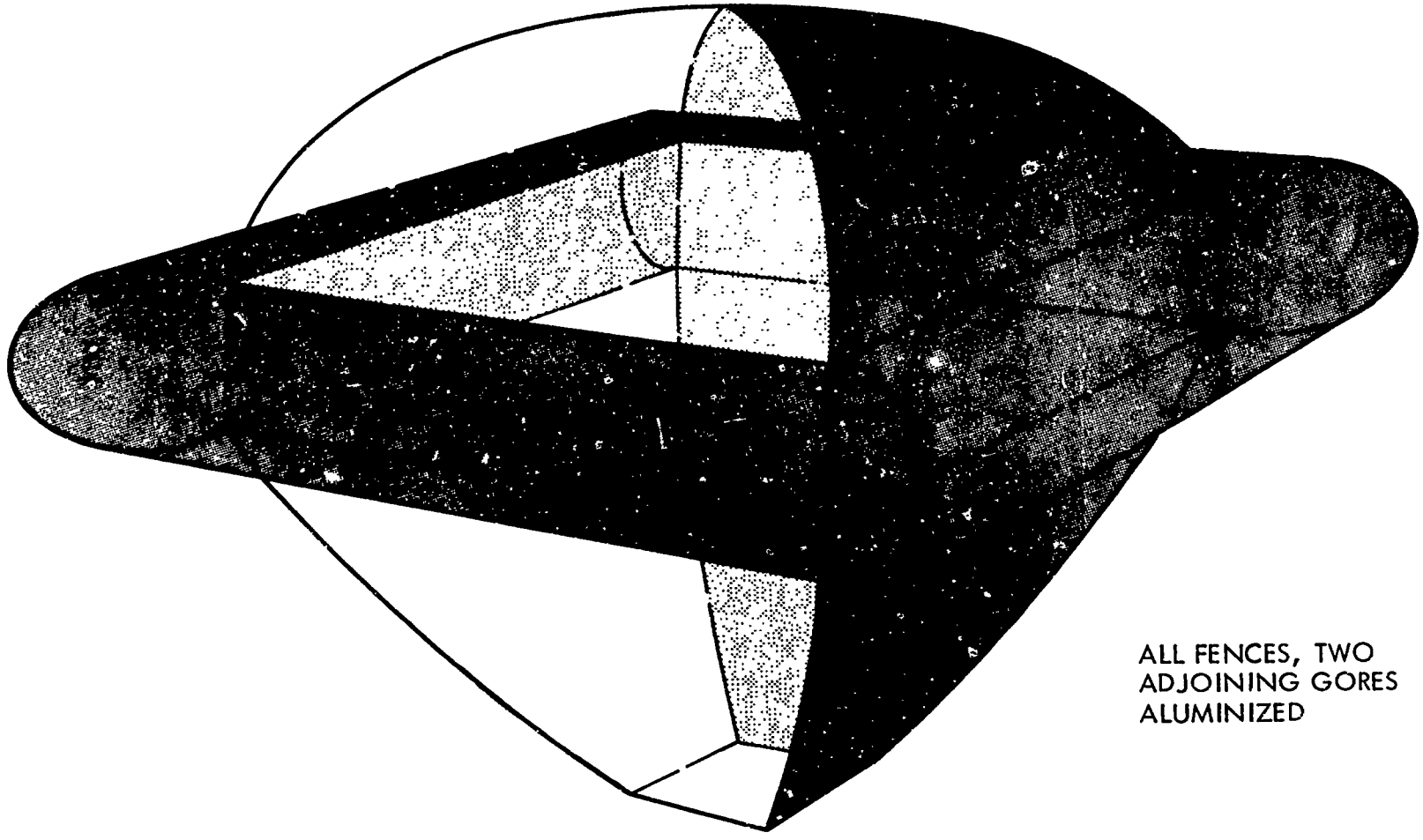

FIGURE 10.3 STARUTE CONFIGURATION 'D'

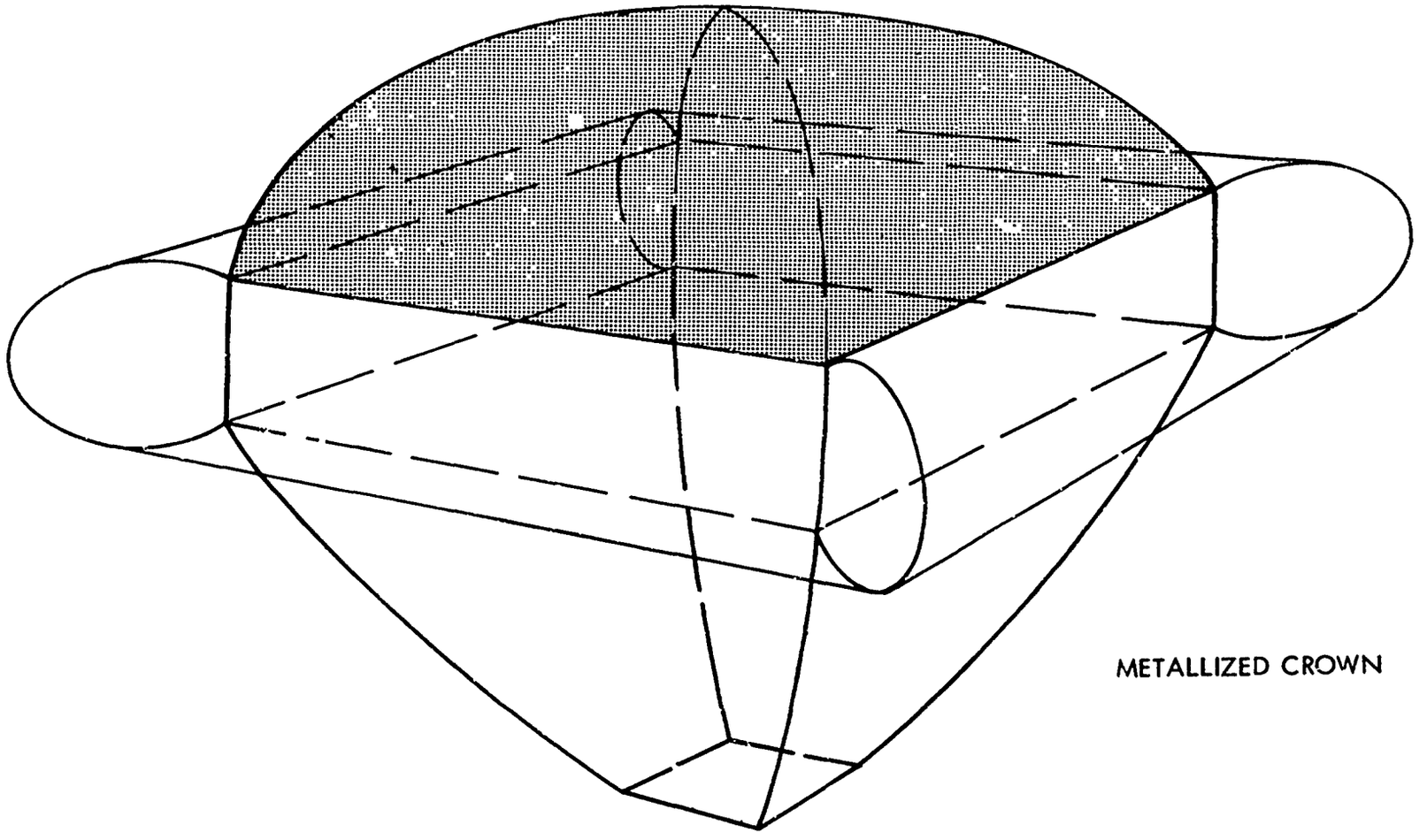

FIGURE 10.4 STARUTE CONFIGURATION 'E'

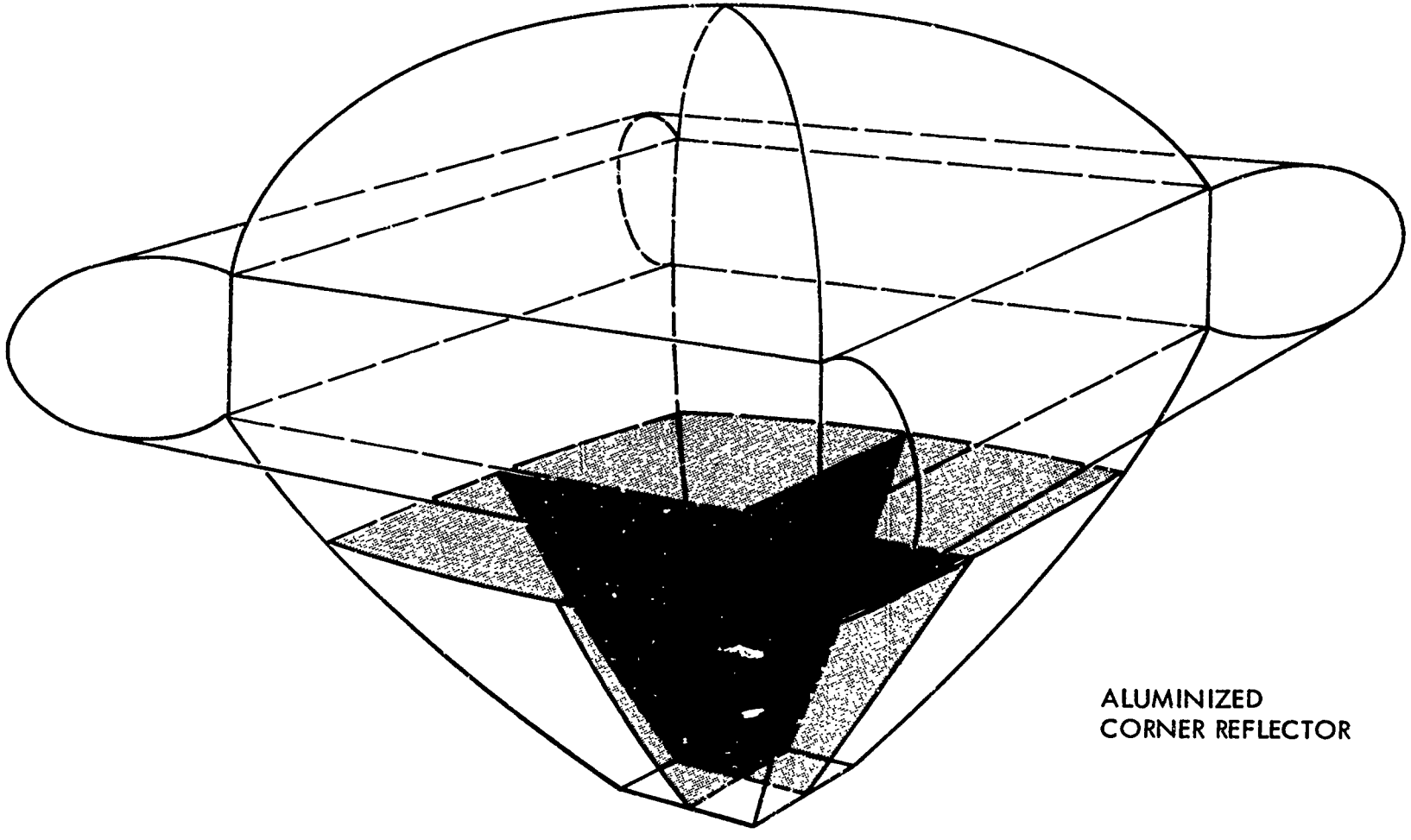

FIGURE 10.5 STARUTE CONFIGURATION 'F'

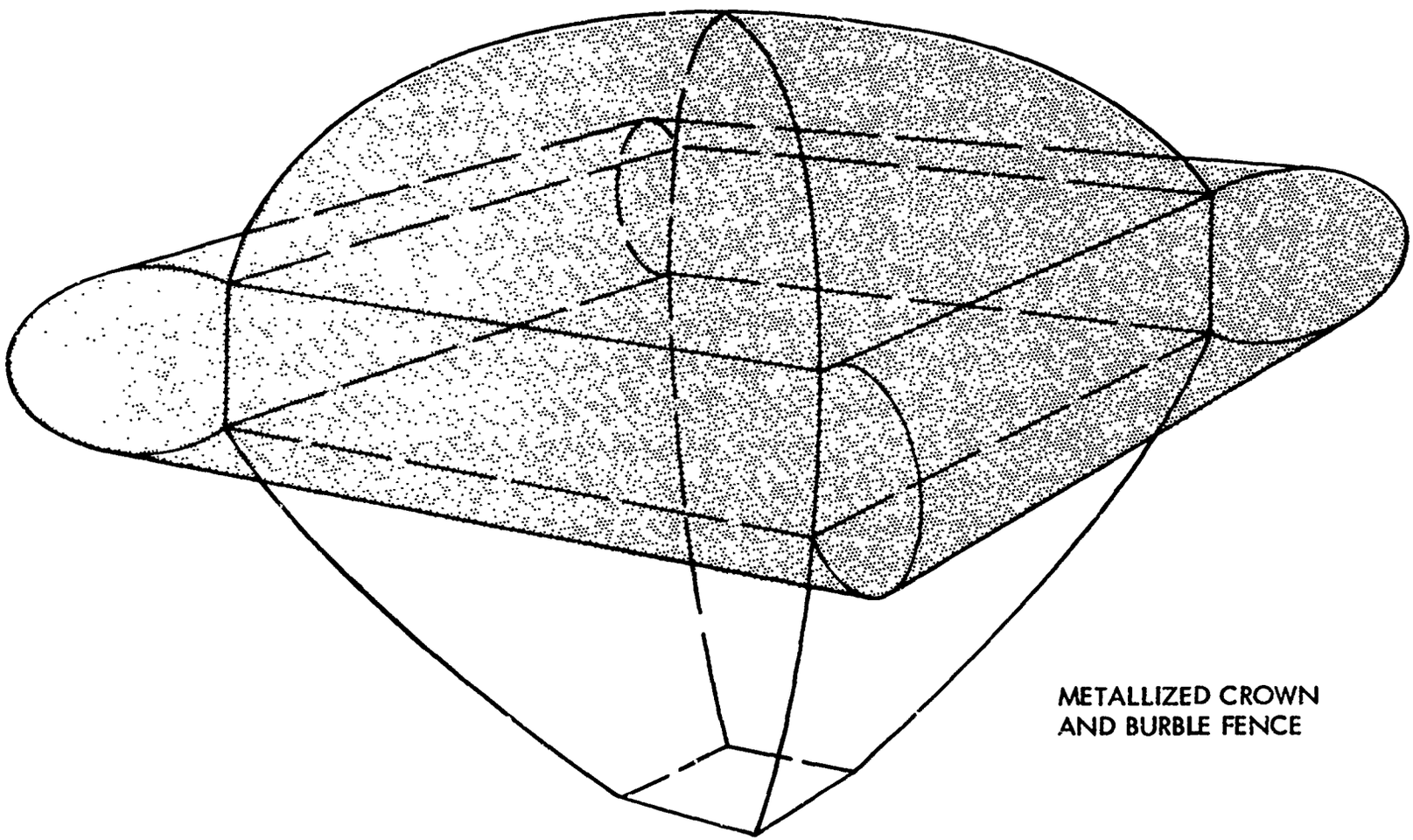

FIGURE 10.6 STARUTE CONFIGURATION 'G'

standard reflectivity pattern (metalized burble fence) was also included in the evaluation.

10.3 Radar Target Analysis

10.3.1 Theoretical Evaluation

Although a large number of factors influence the magnitude of a returned radar signal, the current study has been concerned with the effects which various target reflectivity patterns have upon the reflected signal strength when the target is at a great distance. Other factors being equal, the power returned by a reflective target can be described by the expression

$$P_r = P_t \; K \; \frac{\sigma}{R^4}$$

where P_r = power received from target
P_t = power transmitted by radar
K = proportionality constant which depends upon a number of various influencing parameters
R = slant range distance from radar to the target
σ = radar cross-section of the target

Since the returned power diminishes by the fourth power of the slant range, it is important to maximize the target radar cross-section for long range tracking.

The radar cross-section of a target depends on the size of the reflective area and also upon its geometrical shape. The aspect or viewing angle for non-symetrical shapes can result in significant variations of the reflected signal strength. As the Starute descends, the radar elevation angle generally becomes smaller. Also it has been found that the Starutes rotate about their vertical axis during descent. Both of these factors vary the aspect angle from the tracking radar and influence the returned signal strength. There are so many variables which affect the returned radar signal that flight testing was the only practical way to determine the optimum Starute reflectivity pattern.

10.3.2 Typical Radar Cross-Sections of Simple Target Geometries

Typical radar cross-sections of simple target geometries are presented in Table 10.1 to indicate the dependence of cross-section on shape and wavelength. The various Starute configurations contain complex combinations of some of these simple geometries. The most appropriate relationship, however, is that for a curved surface. It can be seen that for a normal viewing aspect a large radius of curvature is desirable.

TABLE 10.1 RADAR CROSS SECTIONS OF SIMPLE BODIES

Body	σ	Condition or Direction
Sphere	πa^2	When radius $a \gg \lambda$
Sphere	$9(2\pi a/\lambda)^4 \pi a^2$	When radius $a \ll \lambda$
Flat Surface	$4\pi A^2/\lambda^2$	Along normal to surface area A; $A \gg \lambda^2$
Cone	$l^2\lambda/8\pi a$	Transverse direction to height l; a = radius of base
Cone	$\pi a^2 \tan^2\theta$	Longitudinal direction from apex angle 2θ toward base of radius a
Triangular corner reflector	$4\pi L^4/3\lambda^2$	Direction along axis of symmetry with respect to 3Δ planes each of b base length L
Curved surface	$\pi a_1 a_2$	Normal to surface of curvature of radii a_1, a_2
Cylinder	$2\pi L^2 a/\lambda$	Normal to length L; a = radius

However, as the viewing angle deviates from the normal , the signal return diminishes rapidly for surfaces which are close to being flat. In general, surface shapes can be optimized to provide large radar cross-sections at particular aspect angles, but significant degradation may occur as the aspect angle changes. Therefore, constancy of signal return must be considered along with the overall level.

10.3.3 Radar Analysis Procedure

During a flight test the radar maintains track on the descending Starute and payload. The radar AGC (automatic gain control - an index of returned signal strength) records are obtained along with the AGC calibration for the particular day. The AGC calibration S/N values in db are plotted vs. recorder divisions on semilog paper to permit accurate interpolation and determination of AGC S/N in terms of db for each date point. These S/N data points in terms of db are plotted vs. target slant range on semilog paper. Six-inch diameter radar calibration sphere data are also plotted on the same S/N vs slant range graphs for subsequent conversion of the target S/N values (db) to radar cross-section values (dbsm and m^2). At a given slant range, the target S/N (db) value is compared with the calibration sphere S/N (db) value to permit the calculation of the target cross-section for the Cape Kennedy radars utilized in the flight tests. The calibration sphere (6-inch diameter) references are as follows:

"C" - Band Radar 1.16	- 17.00 dbsm.
"S" - Band Mod II	- 16.25 dbsm.

10.4 Flight Test Results

10.4.1 General

The special Starute radar reflectivity flight tests were conducted during series 15, 16, 17 and 19 with an AN/FPS - 16 and a Mod II radar as primary data aquisition radars. Although the data precision was expected to be much better with the FPS - 16, the Mod II was used to more nearly duplicate the remote site problem of a marginal radar.

A typical AGC S/N (db) calibration for the FPS - 16 radar is presented in Figure 10.7 for three successive days. This graph is used to convert AGC recorder divisions to AGC S/N (db) values for the particular day of the flight test.

Typical plots of the AGC S/N (db) versus target slant range are presented in Figs. 10.8 and 10.9 along with the 6"-sphere calibration data. High, medium and low values of the signal return are plotted to give some idea of the aspect angle variability. The plotted values are compared with

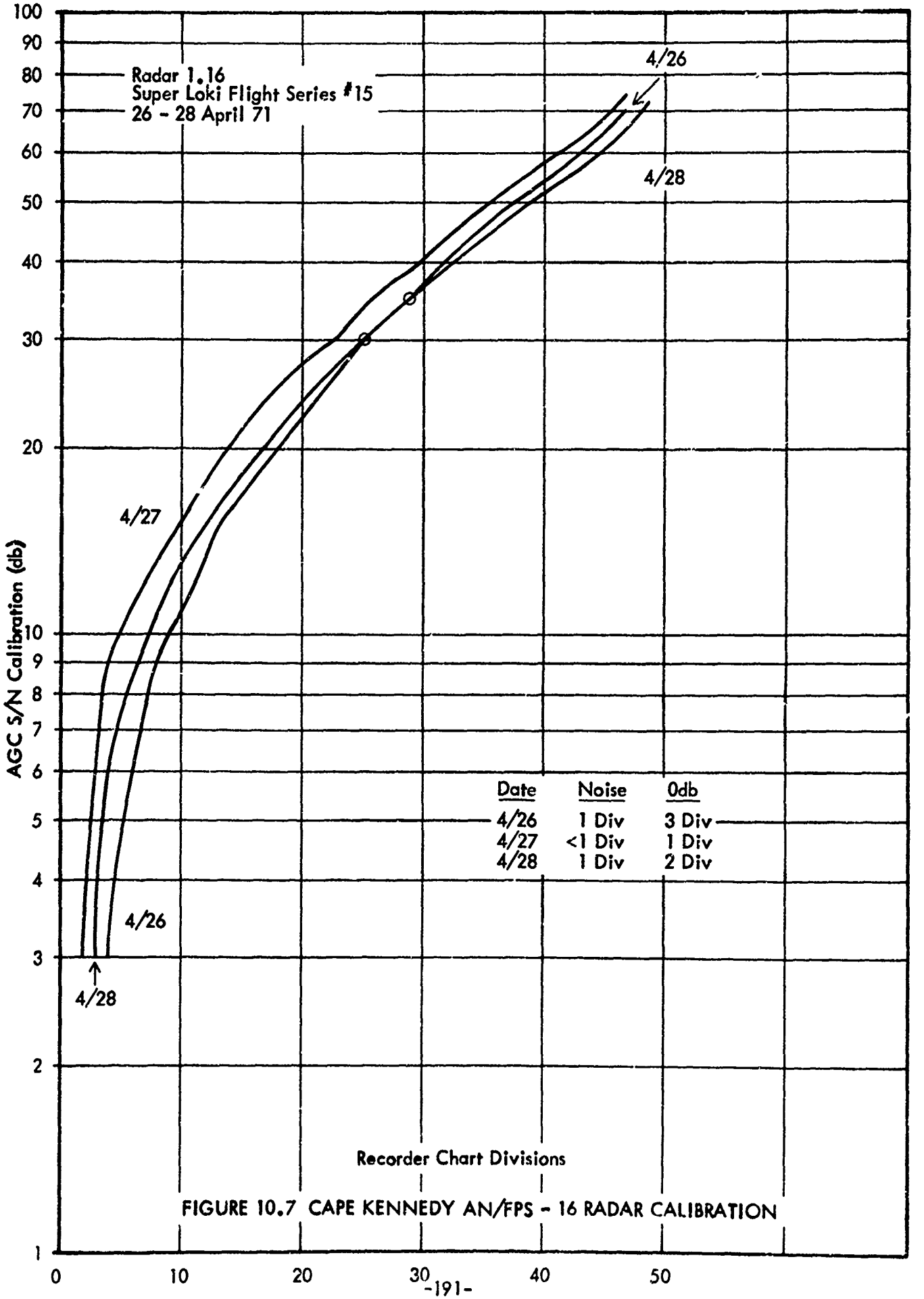

FIGURE 10.7 CAPE KENNEDY AN/FPS - 16 RADAR CALIBRATION

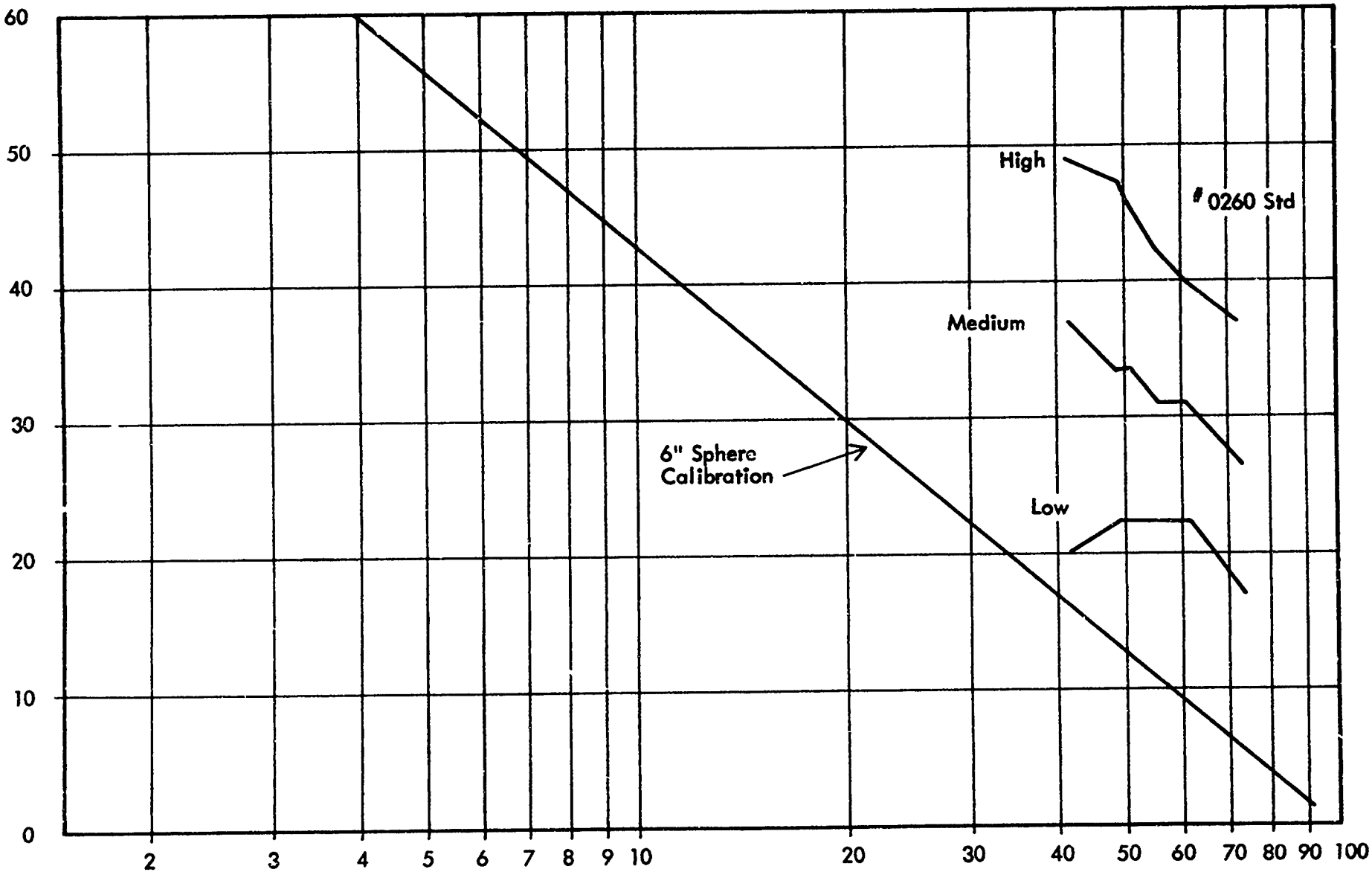

FIGURE 10.8 CAPE KENNEDY AN/FPS - 16 RADAR 1.16 STARUTE DATA 4/26/71

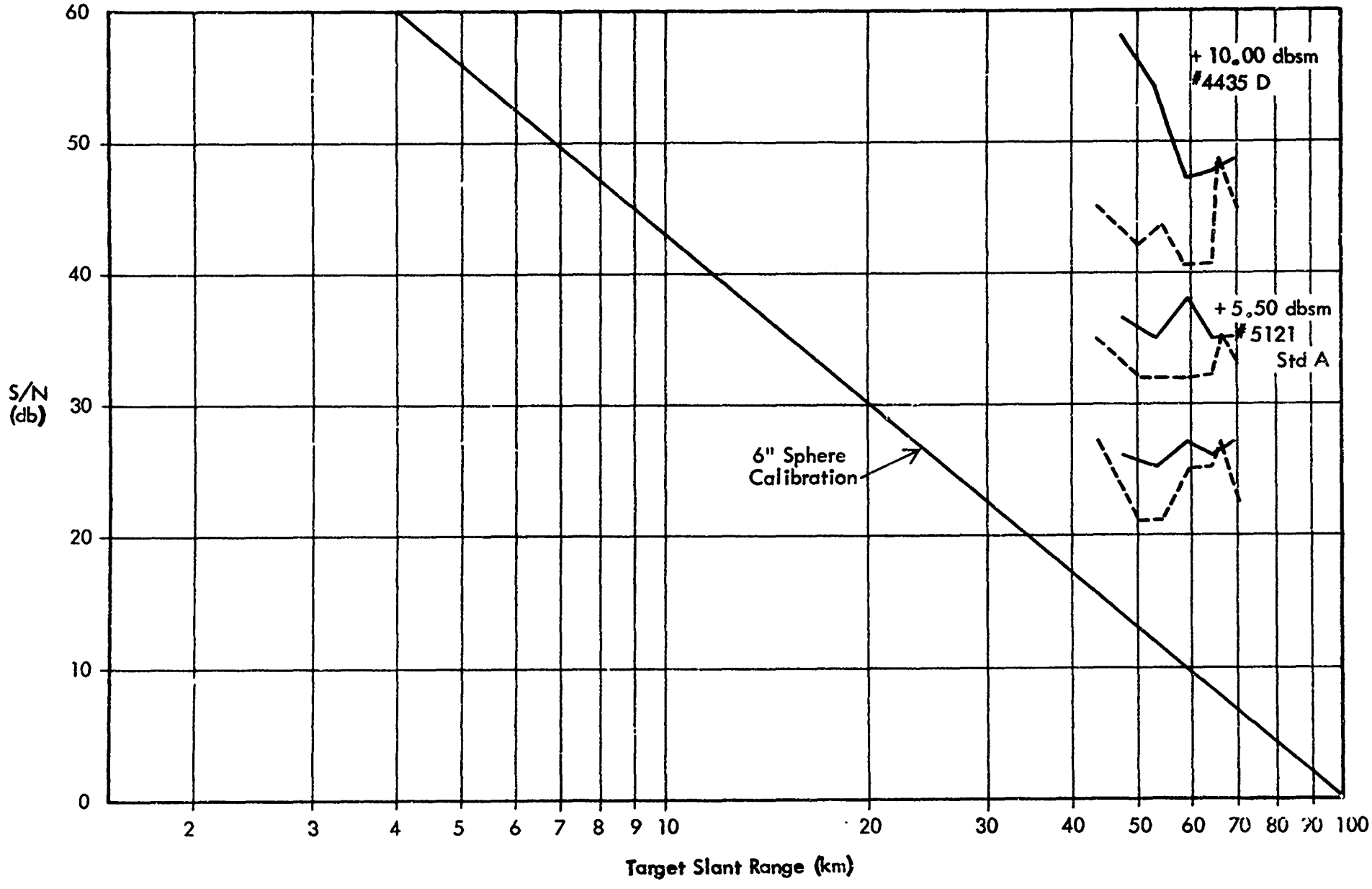

FIGURE 10.9 CAPE KENNEDY AN/FPS - 16 RADAR 1.16 STARUTE DATA 4/27/71

the 6" sphere data at the same slant range to convert the AGC S/N (db) into radar cross-section values, (dbsm and m^2). Comparisons then can be made among the various Starute configurations. Conversion from the AGC S/N (dbsm) data into the actual cross-section area is accomplished by Figures 10.10 and 10.11.

10.4.2 Flight Series 15 Results

The radar cross-section evaluation results for series 15 are presented in Table 10.2 for the FPS - 16 radar. Although some of the Starutes became damaged, there are enough data to indicata that the D configuration is superior to the standard (A through B). When suspicious data are discounted, the average radar cross-section values for the two designs are presented in Table 10.3. As can be seen from the data, there is a large variation in the signal return for a given unit. This is a short term variation which has been related to the rotation of the Starute about its vertical axis and is due to the aspect angle variation.

The Mod II radar data for the same flight series was so poor that comparisons could not be made with any degree of assurance. Although the basic Mod II calibration data was significantly poorer than for the FPS - 16, this does not appear to explain the unpredictable results which were obtained. When the Mod II data were plotted against slant range, the patterns were very inconsistent, and the signal returns were as likely to increase with slant range as to decrease. The data consistency from unit-to-unit of the same design was as poor as that between the different designs. Thus, the Mod II data was judged to be unreliable for purposes of radar cross-section calculation and comparison. Since the Starute target size is considerably greater than the radar wavelengths, it is believed that the wavelength effect is negligible for all configurations except possible for the corner reflector design.

10.4.3 Flight Series 16 Results

The radar cross-section evaluation results for flight series 16 are presented in Table 10.4. Only average values are presented since the high and low signal returns variation was about the same as that for series 15. However, since there is a good deal of judgement in determining the average value of a typical AGC trace, these data must be considered as qualitative estimates only.

Four configurations of Starutes (A, D, F, G) were flown in this flight test series. The results again indicate that the average return for the D configuration is somewhat better than that for the standard or A configuration. This is especially true at the longer slant ranges. The F and G configurations were considerably lower in average signal return than for the standard A configuration. This is true at all of the slant ranges incurred during the flight tests.

FIGURE 10.10 RADAR TARGET CROSS-SECTION CONVERSION

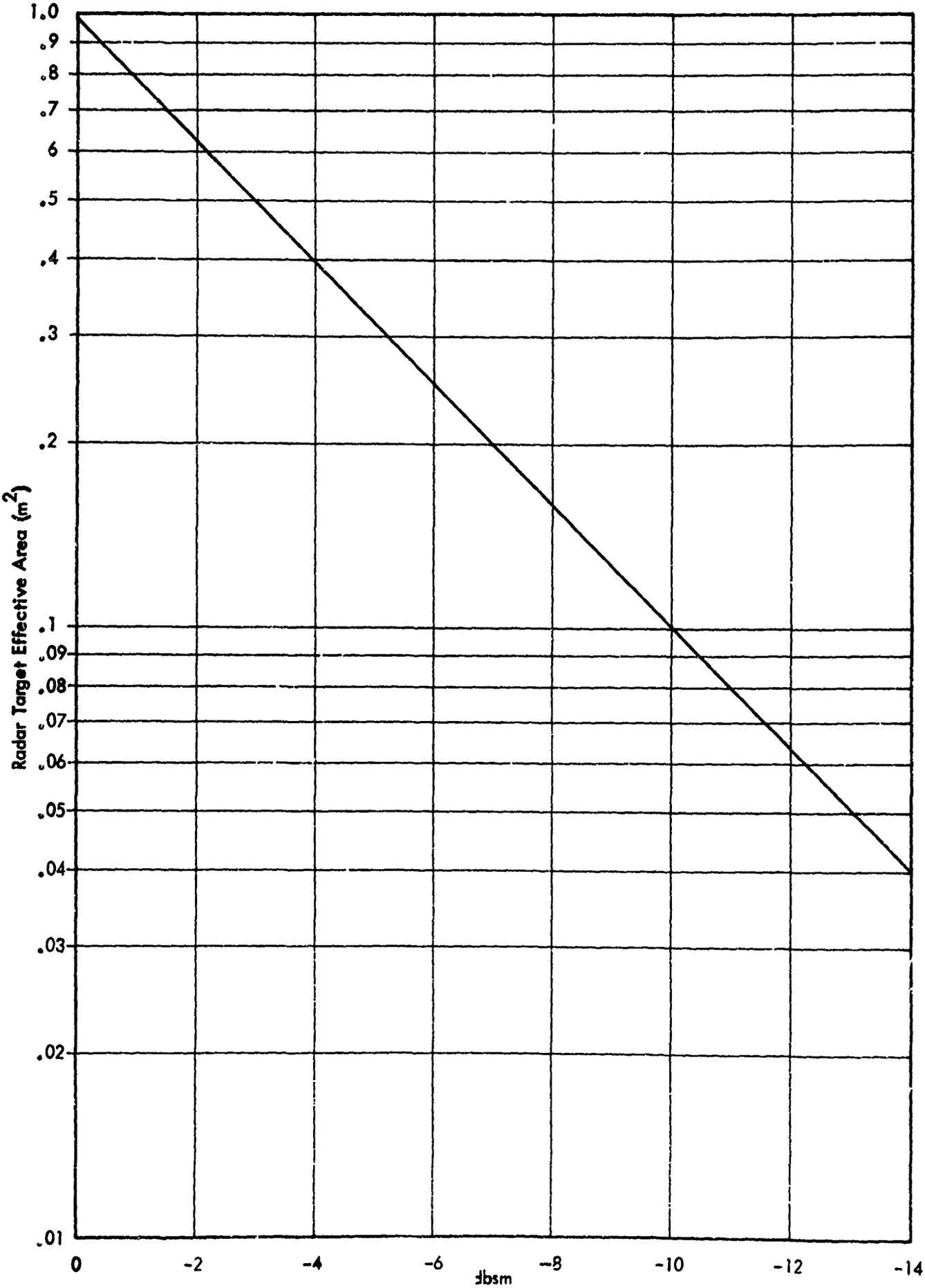

FIGURE 10.11 RADAR TARGET CROSS-SECTION CONVERSION

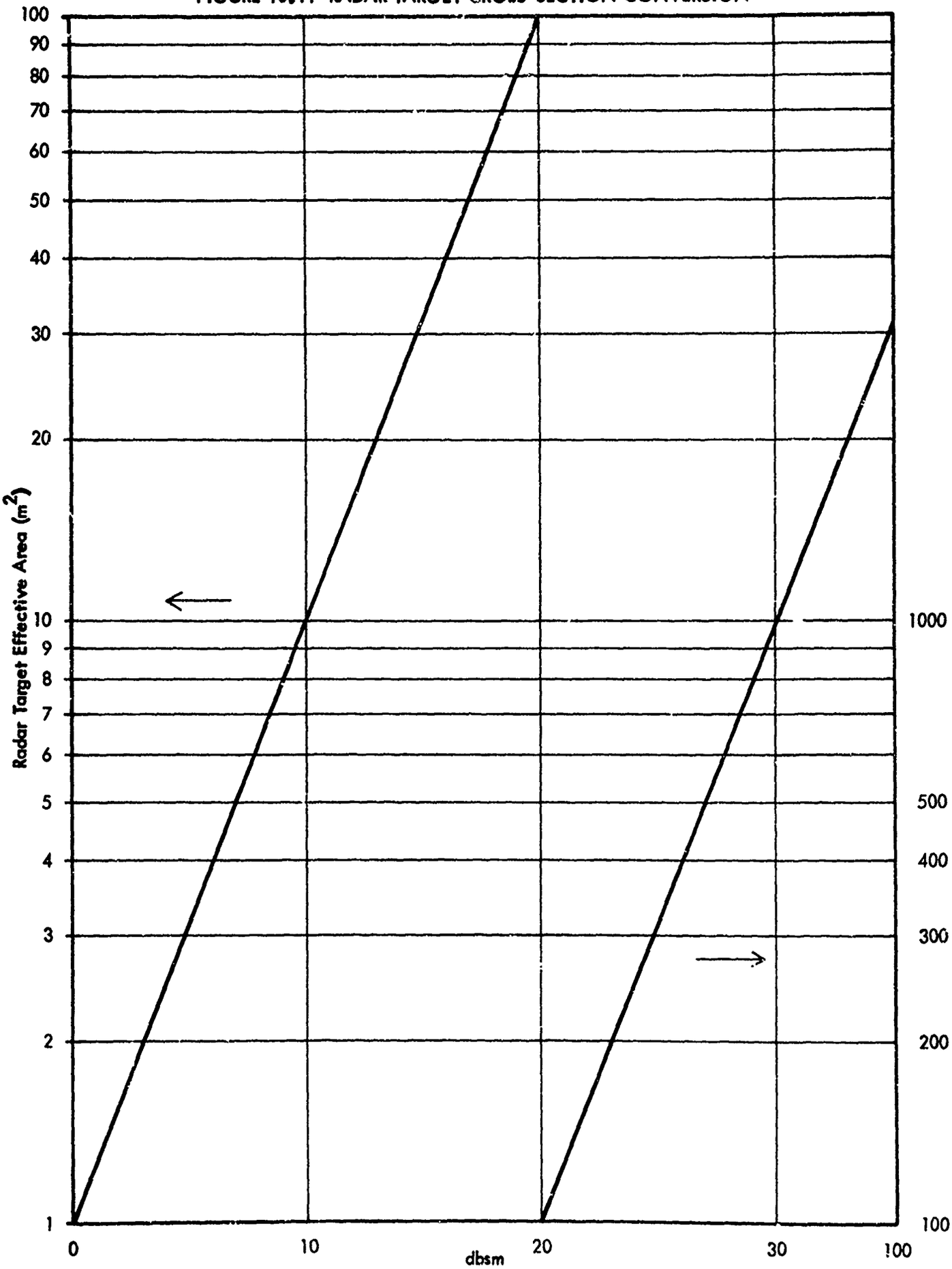

TABLE 10.2 SUPER LOKI STARUTE RADAR CROSS SECTION EVALUATION

FLIGHT SERIES #15 ETR FPS - 16 RADAR #1.16

Date	Test No.	Configuration	Radar Cross-Section dbsm			Effective Area (m^2)			Comments
			Lowest Signal	Medium Signal	Highest Signal	Lowest Signal	Medium Signal	Highest Signal	
26 Apr 71	0260	AStd (T-70)	-4.5	+4.0	+16.0	0.35	2.54	40.00	Pcs Off-Bad
26 Apr 71	7208	AStd (T-68)	-6.0	-0.5	+ 6.0	0.25	0.88	4.00	Good
27 Apr 71	4435	D (TR-102)	-1.1	+8.7	+24.7	0.77	7.50	300.00	Good
27 Apr 71	5121	AStd (T-66)	-3.3	+5.7	+17.7	0.46	3.85	60.00	Good
28 Apr 71	6480	D (TR-101)	-2.8	+9.2	+21.7	0.52	8.50	150.00	1 Pc Off - ?
28 Apr 71	7400	AStd (T-69)	-3.3	+6.7	+16.7	0.46	4.80	47.50	Pcs Off-Bad
28 Apr 71	8419	D (TR-100)	+0.7	+11.2	+19.7	1.20	13.50	95.00	Before damage
			-12.1	- 6.3	+ 6.2	0.06	0.23	4.20	After damage many Pcs off-bac

TABLE 10.3 RADAR CROSS-SECTION AVERAGES, FLIGHT TEST SERIES # 15

Radar Cross-section area (m^2)

Starute Configuration	Lowest Signal	Medium Signal	Highest Signal
Standard	0.42	3.73	49.2
D	0.83	9.83	181.6

TABLE 10.4 SUPER LOKI STARUTE RADAR CROSS-SECTION EVALUATION

FLIGHT SERIES #16 ETR FPS - 16 RADAR 1.16

Date	Test No.	Configuration	(R = 70 km) Radar Cross-section (dbsm)	Effective Area (m^2)
15 June 71	5080	TX - 83 (F)	-1.00	0.785
15 June 71	5989	TX - 82 (F)	-1.00	0.785
16 June 71	3004	TX - 72 (A)	+12.30	17.50
16 June 71	5112	TX - 79 (D)	+14.80	31.00
17 June 71	2069	TX - 71 (A)	+9.10	8.30
17 June 71	4608	TX - 80 (G)	-3.70	0.425

A review of the elevation angle data for both series 15 and 16 indicates that elevation angle has a minor effect as compared with slant range over the region of the flight test data. Configuration D appears to improve in radar cross-section relatively more than the other configurations as the elevation aspect angle becomes lower.

Again for this series the Mod II data were too erratic for reliable analysis.

10.4.4 Flight Series 17 Results

The radar cross-section evaluation results for flight series 17 are presented in Table 10.5. Three standard configuration A Starutes and one H were flown in this series. Although one of the A Starutes resulted in a high value for cross-section, the other two were low. The H Starute was intermediate.

10.4.5 Flight Series 19 Results

The radar cross-section evaluation results for flight series 19 are presented in Table 10.6. One standard configuration A and two H Starutes were evaluated in this series.

10.4.6 Flight Series 23 and 24 Results

The radar cross-section evaluation results for flight series 23 and 24 are presented in Table 10.7. All of these flights were with the 10' Starute and the standard reflectivity pattern (metalized burble fence).

10.4.7 Starute Flight Results Summary

A summary of the Starute radar average cross-section data is presented in Table 10.8 for the various Starute configurations. For all of the configurations there is a large variation in radar cross-section values as obtained from a given AGC trace. A typical trace is shown for the 2 1/8-inch diameter transponder dart and the standard 10' Starute in Fig. 10.12. This pattern is fairly typical of all of the Starutes evaluated.

Based upon average values of radar cross-section it appears that the D configuration is superior, especially at long slant ranges. The 12' D has about ten times the average cross-section as the standard 12' A. The other 12' Starutes are inferior to either of these configurations.

TABLE 10.5 SUPER LOKI STARUTE RADAR CROSS-SECTION EVALUATION

FLIGHT SERIES #17 ETR FPS - 16 RADAR 1.16

Date	Test No.	Configuration	Radar Cross-section (dbsm)	Effective Area (m^2)
8-10-71	5690	TX - 75 (A)	+ 9.00	8.00
8-11-71	7720	TX - 74 (A)	-13.00	0.05
8-11-71	6780	TX - 76 (A)	-14.00	0.04
8-12-71	3528	TX - 85 (H)	+ 1.00	1.26

TABLE 10.6 SUPER LOKI STARUTE RADAR CROSS-SECTION EVALUATION

FLIGHT SERIES #19 ETR FPS - 16 RADAR 1.16

Date	Test No.	Configuration	Radar Cross-section (dbsm)	Effective area (m^2)
10-12-71	1715	TX - 78 (A)	- 8.20	0.15
10-12-71	1632	TX - 88 (H)	- 5.00	0.31
10-14-71	2116	TX - 87 (H)	- 7.30	0.18

TABLE 10.7 SUPER LOKI STARUTE RADAR CROSS-SECTION EVALUATION

FLIGHT SERIES 23 and 24 ETR FPS - 16 RADAR 1.16

Date	Test No.	Configuration	Radar Cross-section (dbsm)	Effective Area (m^2)
3-16-72	7308	10' A	-7.00	0.20
4-4-72	1531	10' A	+2.50	1.80
4-4-72	3163	10' A	+0.80	1.20
4-5-72	2084	10' A	-6.50	0.23

TABLE 10.8 SUPER LOKI STARUTE RADAR CROSS-SECTION EVALUATION

SUMMARY

Starute Configuration	Average Radar Cross-section (dbsm)	Average Effective Target Area (m^2)
12' A	+ 1.11	1.32
12' D	+10.98	12.50
12' F	- 1.00	0.79
12' G	- 3.70	0.43
12' H	- 3.77	0.42
10' A	- 2.55	0.56
7' A	- 7.30	0.19
7' D	- 3.80	0.41

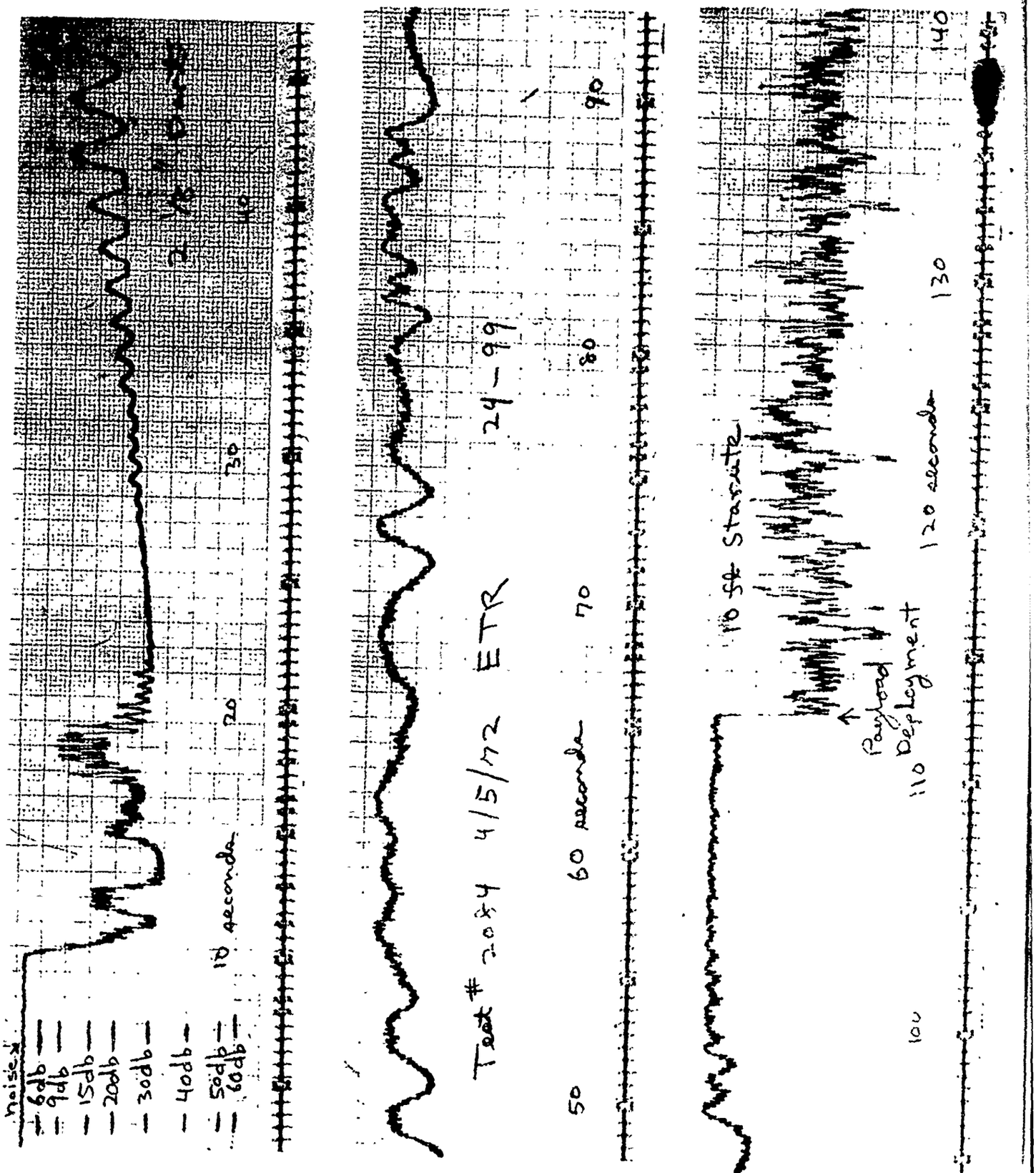

FIGURE 10.12 AGC RECORD FOR 2 1/8" DART AND 10' STARUTE

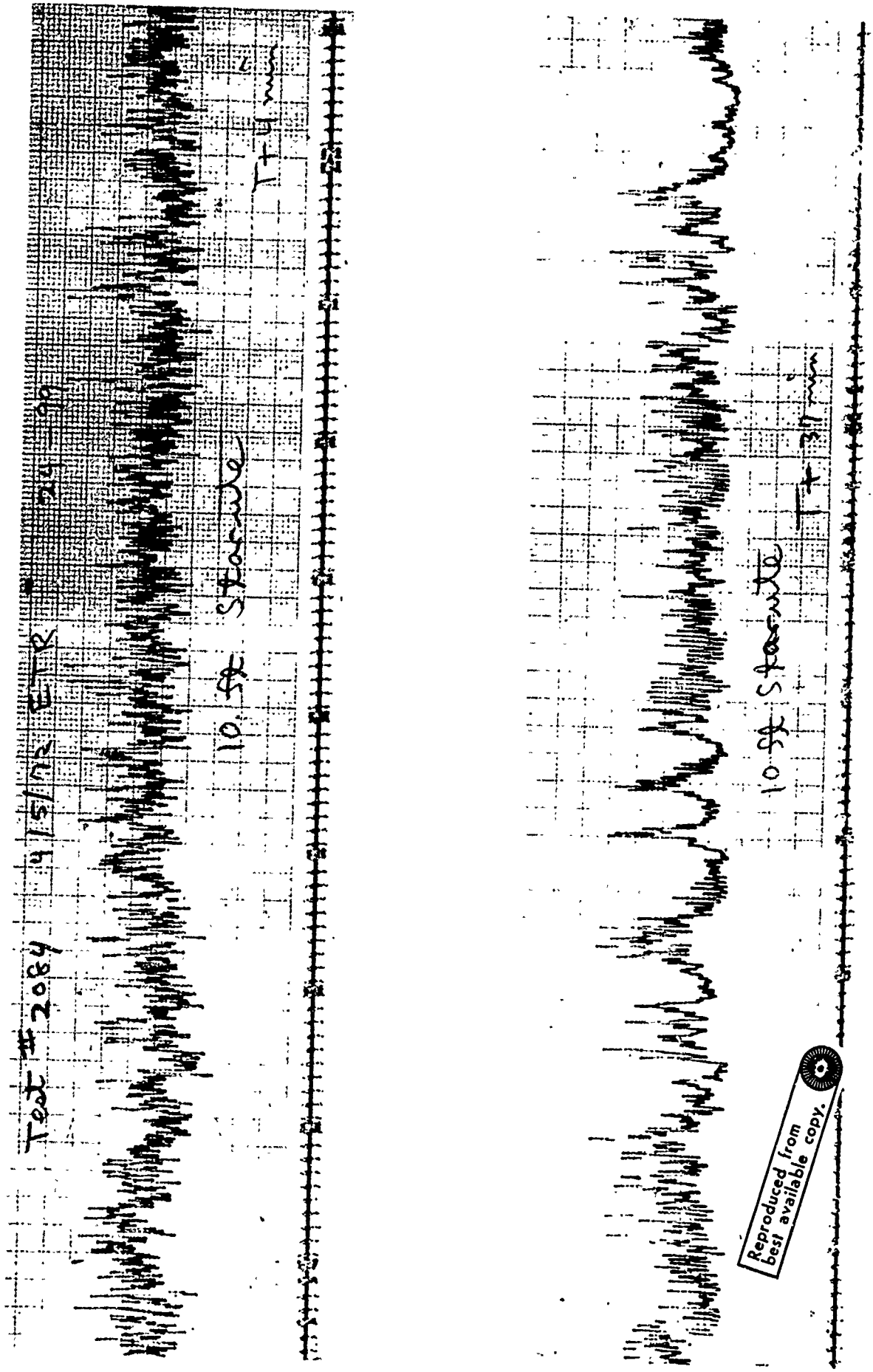

FIGURE 10.12 (continued)

The 10' A Starute has been selected as the final configuration because of aerodynamic heating packaging problems. It has about half the radar cross-section as the 12' A, but has three times the cross-section as the original 7' A Loki configuration. Therefore, the 10' A should be adequate for remote site tracking.

10.4.8 Robin Falling Sphere Flight Test Results

Radar AGC records were taken for the Robin falling sphere flights and were analyzed in the same manner as for the Starutes.

A typical AGC flight sequence for the final design aluminized sphere system is shown in Fig 10.13. From sphere deployment to a flight time of about four minutes, the AGC record is somewhat noisy. This is due to the two set of staves cluttering the radar target gate. At about four minutes the differences in ballistic coefficient between the staves and the sphere is sufficient for the items to separate for enough to clear the gate of the staves. From this time to sphere collapse the signal return is quite constant. The AGC record indicates that sphere collapse takes place over a period of 1.5 minutes and over an altitude layer of about 4,000 feet or 1.2 km. A typical corner reflector sphere AGC record is shown in Fig. 10.14. This record shows wide fluctuations in returned signal strength typical of a corner reflector as it is viewed from different aspect angles. The record indicates that the sphere was spinning immediately after deployment, and that is slowed down in spin rate during its descent.

Radar signal return data for a number of the sphere flights are presented in Figure 10.15. The average signal strengths are plotted at a given slant range along with the spread of highest and lowest signal strengths. The corner reflector sphere has a much greater variation in signal return than the aluminized spheres. A summary of the radar cross-section results is presented in Table 10.9. The average return from the corner reflector is about twice as great as from the aluminized sphere, but the pattern is a great deal more variable. This has been confirmed by means of ground-based anechoic chambers tests at PMR, Point Mugu, where the gore pattern of the aluminized spheres caused only a $\pm$ 1.75 dbsm size wave pattern in an equatorial scan, where the corner reflector spheres caused a $\pm$ 17 dbsm pattern as shown in Figure 10.14. An investigation into the effects of the radar return pattern level and variability upon radar tracking accuracy was beyond the scope of the current program effort.

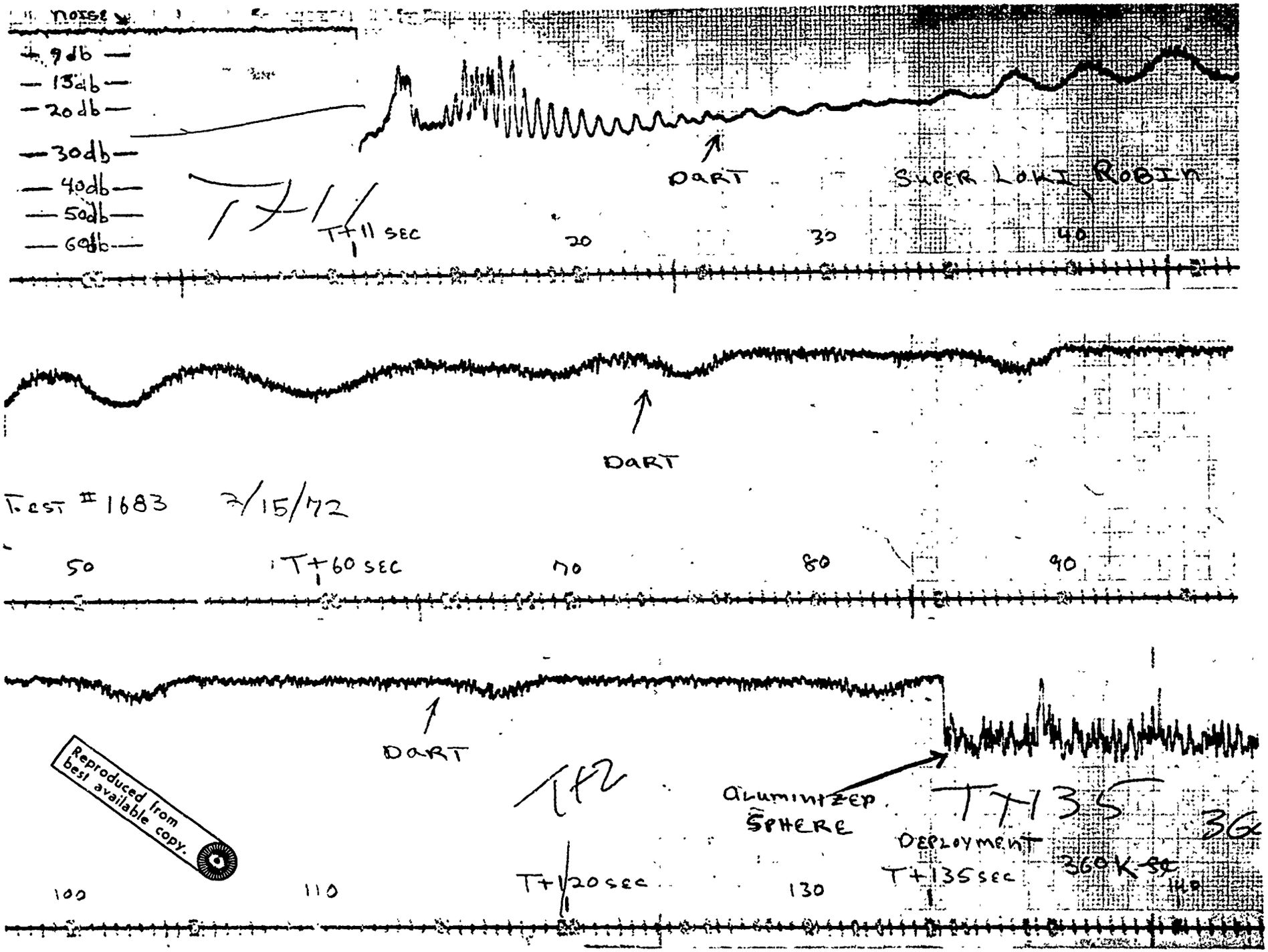

FIGURE 10.13 RADAR AGC RECORD FOR FINAL DESIGN ALUMINIZED SPHERE

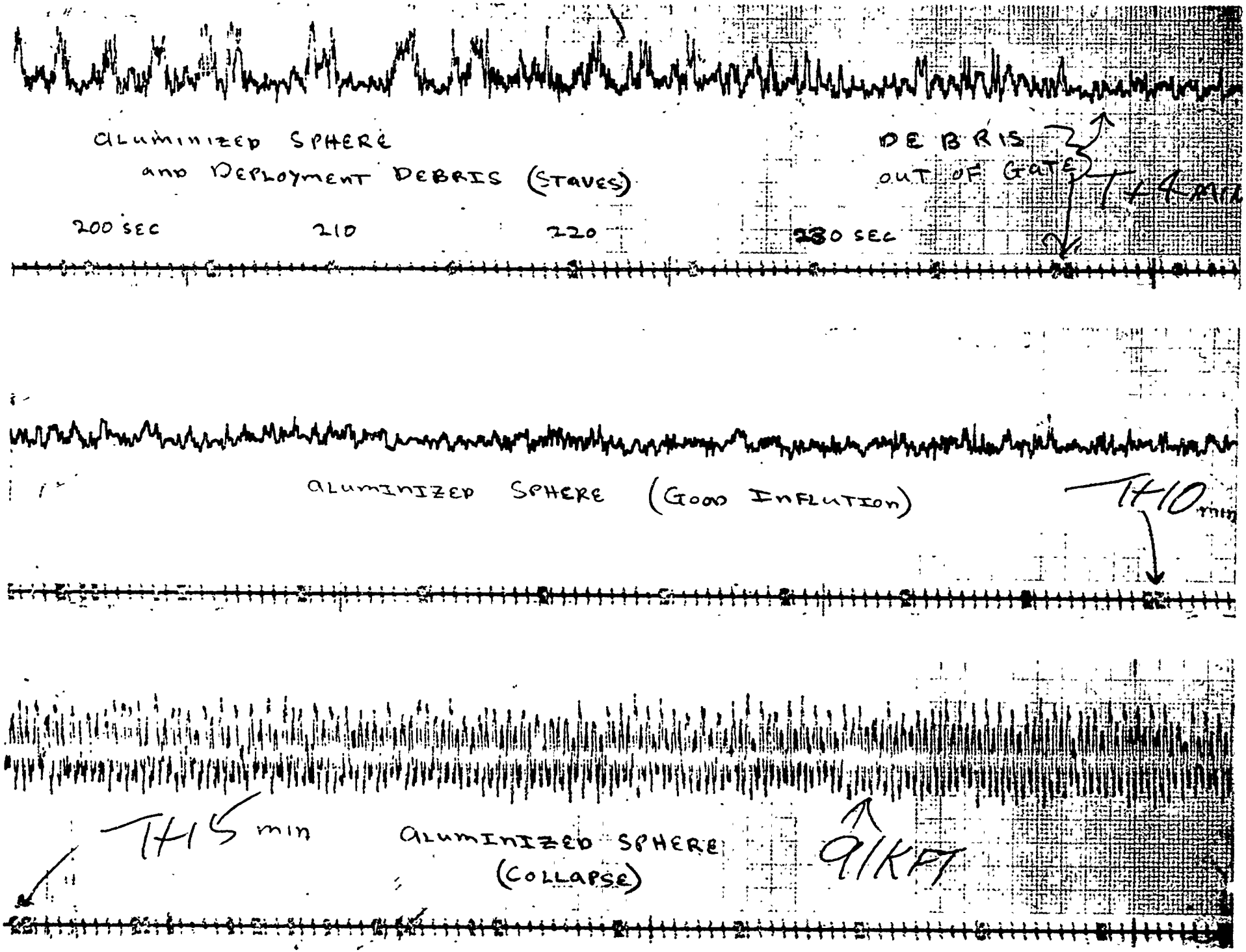

FIGURE 10.13 (continued)

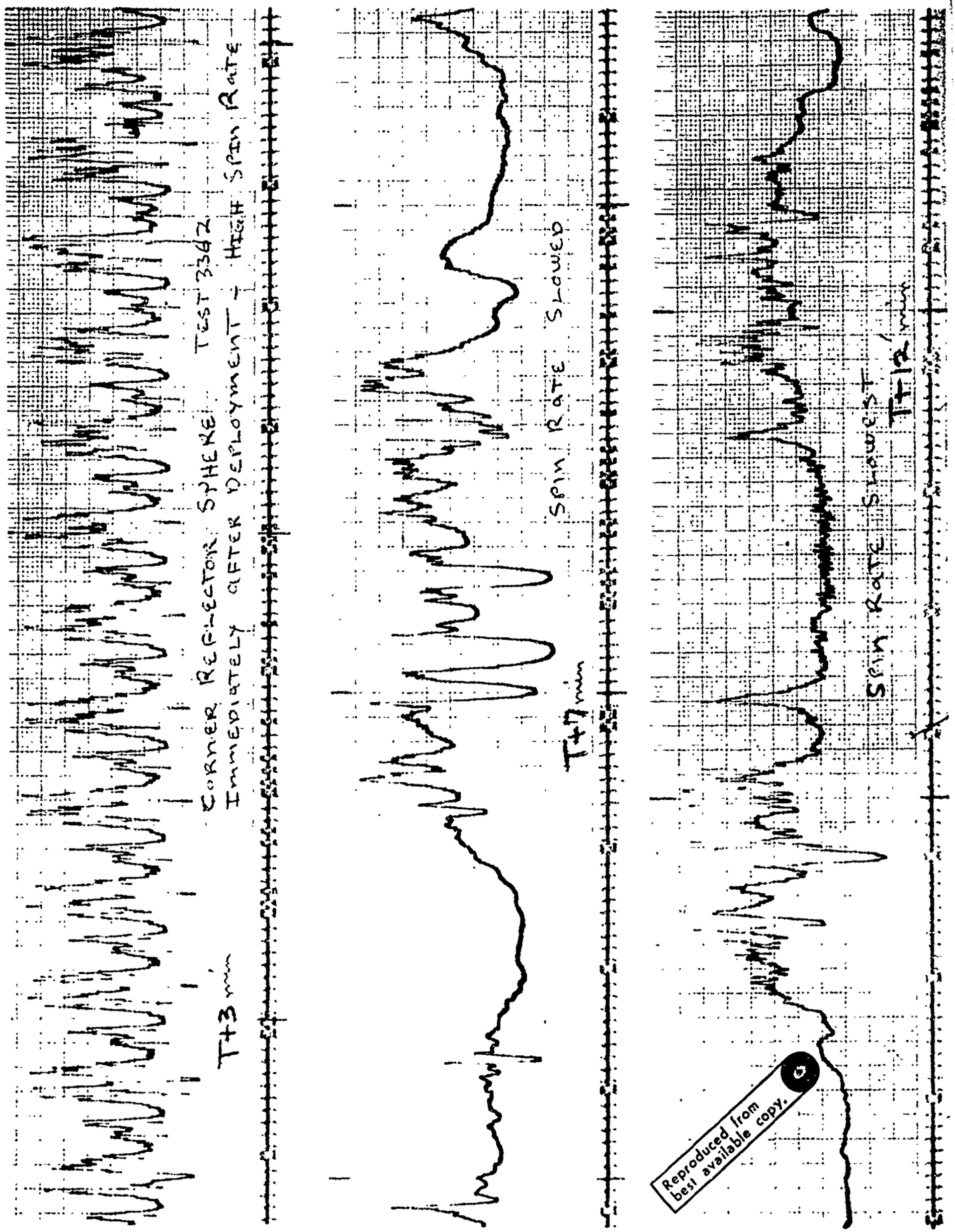

FIGURE 10.14 TYPICAL CORNER REFLECTOR SPHERE AGC RECORD

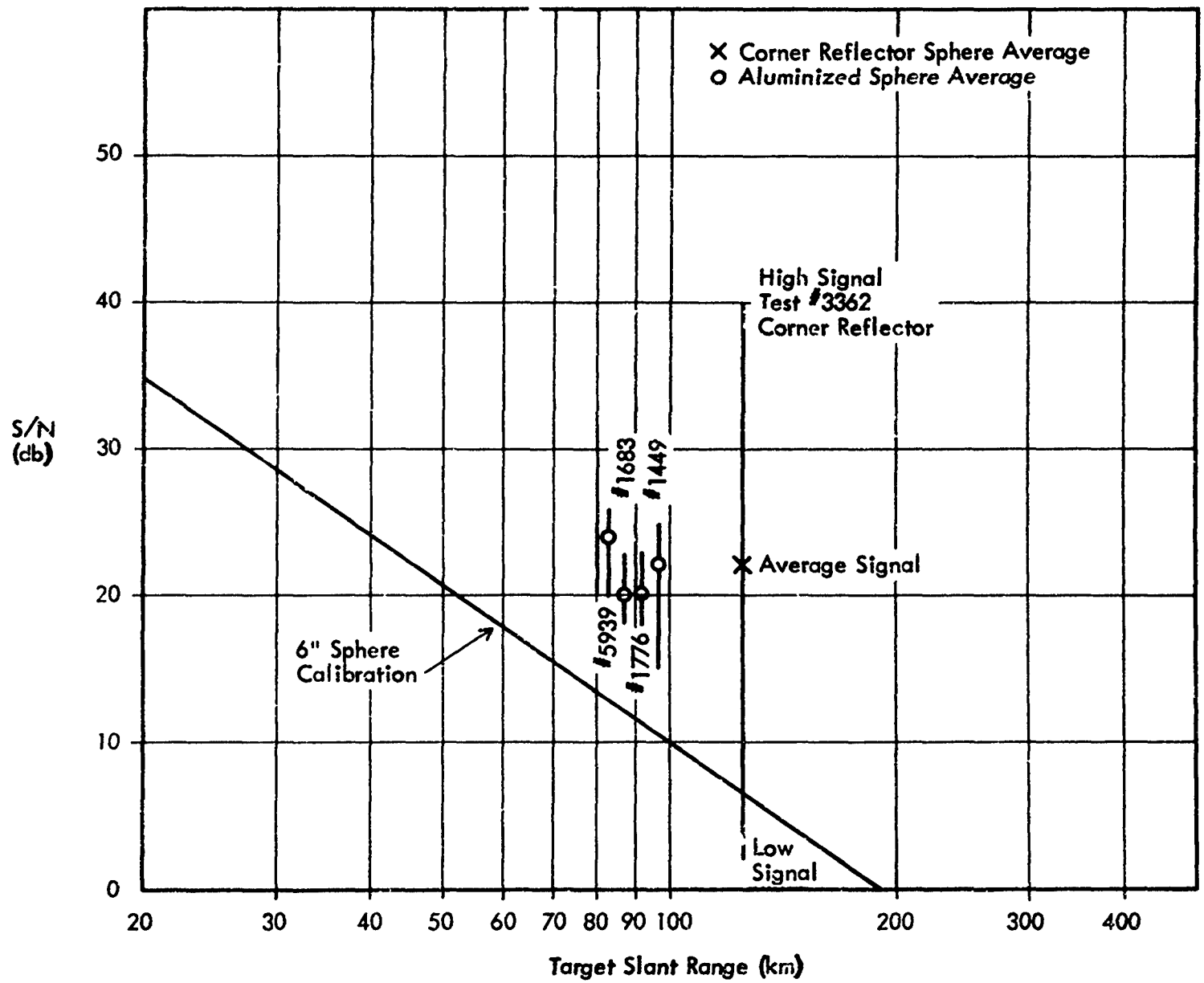

FIGURE 10.15 CAPE KENNEDY AN/FPS - 16 RADAR 1.16 ROBIN FALLING SPHERE DATA

TABLE 10.9 ROBIN FALLING SPHERE RADAR CROSS-SECTION EVALUATION

Date	Test No.	Sphere Configuration	Radar Cross-section (dbsm)			Effective area (m^2)		
			Low Signal	Average Signal	High Signal	Low Signal	Average Signal	High Signal
11-16-71	5939	aluminized	-10.3	- 5.5	-3.5	.095	.280	.442
11-17-71	3136	" "	-11.3	-10.3	-9.3	.090	.095	.118
11-18-71	6750	" "	- 9.5	- 8.5	-7.5	.115	.125	.178
2-15-72	1449	" "	- 9.5	- 4.5	-2.5	.115	.350	.555
2-15-72	1776	" "	-10-2	- 8.2	-5.2	.098	.150	.300
2-15-72	1683	" "	-10.8	- 8.8	-5.8	.092	.130	.261
Average aluminized Spheres			-10.27	- 5.09	-3.76	.097	.310	.420
12-15-71	3362	Corner reflector	-21.3	- 1.3	+16.7	.007	.733	46.50

11.0 Atmospheric Measurements

A typical atmospheric temperature profile obtained with the Super Loki Transponder system is shown in Figure 11.1 along with a near time Loki Datasonde measured profile. There appears to be excellent agreement between the two profiles in spite of the differences in the sensor mounts. The transponder employs a long coiled-wire suspension for the thermistor and the Datasonde employs a thin-film loop mount. Both sets of data agree quite well with the conjective rawinsonde in the lower altitude overlap region.

A typical atmospheric density profile obtained with the Super Loki Robin system is shown in Figure 11.2 along with a near time Viper Dart Robin measured profile. There appears to be excellent agreement between these two profiles, and both agree quite well with the near time Loki Datasonde derived density data from 60km down to collapse altitude. The profiles agree with the conjunctive rawinsonde in the lower altitudes.

There was some concern that the increase in the Robin sphere weight from 115 grams to 165 grams during this development program might degrade the density data accuracy. A study conducted by the University of Dayton under this contract indicates that the heavier sphere is satisfactory for measuring winds below 85 km and density below 88 km with the Super Loki apogee altitude performance and the July 1971 Robin Data Reduction Program.

FIGURE 11.1 ATMOSPHERIC TEMPERATURE PROFILES (Uncorrected Data)

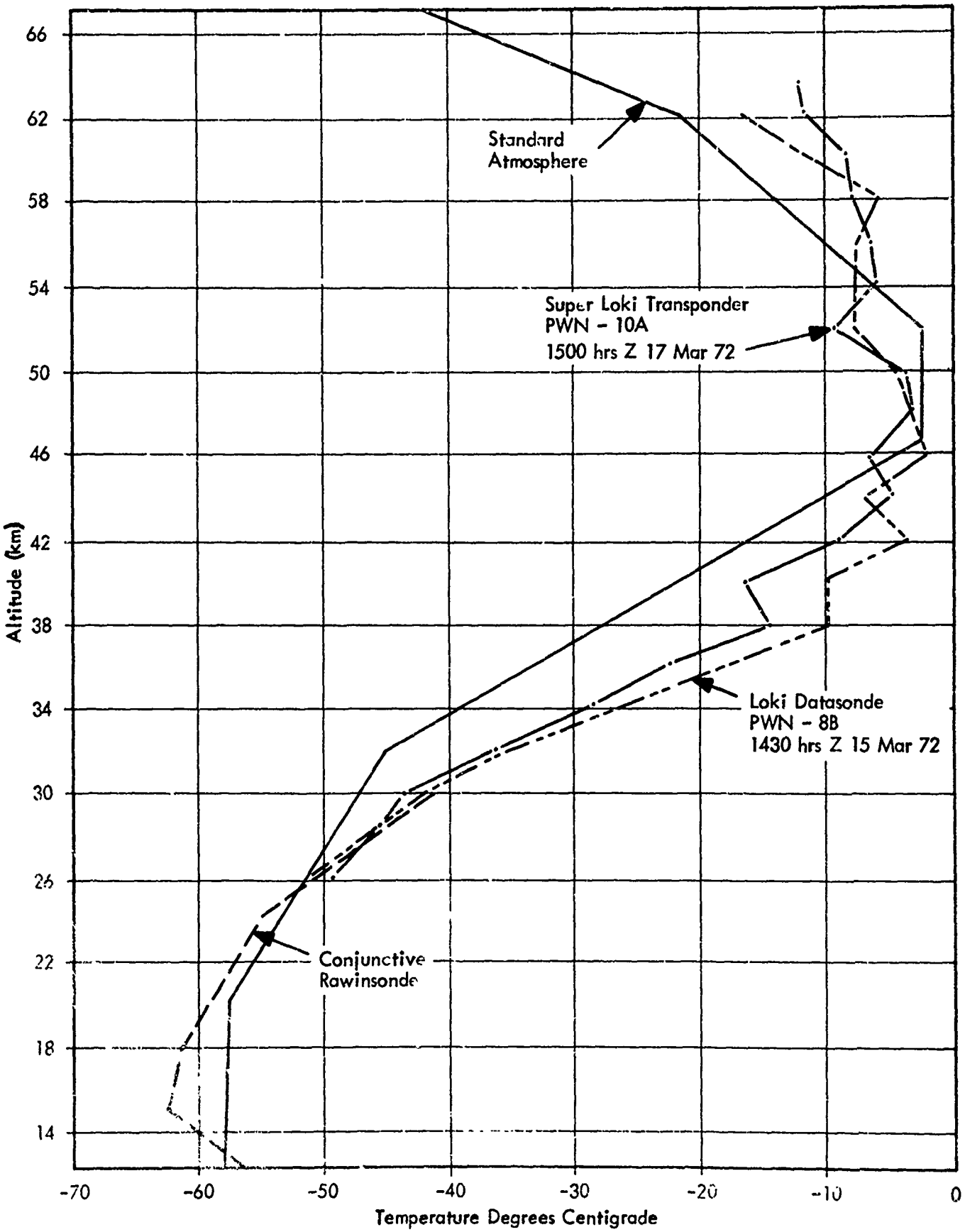

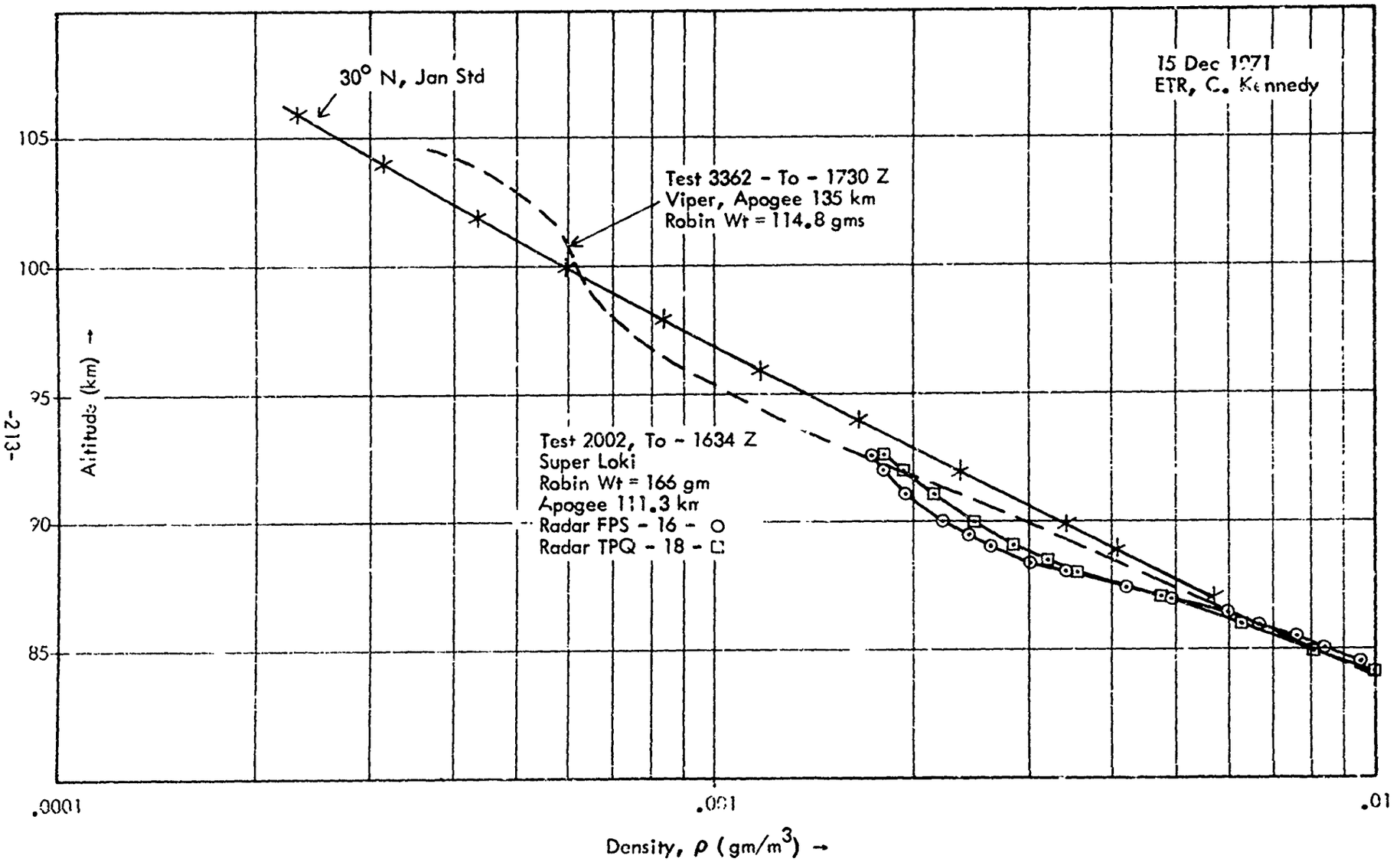

FIGURE 11.2-1 ATMOSPHERIC DENSITY PROFILE

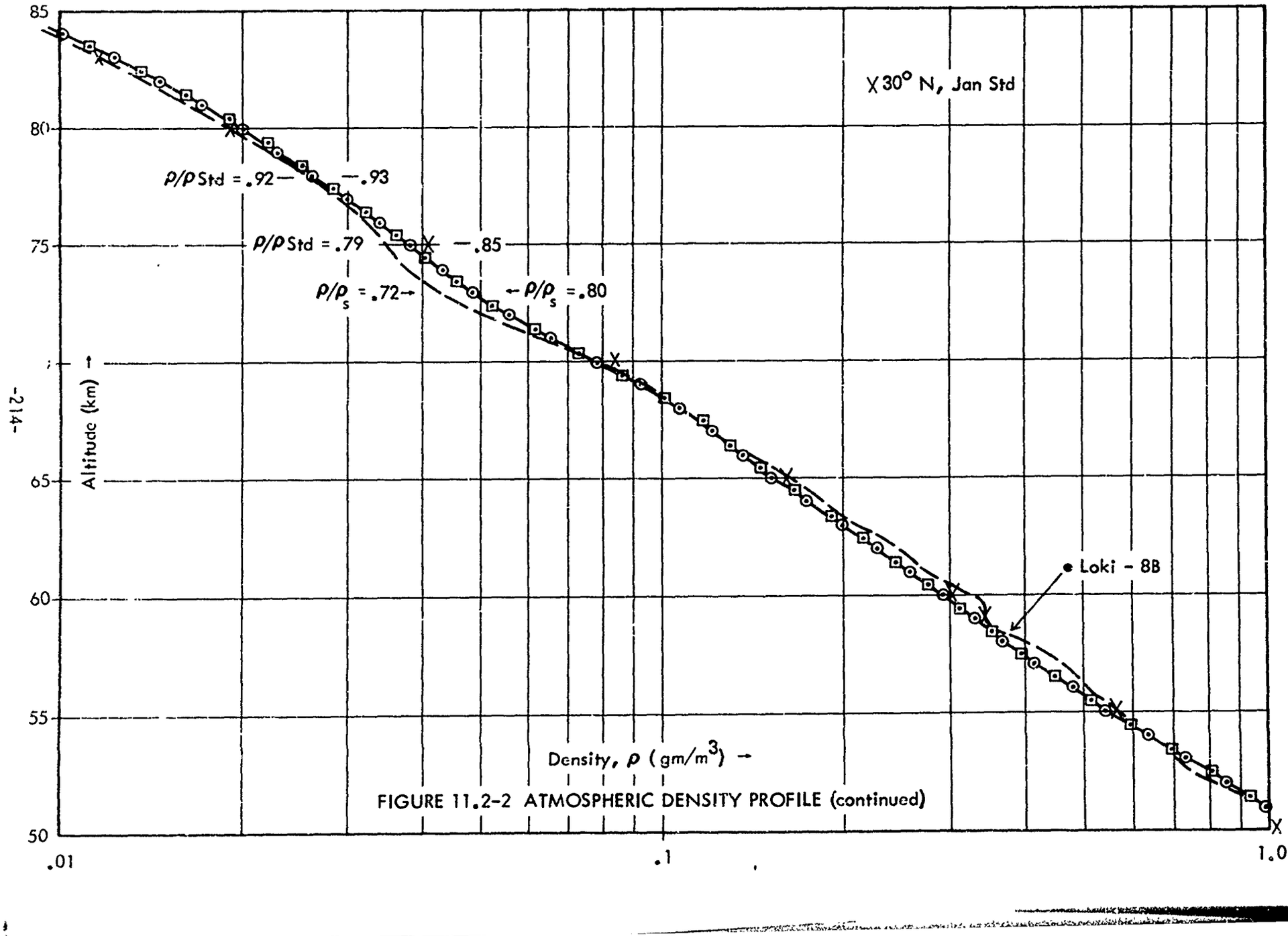

FIGURE 11.2-2 ATMOSPHERIC DENSITY PROFILE (continued)

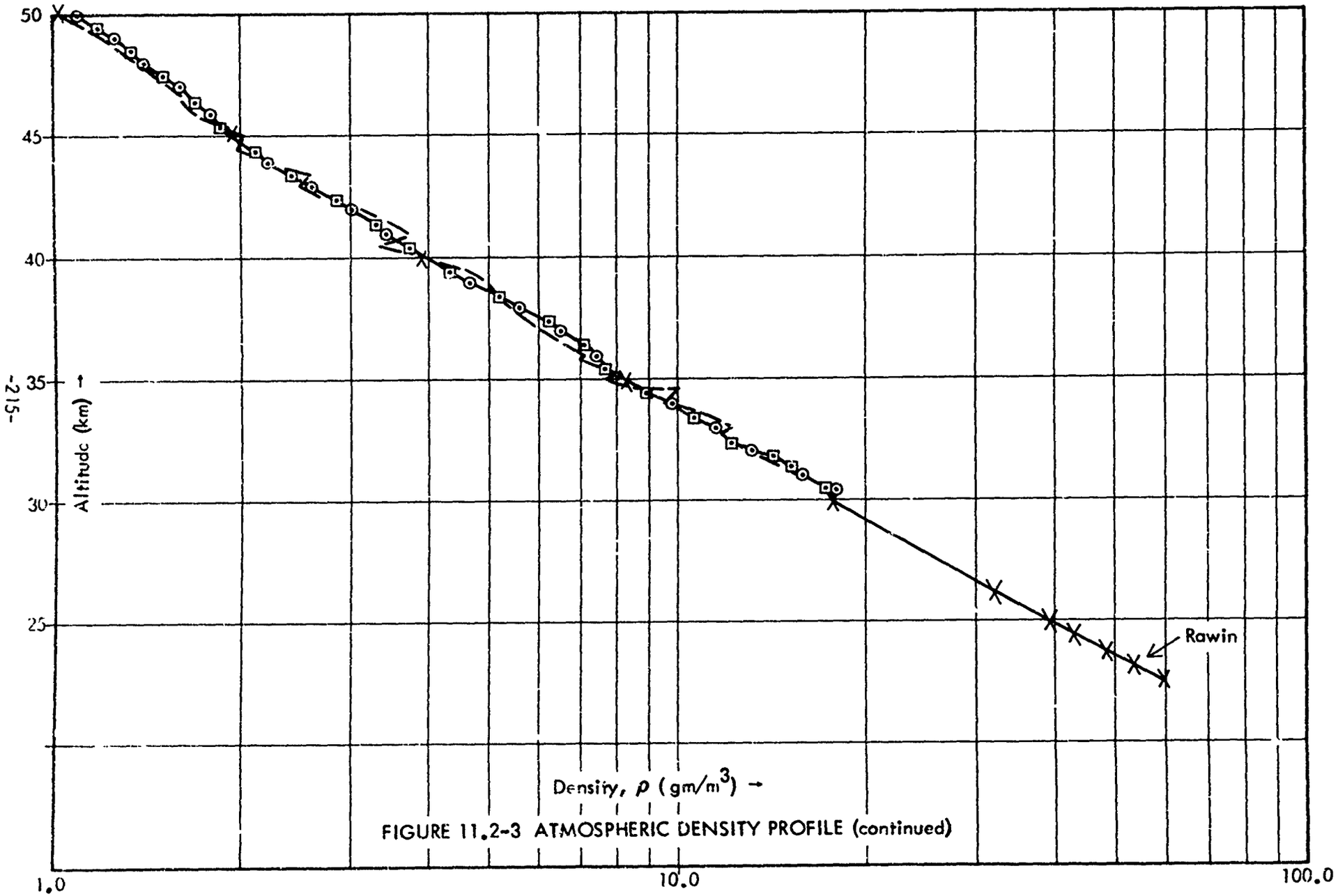

FIGURE 11.2-3 ATMOSPHERIC DENSITY PROFILE (continued)

REFERENCES

1. Wright, John B., The Evolution of a Standard Low Cost Meteorological Rocket System. Pages 183-190. Preprints of the Second Symposium on Meteorological Observations and Instrumentation, AMS, San Diego, Cal. 27-30 March 1972.

2. Georgian, Elefterious J., and Griffin, Jack R., Development of a Transpondersonde for the Super Loki Meteorological Rocket. AFCRL-72-0089, 2 Fegruar 1972.

3. Bollerman, Bruce and Walker, Robert L., Design, Development and Flight Test of the Viper Robin Meteorological Rocket System, Design Improvement. AFCRL-70-0150, 31 January 1970.

4. Fischbach, Frederick F., Allen, Harold F., and Bartman, Fred L., Analyses and Tests of Mylar Falling Spheres. AFCRL-71-0571, 15 December 1971.

5. Georgian, Elefterious J., Transponder Rocketsonde Instrumentation and Data Analysis. Paper Presented at AMS Fourth National Conference on Aerospace Meteorology, Las Vegas, Nevada, 4-7 May 1970.